AN INVESTIGATION OF THE SLIPSTREAMS AND WAKES OF TRAINS AND THE ASSOCIATED EFFECTS ON TRACKSIDE PEOPLE AND OBJECTS.

By

SARAH CATHERINE JORDAN.

A thesis submitted to

The University of Birmingham

for the degree of

DOCTOR OF PHILOSOPHY

Department of Civil Engineering

School of Engineering

The University of Birmingham

January 2008

AT THE BEHEST OF THE UNIVERSITY, THE FOLLOWING PAGES HAVE NOT BEEN SCANNED:

Appendices Section: A1.1-A5.2

ABSTRACT.

A mathematical model is developed which predicts if a person or a pushchair is destabilised by a train's slipstream. The model simulates the mean slipstream velocity time history using the theories of potential flow, boundary layer growth and wake decay. The turbulence-induced fluctuations are reproduced with an autoregressive model. A randomised person is generated and subjected to the simulated slipstream, and their response is modelled by a simple solid object and a mass-spring-damper system. If the slipstream forces cause the person to be displaced by a critical distance the person is destabilised. A randomised pushchair is also generated and positioned so as to be capable of being destabilised by either toppling over or moving along the ground on its wheels. A toppling pushchair is modelled as a simple solid object in a similar manner to that of a person, and a pushchair will move along the ground on its wheels if the slipstream force is greater than the frictional force. Greater numbers of destabilised people and pushchairs are associated with the slipstream of a freightliner than that of a passenger train, increasing train speed and decreasing distance from the train side.

ACKNOWLEDGEMENTS.

I would like to thank my supervisors Dr. Mark Sterling and Prof. Chris Baker for all their guidance, help and constructive criticism throughout this PhD journey. I especially thank Mark for his continued sarcasm. Prof. Roger Gawthorpe also gave feedback to my work and I'd like to thank him for the interest he showed in the developing model. The Railway Safety and Standards Board contributed financially to the project, and Philippe Delpeche and Christian Sacré of CSTB are due thanks for their involvement in subjecting students to sudden gusts. Dr. Dave Boardman and his family generously lent me several 'travel systems' to hurl about the civil engineering lab.

My thanks go to Michael and Fred who were inspirations with regard to mathematics and engineering, and also Roger P. who incited laughter when the mathematics went haywire. Ms Willowes and Mr Huntsman helped me catch the next train even when I did not know there was another due. John and Robin gave me much appreciated support, and my Mercurial Friend was always close by. Finally, I would like to thank the Mater for a most singular genetic inheritance, which includes being quick to laughter and having tungsten in the marrow.

The only way to be sure of catching a train is to miss the one before it. – G. K. Chesterton (1874-1936).

CONTENTS.

FIGURES.

TABLES.

SYMBOLS.

a	Half a cuboid's width in the plane of rotation
a_t	White noise term
A	Boundary layer constant
A	Projected area
A	Cross-sectional area of a train
A_{DU}	Dubois area
B	Decay constant of the vortex at the rear of a train
$\mathbf{c}$	Damping matrix
c_1	Damping between m_1 and m_2
c_2	Damping between m_2 and m_3
c_3	Damping between m_3 and the base
C_n	Generalised damping
C_D	Drag coefficient
C_1	Boundary layer constant
d	Index of Agreement
E	Subscript referring to an elderly person
f	Frequency
f	Natural cyclic frequency
F	Wind induced force
F	Force acting on a pushchair

F_{max}	Maximum frictional force that occurs before the onset of movement between the two objects
g	Acceleration due to gravity
g	Constant
h	Constant
h	Train height
h	Subscript denoting normalisation by vehicle height
h	Person's height
h_1	Height to m_1
h_2	Height to m_2
h_3	Height to m_3
h_p	Height to person's centre of gravity
H	Normalised vehicle height
$H(\omega)$	Heaviside step function
i	Imaginary unit
k	Frequency index
k	Spring stiffness
$\mathbf{k}$	Stiffness matrix
k_1	Stiffness of spring between m_1 and m_2
k_2	Stiffness of spring between m_2 and m_3
k_3	Stiffness of spring between m_3 and the base
k_{eq}	Equivalent stiffness
K_n	Generalised stiffness

L	Total length of train
m	Mass
$\mathbf{m}$	Mass matrix
m_1	Mass representing a person's head
m_2	Mass representing a person's upper body
m_3	Mass representing a person's lower body
m_{tot}	Total mass
M	Measured data
M_F	Force moment
M_n	Generalised mass
M_W	Weight moment
n	Subscript refering to the mode
n	Boundary layer constant
n	Time index
n'	Time index
N	Potential flow constant
N	Number of data points in the time series
N	Normal force
p	Order of the AR model
$p(t)$	Wind force
$\mathbf{p}(t)$	Applied wind load vector
$p_1(t)$	Wind force acting on m_1
$p_2(t)$	Wind force acting on m_2

$p_3(t)$	Wind force acting on m_3
$P_n(t)$	Generalised wind load
$P_n(\tau)$	Impulse load
Q	Source flow rate (m^3/s)
r	Distance between a cuboid's centre of gravity and pivotal edge
R	Normalised radius of the vortex at the rear of a train
Re	Reynolds Number
s	Wavelet scale
S	Simulated data
t	Time
t	Time since the termination of the initial disturbance
T	Normalised time
T_h	Time normalised by vehicle height
T_W	Normalised time at the start of the wake region
T_E	Normalised time at the end of the vortex or the boundary layer region
u	Slipstream velocity
u	Gust velocity
u_τ	Friction velocity
U	Normalised slipstream velocity in the direction of the vehicle's motion
U'	Normalised resultant of the longitudinal and lateral slipstream velocity components
U_{max}	Normalised slipstream velocity at the circumference of vortex at the rear of a train
$\tilde{U}$	Fluctuating normalised velocity
V	Train speed

w	*Person's weight*
w	Train width
W	Normalised vehicle width
$W_n(s)$	Wavelet transform
x	Source position in a ground-fixed reference frame (i.e. the vehicle's longitudinal displacement),
x	Longitudinal distance along a flat plate
x	Horizontal displacement of a cuboid's centre of gravity
$\boldsymbol{x}$	Displacement vector
x_1	Horizontal displacement of m_1
x_2	Horizontal displacement of m_2
x_3	*Horizontal displacement of m_3*
$\dot{\boldsymbol{x}}$	Velocity vector
$\dot{x}_1$	Velocity of m_1
$\dot{x}_2$	Velocity of m_2
$\dot{x}_3$	*Velocity of m_3*
$\ddot{\boldsymbol{x}}$	Acceleration vector
$\ddot{x}_1$	Acceleration of m_1
$\ddot{x}_2$	Acceleration of m_2
$\ddot{x}_3$	Acceleration of m_3
$\hat{x}_1$	Displacement shape of m_1
$\hat{x}_2$	Displacement shape of m_2
$\hat{x}_3$	Displacement shape of m_3

x_n	A signal
x_p	Displacement of the person as a whole
$\hat{x}_k$	Discrete Fourier transform
$\hat{\boldsymbol{x}}$	Displacement shape vector
X	Normalised longitudinal distance from the Centre of the vortex at the rear of a train
X_t	Current value of a time series
y	Lateral distance from the vehicle centreline
y_s	Distance from the side of the train
Y	Subscript referring to a young and middle-aged person
Y	Normalised lateral distance from the vehicle centreline
Y_h	Lateral distance from the vehicle centreline normalised by vehicle height
Y_n	Modal amplitude
Y_V	Normalised lateral distance from the centre of the vortex at the rear of a train
Z_h	Vertical distance from the ground normalised by vehicle height
α	Angle between a cuboid's base and r
α	Wake constant
β	Wake constant
δ	Maximum width of boundary layer
δt	Time interval
δT	Normalised time interval
ε_n	Damping ratio
η	Non-dimensional time parameter
η_r	Relative force amplitude of a force

θ	Angle of rotation
θ	Phase angle
θ	Momentum thickness
λ	Fourier period
μ	Coefficient of static friction
ν	Kinematic viscosity of air
ρ	Density of air
τ_w	Shear stress
ϕ	AR coefficient
ϕ	Eigenvector
$\boldsymbol{\Phi}$	Eigenvector matrix
ψ	Wavelet function
ω	Angular frequency
ω	Undamped natural angular frequency for a Single degree of freedom
ω_k	Angular frequency
ω_{Dn}	Damped angular natural frequency
ω_n	Undamped angular natural frequency
ω_n^2	Eigenvalues
ω_0	Non-dimensional frequency
$*$	Denotes the complex conjugate
$\hat{}$	Indicates the Fourier transform
$\bar{}$	Denotes the mean value
$\lvert\ \rvert$	Brackets representing the determinant of a matrix

CHAPTER 1.

INTRODUCTION.

1.1 Background.

The speeds of trains are getting faster in the UK and elsewhere due to new train designs and the upgrading of tracks. For example, the British Class 390 'Pendolino' train had a top speed of 177km/h (110mph) until 2005, but with the completion of the upgraded West Coast Main Line the speed was able to increase to 200km/h (125mph). There are plans for further track improvements on some sections of the rail network which will enable the 'Pendolino' to travel at a speed of 220km/h (135mph). The Eurostar train running between London and Paris or Brussels on the Channel Tunnel Rail Link (CTRL) is capable of 300km/h (186mph), and there are also plans to run 225km/h (140mph) trains on domestic services between London and Kent along the CTRL in 2009. Furthermore, the proposals for a high-speed rail link between the North and South of England are being considered which would have trains travelling at 320km/h (200mph). On mixed track, such increases in passenger train speed are likely to result in increases of freight train speed in order to improve route capacity.

Transient aerodynamic effects are generated as a train moves through the surrounding air, and the airflow around the moving train is called the slipstream. The slipstream starts upstream of the train's nose and continues into a wake beyond the rear of the train. Although the prevailing airflow is in the same direction as the train's motion, there are also lateral and vertical components of the slipstream. High velocity magnitudes and turbulence levels can be associated with the slipstream, and the subsequent slipstream forces impinge on trackside

objects, such as pushchairs and luggage trolleys situated on station platforms, and on waiting passengers and trackside workers. These forces have the potential of destabilising both the objects and people, for example, pushchairs can move along the platform on their wheels or topple over, and people can lose their balance. Such destabilisation can cause injury to people. Slipstream velocities increase with increasing train speed, therefore, as the speed of trains increase, the risk of people and objects being destabilised also increases.

Sixteen incidents caused by train slipstreams have been recorded on UK station platforms between 1972 and 2002 (Temple and Johnson, 2003). One incident involved a pushchair, which had a child inside, being blown over causing minor head injuries to the child. In another incident a braked pushchair was drawn 3m towards a freightliner, after hitting the train it was pushed across the platform and hit two waiting passengers, injuring one of them. Three people have nearly been swept off their feet by the slipstream of a passing freightliner. Further incidents are likely to occur, especially as train speed is increasing throughout the rail network.

The circumstances that result in destabilisation need to be identified and the likelihood of destabilisation accurately quantified in order to address the increasing risk to people and objects from the effects of train slipstreams. This can be done if the response of a person or an object to a train slipstream can be predicted for given circumstances, e.g. a person standing at 1m from the side of passenger train travelling at 200km/h. This thesis develops a mathematical model to simulate both the characteristics of a train slipstream, and the response of a person and a pushchair to the train slipstream. As train type (i.e. passenger or freight), train speed and distance from the train side affect the slipstream characteristics, these factors

are considered when simulating a slipstream. The model also considers a person's standing orientation and how a pushchair is positioned when simulating the response. The model determines if a particular person or a pushchair will be destabilised by a particular slipstream, and from this calculates the percentage of people and pushchairs destabilised.

If the risk to a person or an object is quantified then appropriate safety measures can be implemented. Such safety practices include platform signs warning people of the dangers of slipstream turbulence, announcements of an oncoming non-stopping train over station speakers, and a yellow line painted parallel to the edge of the platform to keep waiting passengers at a safe distance from non-stopping trains.

1.2 Layout of report.

Chapter 2 of the thesis is a review of the current literature relating to train slipstreams and a person's response. Chapter 3 describes how a train slipstream is modelled. The experiments that were undertaken for the current research in order to investigate the effects of a sudden gust on people are described in Chapter 4. Chapters 5 and 6 are concerned with the modelling of a person's response to a train slipstream and the results obtained from the slipstream/person model respectively. Chapter 7 describes the experiments undertaken to determine the force required to destabilise a pushchair. A pushchair's response to a train slipstream is modelled in Chapter 8 and the results of the slipstream/pushchair model are also presented in this chapter. The final conclusions of the thesis are given in Chapter 9.

CHAPTER 2.

LITERATURE REVIEW.

2.1 Introduction.

This chapter is a review of the literature relevant to the investigation of the effects of a train slipstream upon a person. Section 2.2 describes the full-scale and model-scale experiments undertaken to determine the velocity time history of a vehicle slipstream, and Section 2.3 describes the models used to simulate a train slipstream. The results from experiments undertaken to determine the pressure acting upon people and objects due to a slipstream are given in Section 2.4. Sections 2.5 and 2.6 discuss the literature relating to the effect of wind gusts on people and the proposed safe wind speeds respectively. The literature pertaining to the stability of a person is examined in Section 2.7, and previous work with biomechanical models concludes the literature review in Section 2.8.

2.2 Experiments undertaken to measure a vehicle's slipstream.

A number of experiments have previously been undertaken to measure the slipstream of a vehicle, for example Gawthorpe (1978). However, the most recent experiments include those involving a full-scale passenger train (Liao *et al.*, 1999; Johnson *et al.*, 2004), a full-scale freightliner (Temple and Dalley, 2001), a $1/25^{th}$ model-scale passenger train (Baker *et al.*, 2001), a model-scale lorry (Baker *et al.*, 2000) and a full-scale car (Huggins *et al.*, 2002). Liao *et al.*

(1999) only discuss the maximum slipstream velocity and, therefore, do not allow an investigation into the characteristics of the entire slipstream; however, they do state that the maximum slipstream velocity occurs in the wake of a train. The other papers give details of the slipstream velocities from upstream of the vehicle's nose to the wake beyond the rear of the vehicle, and consequently allow the main slipstream characteristics to be identified.

2.2.1 Results of previous experiments that are used in modelling a train slipstream in the current research.

The measurements of the slipstream velocities taken during the experiments described in Johnson *et al.* (2004), Baker *et al.* (2001), and Temple and Dalley (2001) are used in the development of the train slipstream model presented in this thesis in that the simulated slipstreams are made to reproduce the measured velocity profiles as closely as possible. Table 2.1 gives details of these experiments. The trains involved in the experiments were a full-scale German Intercity Express (ICE2) passenger train, a full-scale UK freightliner, and a model-scale ICE2 passenger train. The passenger trains had a locomotive at the front and rear which tapered in width and height towards their end. The full-scale passenger train had twelve intermediate carriages, whereas the model-scale train had two intermediate carriages. Measurements of the full-scale passenger train and freightliner slipstreams were taken on both a station platform and at the side of an open track. The full-scale ICE2 train past a 0.31m high platform, whereas the freightliner past a 1m high platform. The platforms in Germany are lower than those in the UK, hence the variation in the heights of the platforms involved in the experiments. The measurements were taken at 1.335m and 1m above the German and UK platforms respectively; therefore, the height above the

German and UK track was 1.645m and 2m respectively. The experiments undertaken at the side of an open track were taken at 0.5m and 1m above the German and UK tracks respectively. A platform was not present in the model-scale tests, therefore, the measurements were effectively taken at the side of an open track. The anemometers were positioned at half the height of the model-scale train's body, i.e. at 90mm above the track (2.25m full-scale equivalent). The freightliner slipstream measurements were only taken at one distance from the train side, i.e. at 1.5m and 0.705m on a station platform and along an open track respectively. The passenger train measurements were taken at several distances from the train side, although the distances were not the same for the three experimental setups (see Table 2.1).

The full-scale and model-scale passenger train experiments were undertaken as part of the EU funded Railway Aerodynamics for Passing and Interactions with Dynamic Effects (RAPIDE) project (Schulte-Werning *et al.*, 1999). The project consisted of the above experiments and numerical modelling in order to increase the data on, and better understand, train slipstream effects on people and structures. The technique of ensemble averaging is used when presenting the slipstream velocity time histories. Taking the average of a number of velocity time histories reduces the run-to-run variability of the slipstream data, and the number of runs involved in the ensemble averaging of each train is given in Table 2.1.

Experimental type	Train	Measurement type	Height (m)	Distance from train side (m)	Number of runs in ensemble average
Full-scale	ICE2 14 car	Platform 0.31m high	1.335m above platform	0.57, 1.07, 1.57, 2.07, 2.57, 2.97	11, except for 1.07m from the train side when the number of runs is 8
		Open track	0.5m above track	0.41, 0.75, 1.35, 1.665, 1.915, 2.16	16
	Freightliner	Platform 1m high	1m above platform	1.5	11
		Open track	1m above track	0.705	13
Model-scale	ICE2 4 car	Open track	2.25m above track (full-scale equivalent)	0.125, 0.25, 0.5, 0.75, 1, 1.5, 2	10 runs for a vehicle speed of 32m/s, 8 runs for a vehicle speed of 50m/s

Table 2.1. Experimental series and measurement positions.

2.2.1.1 Full-scale passenger train.

The German ICE2 passenger train involved in the full-scale tests (Johnson *et al.*, 2004) had a total length of 363.8m, and the width and height of an ICE2 train are 3.07m and 3.84m respectively (Köhler, 2001). The speed of the train passing the station platform and travelling along an open track was 51m/s and 69m/s respectively. Figure 2.1 illustrates the ensemble averaged normalised velocity profile of sixteen runs at 0.75m from the train side of an ICE2 passenger train travelling along an open track. The slipstream velocity is normalised by train speed; and time is normalised by train speed (V) and total length of the train (L), i.e. $T = \frac{t.V}{L}$. Therefore, the nose and the rear of the train pass at $T = 0$ and $T = 1$ respectively. The normalised velocity profile has been separated into the u component (the longitudinal velocity travelling in the same direction as the train), the v component (the lateral velocity in the direction away from the side of the train); and the resultant velocity of the u and v components is also given in Figure 2.1. Figure 2.1 shows that a velocity peak occurs as the train's nose passes, followed by increasing velocities and much turbulence along the main body of the train, a peak in velocity immediately after the rear of the train has past, and finally a gradual decay in velocity and turbulence in the wake of the train. The maximum slipstream velocity occurs at the rear of the train, and this agrees with Liao *et al.* (1999). Figure 2.1 also shows that it is the u component of the slipstream that dominates the velocity time history, i.e. the largest slipstream velocity occurs in the direction of the train's motion. Further descriptions of the normalised slipstream velocity profiles of the ICE2 train are given in Section 3.6.1.3. The experiments show that the magnitude of the slipstream velocities increase with decreasing lateral distance from the side of the train.

The slipstream velocity magnitudes and turbulence levels are greater when a train travels along an open track than when passing a station platform at comparable distances from the train side.

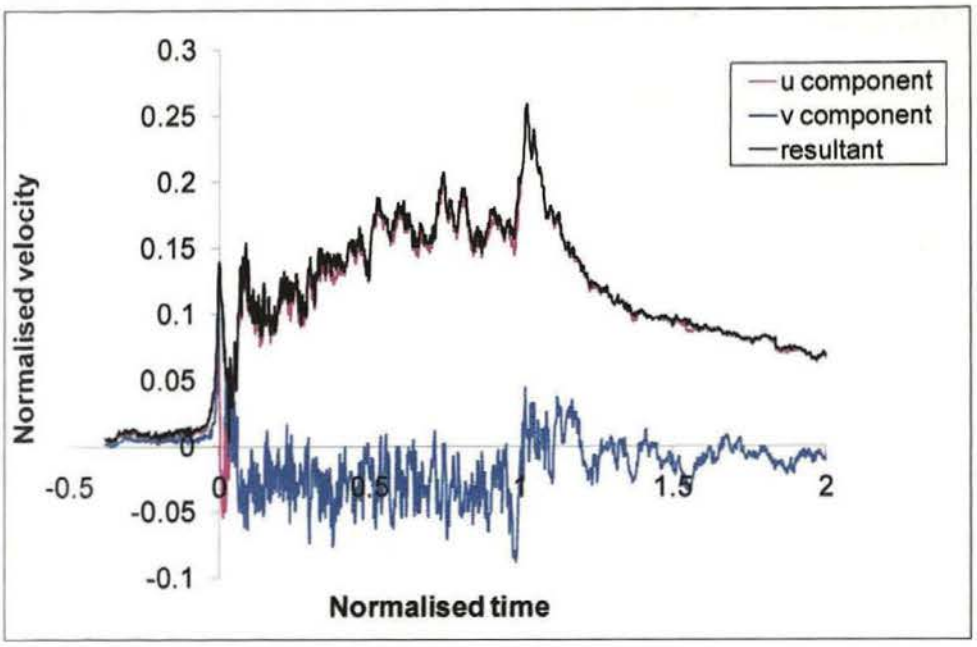

Figure 2.1. Ensemble averaged normalised velocity profile at 0.75m from the side of a full-scale ICE2 passenger train travelling along an open track at 69m/s, showing the u and v components and the resultant velocity. Adapted from Johnson *et al.* (2004).

2.2.1.2 Full-scale freightliner.

The freightliner involved in the full-scale tests (Temple and Dalley, 2001) consisted of a British Rail Class 92 locomotive with forty-six containers which were each sixty percent loaded. All containers were 2.5m wide, 2.59m high, and 6.1m long except for the ten containers at the rear which were 12.2m long. The train had a total length, including the locomotive, of 703.5m, and

was travelling at 33.6m/s. The width, height and length of the Class 92 loco are 2.66m, 3.95m and 21.34m respectively (Wikipedia, 2006a).

Figure 2.2 illustrates the normalised slipstream velocity time history at 0.705m from the side of the freightliner travelling along an open track. The normalised velocity shown is the resultant of the lateral and longitudinal velocity components. The velocity profile of the freightliner slipstream is significantly different to that of the full-scale passenger train. Although there is a slipstream velocity peak at the nose of the freightliner it is larger than that of a passenger train. For example, the normalised velocity at the nose of a train travelling along an open track is 0.336 at 0.705m from the side of a freightliner, whereas it is 0.202 at 0.57m from the side of a passenger train. In this example the nose peak is approximately 60% larger with a freightliner than with a passenger train even though the distance from the passenger train's side is smaller. The boundary layer of a freightliner develops more quickly than that of a passenger train, with higher normalised velocities and turbulence levels at comparable distances from the train side. Also, there is no velocity peak at the rear of the freightliner. Further descriptions of the normalised slipstream velocity profiles of the freightliner are given in Section 3.6.2.3.

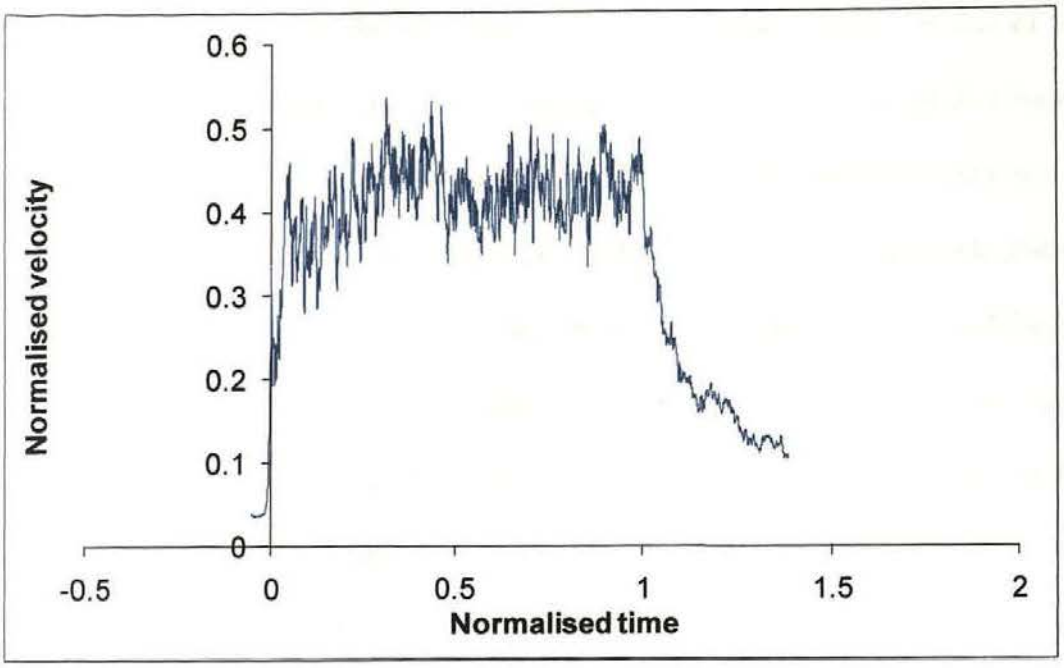

Figure 2.2. Ensemble averaged normalised velocity profile at 0.705m from the side of a full-scale freightliner travelling along an open track at 33.6m/s. Adapted from Temple and Dalley (2001).

2.2.1.3 Model-scale passenger train.

The model-scale ICE2 train involved in the tests on a moving model rig (Baker *et al.*, 2001) had a total length of 4.2m (105m full-scale equivalent). Figure 2.3 shows the ensemble averaged normalised velocity profile at 10mm (0.25m full-scale equivalent) from the side of a train travelling at 32m/s. As with the full-scale tests, the resultant of the lateral and longitudinal components of the velocity is presented. The slipstream of a model-scale passenger train has an essentially inviscid region upstream and around the nose with a velocity peak that occurs as the nose passes, and increasing velocities and turbulence along the main body of the train which gradually decrease in the wake. The slipstream velocities increase with train speed and

decreasing distance from the train side. The shape of the velocity profile of the model-scale passenger train is similar to that of the full-scale passenger train except that there is no velocity peak at the rear of the model-scale train. That the model-scale passenger train slipstream does not reproduce the significant velocity peak recorded at the rear of the full-scale passenger train may be a deficiency of the experiments. However, the measurements of the model-scale experiments were taken at 2.25m (full-scale equivalent) above the track, whereas they were taken at 0.5m and 1.645m above the track during the experiments involving the full-scale passenger train travelling along an open track and passing a station platform respectively. Therefore, the discrepancy between the results may be due to the measurements of the model-scale tests being taken at a greater height than those of the full-scale tests. The normalised nose peak velocity is of a similar magnitude in both the model-scale and full-scale passenger train slipstreams at comparable distances from the train side. However, there is a delayed boundary layer growth as well as lower wake velocities associated with the model-scale train. Further descriptions of the normalised slipstream velocity profiles of the model-scale train are given in Section 3.6.3.3. The model-scale tests used two different train speeds and demonstrated that when slipstream velocity is normalised by train speed, train speed has a negligible effect on the normalised slipstream velocity. This is also in agreement with the model-scale lorry experiments of Baker *et al.* (2000).

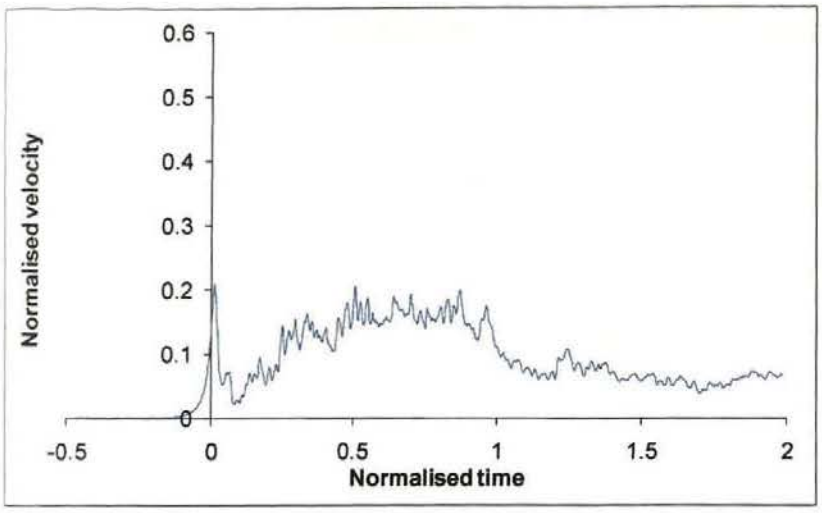

Figure 2.3. Ensemble averaged normalised velocity profile at 10mm (0.25m full-scale equivalent) from the side of a model-scale passenger train travelling at 32m/s. Adapted from Baker *et al.* (2001).

2.2.1.4 Summarising the train slipstream velocity profiles.

The following summarises the results of the above measurements of a train slipstream:

- There is an essentially inviscid region upstream and around the train nose with a velocity peak occurring as the nose passes.
- The normalised velocity peak at the train's nose is larger with a freightliner than a passenger train at comparable distances from the train side.
- There is boundary layer flow along the main body of the train with increasing velocities and turbulence.
- Higher normalised velocities and turbulence are associated with a freightliner.

- A velocity peak was recorded after the rear of a full-scale passenger train.
- The velocities and turbulence gradually decay within the wake.
- The slipstream velocities increase with decreasing distance from the train side.
- The slipstream velocities increase with increasing train speed, however, the effect of train speed is small when the slipstream velocities are normalised by train speed.

2.2.2 Differences in the slipstreams between vehicle types.

The differences in the slipstreams between vehicle types are mostly due to the extent of the streamlining of the vehicles, with a more streamlined vehicle having lower normalised slipstream velocities and turbulence levels. The experiments of Liao *et al.* (1999) used a cylindrical dummy representing a person's trunk to measure the force acting on a person due to a train slipstream, and show that a significantly smaller force is due to the slipstream of a train with a tapered locomotive at each end than a more bluff bodied train. A smaller velocity peak at the vehicle's nose is associated with streamline-nosed passenger trains (Johnson *et al.*, 2004; Baker *et al.*, 2001) than with the bluff-nosed freightliners (Temple and Dalley, 2001) and lorries (Baker *et al.*, 2000). Figure 2.4 shows the resultant ensemble averaged normalised slipstream velocity profile measured at various distances from the side of a model-scale lorry travelling at 30m/s (after Baker *et al.*, 2000). Considering that the height at which the measurements were taken affects the results, Figure 2.4 can be compared to Figure 2.3 as both the model-scale lorry and model-scale passenger train measurements were taken at the full-scale equivalent of 2.25m above the ground/track. The normalised nose peak velocity is of the order of 0.2 at a distance of 0.25m

(full-scale equivalent) from the train's side. However, this peak velocity magnitude would occur at a distance of between 0.75m and 1.50m (full-scale equivalent) from the lorry's side. Therefore, higher velocities occur at the front of a lorry than at the front of a passenger train at corresponding distances from the vehicle's side. There is also a more well-defined boundary layer along the train than with any other vehicle due to the train's longer length facilitating more boundary layer development. Liao *et al.* (1999) show that higher slipstream velocities occur on lower platforms than higher platforms, which is likely to be due to the exposed bogies increasing the aerodynamic roughness of the train. This implies that workers situated on an open track are subjected to higher slipstream velocities than passengers on a station platform for a given train type, train speed and distance from the train side. Figure 2.5 illustrates the longitudinal, lateral and vertical components of the normalised velocity profile of a full-scale car measured during the experiments of Huggins *et al.* (2002). The velocity peaks in a car's slipstream associated with the passing of wheels were recorded as the anemometers used in the tests were positioned close to the ground. From this it can be conjectured that the velocity peaks occurring along the main body of the full-scale passenger train (Figure 2.1) are due to the passing of the inter-carriage gaps.

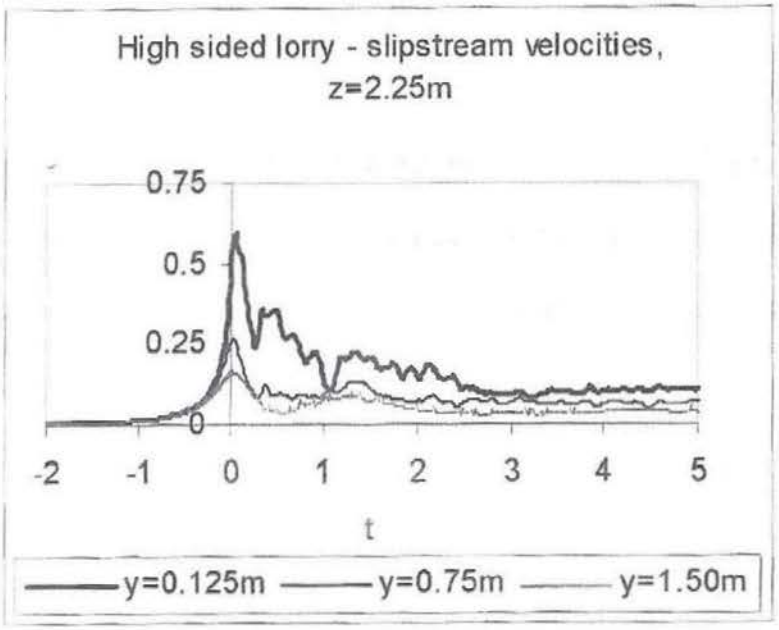

Figure 2.4. Normalised velocity against normalised time for the slipstream of a model-scale lorry travelling at 30m/s (after Baker *et al.*, 2000).

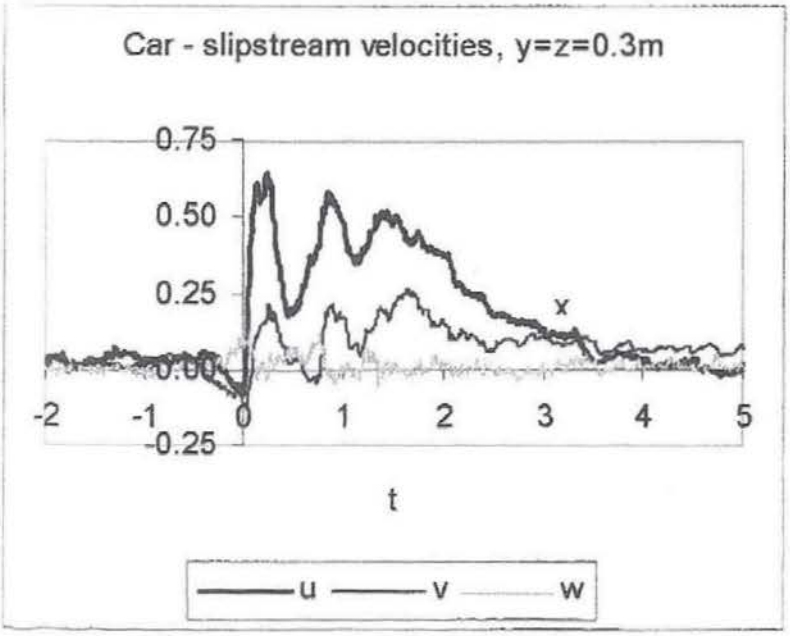

Figure 2.5. Normalised velocity against normalised time for the slipstream of a full-scale car travelling at 18m/s (after Huggins *et al.*, 2002).

2.3 Modelling a slipstream.

As part of the project investigating the aerodynamic effects of high speed trains, Liao *et al.* (1999) simulated the slipstream of a train using a Computational Fluid Dynamics (CFD) model. The results are used to compare the slipstream velocities by slipstream region, platform height and distance from the train side. They are also used to compare the slipstream of a streamlined train with that of a bluff-nosed, non-streamlined train. Figure 2.6 shows the results of the CFD model, presented in a plan view, for 0.762m and 1.524m above a platform by the side of a streamlined passenger train travelling at 67m/s (after Liao *et al.*, 1999). Figures 2.6a and 2.6b show the results associated with a low and high level platform respectively. The results of the CFD model show that the wake is the significant region for a streamlined train, which agrees with the measurements of the full-scale experiments described by Liao *et al.* (1999). The CFD model of the bluff-nosed train predicts larger velocities around the nose and in the boundary layer than with the streamlined train, which also agrees with the experiments. However, the model predicts that the bluff-nosed train has higher slipstream velocities around the nose and in the boundary layer than in the wake, which does not agree with the experiments. During the full-scale tests it was observed that the wake of the bluff-nosed train extends by a greater lateral distance than predicted by the CFD model resulting in the maximum slipstream velocity occurring in the wake. There was little data available to model the bluff-nosed train and this is conjectured by Liao *et al.* (1999) to contribute to the deficiencies in the CFD results of this particular train. The CFD model predicts lower levels of turbulence in the slipstream of the streamlined train than in that of the bluff-nosed train. Freightliners are bluff-nosed, non-streamlined vehicles, therefore, they would be expected to have larger slipstream velocities and levels of turbulence, and this agrees with the

findings of Temple and Johnson (2003), which show that freightliners have caused the most slipstream incidents on UK station platforms. The CFD model reproduces the full-scale measurements of Baker *et al.* (2000), Baker *et al.* (2001) and Huggins *et al.* (2002) in that the slipstream velocities increase with increasing vehicle speed and decreasing distance from the vehicle side. It also shows that a low platform results in a more intense aerodynamic effect than a higher platform, which is verified by the full-scale experiments undertaken as part of the same project. Figure 2.6a shows that a higher wake velocity is associated with a smaller vertical position for a given lateral distance. This variation due to height may explain why a slipstream velocity peak at the rear of a train was recorded during the full-scale experiments of Johnson *et al.* (2004) but not in the model-scale tests of Baker *et al.* (2001), as the anemometers in the latter tests were positioned at a greater height. The CFD model predicts that high-speed trains generate slipstream velocities that routinely exceed the limits determined by British Rail for the safety of pedestrians and trackside workers, which are 25mph (11.2m/s) and 38mph (17.0m/s) respectively. Liao *et al.* (1999) compare the predicted slipstream velocities to the Beaufort Scale in order to investigate the slipstream effects on a person. However, the Beaufort Scale relates to a sustained wind velocity and is not entirely appropriate for this use as a slipstream acts more like a gusty wind which has a greater effect on a person's stability than a constant wind.

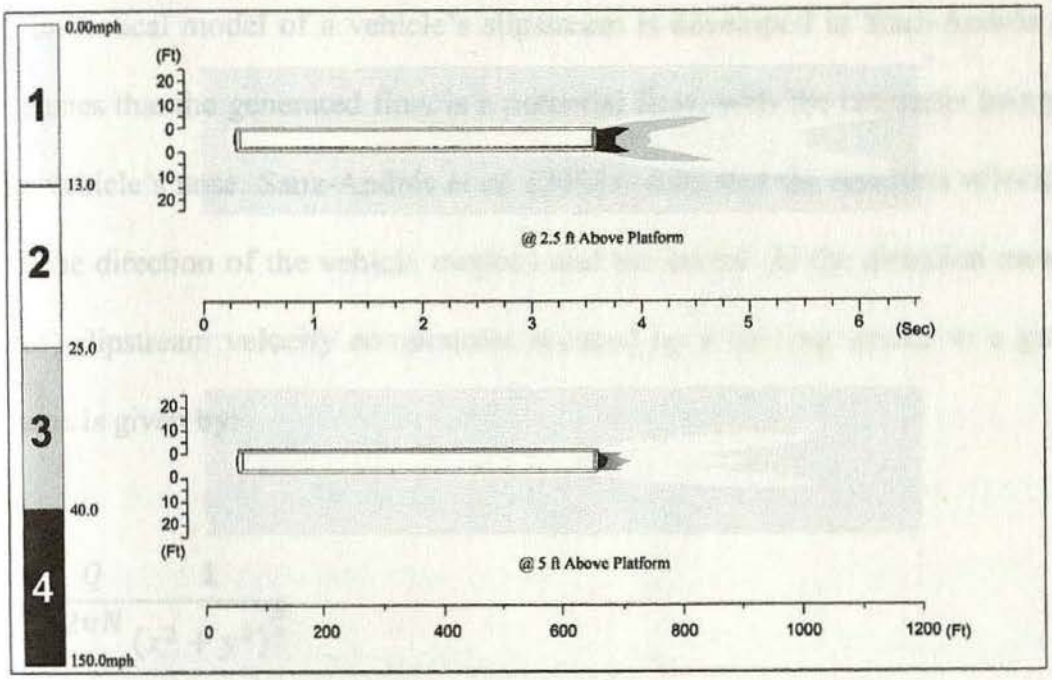

Figure 2.6a. Low level platform.

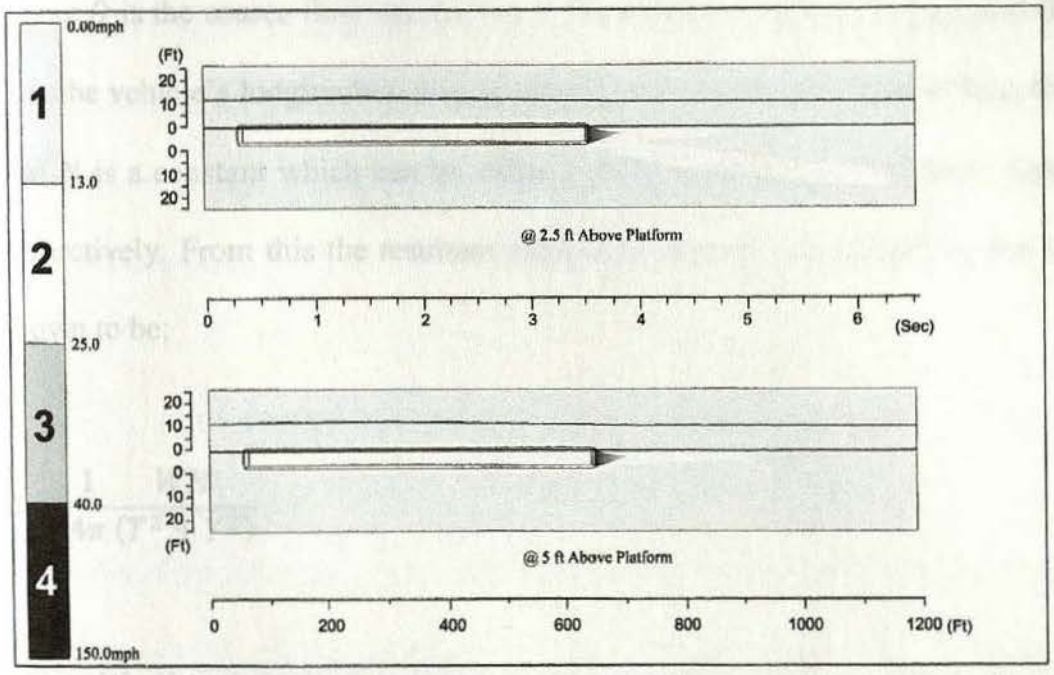

Figure 2.6b. High level platform.

Figure 2.6. CFD analysis results of the mean slipstream velocity of a passenger train travelling at 67m/s (150mph) for 0.762m (2.5') and 1.524 (5') above the platform (after Liao *et al.*, 1999).

A theoretical model of a vehicle's slipstream is developed in Sanz-Andrés *et al.* (2004a) which assumes that the generated flow is a potential flow, with the emphasis being on the effect due to the vehicle's nose. Sanz-Andrés *et al.* (2004a) state that the resultant velocity of the longitudinal (in the direction of the vehicle motion) and the lateral (in the direction away from the vehicle's side) slipstream velocity components induced by a moving source in a ground-fixed reference frame is given by:

$$u = \frac{Q}{2\pi N} \frac{1}{(x^2 + y^2)^{\frac{N}{2}}} \tag{2.1}$$

where Q is the source flow rate (m^3/s), x is the source position in a ground-fixed reference frame (i.e. the vehicle's longitudinal displacement), y is the lateral distance from the vehicle centreline, and N is a constant which can be either 1 or 2 to denote two- or three- dimensional flow fields respectively. From this the resultant slipstream velocity normalised by the vehicle speed can be shown to be:

$$U = \frac{1}{4\pi} \frac{WH}{(T^2 + Y^2)} \tag{2.2}$$

where W, H and Y are the vehicle width, vehicle height and lateral distance from the vehicle centreline, respectively, all normalised by the vehicle length; and T is the time normalised by vehicle speed and length. Equation (2.2) is derived in Appendix 1.

A theoretical model was developed by Baker and Sterling (2004) to reproduce the effects of high-speed train slipstreams on people standing on a station platform, and it is this model that forms the basis of the model developed in this thesis. However, in simulating train slipstreams, the model of Baker and Sterling (2004) has a number of deficiencies, including that it only simulates the slipstreams generated by the model-scale passenger train (Baker *et al.*, 2001). Consequently, it does not reproduce the velocity peak which was measured at the rear of a full-scale passenger train; as this peak results in the largest slipstream velocity of a passenger train, the theoretical model underestimates the maximum force acting on a person due to a slipstream. Also, a freightliner generates larger slipstream velocities than a passenger train and so has the potential to cause a more dangerous environment than a passenger train; however, the model does not simulate this worse case scenario. In order to create a tool which can better investigate the effects of a slipstream on a person the model needs be able to simulate the slipstream of a full-scale passenger train and a freightliner, and the theoretical model presented in this thesis addresses these deficiencies.

2.4 Pressure on people and objects.

A number of experiments have been undertaken to measure the pressure changes on a person and an object due to a slipstream. Model-scale experiments described in Gerhardt and Krüger (1998) measured the transient pressure changes due to the passing of a train on a plate representing a person at various distances from the train side, and the model-scale tests of Cali and Covert (2000) investigated the slipstream effects of a vehicle on an overhead sign. The full-scale experiments of Robertson *et al.* (2004) investigated the slipstream effects of a light goods vehicle

(LGV) on an overhead sign, and the full-scale tests of Quinn *et al.* (2001) measured the pressure changes on road signs due to the slipstreams of cars. All of these show that there is a positive static pressure peak as the vehicle approaches followed by a larger negative pressure (suction) peak due to flow separation as the leading edge of the vehicle passes. The model train described in Gerhardt and Krüger (1998) consisted only of a train head, therefore, the experiments only investigated the pressure changes around the nose and front of a train. However, Cali and Covert (2000) and Robertson *et al.* (2004) looked at the pressure along the whole length of the vehicle, and recorded small suctions along the length of the vehicle. Robertson *et al.* (2004) recorded a small suction due to flow separation after the rear of the vehicle had past; however, Cali and Covert (2000) actually recorded a small positive pressure peak beyond the rear of the vehicle, but this was due to the wake interfering with the effect of the flow separation. Cali and Covert (2000) use a dimensionless force coefficient based on sign area and vehicle speed, and the experiments show that vehicle shape has a significant effect on the magnitude of the force coefficient, with the upstream and nose peaks being lower with a streamlined vehicle than with a more bluff bodied vehicle. The measurements in Gerhardt and Krüger (1998) give a pressure gradient which is twice as large as that considered dangerous to people during storms (Melbourne, 1978), and infer an allowable pressure gradient from Melbourne (1978) which is calculated to occur at 2m from the tracks. Therefore, a safety zone within a lateral distance of 2m from the tracks is proposed.

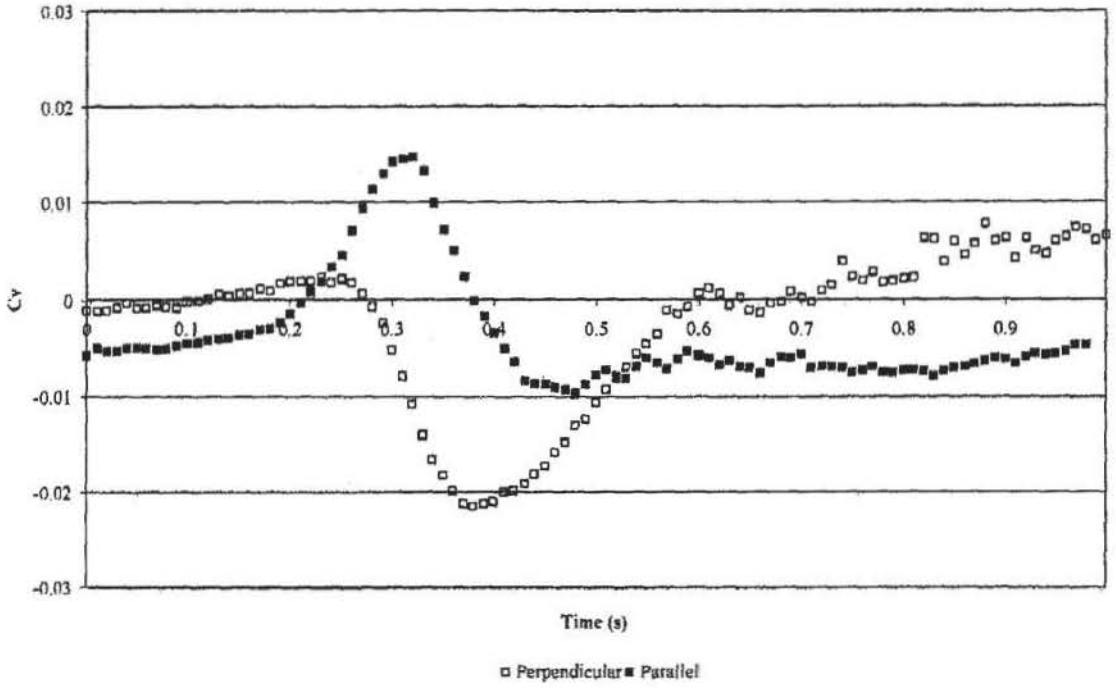

Figure 2.7. Ensemble average vehicle force coefficient for pedestrian barriers (□ perpendicular, ■ parallel) (after Quinn *et al.*, 2001).

Full-scale tests undertaken on road signs and pedestrian barriers (Quinn *et al.*, 2001) show that the effect of a passing car is due to a static pressure pulse rather than being a slipstream gust effect. The static pressure acting on signs and barriers positioned perpendicular to the direction of travel increases slightly and then reaches a larger negative peak, i.e. is pushed in the direction of travel then pulled in the opposite direction. Barriers placed parallel to the direction of travel show a different pattern in that they are first pushed away from the car to a greater extent than those positioned perpendicular, then pulled towards the car with an approximately equal force. Figure 2.7 shows the ensemble average vehicle force coefficient for pedestrian barriers, where the force coefficient is based on car speed and the area of the sign or barrier. The experimental results show that size, but not shape, of a sign or barrier has an influence on the force coefficient. The

force coefficients obtained by Quinn *et al.* (2001) for the perpendicular signs and barriers, and those obtained by Cali and Covert (2000) for the overhead signs, have similar values. Cali and Covert (2000) suggest that the decay in the force coefficient is inversely proportional to the fourth power of the distance between the vehicle and sign, however, Quinn *et al.* (2001) suggest a decrease inversely proportional to the square of this distance.

Sanz-Andrés *et al.* (2003) use a theoretical model of the pressure changes to predict those occurring on road signs and pedestrian barriers and compare the prediction with the experimental results of Quinn *et al.* (2001). The theoretical values of the elapsed time between the two pressure peaks occurring on the signs and barriers positioned perpendicular to the direction of travel, and the elapsed time between the time origin and the first peak of the signs and barriers parallel to the direction of travel are compared with those of the measured data. The theoretical force coefficients are also compared with those of the experiments. The model predicts the shape of the force coefficient time history, the elapsed time and order of magnitude of the force coefficients associated with the road signs. The theoretical model of the pedestrian barriers also correctly predicts the shape of the force coefficient time history and the elapsed time between the time origin and the force coefficient peak; however, the predicted force coefficients are significantly larger than those of the experimental data for both perpendicular and parallel barrier positions. The theoretical model of Sanz-Andrés *et al.* (2003) accurately predicts the force coefficient time history around the nose of the streamlined vehicle involved in the experiments of Cali and Covert (2000); however, it does not predict the pressure pulse measured after the rear of this vehicle. Sanz-Andrés *et al.* (2003) conclude that the theoretical model gives a qualitative representation of the forces acting on road signs and pedestrian barriers due to the pressure pulse at the nose of a

vehicle, and a quantitative representation when the vehicle is streamlined. Sanz-Andrés *et al.* (2004b) adapt the work of Sanz-Andrés *et al.* (2003) to more accurately reproduce the forces on a pedestrian barrier parallel to the direction of vehicular travel.

2.5 Gust effects.

The transient nature of the aerodynamic effects of a train results in a person experiencing a slipstream as a sudden gust; however, there has been little work undertaken to investigate the effect a sudden gust has on a person. A gusty wind can affect a person's stability more than a wind with little turbulence, as shown by the experiments described in Hunt *et al.* (1976), and by the observations of Melbourne and Jourbert (1971). The experiments described in Hunt *et al.* (1976) involved people walking into a wind tunnel with a mean wind speed of 4m/s or 8.5m/s, with or without turbulence. The turbulence intensity was 0.13 and 0.12 with the mean wind speed of 4m/s and 8.5m/s respectively. These experiments show that people are deflected more when walking into a turbulent wind, as well as finding it more difficult to retrace their steps in a turbulent wind. Melbourne and Jourbert (1971) also observed that people struggle against gusty winds in the built environment, and remark upon two girls falling in the street when a wind speed of 12m/s rose to a maximum gust of 23m/s. Murakami and Deguchi (1981) reproduced the effect of experiencing a sudden gust by having individuals walk out from behind a fence into the wind in a wind tunnel. The slats of the fence could be opened by various amounts, and the experiments showed that the largest deflections in the path of a person occurred when the slats were fully closed and, therefore, the change in wind speed experienced was the greatest.

2.6 Safe winds.

Durov (1967) defines a loss of balance of a person as occurring when the initial posture has to be altered so as to prevent falling; this change in posture could be the act of taking steps, moving the legs, etc. An unsafe wind speed is said to be one that causes a person to lose their balance. Temple and Johnson (2003) collated from various literature the wind speeds at (and above) which a person can be blown over. This shows that there is a lower allowable wind speed for elderly people than for younger people (Bottema, 1992), and a lower allowable wind speed for passengers on a station platform than for trackside workers. From observations of people in the wind, including those made by Melbourne and Joubert (1971), Hunt *et al.* (1976) conclude that a steady uniform wind of less than 20-30m/s is safe for walking. When determining the gusty wind that is safe for walking they estimate an equivalent steady wind speed using a formula based on the mean wind speed and the turbulence intensity, and conclude that an equivalent steady speed of less than 20m/s is safe for walking. With a turbulence intensity of 0.13, as occurred in the experiments of Hunt *et al.* (1976), the mean speed of the gusty wind would have to be less than 14m/s to ensure safety whilst walking. Hunt *et al.* (1976) also conclude that a non-uniform wind which varies by 70% over 2m should be less than 13-20m/s for safety. This work highlights that a sudden change in wind speed is more destabilising than a steady uniform wind.

Acceleration, as well as the magnitude, of the wind speed affects a person's stability (Baker *et al.*, 2001; Vuchic, 1981). Limiting accelerations of $0.61m/s^2$, $0.54m/s^2$ and $0.43m/s^2$ cause a person to be destabilised by falling forwards, backwards and sideways respectively (De Graaf and Van Weperen, 1997). These values show that a person can withstand greater slipstream

accelerations when standing with their back to the oncoming flow than when facing it. The limiting acceleration values also show that a person standing side on to the flow can withstand the least amount of acceleration. However, as the projected area of a person side-on to the flow is smaller than that of a person either facing the flow or with their back to the flow, the force acting on a side-on person is smaller. This compensates for the lower tolerance of acceleration when side-on, and so standing facing the flow is the least stable orientation, as is shown in the experiments described in Chapter 4.

Temple and Johnson (2003) identify sixteen incidents which occurred on a UK station platform due to the slipstreams of passing trains, including people nearly being swept off their feet by the slipstream of a freightliner. However, most of the incidents involved pushchairs affected by a freightliner's slipstream. For example, a braked pushchair positioned 3m from the platform edge was drawn towards and hit a freightliner travelling at 70mph (31m/s), the pushchair was then propelled along the platform and hit two people causing one to be injured. The incidents compiled by Temple and Johnson (2003) highlight the dangers associated with a train slipstream.

2.7 Stability of a person.

A person needs to control their balance whilst standing when experiencing spontaneous postural sway and when subjected to an applied force. This balance control may involve changing the position of the body's centre of gravity without altering the base of support, e.g. by bending their legs, or increasing the base of support by either stepping or reaching out to grasp a rail etc. (Hsiao and Robinovich, 1999; Maki *et al.*, 2003).

The experiments described in Laughton *et al.* (2003) show that postural sway is related to age, with elderly people swaying over greater distances than younger people. This larger sway is a factor in an elderly person's risk of falling. Laughton *et al.* (2003) recorded greater muscular activity in the elderly which is correlated to sway, but does not conclude whether the increased muscular activity contributes to the decline in stability or is activated to compensate for the instability. Mackey and Robinovich (2006) describe experiments in which individuals stood in an inclined position and contracted their ankle muscles in order to recover a vertical position. These experiments show that, compared to a younger person, an elderly person's reaction is slower and their ankle torque smaller. Also, the maximum angle of inclination that an elderly person can recover from is smaller. When a person was subjected to surface roll (lateral motion) and their support base was fixed, their response was dependent upon age (Allum *et al.*, 2002). The young people involved in the experiments counterbalanced the motion by large movements of their trunk in the opposite direction to that of the fall. The middle-aged participants reacted similarly but with a smaller movement, whereas the elderly participants had the smallest movement due to their greater trunk stiffness. This resulted in a young and middle-aged person's trunk orientation being in the opposite direction to and away from the direction of the downwards surface. An elderly person's trunk, however, was displaced in the direction of the fall, thereby increasing their risk of falling. The young and middle-aged people also made arm movements in the opposite direction to the downwards surface to counterbalance the roll, but elderly people took their arms towards the direction of the fall in order to cushion themselves when falling which further increased their risk of falling.

When a person's balance is recovered by either stepping or grasping an object, there is a greater moment produced to counteract the falling motion due to an increase in the distance between the person's centre of gravity and the point of rotation. Additionally, a person's base of support increases so allowing a greater distance for the centre of gravity to move without loss of stability. The balance recovery reactions of stepping and grasping provide a better means of stabilisation than just altering the position of the body's centre of gravity without altering the base of support (e.g. by bending the legs). The stepping and grasping reactions are initiated early and are a person's preferred response mechanisms to loss of balance (Maki *et al.*, 2003). When a person steps to prevent falling their step length increases with increasing perturbation and the time taken to complete the step decreases (Luchies *et al.*, 1994; Hsiao and Robinovich, 1999). The step length of an elderly person is smaller than that of a younger person, and they rely more on multi-step responses (Hsiao and Robinovich, 1999). An elderly person is also more likely to grasp at an object in order to recover their balance; however, as with stepping, this action is slower for an elderly person than for a younger person (Maki *et al.*, 2003).

2.8 Biomechanical model.

Previous work has been undertaken to develop a model of a person responding to a force. Mass-spring-damper models have been developed where the springs and dampers contribute stiffness and damping to the system. The stiffness is the resistance of the elastic components of a person's muscles to deflection and deformation (Wexler *et al.*, 1997). The damping is the viscous resistance of the muscles which reduces the amplitude of the system's oscillations (Martin *et al.*, 1994). Simple mass-spring-damper models consisting of an inverted pendulum with a mass-less

rod and a lumped mass representing the total mass of a person are used by, for example, Yu and Luo (2004). Mass-spring-damper models with more than one mass are also used for a variety of situations. Zong and Lam (2002), for instance, use a model with four masses to study the response of a seated person to ship motion due to an underwater explosion, whereas Nigg and Liu (1999) utilise a multi-mass model to investigate the muscle stiffness and damping of a runner. Matsumoto and Griffin (2003) develop a number of models with one or two masses representing a standing person subjected to vertical vibration in order to identify the most practical model. Whereas Matsumoto and Griffin (2003) only investigate the vertical stiffness and damping in the models, Kim *et al.* (2005) and Matsumoto and Griffin (2001) consider both rotational and vertical stiffness and damping in their models of a seated person. All of these models represent the full body of a person except for the one developed in Zong *et al.* (2002) which only models a person's body between the head and pelvis. As the various models generally differ significantly it is difficult to compare the values of the stiffness and damping used, but one model developed by Kim *et al.* (2005) and one model of Matsumoto and Griffin (2001) are sufficiently similar to allow comparison. There are differences in values of stiffness and damping between these two models; for instance, the vertical stiffness of the buttocks is stated to be 0.905kN/m and 153kN/m in Kim *et al.* (2005) and Matsumoto and Griffin (2001) respectively. Also, the vertical damping of the buttocks is 47Ns/m and 3150Ns/m in Kim *et al.* (2005) and Matsumoto and Griffin (2001) respectively. This illustrates that there is a wide range of values for the stiffness and damping used in the various mass-spring-damper models of a person.

A person's muscles are not able to react instantaneously when a person is subjected to an applied force, therefore, there is a short time delay from the start of the force and the inception of a

person's muscular response. Throughout this short duration a person's body is effectively a non-responsive object. Fukuchi (1961) (cited in Johnson *et al.*, 2004) takes a person's muscular response to start after 0.25s have elapsed since the application of the force, and that 63% of the response has developed after 0.375s. This concept that a person's response can be considered to be that of a simple solid object for the initial 0.375s is the basis of a model developed in Johnson *et al.* (2004) to reproduce the response of a person subjected to the slipstream of a high-speed train. In the model a rectangular cuboid represents a person which rotates about an axis when the force due to the slipstream results in a moment larger than the mass moment. The cuboid, and hence the person, becomes unstable when the centre of gravity moves beyond the axis of rotation. This model is further described in Section 5.2. A parametric analysis of the model, which uses a male standing facing into the slipstream as the base case, shows that a person's risk of losing their balance decreases with increasing body mass and decreasing height, and the most stable standing orientation is side-on to the oncoming flow. Clothing is also shown to affect a person's response, with an open coat resulting in an increased risk of a person losing their balance. Gender does not affect the response, however, a child is more susceptible to the effects of a slipstream than an adult.

The theoretical model developed by Baker and Sterling (2004) to reproduce the effects of a high-speed passenger train slipstream on a person at a station platform, and which forms the basis of the theoretical model developed in this thesis, models a person as a mass-spring-damper system. The model generates the same response for all people for a given weight, height, standing orientation and slipstream. However, an elderly person can be expected to have a different response to a train slipstream than a younger person but the model does not allow for this. Also,

the values of a person's stiffness and damping are taken from one particular mass-spring-damper system of Matsumoto and Griffin (2001), but there are other models to consider including those developed by other authors. Finally, most slipstream incidents involve pushchairs (Temple and Johnson, 2003), however, Baker and Sterling (2004) do not incorporate a pushchair's response into the theoretical model, but doing so would have allowed a more thorough investigation into the potential dangers of a train slipstream. The theoretical model presented in this thesis addresses these omissions.

2.9 Knowledge gap and aim of research.

The full-scale and model-scale experiments described in Johnson *et al.* (2004), Baker *et al.* (2001), and Temple and Dalley (2001) show that the slipstream velocity of a train increases rapidly at the train's nose, and that high velocities and turbulence levels can be associated with a slipstream. As a gusty wind can have a greater effect upon a person's stability than a steady wind it can be conjectured that a train slipstream will adversely affect the stability of a person standing by the side of a train. However, little work has been undertaken to simulate and quantify a person's response to a train slipstream, and the current research aims to address this deficiency.

Although Liao *et al.* (1999) develop a CFD model of a train's slipstream the turbulence, which is an important factor in the stability of a person, is not reproduced. Furthermore, the experiments of Gerhardt and Krüger (1998) only measured the pressure changes due to the slipstream occurring at a train's nose, however, high velocities and turbulence levels occur along the length of a train. The current research aims to develop a model to simulate the turbulent slipstream, and

hence the forces due to the slipstream, for the whole length of a train and into the wake. Johnson *et al.* (2004) develop a biomechanical model of a non-responsive object to simulate a person's displacement due to a force; however, the inception of a person's muscular response occurs soon after the nose of a high-speed train has past. Therefore, the complete simulation of a person's response to a train slipstream needs to incorporate the displacements occurring after the inception of the muscular response. The current research aims to reproduce the movement of a person before and after the inception of the muscular response. Although various models have been developed (for example, by Matsumoto and Griffin, 2003) which allow for the muscular response of a person, they are in relation to vertical vibration and do not investigate the response to a horizontal force such as that produced by a slipstream. The current research aims to address this and thereby simulate a person's response to the forces generated by a slipstream before and after the inception of the muscular response for the whole length of the slipstream.

CHAPTER 3.

MODELLING THE SLIPSTREAM OF A TRAIN.

3.1 Introduction.

Previous experiments have measured the slipstream velocities of a full-scale passenger train (Johnson *et al.*, 2004), a full-scale freightliner (Temple and Dalley, 2001), and a model-scale passenger train (Baker *et al.*, 2001), as described in Section 2.2.1. These measurements are used in the development of the train slipstream model presented in this thesis in that the simulated slipstreams of the model are made to reproduce the measured slipstream velocity profiles as closely as possible. The technique of ensemble averaging is used in order to reduce the run-to-run variability of the measured and simulated slipstream velocity time histories, and hence facilitate comparison and modelling. The number of runs of an ensemble average for each train type depends upon the number of runs from the measured data that could be used in the analysis. The ensemble average of the simulated slipstream comprises the same number of runs of that of the measured data in order to facilitate comparison. Table 2.1 gives details of the trains, distances from the train side that the measurements were taken at, and the number of runs occurring in the ensemble averages.

3.2 Investigating the velocity peak at the rear of the full-scale passenger train.

The slipstream of a full-scale passenger train has a velocity peak immediately after the rear of the train, and in order to be able to model this velocity increase as accurately as possible a good understanding of what is happening within this region is required. Hence, this section

closely inspects the slipstream velocity around the rear of a full-scale passenger train. Figure 2.1 of Section 2.2.1.1 gives the ensemble averaged normalised velocity profile at 0.75m from the side of a full-scale passenger train travelling along an open track at 69m/s. As with all subsequent slipstream velocity time histories, time is normalised by the train speed and the length of the train, so that the nose and the rear of the train pass at $T = 0$ and $T = 1$ respectively. Figure 2.1 gives the resultant velocity, the u component of the velocity (the longitudinal velocity in the same direction as the train's motion) and the v component of the velocity (the lateral velocity in the direction away from the train side). Figure 2.1 shows that the velocity peak at the rear of the train is due to an increase in the u component of the slipstream velocity.

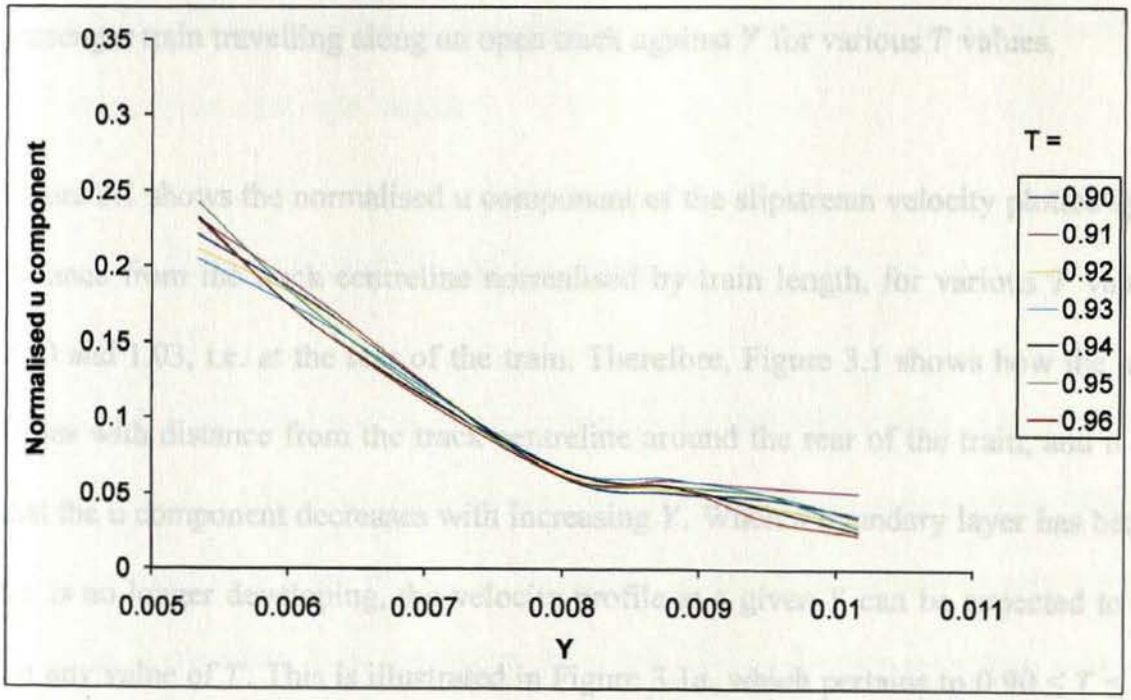

Figure 3.1a. The normalised u component against Y values for $0.90 \leq T \leq 0.96$.

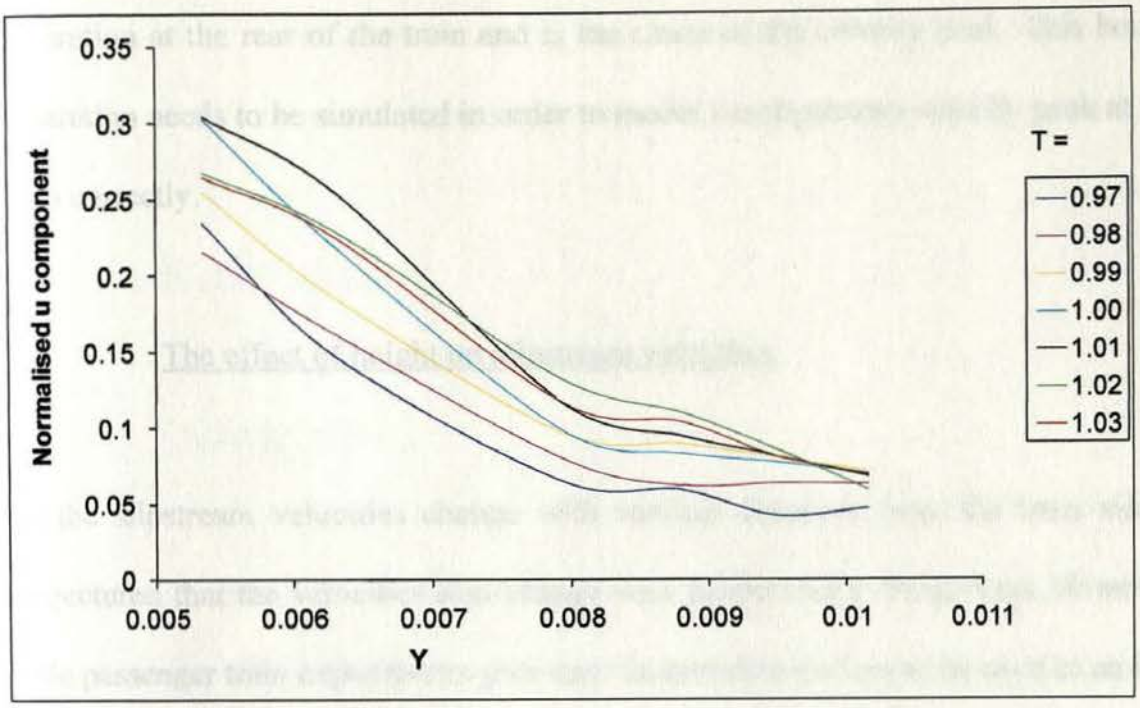

Figure 3.1b. The normalised u component against Y values for $0.97 \leq T \leq 1.03$.

Figure 3.1. The normalised u component of the slipstream velocity of a full-scale passenger train travelling along an open track against Y for various T values.

Figure 3.1 shows the normalised u component of the slipstream velocity plotted against Y, the distance from the track centreline normalised by train length, for various T values between 0.90 and 1.03, i.e. at the rear of the train. Therefore, Figure 3.1 shows how the u component varies with distance from the track centreline around the rear of the train, and it can be seen that the u component decreases with increasing Y. When a boundary layer has become stable, i.e. is no longer developing, the velocity profile at a given Y can be expected to be identical for any value of T. This is illustrated in Figure 3.1a, which pertains to $0.90 \leq T \leq 0.96$, where the velocity profiles for each value of T are similar at each Y value. However, Figure 3.1b, which pertains to $0.97 \leq T \leq 1.03$, illustrates that the velocity increases with T at a given Y. This starts at $T = 0.97$, which is just before the rear of the train. This stability of the velocity profile followed by an increase in velocity for a given Y value is indicative of boundary layer

separation at the rear of the train and is the cause of the velocity peak. This boundary layer separation needs to be simulated in order to model the slipstream velocity peak at the rear of a train correctly.

3.3 The effect of height on slipstream velocities.

As the slipstream velocities change with varying distances from the train side, it can be conjectured that the velocities also change with height above the ground. However, the full-scale passenger train experiments give only limited data that could be used in an investigation of the effect of height, and the full-scale freightliner and model-scale passenger train data only relate to one height. Therefore, an investigation of how slipstream velocities change with height cannot be satisfactorily undertaken, and consequently the model assumes that the velocities do not alter with height.

3.4 Theoretical modelling of the slipstream.

Section 2.2.1 identifies specific flow regions associated with a train slipstream, and the fluid dynamics theory related to the upstream, boundary layer and wake regions form the basis of the theoretical slipstream model. A theoretical vortex is developed to simulate the velocity peak due to boundary layer separation at the rear of the full-scale passenger train. The wake is delayed until $T = 1.5$ and a transitional region exists between the region around the rear of the train and the wake. Each of the flow regions is considered separately and then combined to form the entire continuous flow field around a train. This process results in a mean velocity time history, and the turbulence-induced fluctuations are incorporated into the model by the

use of a modified autoregressive model. A complete derivation of the equations used in the slipstream model is given in Appendix 1.

3.4.1 Mean velocities.

3.4.1.1 Upstream region.

The slipstream velocities associated with the region immediately upstream of the train ($T \leq 0$) are essentially inviscid and are modelled using potential flow theory as adapted by Sanz-Andrés *et al.* (2004a), which is described in Section 2.3 and given in equation (2.1). The parameter N of equation (2.1) takes the value of two in the model in order to reproduce the three-dimensional flow of a slipstream. The resultant of the longitudinal (in the direction of the vehicle's motion) and lateral (in the direction away from the vehicle side) slipstream velocity components normalised by train speed can be shown to be:

$$U = \frac{1}{4\pi} \frac{WH}{(T^2 + Y^2)} \tag{3.1}$$

where W, H and Y are the train width, train height and lateral distance from the train centreline, respectively, all normalised by the train length. T is the normalised time. The maximum value of U occurs when the value of $T^2 + Y^2$ is at a minimum, which is when T^2 is at a minimum for a given value of Y^2, i.e. when $T = 0$. Hence there will be a velocity peak generated at $T = 0$, so reproducing the measured slipstream velocity profiles. Equation (3.1) is derived in Appendix 1.

Sanz-Andrés *et al.* (2004a) use the potential flow theory to try to predict the pressure due to a slipstream along the whole length of the vehicle and beyond, although they recognise that the main contribution of the potential flow theory lies around the vehicle nose. Therefore, the model uses the potential flow theory for the entire length of the generated slipstream, although its contribution to the normalised velocity is negligible beyond the train's nose.

3.4.1.2 Boundary layer region.

The flow along the main body of the vehicle ($0 \leq T \leq 1$) is assumed to approximate the flow along a flat plate. Hence, the velocity profile of this region is, in part, obtained from the boundary layer theory of a flat plate (Duncan *et al.*, 1970). The normalised slipstream velocity can then be given as:

$$U = 1 - T^{\frac{(n+1)}{n(n+3)}}\left(Y - \frac{W}{2}\right)^{\frac{1}{n}} A^{-\frac{1}{n}} Re^{\frac{2}{n(n+3)}} \tag{3.2}$$

where T, Y and W are as for equation (3.1) and Re is the Reynolds Number defined as $\frac{VL}{\nu}$ with V as the train speed, L as the length of the train, and ν as the kinematic viscosity of air which, for the current work, is taken as $1.46\text{x}10^{-5}\text{m}^2/\text{s}$. A is defined as $\left[\frac{(n+2)(n+3)}{n} C_1^{-\frac{2n}{(n+1)}}\right]^{\frac{(n+1)}{(n+3)}}$, where n and C_1 are constants dependent upon the train type and distance from the train side, the values of which are given in Section 3.6. Note that $Y - \frac{W}{2}$ is the normalised lateral distance from the train side. Equation (3.2) is derived in Appendix 1.

The potential flow theory is used in conjunction with the boundary layer theory for the region along the main body of the train. Equation (3.3) is a combination of equations (3.1) and (3.2), and gives the complete normalised slipstream velocity equation used in the model for the region where $0 \leq T \leq 1$.

$$U = 1 - T^{-\frac{(n+1)}{n(n+3)}}\left(Y - \frac{W}{2}\right)^{\frac{1}{n}} A^{-\frac{1}{n}} Re^{\frac{2}{n(n+3)}} + \frac{1}{4\pi}\frac{WH}{(T^2 + Y^2)} \tag{3.3}$$

It must be noted that the potential flow theory (equation (3.1)) results in a velocity that is at a varying angle to the side of the train, whereas the boundary layer theory (equation (3.2)) results in a flow that occurs in the same direction as the motion of the train. Therefore, the velocities due to the two theories act in different directions. However, the longitudinal component of the velocity dominates the flow along the main body of the train, as shown by Figure 2.1, hence the boundary layer flow dominates and the contribution of the potential flow theory is negligible. As the motivation behind the creation of the slipstream model is its application to person and pushchair stability (which Chapters 5 and 8 show is related to the square of the resultant velocity), it is felt that the engineering approximation of the combination of the two equations is justified in this context.

The constants n and C_1 influence both the first and final slipstream velocity of the boundary layer region and consequently the shape of the mean boundary layer velocity profile. An increase in n results in a larger first boundary layer velocity and a smaller final boundary layer velocity. An increase in C_1 reduces both the first and final velocities. Therefore, the

values of n and C_1 are chosen in combination to generate the correct magnitude and shape of the boundary layer velocity profile.

3.4.1.3 Velocity peak at the rear of the train.

The model simulates the boundary layer separation occurring at the rear of a full-scale passenger train by generating a vertical cylindrical vortex immediately behind the train in the wake. The vortex has a diameter equal to half the train's width, and is positioned so as to occupy half the width of the train, as illustrated in Figure 3.2. The effect of the vortex is modelled to last for the diameter of the vortex, as indicated in Figure 3.2 by the 'zone of vortex influence'.

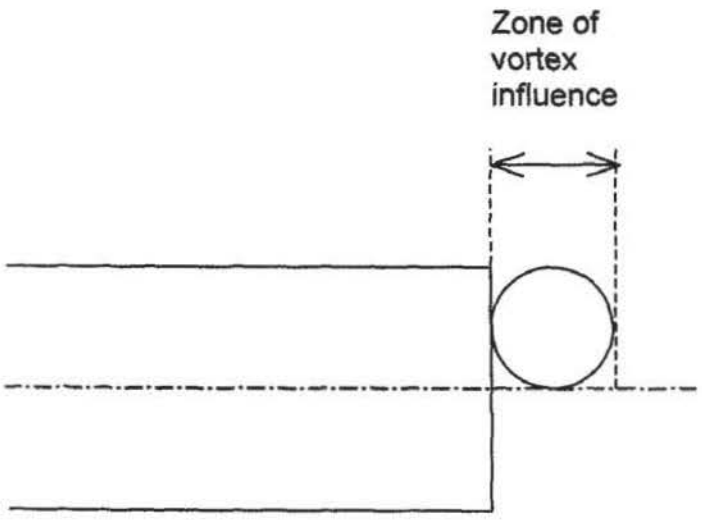

Figure 3.2. Plan view of the rear of the train with an idealised embedded vortex.

From a maximum at the circumference of the vortex, the normalised velocity decays exponentially outside the vortex, so that:

$$U = U_{max} e^{-B\left(\sqrt{(X^2+Y_V^2)}-R\right)} \tag{3.4}$$

where U_{max} is the normalised slipstream velocity at the circumference of the vortex, B is a decay constant; and R, X, and Y_V are the vortex radius, the longitudinal distance from the centre of the vortex, and the lateral distance from the centre of the vortex respectively, all normalised by the train length. X has a negative value if the point lies between the rear of the train and the vortex centre. Figure 3.3 gives the plan view of the vortex. Due to the size and the position of the vortex, everyone standing by the side of the train is outside of the vortex and so subjected to the decaying velocity. The term $\sqrt{(X^2 + Y_V^2)} - R$ in equation (3.4) allows the model to generate a normalised slipstream velocity depending upon the distance beyond the vortex's circumference at which a person is standing. As the velocity peak at the rear of a train was only recorded during the full-scale passenger train tests the vortex is not incorporated into the simulated slipstream of a freightliner or a model-scale passenger train.

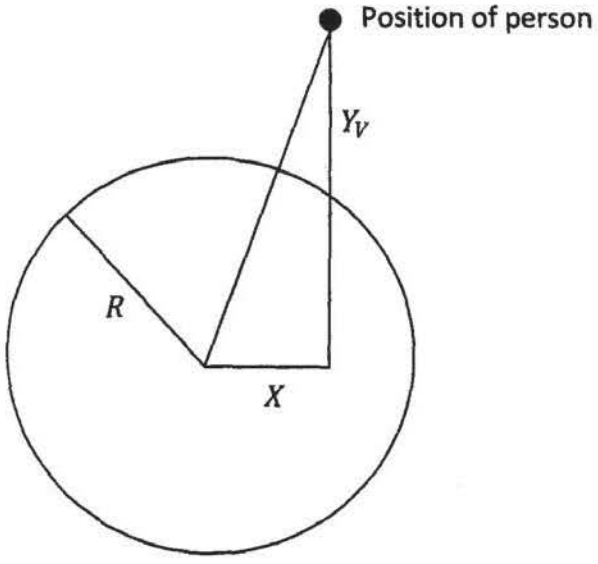

Figure 3.3. Plan view of the vortex.

The vortex model reproduces the mean characteristics of the slipstream velocity at the rear of a passenger train, with the velocity increasing at $T = 1$ which reaches a peak a little after $T = 1$ and then decays after the rear of the train has past. During the development of the theoretical model a Rankine vortex with linear velocity decay outside the circumference was also tested, but was rejected as no combination of the decay constants was found that generated the correct maximum velocity magnitude for all lateral distances from the train side.

3.4.1.4 Transition.

The final simulated velocities of the full-scale passenger train's vortex, the freightliner's boundary layer, and the model-scale passenger train's boundary layer are higher than the first simulated wake velocity. Therefore, the onset of the wake is delayed until $T = 1.5$, and a transitional region is assumed to exist before the wake region. As no theory exists to determine the velocities in this region, a quadratic equation is devised to connect the wake to the vortex or boundary layer in this transitional region:

$$U = U(T_W) + \frac{\big(U(T_E) - U(T_W)\big)(T - T_W)^2}{(T_W - T_E)^2} \tag{3.5}$$

where T_W is the normalised time at the start of the wake region, i.e. $T_W = 1.5$, and T_E is the normalised time at the end of the vortex or the boundary layer region. $T_E = 1$ for the full-scale freight and model-scale passenger trains as this relates to the end of the boundary layer region, and T_E for the full-scale passenger train relates to the end of the vortex which is dependent upon the diameter of the vortex which in turn is dependent upon the train width.

3.4.1.5 Wake region.

From the expression given by Baker (2001) the decay in the normalised resultant of the longitudinal and lateral velocity components in ground vehicle wakes, U, can be shown to be:

$$U = \alpha \frac{H}{2(T - T_W)} \left(1 + \frac{Y^2}{4(T - T_W)^2}\right)^{0.5} exp\left(-\beta \frac{Y^2 + \frac{H^2}{4}}{H^{1.5}(T - T_W)^{0.5}}\right) \tag{3.6}$$

where H, T, and Y are as for equation (3.1) and T_W as for equation (3.5). The parameters α and β are decay constants and take the values of 2.5 and 1 respectively based on work undertaken in Baker (2001). Note that as T increases U decreases. Equation (3.6) is derived in Appendix 1. Incorporating potential flow theory, the full equation for the normalised velocity in the wake becomes:

$$U' = \alpha \frac{H}{2(T - T_W)} \left(1 + \frac{Y^2}{4(T - T_W)^2}\right)^{0.5} exp\left(-\beta \frac{Y^2 + \frac{H^2}{4}}{H^{1.5}(T - T_W)^{0.5}}\right) + \frac{1}{4\pi} \frac{WH}{(T^2 + Y^2)} \tag{3.7}$$

3.4.1.6 Combining the theories of the flow regions.

Combining equations (3.1), (3.3), (3.5) and (3.7) gives the mean flow field around the full-scale freightliner and the model-scale passenger train. With the addition of equation (3.4) to generate a vortex at the rear of the train the mean flow of the full-scale passenger train is also simulated. Figure 3.4 shows the simulated mean normalised flow of the slipstream at 0.57m from the side of a full-scale passenger train travelling at 51m/s past a station platform. The

nose and the rear of the vehicle pass at $T = 0$ and $T = 1$, respectively. Figure 3.4 illustrates that the slipstream model generates a continuous flow, and that the flow regions identified from the experimental data are reproduced, i.e. velocities increase upstream of the train reaching a peak at the train nose, a boundary layer develops with increasing velocities along the train side, a peak occurs at the rear of the train, and the velocities decay gradually in the wake. Although the general mean profile of the flow is reproduced, the turbulence-induced velocity fluctuations are absent.

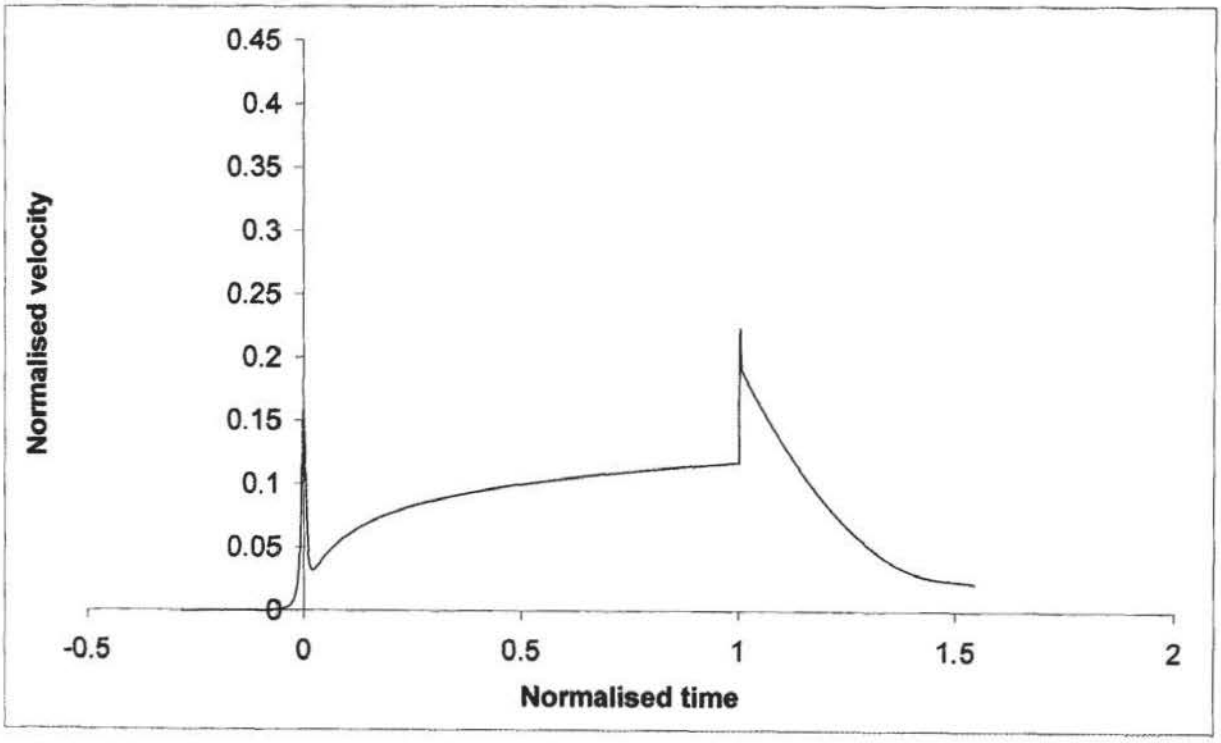

Figure 3.4. Simulated mean normalised velocity time history of the slipstream at 0.57m from the side of a full-scale passenger train travelling at 51m/s past a station platform.

3.4.2 Reproducing turbulence.

A slipstream with a high level of turbulence will have larger velocities and larger changes in velocity than a slipstream with the same mean flow but a low level of turbulence. Thus, a

person subjected to a high level of turbulence will be exposed to larger applied forces and greater gustiness. This will increase their risk of losing their balance; therefore, it is important that turbulence is incorporated into the slipstream model to enable a person's response to be reproduced accurately.

3.4.2.1 AR modelling.

An adapted autoregressive (AR) model is used to incorporate the turbulence-induced velocity fluctuations into the slipstream model. In general, an AR model is a mathematical model of the autocorrelation in a time series, which is the correlation of the values of a time series with previous values of the same series. The AR model expresses a value of a time series as a finite linear function of its previous values along with one white noise term, i.e.:

$$X_t = \phi_1 X_{t-1} + \cdots + \phi_p X_{t-p} + a_t \tag{3.8}$$

where X_t is the current value of a time series, p is the order of the AR model, ϕ is an AR coefficient, and a_t is the white noise term (see Box and Jenkins, 1970). An AR model is used to forecast a stationary time series, i.e. a stochastic time series with a probability distribution that is the same at all the times so that the mean and variance do not change with time. However, the turbulence-induced velocity fluctuations within a slipstream vary with time, for example the boundary layer region has greater levels of turbulence than any other region, and the turbulence in the wake decays with time. In order to reproduce the turbulence-induced velocity fluctuations an AR model of order two is modified as follows:

$$\widetilde{U}_T = U_T + \phi_1\left(\widetilde{U}_{T-1} - U_{T-1}\right) + \phi_2\left(\widetilde{U}_{T-2} - U_{T-2}\right) + \phi_3 a_t \tag{3.9}$$

where $\widetilde{U}$ is the fluctuating normalised velocity, U is the normalised mean velocity, and a_t and ϕ are as for equation (3.8). Therefore, the AR model is based on previous fluctuating normalised velocities minus previous normalised mean velocities. The values of ϕ_1, ϕ_2 and ϕ_3 depend upon the slipstream region, and ϕ_3 is dependent upon the lateral distance from the train side. The white noise term in an AR model is random in time, normally distributed and with a mean value of zero. In the AR model used by the slipstream model the standard deviation of the white noise term is of the value one. The AR coefficients of ϕ_1 and ϕ_2 affect the slipstream's larger scale turbulence, and as ϕ_3 is associated with the white noise term it affects the magnitude of the smaller scale turbulence. In order to correctly model the turbulence-induced velocity fluctuations the order of the model (in this case two) needed to be identified and the AR coefficients estimated. Box and Jenkins (1970) describe a method using plots of the autocorrelation functions and partial autocorrelation functions to identify the order of the AR model. However, as the AR model is modified this method has not been adopted, instead the order and values of the AR coefficients are obtained by a process of trial and improvement, and by using the technique of wavelet analysis to examine the frequency domain to check that the correct energy distribution has been produced. The technique of wavelet analysis is appropriate as the slipstream model needs not only to have the correct velocity time history but also a realistic energy distribution in the frequency domain, i.e. realistic turbulence.

The simulated mean velocity at 0.57m from the side of a full-scale passenger train travelling at 51m/s past a station platform is given in Figure 3.4, and Figure 3.5 shows how

incorporating the AR model into the slipstream model results in the generation of the turbulence-induced velocity fluctuations of a slipstream.

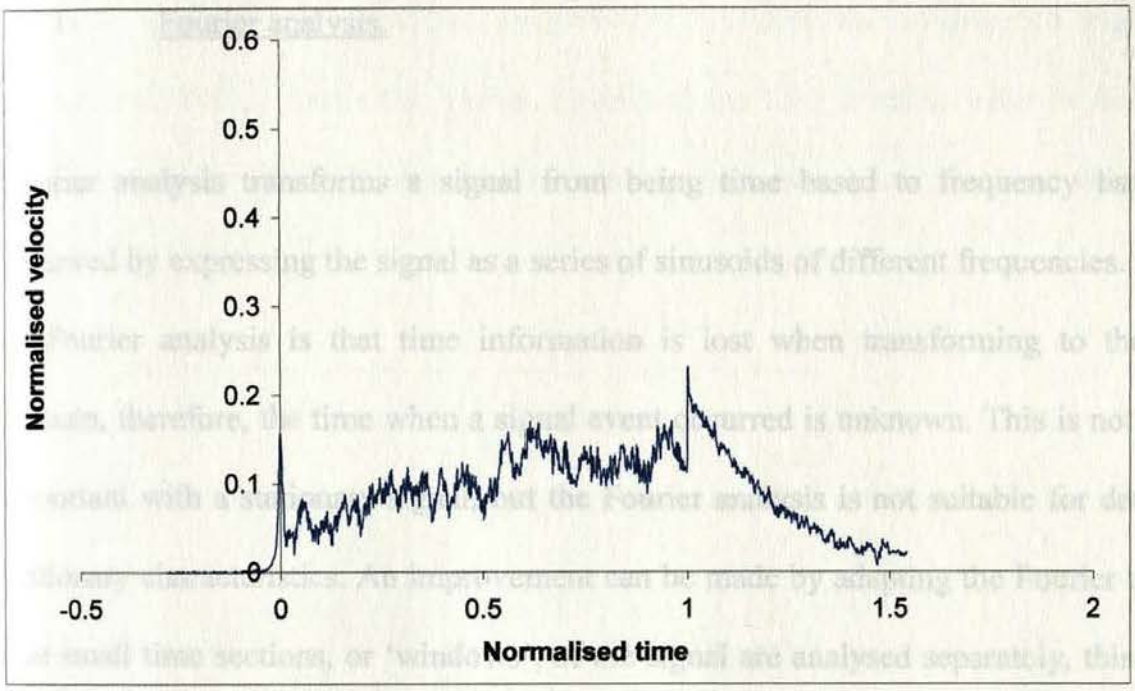

Figure 3.5. Simulated normalised ensemble average velocity time history with turbulence of the slipstream at 0.57m from the side of a full-scale passenger train travelling at 51m/s past a station platform.

3.5 Investigating the frequency domain of a train slipstream velocity fluctuation.

The frequency domain of a train slipstream needs to be investigated in order to determine if the turbulence-induced velocity fluctuations of the slipstream are simulated correctly by the AR model. The mathematical techniques of Fourier analysis and wavelet analysis are described in Sections 3.5.1 and 3.5.2 respectively. Wavelet analysis has an advantage over Fourier transforms in that it is suitable for investigating non-stationary signals, such as that of

a train slipstream; therefore, this method is used to investigate the frequency domain of a train slipstream in the current research.

3.5.1 Fourier analysis.

Fourier analysis transforms a signal from being time based to frequency based. This is achieved by expressing the signal as a series of sinusoids of different frequencies. A drawback of Fourier analysis is that time information is lost when transforming to the frequency domain, therefore, the time when a signal event occurred is unknown. This is not particularly important with a stationary signal, but the Fourier analysis is not suitable for detecting non-stationary characteristics. An improvement can be made by adapting the Fourier transform so that small time sections, or 'windows', of the signal are analysed separately, this gives some information on when a signal event occurs. However, the windowed Fourier analysis can determine the frequencies inaccurately as the size of the window is the same throughout the analysis. For instance, if the window is too large then high frequencies of the signal can be mistaken for lower frequencies. The accuracy would be improved by a method that utilises a varying window size, so that a large and small window could be used when information on low-frequencies and high-frequencies are required respectively. Such a method is wavelet analysis which breaks down a signal into a time and frequency space simultaneously.

3.5.2 Wavelet analysis.

A wavelet is a mathematical function that resembles a small waveform and is of finite length and zero mean amplitude. In a wavelet analysis, the wavelet's scale is varied by changing its

width, and for each scale the wavelet is shifted (translated) along the signal, so that a number of translations occur for each scale. This results in a relationship between amplitude, scale and time of the signal. The wavelet function used in the current research uses a Morlet wavelet, which is a sine curve modified by a Gaussian curve, and shown in Figure 3.6. Figure 3.6, after Wikipedia (2007a), shows the Morlet wavelet in the time domain, with the horizontal axis corresponding to time and the vertical axis to amplitude normalised by the greatest amplitude.

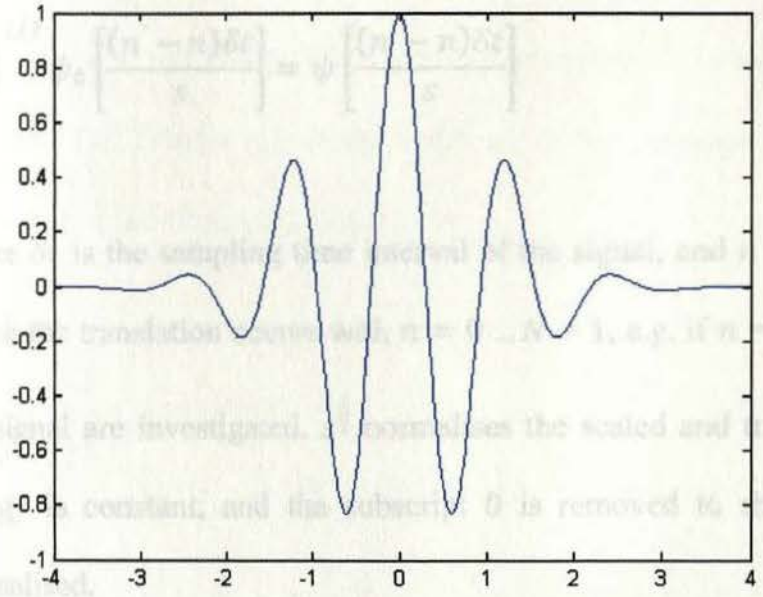

Figure 3.6. Morlet Wavelet (after Wikipedia, 2007a).

As it is the wavelet power spectrum of the slipstreams that is used to compare the simulated and measured train slipstreams then the particular wavelet function is not critical (Torrence and Compo, 1998). Therefore, a Morlet wavelet is chosen as it is commonly used and relatively simple. The equation of the Morlet wavelet is given by:

$$\psi_0(\eta) = \pi^{-\frac{1}{4}} e^{i\omega_0 \eta} e^{-\frac{\eta^2}{2}} \tag{3.10}$$

where $\psi_0(\eta)$ is the wavelet function, $\eta = \frac{t}{s}$ a non-dimensional time parameter with t and s as the time and wavelet scale respectively, i is the imaginary unit ($\sqrt{-1}$), and ω_0 is the non-dimensional frequency. Equation (3.10) gives the mother wavelet, which is then scaled, translated and normalised:

$$\left(\frac{\delta t}{s}\right)^{1/2} \psi_0 \left[\frac{(n' - n)\delta t}{s}\right] = \psi \left[\frac{(n' - n)\delta t}{s}\right] \tag{3.11}$$

where δt is the sampling time interval of the signal, and n and n' are the time indices along which the translation occurs with $n = 0 \ldots N - 1$, e.g. if $n = 0$ then events at the beginning of the signal are investigated. $s^{\frac{1}{2}}$ normalises the scaled and translated wavelet so that the total energy is constant, and the subscript 0 is removed to show that the wavelet function is normalised.

A continuous wavelet transform of a signal is:

$$W_n(s) = \sum_{n'=0}^{N-1} x_{n'} \psi * \left[\frac{(n' - n)\delta t}{s}\right] \tag{3.12}$$

where x_n is the signal, N is the number of data points in the time series, and the asterix ($*$) denotes the complex conjugate, i.e. the negation of the i term to $-i$. The wavelet transform can be computed in the time domain directly from equation (3.12); however, it is simpler and

faster to undertake the wavelet transform in Fourier space using the Fast Fourier Transform. The Fourier transform is taken of equation (3.12) and then the inverse Fourier transform is taken, thus the wavelet transform is:

$$W_n(s) = FFT^{-1}\left[\sum_{k=0}^{N-1} \hat{x}_k \hat{\psi} * (s\omega_k) e^{i\omega_k n \delta t}\right] \tag{3.13}$$

where FFT^{-1} indicates that the inverse Fast Fourier Transform is taken of the product within the brackets, $k = 0 \ldots N-1$ is the frequency index, $\hat{x}_k$ is the discrete Fourier transform, the ^ indicates the Fourier transform, and ω_k is the angular frequency. The discrete Fourier transform of the signal, $\hat{x}_k$, is given by:

$$\hat{x}_k = \frac{1}{N}\sum_{n=0}^{N-1} x_n e^{-2\pi i k n/N} \tag{3.14}$$

At each scale, s, the wavelet function is normalised to have unit energy, so that:

$$\left(\frac{2\pi s}{\delta t}\right)^{1/2} \hat{\psi}_0(s\omega_k) = \hat{\psi}(s\omega_k) \tag{3.15}$$

With the Fourier transform of the Morlet wavelet function being:

$$\hat{\psi}_0(s\omega) = \pi^{1/4} H(\omega) e^{-(s\omega-\omega_0)^2/2} \tag{3.16}$$

where $H(\omega)$ is the Heaviside step function. $H(\omega) = 1$ if $\omega > 0$, $H(\omega) = 0$ otherwise. Each of the unscaled $\hat{\psi}_0$ are normalised to have unit energy:

$$\int_{-\infty}^{+\infty} |\hat{\psi}_0(\omega')|^2 \, d\omega' = 1 \tag{3.17}$$

and the angular frequency is:

$$\omega_k = \begin{cases} \dfrac{2\pi k}{N\delta t}, & k \leq \dfrac{N}{2} \\ -\dfrac{2\pi k}{N\delta t}, & k > \dfrac{N}{2} \end{cases} \tag{3.18}$$

The wavelet power spectrum is defined as the square of the absolute value of the amplitude of the wavelet transform, i.e. $|W_n(s)|^2$. A plot of the wavelet power spectrum in a scalogram gives the relationship between power (energy per unit time), wavelet scale and time, see Section 3.5.2.2.

3.5.2.1 Values of the wavelet function parameters.

In order to calculate the wavelet power spectrum of both the simulated and measured train slipstreams the correct values of the parameters involved in the wavelet analysis need to be determined. The value of ω_0 is 6 to ensure admissibility of a Morlet wavelet (Farge, 1992). The relationship between the equivalent Fourier period, λ, and the wavelet scale, is:

$$\lambda = \frac{4\pi s}{\omega_0 + \sqrt{2 + \omega_0{}^2}} \tag{3.19}$$

with $\omega_0 = 6$, equation (3.19) becomes $\lambda = 1.03s$. Therefore, the Morlet wavelet scale is approximately equal to the Fourier period. In order to satisfactorily sample all the frequencies within the slipstream velocity time series the smallest wavelet scale, s_0, takes a value so that λ is approximately $2\delta t$. As λ and s are approximately equal, the value of s_0 is such that:

$$s_0 = 2\delta t \tag{3.20}$$

The angular frequency, ω, relates to the frequency, f, by the relationship $\omega = 2\pi f$. The parameter δt is normalised in the wavelet analysis undertaken on the train slipstreams so that δT is actually used, thereby corresponding to the normalised time used to present the slipstream data.

3.5.2.2 Wavelet power spectra.

The wavelet analysis described in Section 3.5.2 gives the relationship between the wavelet power spectra, wavelet scale and time which can be represented in a contour plot referred to as a scalogram. Figure 3.7 gives an example of such a scalogram and was produced by using a program on the website of the University of Colorado (Torrence and Compo, n.d.). This figure is for a single measured slipstream at 0.57m from the side of a full-scale passenger train travelling past a station platform at 51m/s. Figure 3.7 shows the normalised time, T, the wavelet scale (which is dimensionless as it is based on normalised time), and the power (which is also dimensionless as it is based on normalised velocity). In Figure 3.7 the highest

powers are associated with the largest scales, i.e. the lowest frequencies, and not in the high frequency turbulence. However, there is an increase in the energy in the smaller scales for $0 \leq T \leq 1$, therefore, the scalogram shows that there are greater turbulence levels in the slipstream along the main body of the train, i.e. in the boundary layer. This agrees with the normalised slipstream velocity time history of Figure 2.1.

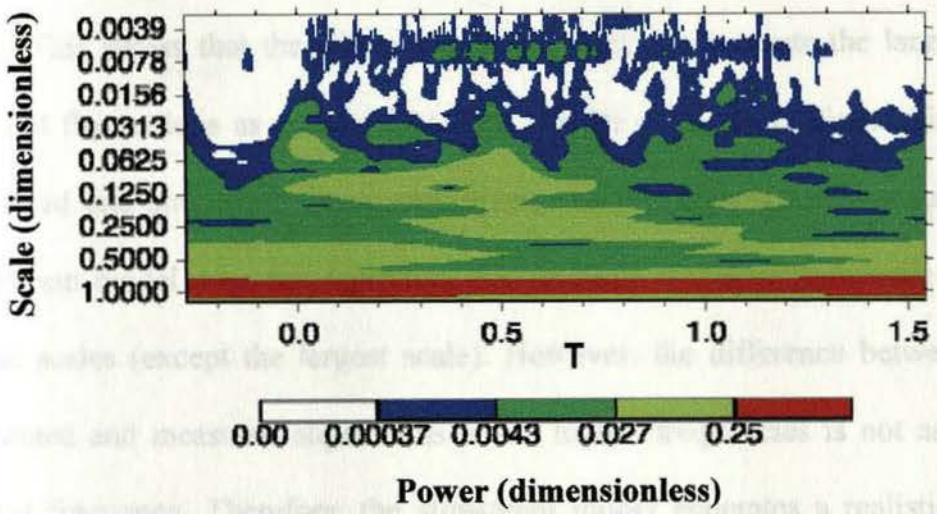

Figure 3.7. Wavelet scalogram of the measured slipstream at 0.57m from the side of a full-scale passenger train travelling at 51m/s past a station platform.

Further investigation is carried out by effectively taking a vertical slice from a scalogram at any particular time so giving the relationship between the dimensionless power and the dimensionless wavelet scale for that time. Using equation (3.19) the equivalent Fourier period, and hence frequency, can be calculated for each of the wavelet scales. The relationship between power and frequency can be seen in a power spectra plot, the curve of which is analogous to spectra obtained from Fourier transform techniques, and an example of such a plot is given in Figure 3.8. The two curves of Figure 3.8 illustrate the ensemble average of the

data from eleven scalograms at $T = 1$ for simulated and measured train slipstream data. The slipstreams occur at 0.57m from the side of a passenger train travelling at 51m/s past a station platform. The horizontal axis of Figure 3.8 is the frequency (which is dimensionless as it is based on normalised time), and the vertical axis is the dimensionless power, both axes have a logarithmic scale. Figure 3.8 illustrates that for this particular train type, train position, train speed, distance from the train side, and T value, the measured and simulated slipstream power is similar for each frequency. The exception to this is at the lowest frequency, i.e. the largest scale. This shows that the slipstream model does not generate the largest scale turbulence-induced fluctuations as accurately as the smaller scale fluctuations. Also, the power of the measured and simulated slipstreams diverge at the highest frequencies, indicating that the slipstream model does not reproduce the smallest scales of turbulence as accurately as the larger scales (except the largest scale). However, the difference between the power of the simulated and measured slipstreams at the higher frequencies is not as great as that at the lowest frequency. Therefore, the slipstream model generates a realistic flow except at the largest scale for this particular train setup and value of T.

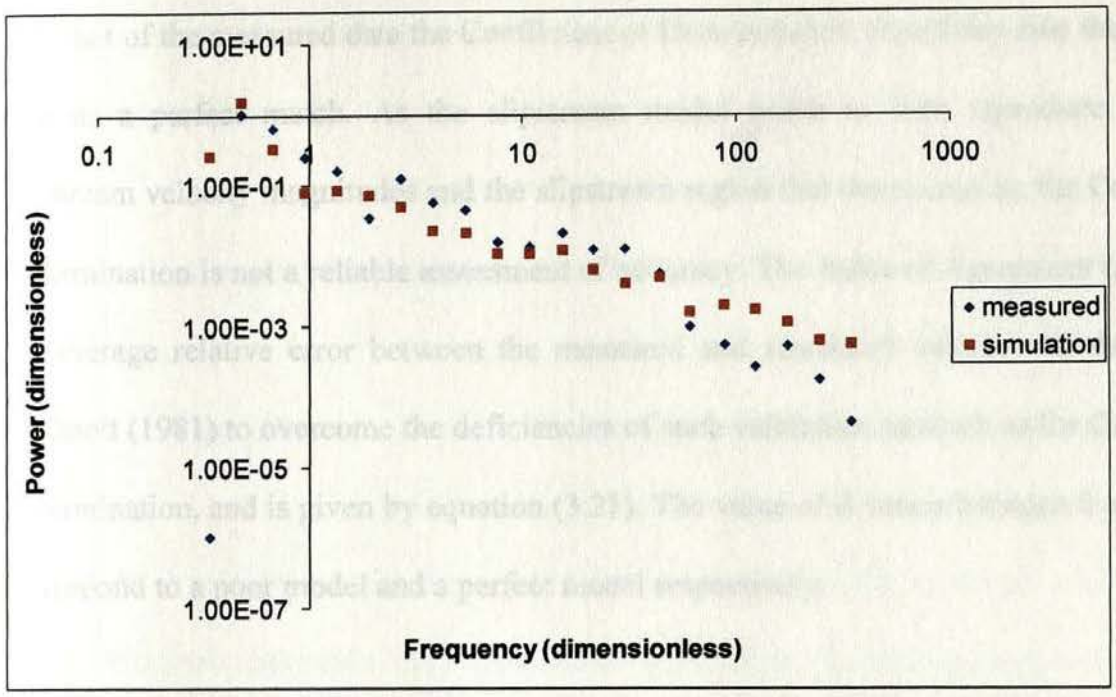

Figure 3.8. Wavelet spectra plots of the measured and simulated slipstreams at T = 1, 0.57m from the side of a full-scale passenger train travelling at 51m/s past a station platform.

3.5.2.3 Model validation.

The slipstream model needs to accurately simulate a train slipstream in order to be a useful tool, with the magnitudes of the simulated velocities being the same as those determined from experiment. The method of quantifying the goodness-of-fit of the model has to be carefully selected as some methods have limitations that allow a poor model to be described as good. For example, the Coefficient of Determination is $\frac{\sum_{i=1}^{N}(M_i-\bar{M})(S_i-\bar{S})}{\left[\sum_{i=1}^{N}(M_i-\bar{M})^2\right]^{0.5}\left[\sum_{i=1}^{N}(S_i-\bar{S})^2\right]^{0.5}}$, where M and S refer to the measured data and simulated data respectively, and the overbar refers to the mean of the data (Legates and McCabe, 1999). This validation method is not sensitive to proportional or additive differences between the measured and the simulated values. Therefore, if the power of the simulated data at each frequency was a hundred times greater

than that of the measured data the Coefficient of Determination would describe the two sets of data as a perfect match. As the slipstream model needs to both reproduce the correct slipstream velocity magnitudes and the slipstream region that they occur in, the Coefficient of Determination is not a reliable assessment of accuracy. The Index of Agreement (d), which is the average relative error between the measured and simulated values, was developed by Willmott (1981) to overcome the deficiencies of such validation methods as the Coefficient of Determination, and is given by equation (3.21). The value of d varies between 0 and 1, which correspond to a poor model and a perfect model respectively.

$$d = 1 - \frac{\sum_{i=1}^{N}(M_i - S_i)^2}{\sum_{i=1}^{N}\left((|S_i - \bar{M}|) + (|M_i - \bar{M}|)\right)^2} \tag{3.21}$$

This method of validation is used to analyse the accuracy of the slipstream model in both the time and frequency domains.

3.6 Modelling the slipstream of various train types.

This section shows how the model reproduces the slipstreams of the various train types that were measured during the full-scale and model-scale experiments. The details of the trains are given in Section 2.2. The relevant fluid dynamics theories are utilised by the model, and the parameters of n and C_1 of the boundary layer equation (equation (3.2)) are determined for each train type, as well as the parameters U_{max} and B of the vortex equation (equation (3.4)) when modelling the full-scale passenger train. The dimensions of each train type are

incorporated into the model as train shape has been found to affect the slipstream velocities (see Section 2.2.2).

3.6.1 Full-scale passenger train.

3.6.1.1 Mean velocity.

In order to simulate the mean slipstream velocities of a full-scale passenger train the theories of potential flow, boundary layer growth and wake decay are used along with the equations for a vortex at the rear of the train and a transitional region between the vortex and the wake. The tapering of the locomotive's nose is modelled as it affects the velocity peak at the train's nose. A plan of an ICE2 train, including its tapering nose, is given by Köhler (2001) and is used to model the tapered region. Although the plan specifies neither the width of the train's nose at its narrowest nor the length of the tapered region, these can be approximated from the plan using the known width of the main body of the train (3.07m). The narrowest width of the train's nose is half the width of the main body of the train. The tapering nose width is approximated by using the average nose width along the full length of the nose, and is therefore three quarters of the width of the main body of the train, i.e. 2.303m. The ratio of the nose length to the width of the main body of the train is 0.5173, therefore, the nose length is 1.588m. The tapering of the width of the train's nose results in a smaller normalised velocity peak in this region than would have occurred if the tapering had not been modelled. The height of the train nose also tapers; however, when this was also reproduced in the slipstream model the normalised velocity peak at the train's nose was too low, i.e. smaller than the

measured normalised velocity nose peak of the full-scale tests. Therefore, only the tapering nose width is modelled.

The constants n and C_1 in the equation for the boundary layer growth along a flat plate were originally taken to depend upon the Reynolds Number, as described for flow in pipes by Duncan *et al.* (1970). However, this method neither reproduces the shape of the velocity time history of the boundary layer growth nor the velocity magnitudes in this region. Therefore, a trial and improvement approach is taken to identify the values of the constants that, in combination, generate the correct velocity time history along the main body of the train. The values of n and C_1 used to model a full-scale passenger train have an approximate linear relationship with the distance, in metres, from the side of the train (y_s). For the train passing by a station platform the parameters used in the model are given by:

$$n = 56.153y_s + 2.237 \tag{3.22}$$

$$C_1 = 12y_s + 5.160 \tag{3.23}$$

For a train travelling along an open track the parameters are given by:

$$n = 28.8y_s + 5.8456 \tag{3.24}$$

$$C_1 = 8.4903y_s + 2.5631 \tag{3.25}$$

The values of n and C_1 increase with increasing y_s, and C_1 is greater for a passenger train passing a station platform than when travelling along an open track. Varying the boundary layer parameters in this manner is an arbitrary allowance made in order to fit the two-

dimensional boundary layer theory to a three-dimensional reality. Although n and C_1 have roots in boundary layer theory, in the current work they are considered as 'curve fit' parameters, and so are altered to reproduce the shape and magnitude of the velocity profile along the main body of a train.

In order to generate a vortex at the rear of the train which produces the correct velocity peak magnitude in this region a trial and improvement process was used to determine the appropriate values of the constants B and U_{max}. With a full-scale passenger train, B = 284, and U_{max} is 35% and 50% of the speed of the train passing by a station platform and travelling along an open track respectively.

3.6.1.2 Turbulence.

The AR coefficients used to simulate the turbulence-induced velocity fluctuations within the full-scale passenger train's slipstream are given in Table 3.1. The values of ϕ_1 and ϕ_2 do not change with y_s, whereas ϕ_3 decreases with increasing y_s reflecting the reduction in the magnitude of the turbulence levels as the distance from the train side increases. The value of ϕ_1 is the same for both the train passing a station platform and travelling along an open track, except along the main body of the train where the value of ϕ_1 is greater at a station platform. This is also the case with ϕ_2. The values of ϕ_3 are smaller with a train passing a station platform than with a train travelling along an open track for all of the slipstream regions, except upstream and around the train nose. Hence, there are smaller turbulence magnitudes in the slipstream of a train passing a station platform. The differences between the slipstreams of a train travelling along an open track and passing a station platform are likely to be due to the

interaction of the platform with the slipstream, with the exposed bogies of a train travelling along an open track increasing the aerodynamic roughness of the train. The values of ϕ_3 are the same for both train types upstream and around the train nose as the turbulence levels in this region are very small for both train types. The largest values of ϕ_3, and hence the largest turbulence magnitudes, occur along the main body of the train reflecting the large turbulence levels measured in the boundary layer as described in Section 2.2.1.1. The next largest values of ϕ_3 occur in the vortex and transition region, then in the wake region, and finally in the upstream and nose region.

The values of y_s associated with ϕ_3, as given in Table 3.1, are based upon the y_s values that the slipstream measurements were taken at during the full-scale tests. For example, at y_s = 0.57m and y_s = 1.07m, the ϕ_3 values used along the main body of a train passing a station platform are 0.03 and 0.015 respectively. When y_s is 1.57m, 2.07m, 2.57m and 2.97m, ϕ_3 = 0.0113. Thus, in the model $\phi_3 = 0.03$ when $y_s \leq 0.75$m, $\phi_3 = 0.015$ when $0.75 < y_s \leq 0.125$m, and $\phi_3 = 0.0113$ otherwise. In this example, the limiting y_s value of 0.75m is chosen as it lies between the distances of 0.57m and 1.07m used in the full-scale tests; similarly, the limiting y_s value of 1.25m lies between the distances of 1.07m and 1.57m used in the full-scale tests.

Region of train	ϕ	AR coefficient values	
		Train travelling past a station platform	Train travelling along an open track
Upstream and around nose	ϕ_1	0.5	0.5
	ϕ_2	0.2	0.2
	ϕ_3	0.003 if $y_s \leq 0.75$m, 0.0017 otherwise	0.003 if $y_s \leq 0.5$m, 0.0017 otherwise
Main body	ϕ_1	0.35	0.3
	ϕ_2	0.55	0.5
	ϕ_3	0.03 if $y_s \leq 0.75$m, 0.015 if 0.75m $< y_s \leq 1.25$m, 0.0113 otherwise	0.08 if $y_s \leq 0.5$m, 0.045 if 0.5m $< y_s \leq 1$m, 0.0225 otherwise
Vortex and transition	ϕ_1	0.5	0.5
	ϕ_2	0.2	0.2
	ϕ_3	0.0141 if $y_s \leq 0.75$m, 0.007 otherwise	0.025 if $y_s \leq 0.5$m, 0.0141 otherwise
Wake	ϕ_1	0.65	0.65
	ϕ_2	0.1	0.1
	ϕ_3	0.0039 if $y_s \leq 0.75$m, 0.002 otherwise	0.007 if $y_s \leq 0.5$m, 0.0039 otherwise

Table 3.1. AR coefficients used to simulate the turbulence within the slipstream of the full-scale passenger train.

3.6.1.3 Simulated velocity time histories.

Figure 3.9 shows both the simulated and measured normalised ensemble averaged slipstream velocity profiles of a full-scale passenger train passing by a station platform at 51m/s at various distances from the train side. Figure 3.10 shows the simulated and measured normalised ensemble averaged slipstream velocity profiles when the train is travelling along an open track at 69m/s. The normalised velocity upstream of the trains involved in the full-scale tests was not zero; therefore, there was an ambient wind velocity during the tests that is not reproduced by the model. The ambient normalised wind velocities were 0.03 and 0.02 for the train passing a station platform and travelling along an open track respectively. Hence, the magnitudes of the simulated normalised velocities are less than those of the measured normalised velocities by this amount, and this needs to be taken into consideration when comparing the simulated and the measured normalised velocity profiles.

Figures 3.9 and 3.10 show that the general shape and velocity magnitudes of the measured slipstreams are reproduced in the simulation. The two main points of reference for comparison are the maximum values of the normalised velocity peaks at the nose and the rear of the train, and Tables 3.2 and 3.3 give the magnitudes of these peaks for a train passing a station platform at 51m/s and along an open track at 69m/s respectively. The peaks measured during the full-scale tests are reduced to remove the ambient wind velocity associated with each train. Tables 3.2 and 3.3 also give the percentage difference between the simulated and measured normalised velocity peaks, where a negative percentage difference reflects that the simulated velocity peak is less than that of the measured slipstream, and vice versa.

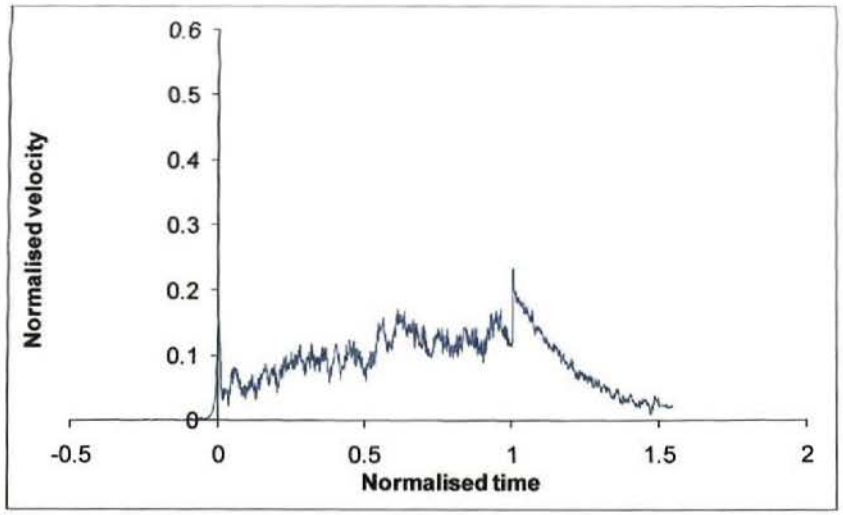

Figure 3.9a. Simulated normalised slipstream at y_s = 0.57m.

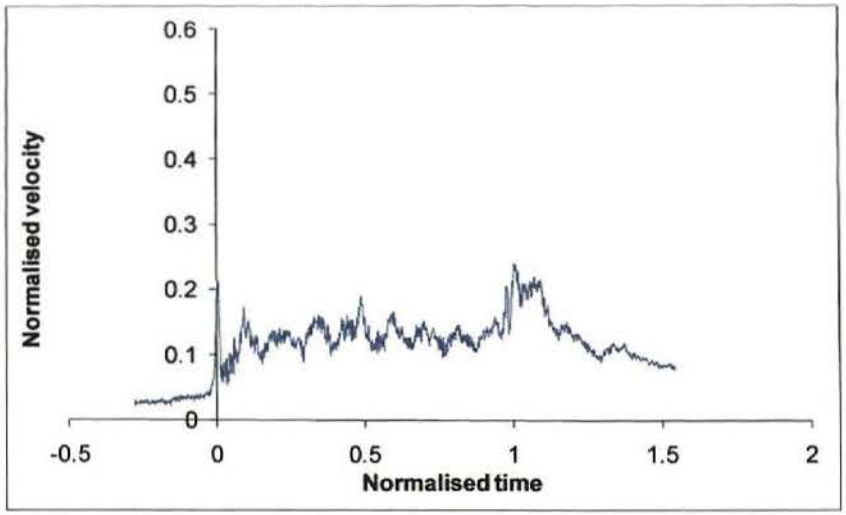

Figure 3.9b. Measured normalised slipstream at y_s = 0.57m.

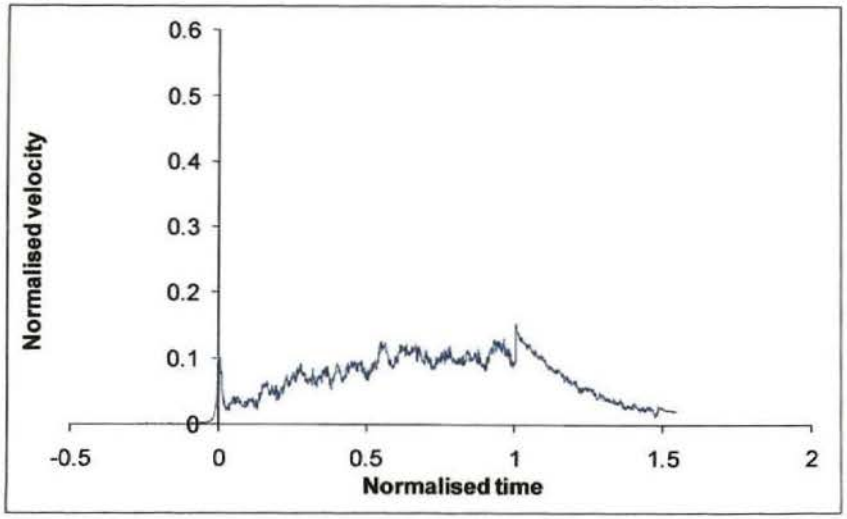

Figure 3.9c. Simulated normalised slipstream at y_s = 1.07m.

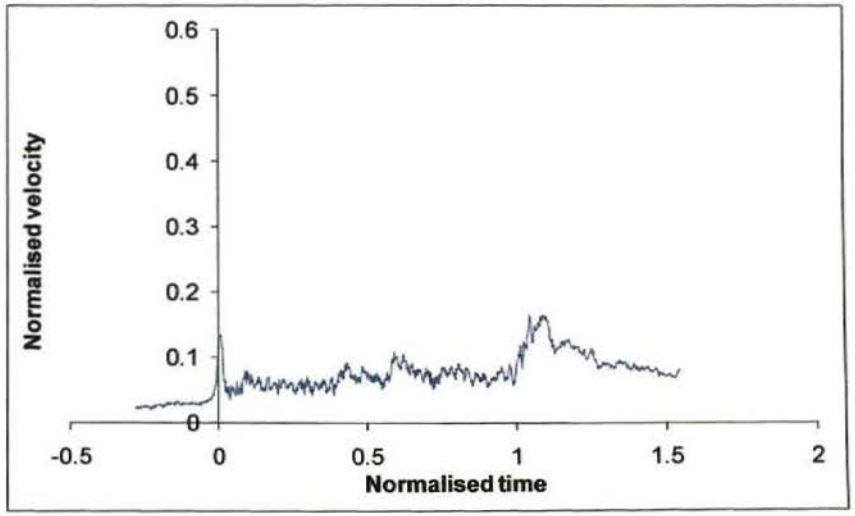

Figure 3.9d. Measured normalised slipstream at y_s = 1.07m.

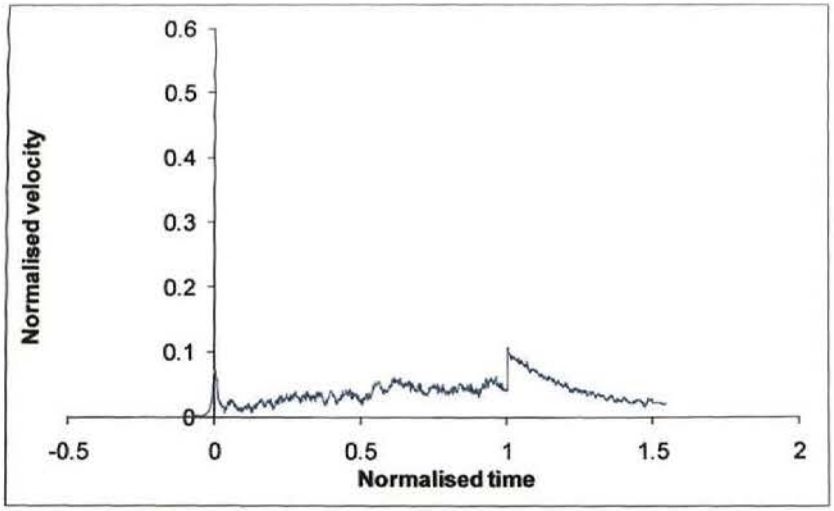

Figure 3.9e. Simulated normalised slipstream at y_s = 1.57m.

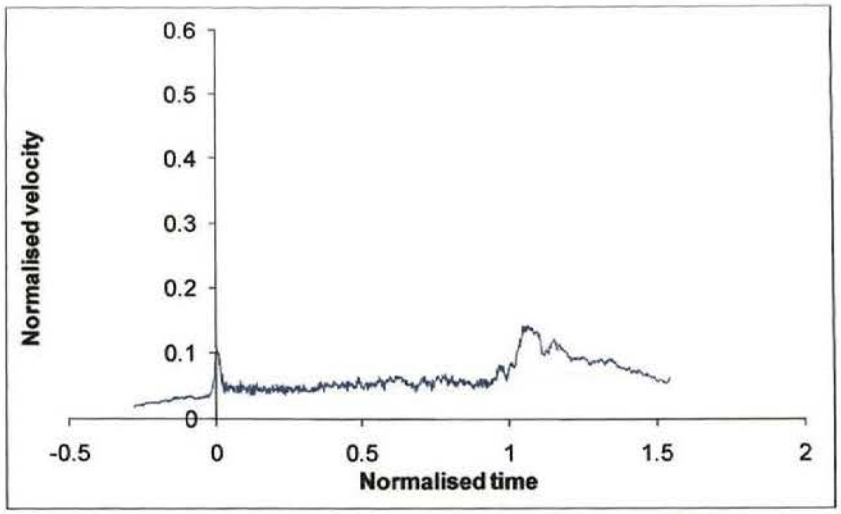

Figure 3.9f. Measured normalised slipstream at y_s = 1.57m.

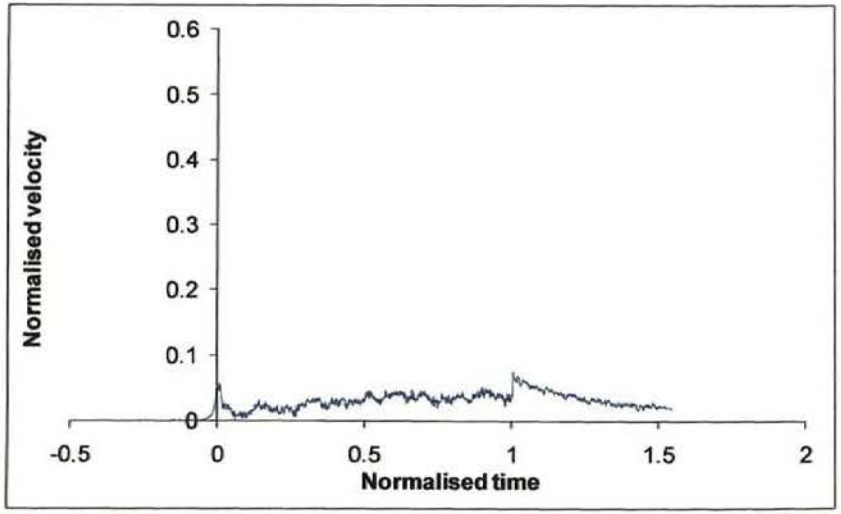

Figure 3.9g. Simulated normalised slipstream at y_s = 2.07m.

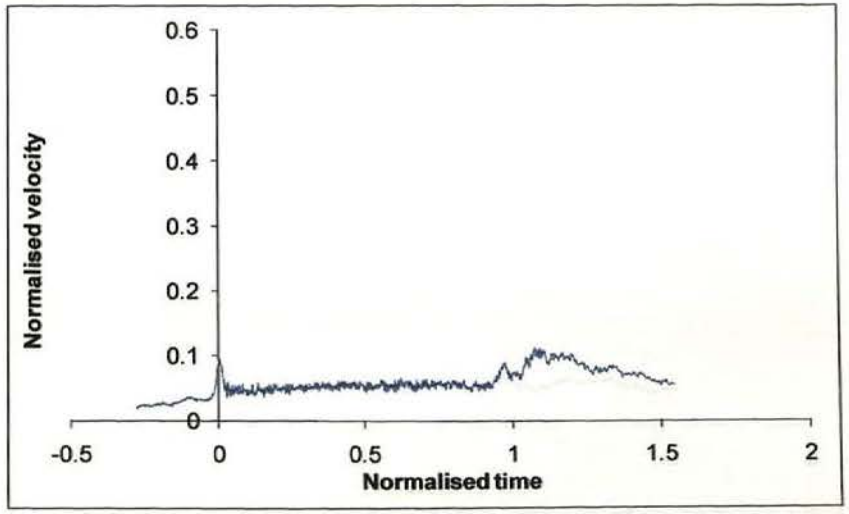

Figure 3.9h. Measured normalised slipstream at y_s = 2.07m.

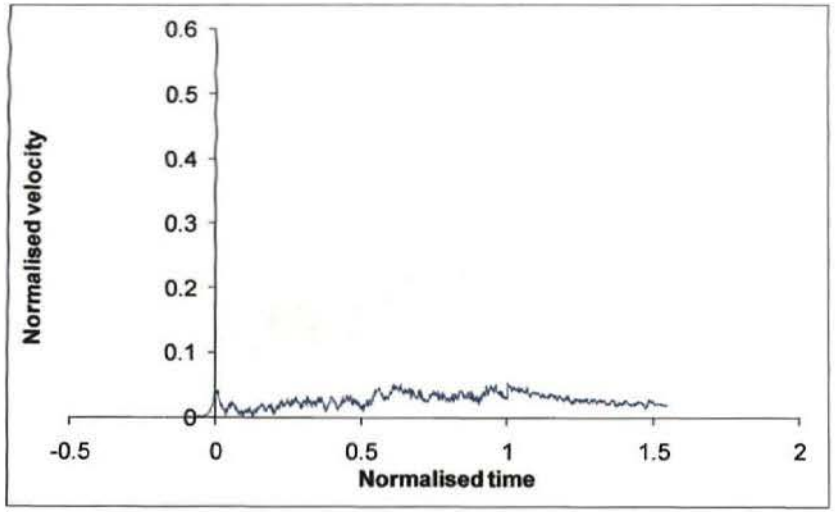

Figure 3.9i. Simulated normalised slipstream at y_s = 2.57m.

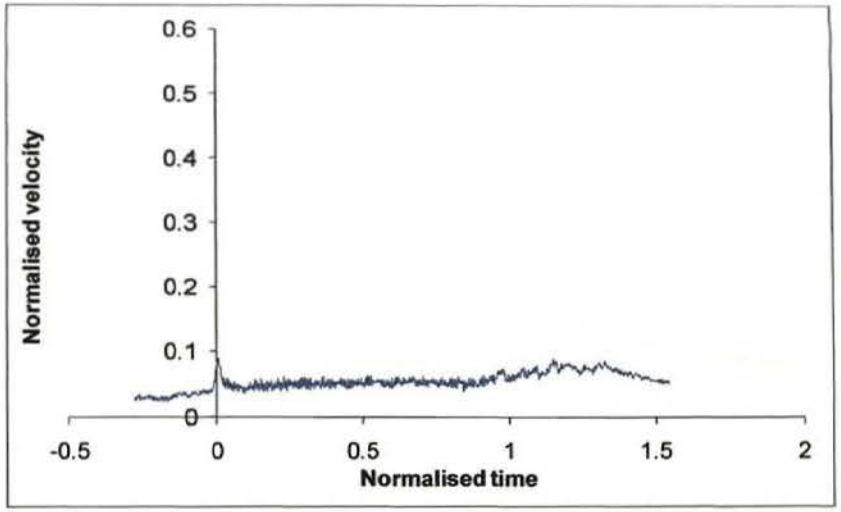

Figure 3.9j. Measured normalised slipstream at y_s = 2.57m.

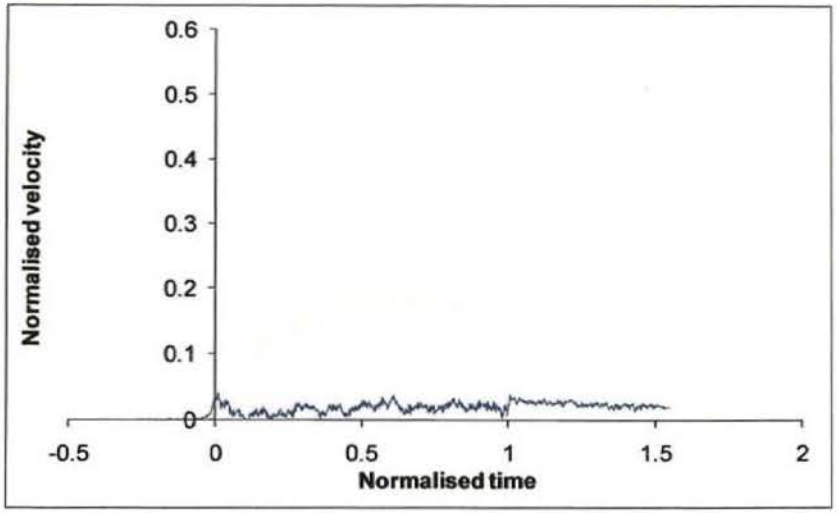

Figure 3.9k. Simulated normalised slipstream at y_s = 2.97m.

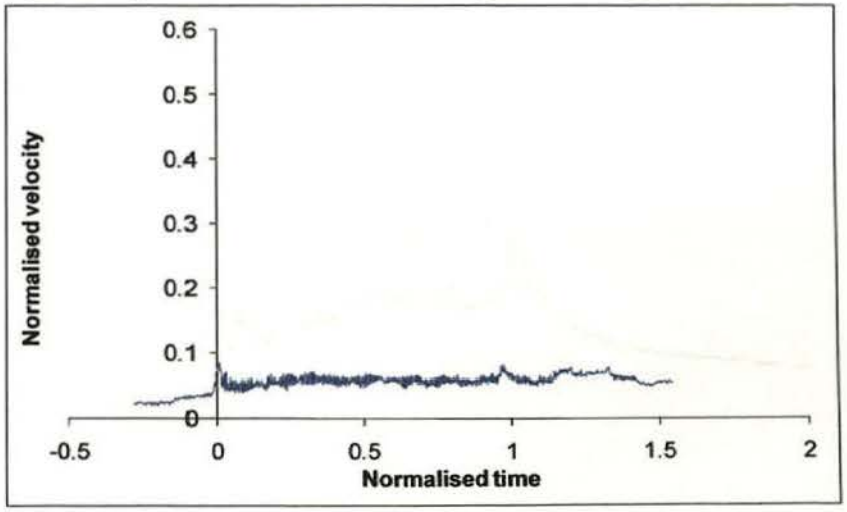

Figure 3.9l. Measured normalised slipstream at y_s = 2.97m.

Figure 3.9. Simulated and measured normalised slipstreams of a full-scale passenger train passing by a station platform at 51m/s.

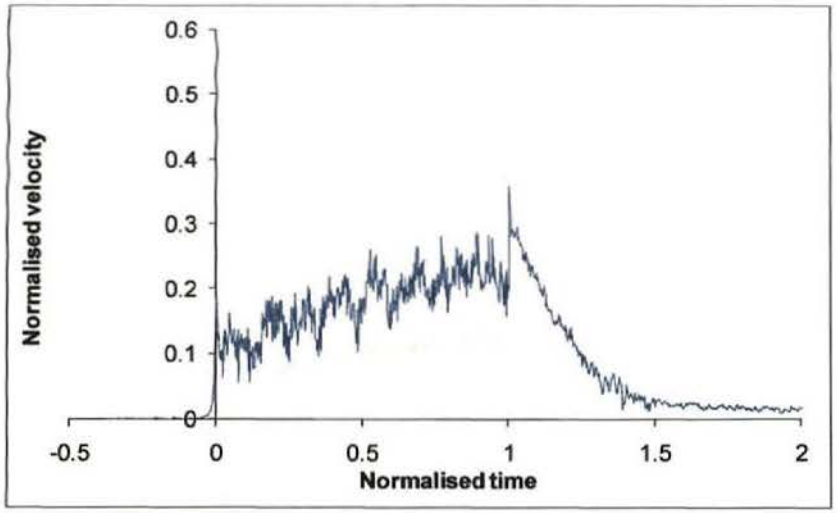

Figure 3.10a. Simulated normalised slipstream at y_s = 0.41m.

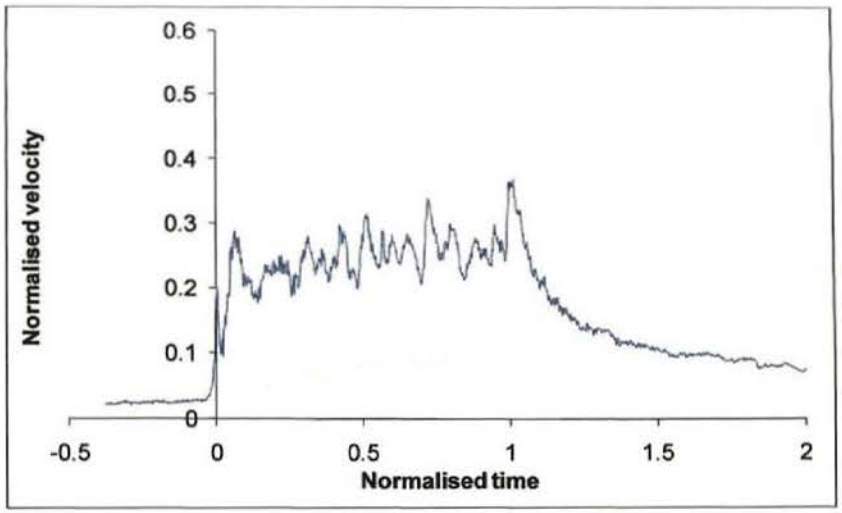

Figure 3.10b. Measured normalised slipstream at y_s = 0.41m.

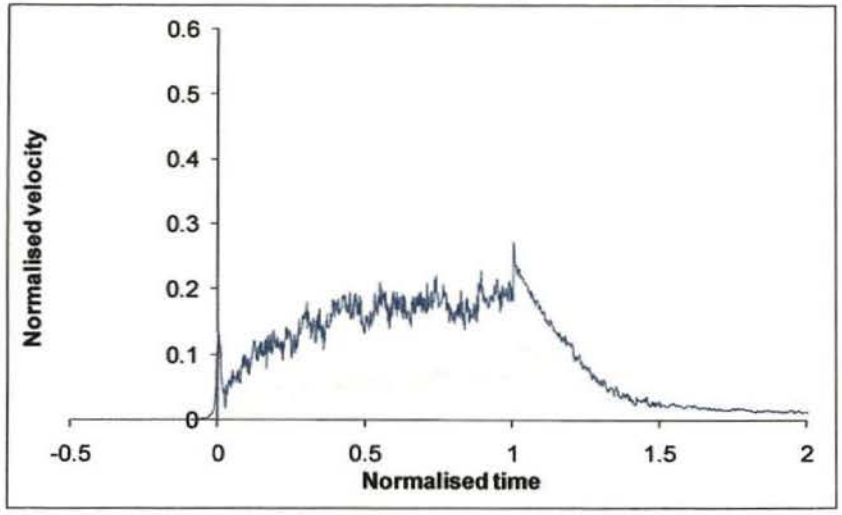

Figure 3.10c. Simulated normalised slipstream at y_s = 0.75m.

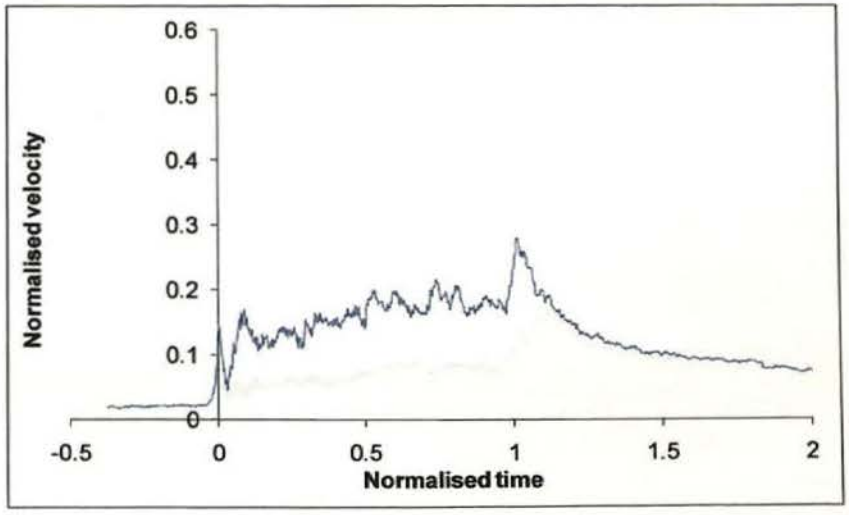

Figure 3.10d. Measured normalised slipstream at y_s = 0.75m.

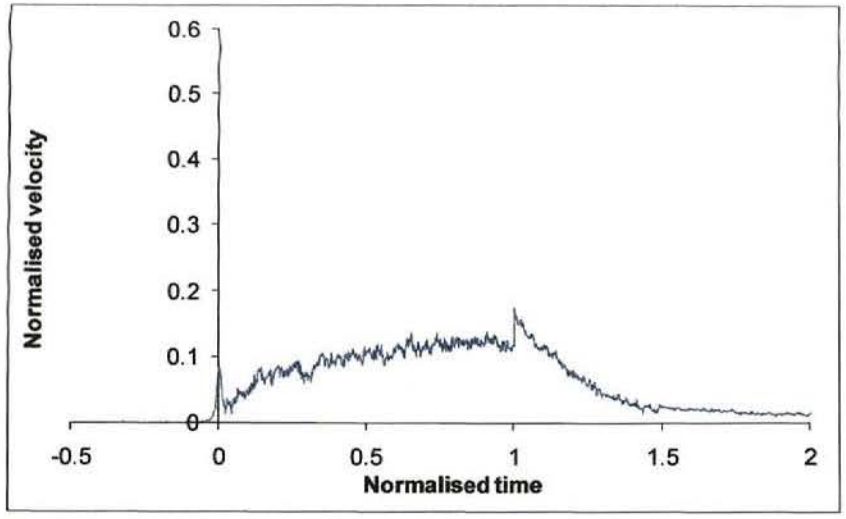

Figure 3.10e. Simulated normalised slipstream at y_s = 1.35m.

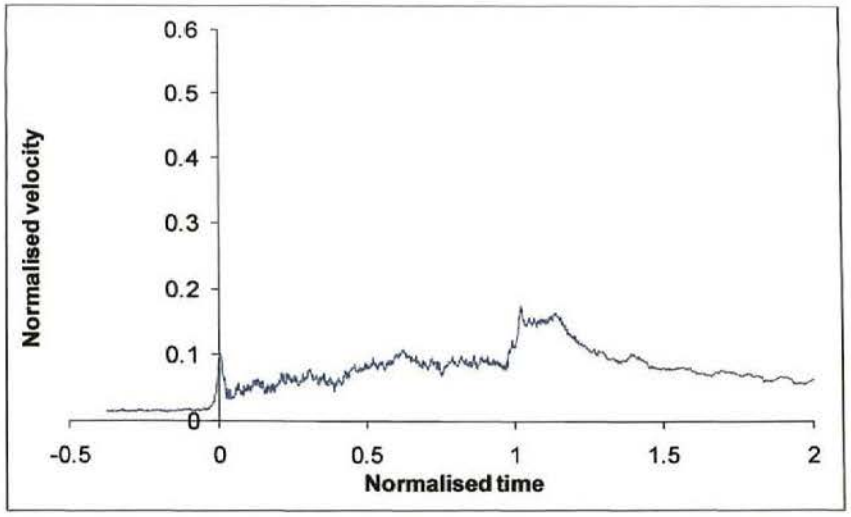

Figure 3.10f. Measured normalised slipstream at y_s = 1.35m.

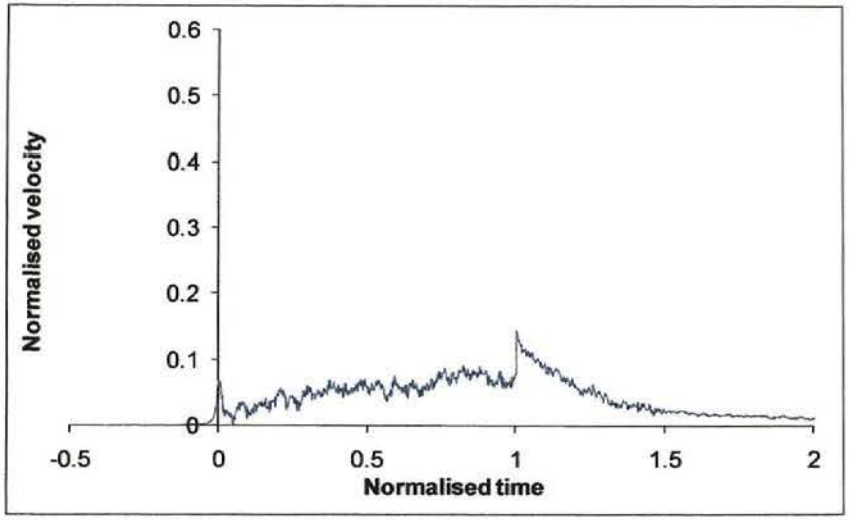

Figure 3.10g. Simulated normalised slipstream at y_s = 1.665m.

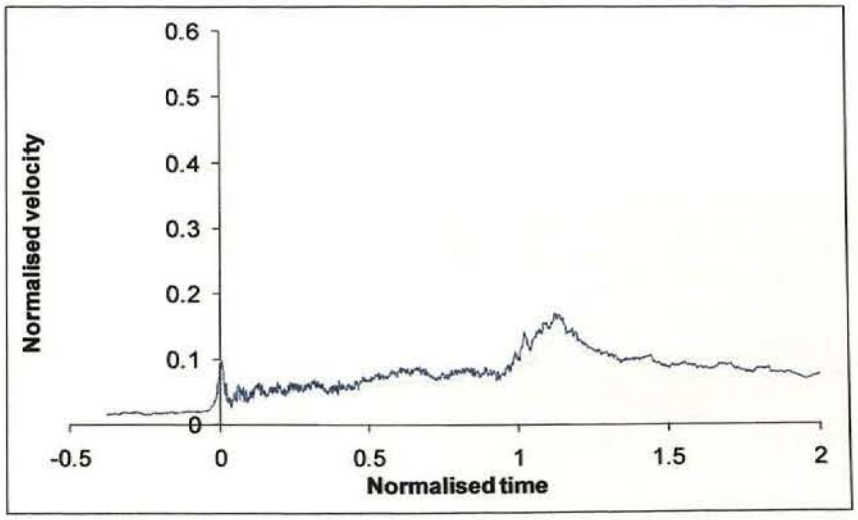

Figure 3.10h. Measured normalised slipstream at y_s = 1.665m.

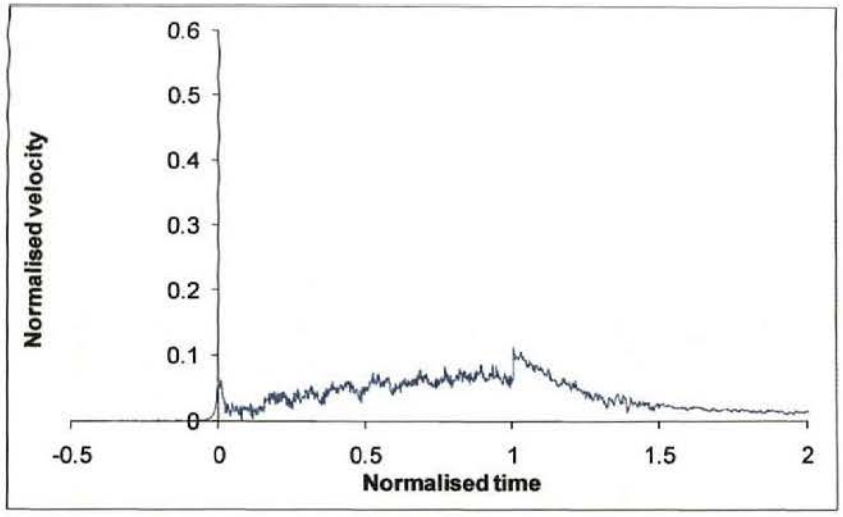

Figure 3.10i. Simulated normalised slipstream at y_s = 1.915m.

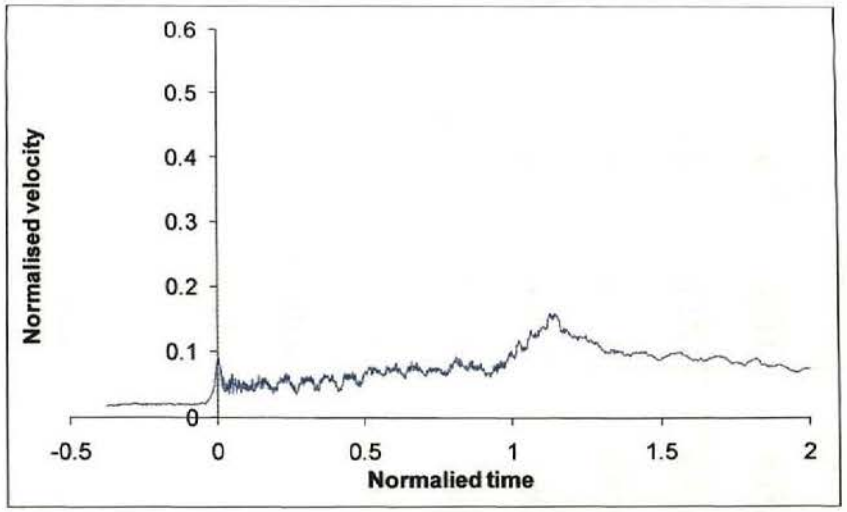

Figure 3.10j. Measured normalised slipstream at y_s = 1.915m.

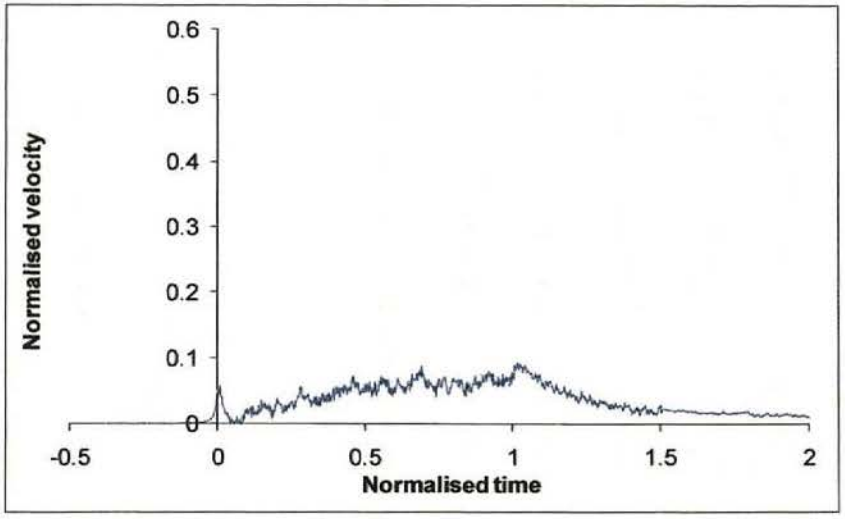

Figure 3.10k. Simulated normalised slipstream at y_s = 2.16m.

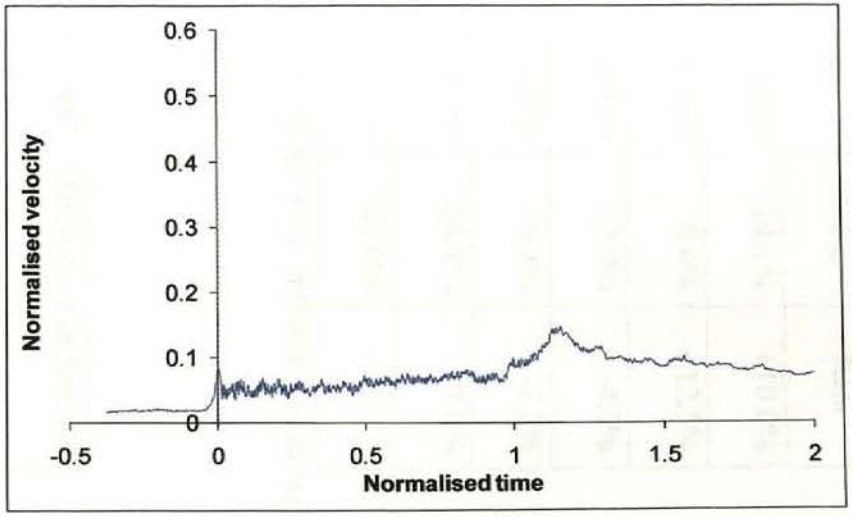

Figure 3.10l. Measured normalised slipstream at y_s = 2.16m.

Figure 3.10. Simulated and measured normalised slipstreams of a full-scale passenger train travelling along an open track at 69m/s.

y_s (m)	Measured velocity peak		Simulated velocity peak		Percentage difference	
	Nose	Rear	Nose	Rear	Nose	Rear
0.57	0.184	0.211	0.158	0.232	-14.1%	+10.0%
1.07	0.103	0.136	0.103	0.153	0.0%	+12.5%
1.57	0.073	0.111	0.071	0.106	-2.7%	-4.5%
2.07	0.064	0.082	0.058	0.076	-9.4%	-7.3%
2.57	0.059	0.057	0.042	0.053	-28.8%	-7.0%
2.97	0.055	0.052	0.042	0.038	-23.6%	-26.9%

Table 3.2. Normalised slipstream velocity peak magnitudes of a full-scale passenger train passing a station platform at 51m/s.

y_s (m)	Measured velocity peak		Simulated velocity peak		Percentage difference	
	Nose	Rear	Nose	Rear	Nose	Rear
0.41	0.182	0.348	0.186	0.354	+2.2%	+1.7%
0.75	0.126	0.261	0.135	0.259	+7.1%	-0.8%
1.35	0.082	0.156	0.085	0.175	+3.7%	+12.2%
1.665	0.076	0.150	0.069	0.144	-9.2%	-4.0%
1.915	0.068	0.137	0.062	0.112	-8.8%	-18.2%
2.16	0.065	0.128	0.058	0.093	-10.8%	-27.3%

Table 3.3. Normalised slipstream velocity peak magnitudes of a full-scale passenger train travelling along an open track at 69m/s.

The best match between the simulated and measured peaks is associated with the nose of the passenger train passing a station platform at y_s = 1.07m, where both the simulated and

measured nose peaks have a value of 0.103. The largest percentage differences are associated with the larger values of y_s. There is a -28.8% and -23.6% difference associated with the nose peak of a train passing a station platform at y_s values of 2.57m and 2.97m respectively. For the rear peaks, there is a -26.9% difference associated with the train passing a station platform at y_s = 2.97m, and a -27.3% difference with a train travelling along an open track at y_s = 2.16m. Although the percentage differences at the larger values of y_s are quite large they are associated with small normalised velocity magnitudes. A person is more vulnerable to being displaced by the large slipstream velocities occurring close to the train side, and the model simulates these velocities with greater accuracy. The simulated normalised velocity magnitudes along the main body of the train and in the wake are also similar to those of the measured slipstreams; however, there is a more gradual increase in normalised velocity towards the peak at the rear of the train in the measured slipstream than generated by the model. This results in the maximum measured rear peak velocity occurring later than in the simulated slipstream at large values of y_s. A second velocity peak at the rear of the train is evident in the measured slipstreams at y_s values of 0.57m, 1.07m and 1.57m, which will be due to vortex shedding occurring in the wake of the train. This phenomenon is not simulated by the slipstream model as it is not possible to predict the rate of the vortex shedding for the various train types or speeds. 3.6.1.5 gives a further quantitative comparison of the simulated and measured normalised slipstream velocity profiles of a full-scale passenger train.

From a visual inspection of Figures 3.9 and 3.10 the turbulence levels of the measured slipstreams appear to be reasonably well reproduced by the model. The exception to this occurs along the main body of a train travelling along an open track at the smallest distance from the train side, i.e. at y_s = 0.41m, where the larger scale turbulence is not accurately

simulated. Theoretically, increasing the values of ϕ_1 and ϕ_2 would result in an improved simulation. However, the values of ϕ_1 and ϕ_2 are as large as they can be as a further increase in either ϕ_1 or ϕ_2 results in an unrealistic simulated velocity profile that bears no resemblance to an actual velocity profile along the main body of a train.

3.6.1.4 Wavelet spectra plot.

The wavelet spectra plots of Figure 3.8 in Section 3.5.2.2 are concerned with a passenger train travelling by a station platform at 51m/s when $T = 1$ and $y_s = 0.57$m. Figure 3.11 gives this information but for $y_s = 1.07$m. The two curves of Figure 3.8 are a closer match than those of Figure 3.11, hence the model simulates a more accurate slipstream at $y_s = 0.57$m than at $y_s = 1.07$m when $T = 1$. The curves in Figure 3.12 are concerned with a passenger train travelling along an open track at 69m/s when $T = 1$ and $y_s = 0.41$m, and are not as close a match as those in either Figure 3.8 or Figure 3.11. Therefore, the slipstream of a train travelling along an open track is not as accurately simulated as the train passing a station platform at $T = 1$ for the particular distances from the train side investigated. As with Figure 3.8, Figures 3.11 and 3.12 show that the measured and simulated dimensionless power is similar for each dimensionless frequency, except at the lowest frequency (largest scale) and at the highest frequencies (smallest scales).

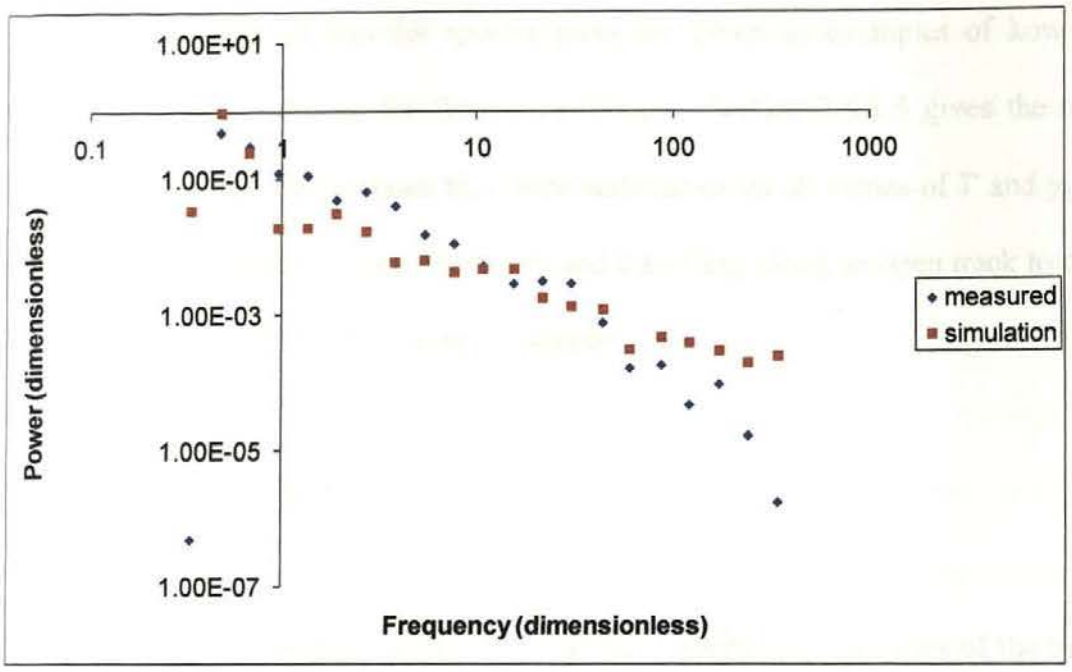

Figure 3.11. Wavelet spectra plots of the measured and simulated slipstreams at T = 1 and y_s = 1.07m for a full-scale passenger train travelling at 51m/s past a station platform.

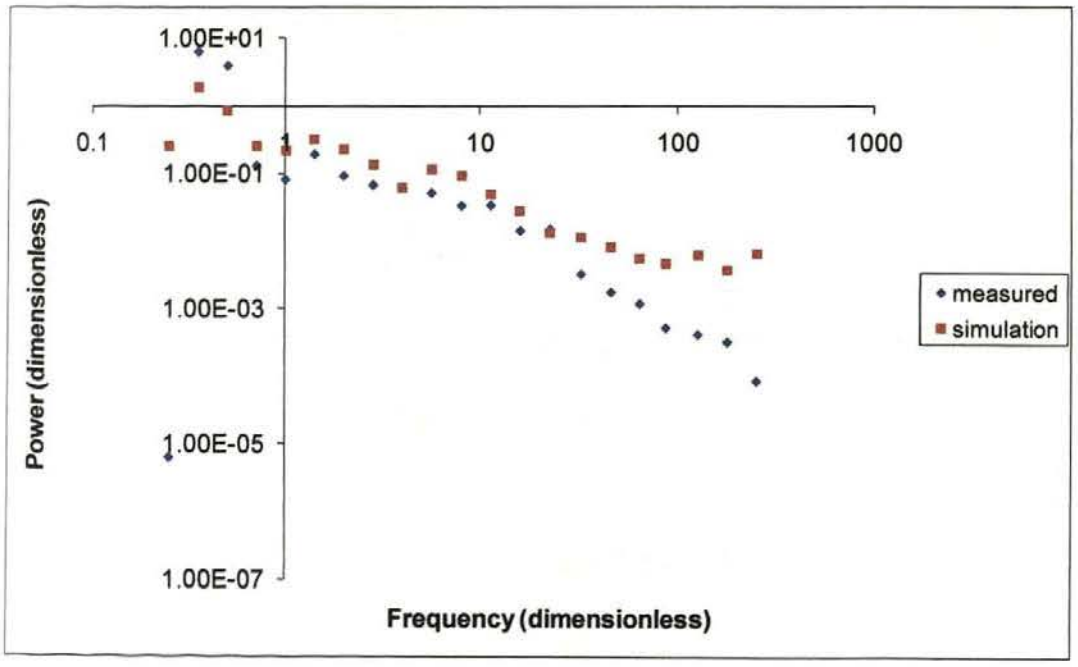

Figure 3.12. Wavelet spectra plots of the measured and simulated slipstreams at T = 1 and y_s = 0.41m for a full-scale passenger train travelling at 69m/s along an open track.

These three figures of wavelet spectra plots are given as examples of how the model's accuracy is investigated in the frequency domain. Section 3.6.1.5 gives the results of the Index of Agreement calculations that were undertaken on all values of T and y_s for both the passenger train passing a station platform and travelling along an open track to determine the accuracy of the model in the frequency domain.

3.6.1.5. Model validation.

The Index of Agreement (d) for the normalised velocity time histories of the train passing a station platform and travelling along an open track are given in Tables 3.4 and 3.5 respectively. The normalised velocities of the measured slipstreams have been reduced to allow for the ambient wind velocities so that they are comparable with the simulated slipstreams, and the value of d is dimensionless.

y_s (m)	0.57	1.07	1.57	2.07	2.57	2.97
d	0.902	0.661	0.852	0.835	0.783	0.750

Table 3.4. Index of Agreement (d) pertaining to the normalised velocity time history of the full-scale passenger train passing a station platform.

y_s (m)	0.41	0.75	1.35	1.665	1.915	2.16
d	0.923	0.929	0.777	0.725	0.674	0.622

Table 3.5. Index of Agreement (d) pertaining to the normalised velocity time history of the full-scale passenger train travelling along an open track.

Tables 3.4 and 3.5 show that the value of d lies between 0.902 and 0.661 when the full-scale passenger train passes a station platform, and between 0.929 to 0.622 when the train travels along an open track. In general, the value of d increases with decreasing y_s, therefore, the model accurately simulates the slipstream velocities close to the train side where the slipstream velocities are highest and therefore the risk to a person is greatest. The main exception to this is at 1.07m from the side of a train passing a station platform, which is the second smallest distance but is modelled the least accurately for this train. Although Table 3.2 shows that the magnitudes of the velocity peaks are simulated with reasonable accuracy at y_s = 1.07m, the model does not reproduce the 'flat' shape of the normalised velocity profile of the measured slipstream along the main body of the train (see Figures 3.9c and 3.9d). The measured velocities along the entire length of the main body of the train at y_s = 1.07m are only slightly larger than those upstream of the train, however, the simulated velocities increase along the train's main body. No combination of the boundary layer parameters n and C_1 result in such a 'flat' velocity profile, but the values of the constants used in the model give the best possible simulation of this region.

Figures 3.13 and 3.14 give the values of d relating to the dimensionless power of the full-scale passenger train passing a station platform and travelling along an open track respectively. The value of d of a train passing a station platform lies between 0.81 and 0.93 for all values of T and y_s. These are reasonably high values and, therefore, indicate that the model simulates the slipstream turbulence with reasonable accuracy. In Figure 3.13 the value of d lies between 0.88 and 0.89 at y_s = 1.07m showing that although the normalised velocity is not reproduced with great accuracy in the time domain (as indicated by a low value of d in Table 3.4) the turbulence levels are reproduced with reasonable accuracy in the frequency

domain. The smallest y_s value (0.57m) is associated with the largest values of d, which lie between 0.92 and 0.93, therefore, the most accurate reproduction of the turbulence levels occurs at this value of y_s. Figure 3.14 shows that d lies between 0.78 and 0.99 for all values of T and y_s, except at the smallest distance from the train side, for a train travelling along an open track. These values are reasonably high indicating that the model reproduces the turbulence levels of this train with reasonable accuracy. However, the smallest distance from the train side, y_s = 0.41m, is associated with the lowest range of d values (0.61 to 0.64), indicating a poorer simulation of the turbulence levels, as also described in Section 3.6.1.3. The highest values of d in either Figure 3.13 or 3.14 occur at 0.75m from the side of a train travelling along an open track and lie between 0.98 and 0.99.

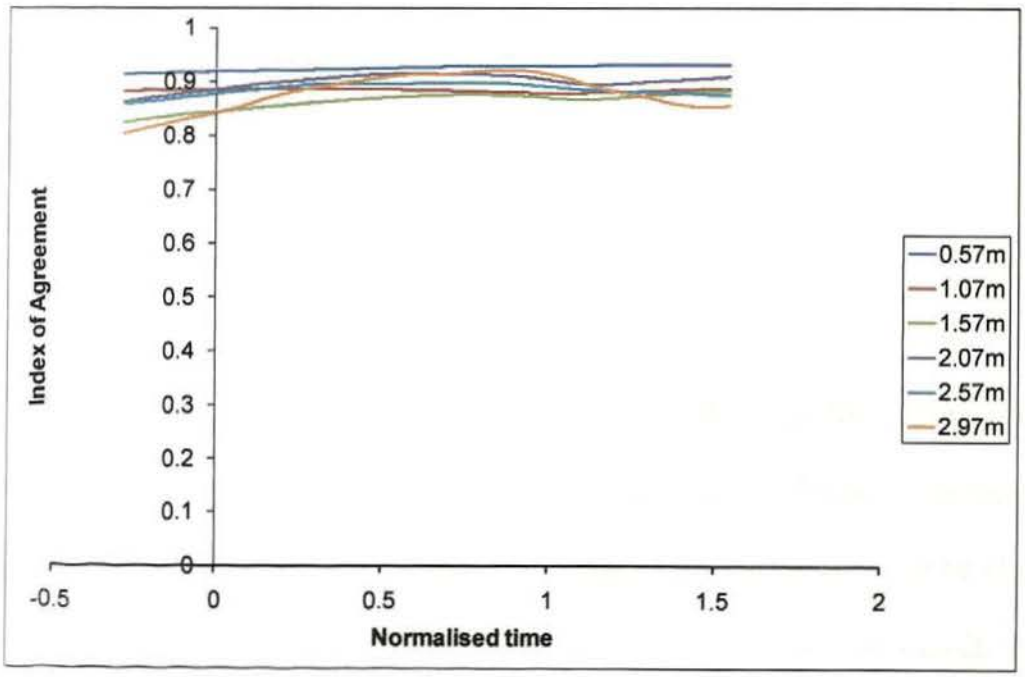

Figure 3.13. Index of Agreement (d) relating to the dimensionless power of the full-scale passenger train passing a station platform.

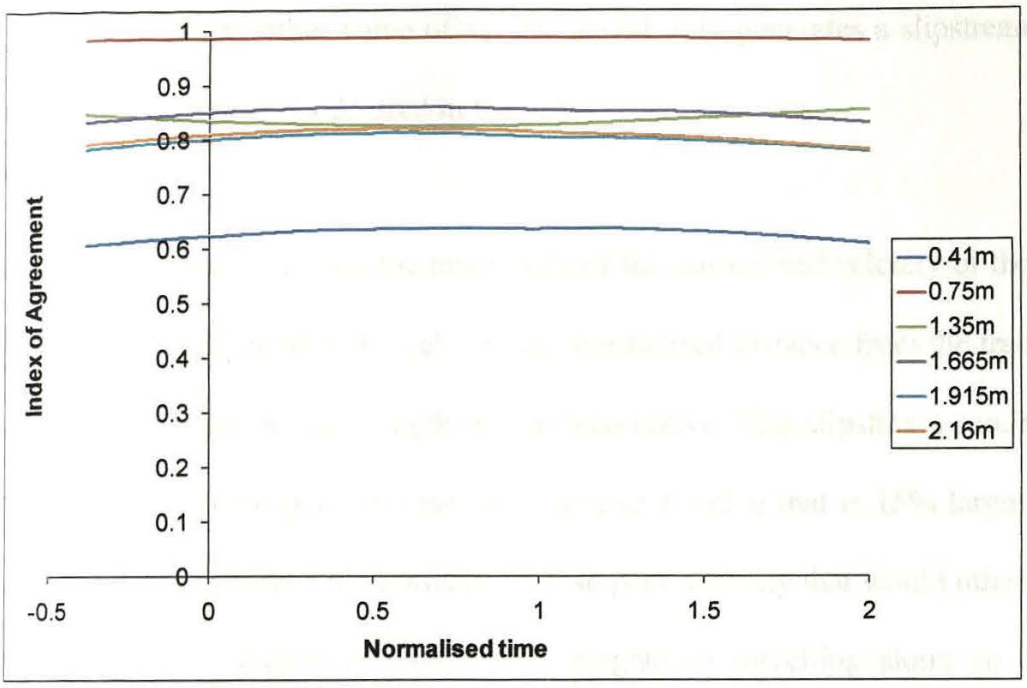

Figure 3.14. Index of Agreement (d) relating to the dimensionless power of the full-scale passenger train travelling along an open track.

3.6.2 Freightliner.

3.6.2.1 Mean velocity

The full-scale freightliner slipstream is modelled using the theories of potential flow, boundary layer development and wake decay, as for the full-scale passenger train described in Section 3.6.1. However, as no peak at the rear of the freightliner can be identified, a vortex is not included in the freightliner slipstream model, and so the transition region links the boundary layer and wake regions. The parameters n, C_1, and ϕ_3 used in the simulation of a full-scale passenger train vary with y_s. However, the full-scale tests only took slipstream measurements at y_s = 1.5m and y_s = 0.705m for a freightliner passing a station platform and travelling along an open track respectively. As there is no data on which to base slipstream

simulations at any other value of y_s, the model only generates a slipstream for the distances from the freightliner's side used in the tests.

In order to correctly model the magnitude of the normalised velocity of the nose peak, it was found appropriate to alter the value of the normalised distance from the track centreline (Y) to an effective value for the length of the locomotive. The slipstream model of a freightliner passing by a station platform uses an effective Y value that is 15% larger than the actual Y value in order to reduce the normalised nose peak velocity that would otherwise be generated. Conversely, the slipstream model of a freightliner travelling along an open track has an effective Y value 18% lower than the actual Y value to increase the normalised nose peak velocity to be the same magnitude as that of the measured slipstream.

Freightliner position	n	C_1
Passing a station platform	8	1.3
Travelling along an open track	10	2.5

Table 3.6. Boundary layer parameters n and C_1 used in the freightliner slipstream model.

Table 3.6 gives the values of the boundary layer parameters n and C_1 used in the freightliner slipstream model. The values of n and C_1 for the freightliner travelling along an open track are larger than for a freightliner passing a station platform reflecting that the shape of the normalised boundary layer velocity profiles are different for the two trains.

3.6.2.2 Turbulence.

Table 3.7 gives the values of the AR coefficients used to model the turbulence within the slipstream of a freightliner. The values of ϕ_1 are the same for both the freightliner passing a station platform and travelling along an open track, except along the locomotive and the main body where they are greater for a freightliner passing a station platform. The values of ϕ_2 are also independent of train location, except along the locomotive and in the wake.

The value of ϕ_3 is also independent of train location, except along the locomotive and the main body. The largest values of ϕ_3, hence the greatest small scale turbulence magnitudes, occur along the freightliner's main body as with the full-scale passenger train described in Section 3.6.1.2. The next largest ϕ_3 of the freightliner passing a station platform occurs in the transition region, followed by the locomotive, then the wake, and finally the upstream region has the lowest small scale turbulence magnitudes. This sequence differs from that of the train travelling along an open track in that the second and third largest turbulence magnitudes occur along the locomotive and in the transition region respectively, which is the reverse order for the train passing a station platform. The difference in turbulence levels between the train locations is likely to be due to the interaction of the station platform and the slipstream, and the exposed bogies of a train travelling along an open track.

Region of train	ϕ	AR coefficient values	
		Train passing by a station platform (y_s = 1.5m)	Train travelling along an open track (y_s = 0.705m)
Upstream	ϕ_1	0.5	0.5
	ϕ_2	0.2	0.2
	ϕ_3	0.0017	0.0017
Locomotive	ϕ_1	0.35	0.3
	ϕ_2	0.55	0.5
	ϕ_3	0.015	0.045
Main body	ϕ_1	0.35	0.3
	ϕ_2	0.6	0.6
	ϕ_3	0.04	0.065
Transition	ϕ_1	0.5	0.5
	ϕ_2	0.45	0.45
	ϕ_3	0.02	0.02
Wake	ϕ_1	0.65	0.65
	ϕ_2	0.1	0.2
	ϕ_3	0.0039	0.0039

Table 3.7. AR coefficients used to simulate the turbulence within the slipstream of the full-scale freightliner.

3.6.2.3 Simulated velocity time histories.

Figures 3.15 and 3.16 show the simulated and measured normalised ensemble averaged slipstream velocity time histories of a freightliner passing by a station platform and travelling along an open track respectively. The speed of both trains is 33.6m/s. As with the full-scale passenger train tests, an ambient wind velocity was recorded during the freightliner tests. The normalised ambient wind velocity of 0.04 is not reproduced by the model, therefore, the simulated normalised slipstream velocity magnitudes are less than those of the measured slipstreams by 0.04. Figures 3.15 and 3.16 show that the general shape, velocity magnitudes and turbulence levels of the measured slipstreams are reproduced in the simulation. However, the model does not reproduce the very rapid increase in velocities along the main body of the train immediately after the nose peak for a train travelling along an open track.

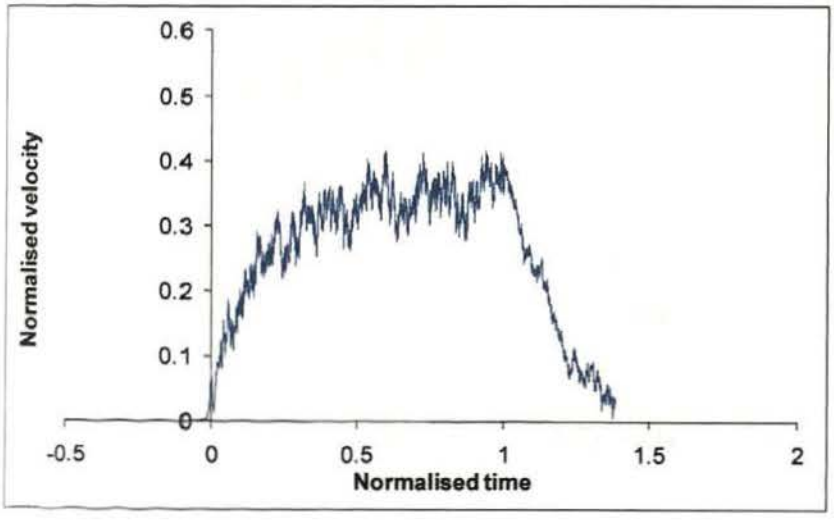

Figure 3.15a. Simulated normalised slipstream at y_s = 1.5m.

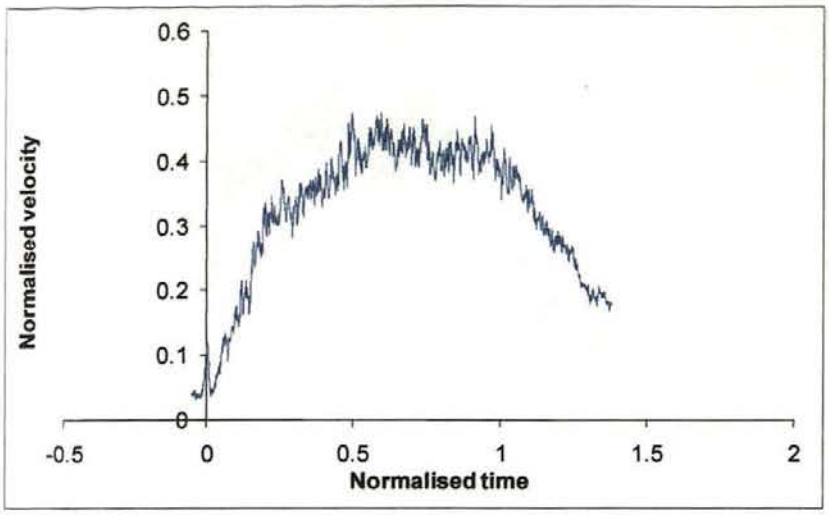

Figure 3.15b. Measured normalised slipstream at y_s = 1.5m.

Figure 3.15. Simulated and measured normalised slipstreams of a freightliner passing by a station platform at 33.6m/s.

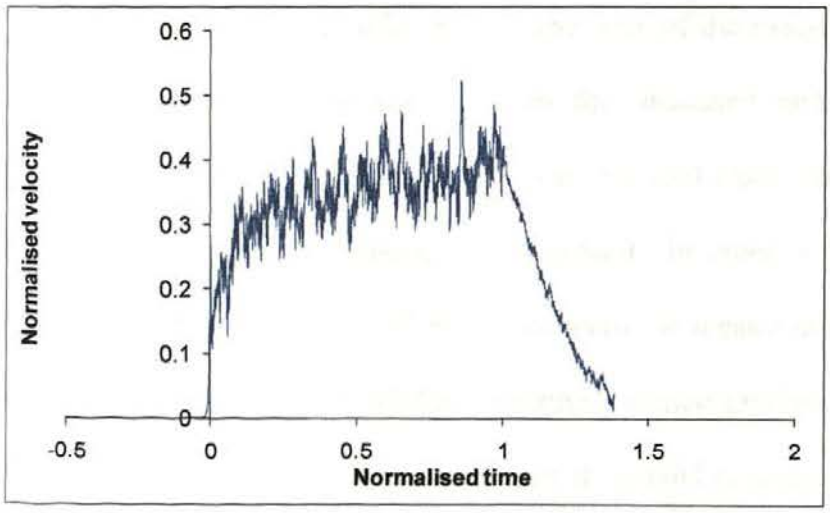

Figure 3.16a. Simulated normalised slipstream at y_s = 0.705m.

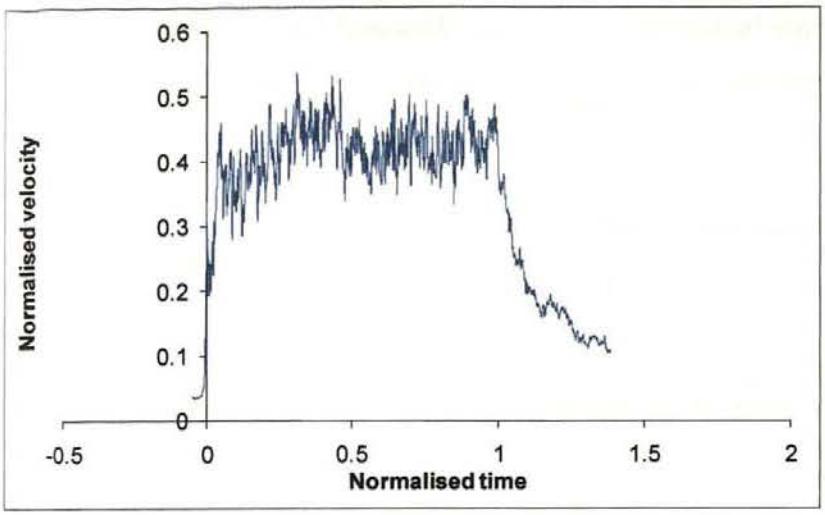

Figure 3.16b. Measured normalised slipstream at y_s = 0.705m.

Figure 3.16. Simulated and measured normalised slipstreams of a freightliner travelling along an open track at 33.6m/s.

Table 3.8 gives the magnitudes of the nose peak of the measured and simulated slipstreams, and the percentage difference between the measured and simulated peak values. The measured nose peak in Table 3.8 has been reduced from that shown in Figures 3.15b and 3.16b by the ambient normalised wind velocity in order to facilitate comparison with the simulation. The percentage differences between the measured and simulated nose peaks are -1.3% and -0.3% for the freightliner passing a station platform and travelling along an open track respectively. As these values are low the model is generating normalised velocity peaks at the nose of a freightliner with reasonable accuracy. Section 3.6.2.5 gives a further quantitative comparison of the simulated and measured normalised slipstream velocity profiles of a freightliner.

Freightliner	Measured slipstream	Simulated slipstream	Percentage difference
Passing a station platform	0.079	0.078	-1.3%
Travelling along an open track	0.296	0295	-0.3%

Table 3.8. Normalised velocity peak magnitudes at the nose of a full-scale freightliner with a speed of 33.6m/s.

3.6.2.4 Wavelet spectra plot.

The wavelet spectra plots for a freightliner passing a station platform when y_s = 1.5m and a freightliner travelling along an open track when y_s = 0.705m are given in Figures 3.17 and 3.18 respectively, for T = 1. The simulated and measured wavelet spectra plots are very similar at low frequencies, but diverge at higher frequencies, indicating that the model reproduces the large scale turbulence of a freightliner more accurately than the small scale turbulence. Section 3.6.2.5 gives the values of d for a freightliner at all values of T to determine the accuracy of the model in the frequency domain.

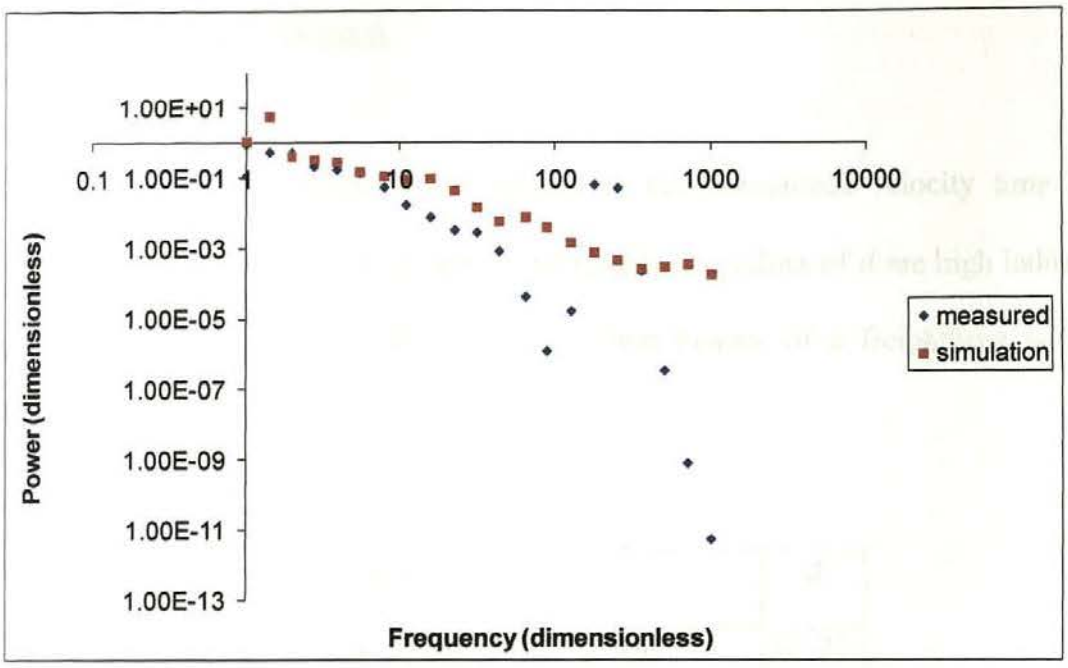

Figure 3.17. Wavelet spectra plots of the measured and simulated slipstreams at T = 1 and y_s = 1.5m for a full-scale freightliner travelling at 33.6m/s past a station platform.

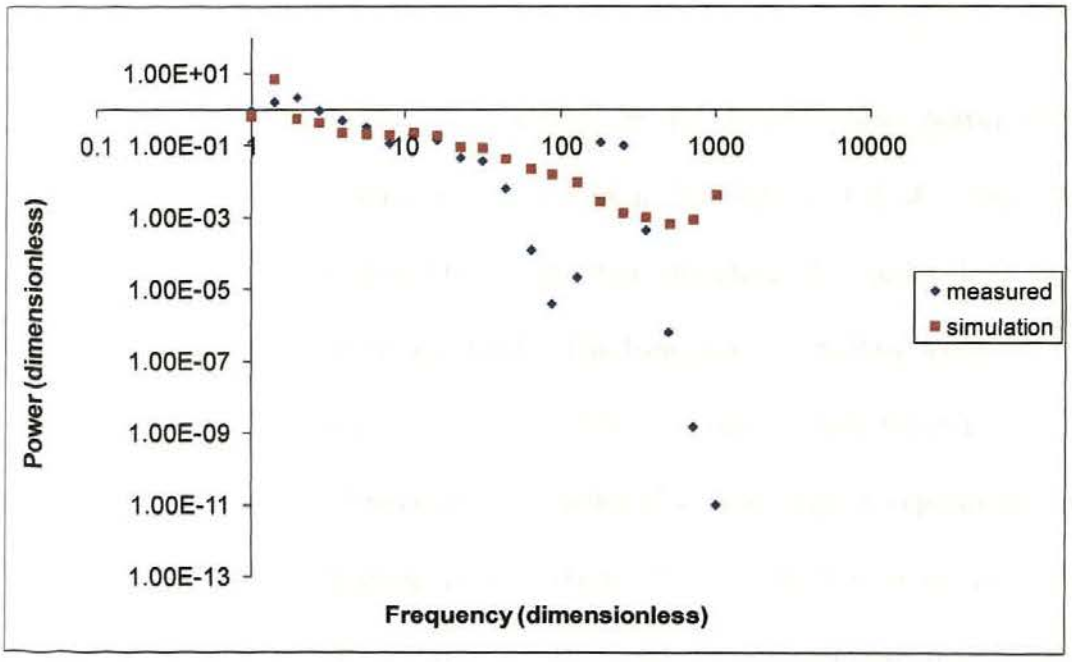

Figure 3.18. Wavelet spectra plots of the measured and simulated slipstreams at T = 1 and y_s = 0.705m for a full-scale freightliner travelling at 33.6m/s along an open track.

3.6.2.5 Model Validation.

Table 3.9 gives the values of d relating to the normalised velocity time history of a freightliner, allowing for the ambient wind speed. The values of d are high indicating that the model reproduces the normalised velocity time history of a freightliner with reasonable accuracy.

Train	d
Freightliner passing a station platform (y_s = 1.5m)	0.923
Freightliner travelling along an open track (y_s = 0.705m)	0.934

Table 3.9. Index of Agreement (d) relating to the normalised velocity time history of a full-scale freightliner.

Figure 3.19 gives the values of d relating to the dimensionless power of the full-scale freightliner, which clearly have a wide variation. The values of d of a freightliner passing a station platform vary between 0.079 and 0.624, therefore, the model does not simulate the turbulence levels of this train accurately. The freightliner travelling along an open track has values of d that vary between 0.078 and 0.869, and only around the rear of the train are the values greater than 0.8. Therefore, the model also inadequately reproduces the turbulence levels of a train travelling along an open track. This was the best model of a freightliner that could be developed within the time available, and the low values of d in Figure 3.19 reflect the difficulty in modelling the turbulence within a freightliner's slipstream. The difficulty is likely to be due to the complexity of the turbulence of the freightliner involved in the full-

scale tests which consisted of wagons of various types and various loadings, and which would have been much more aerodynamically rough than a passenger train.

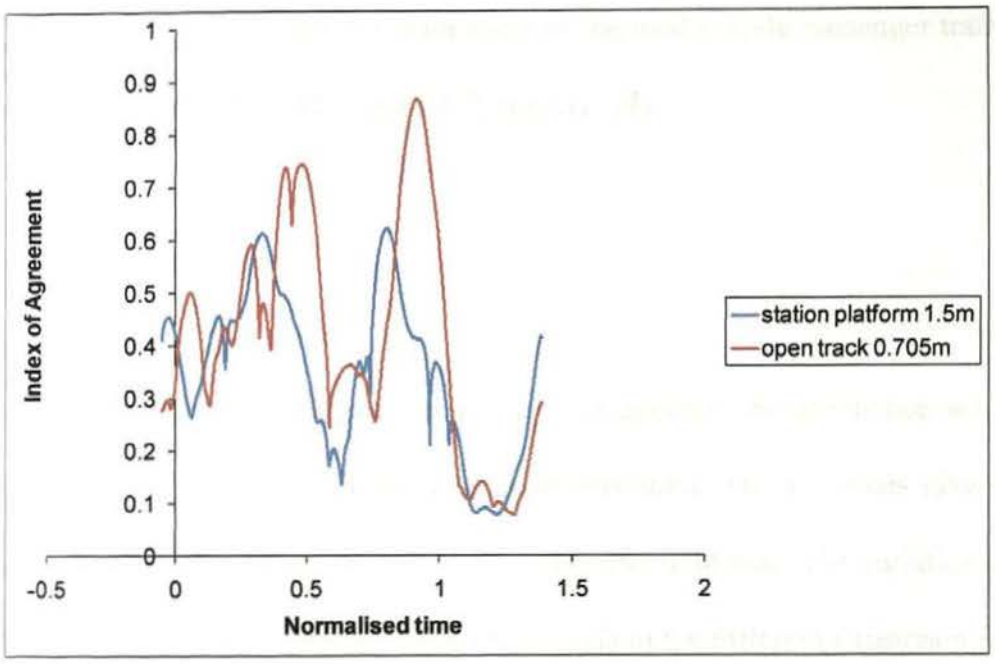

Figure 3.19. Index of Agreement (d) relating to the dimensionless power of the full-scale freightliner.

3.6.3 Model-scale passenger train.

3.6.3.1 Mean velocity.

The mean slipstream velocity of the model-scale passenger train is simulated using the theories of potential flow, boundary layer development and wake decay, as for the full-scale passenger train and freightliner. The experimental results did not show a velocity peak at the rear of the train, therefore, a vortex is not included in the slipstream model for this train type. The model-scale train nose width is modelled to taper in the same manner as that of the full-

scale passenger train. As with the full-scale passenger train, modelling a tapering nose height resulted in a normalised velocity nose peak that was too small, therefore, only the tapering nose width is modelled. In order to reproduce the shape of the normalised velocity profile of the boundary layer along the main body of the model-scale passenger train the parameters n and C_1 take the values 11.5 and 10.75 respectively.

3.6.3.2 Turbulence.

Table 3.10 gives the AR coefficients used to generate the turbulence within the normalised slipstream of the 1/25th model-scale passenger train. The y_s values given are the full-scale equivalents of the distances from the model-scale train side. The variation in the values of ϕ_1 and ϕ_2 are due to the varying turbulence levels in the different slipstream regions of the train. The largest value of ϕ_3 occurs along the main body of the train indicating that this region has the greatest small scale turbulence magnitudes, which is also the case for the full-scale passenger train and freightliner. The transition region has the next highest value of ϕ_3, and then the wake. Finally, the region in front of and around the train's nose has such a low level of turbulence that $\phi_3 = 0$.

Region of train	ϕ	AR coefficient values
Upstream and around nose	ϕ_1	0.5
	ϕ_2	0.2
	ϕ_3	0
Main body	ϕ_1	0.35
	ϕ_2	0.55
	ϕ_3	0.03 if $y_s \leq 0.375$m, 0.0225 if $0.375\text{m} < y_s \leq 0.75$m, 0.0113 otherwise
Transition	ϕ_1	0.5
	ϕ_2	0.2
	ϕ_3	0.0141 if $y_s \leq 0.375$m, 0.0094 if $0.375\text{m} < y_s \leq 0.75$m, 0.007 otherwise
Wake	ϕ_1	0.65
	ϕ_2	0.1
	ϕ_3	0.0039 if $y_s \leq 0.375$m, 0.0026 if $0.375\text{m} < y_s \leq 0.0.75$m, 0.002 otherwise

Table 3.10. AR coefficients used to simulate the turbulence within the slipstream of the model-scale passenger train.

3.6.3.3 Simulated velocity time histories.

Figure 3.20 illustrates the simulated and measured normalised ensemble averaged slipstream velocity profiles of a model-scale passenger train travelling at 32m/s. The normalised velocity upstream of the train was zero, reflecting the still air environment around the moving model

rig. therefore, the simulated and measured normalised velocity profiles can be compared directly without having to allow for an ambient wind velocity. Table 3.11 gives the maximum values of the normalised velocity peak at the train's nose, as well as the percentage difference between the peak values. The model generates normalised velocity peaks that are of smaller magnitudes than those of the measured slipstreams, and the percentage difference between the simulated and measured peaks becomes smaller with decreasing values of y_s. Hence, at small values of y_s, where the large slipstream nose peak velocities occur, the model simulates the peak velocity with greater accuracy. The general shape of the measured normalised velocity profile is reproduced in the simulation. The model simulates normalised velocity magnitudes along the main body of the train, in the transition region and in the wake that are similar to those of the measured slipstreams. The delay in the growth of the measured boundary layer velocities of the model-scale passenger train is also reproduced by the simulation, as is the fact that the delay increases with increasing y_s. A visual inspection shows that the turbulence levels are reasonably well reproduced by the model, although the turbulence levels are not as accurately simulated at y_s = 10mm (0.25m full-scale equivalent) compared to the larger values of y_s. A quantitative comparison of the simulated and measured normalised slipstream velocities, including turbulence, is given in Section 3.6.3.5.

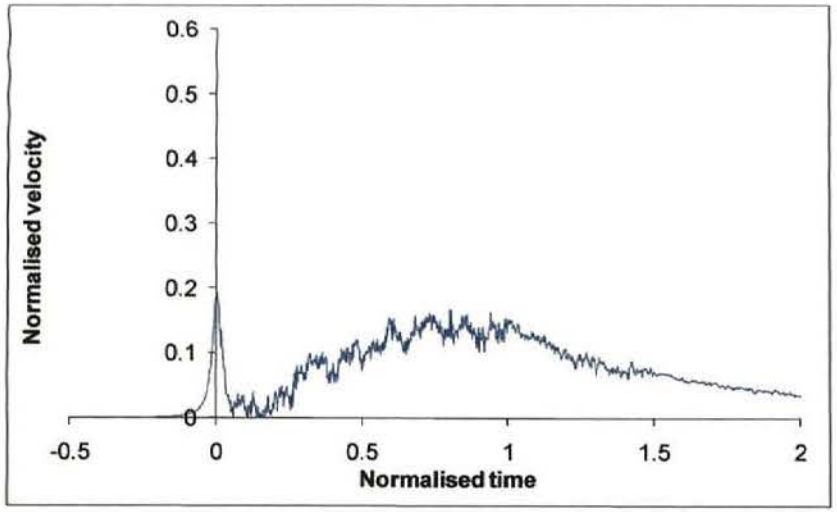

Figure 3.20a. Simulated normalised slipstream at y_s = 10mm.

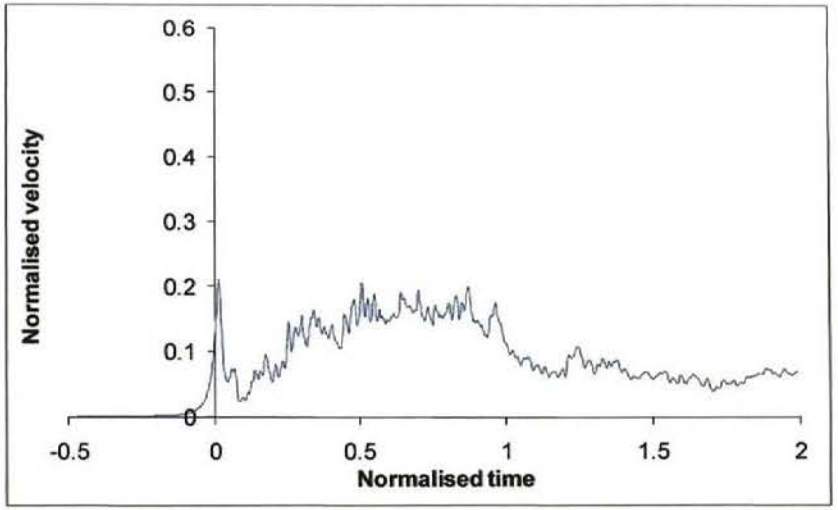

Figure 3.20b. Measured normalised slipstream at y_s = 10mm.

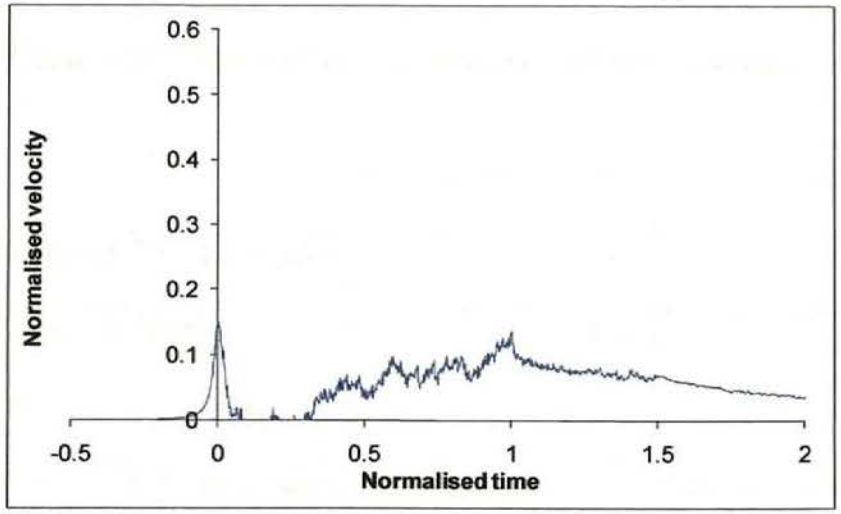

Figure 3.20c. Simulated normalised slipstream at y_s = 20mm.

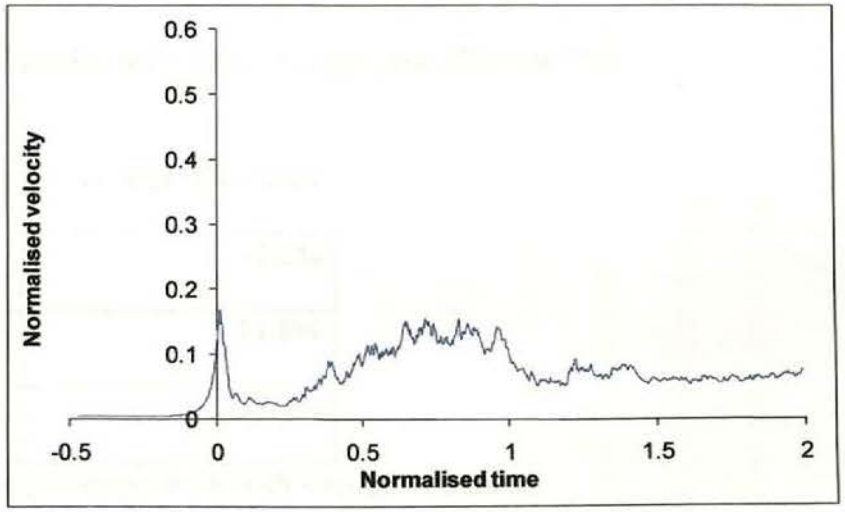

Figure 3.20d. Measured normalised slipstream at y_s = 20mm.

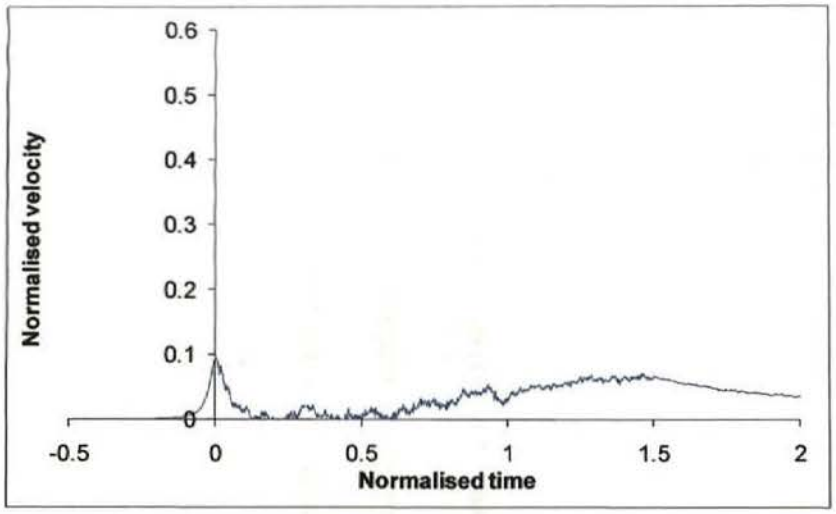

Figure 3.20e. Simulated normalised slipstream at y_s = 40mm.

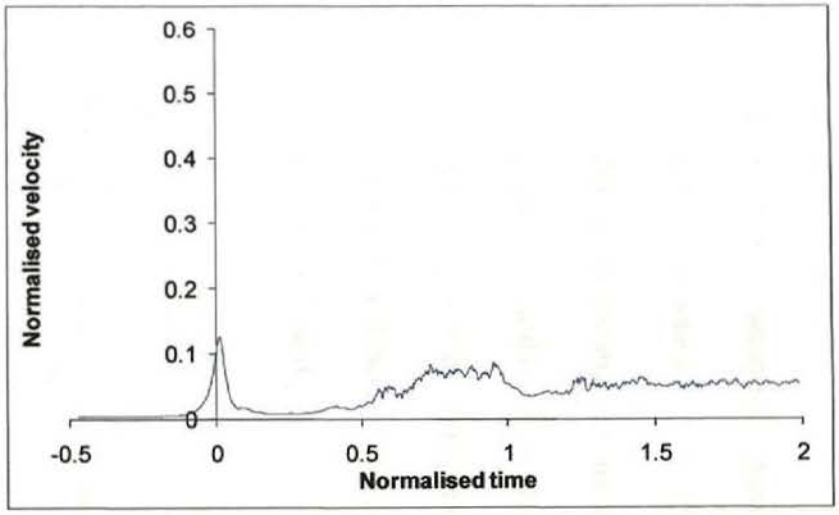

Figure 3.20f. Measured normalised slipstream at y_s = 40mm.

Figure 3.20. Simulated and measured normalised slipstreams of a 1/25th model-scale passenger train travelling at 32m/s.

y_s	Measured slipstream	Simulated slipstream	Percentage difference
10mm (0.25m full-scale)	0.211	0.195	-7.6%
20mm (0.5m full-scale)	0.169	0.149	-11.8%
40mm (1m full-scale)	0.126	0.096	-23.8%

Table 3.11. Normalised velocity nose peak magnitudes of a model-scale passenger train with a speed of 32m/s.

3.6.3.4 Wavelet spectra plot.

Figure 3.21 shows the wavelet spectra plots of the measured and simulated slipstreams at y_s = 10mm (0.25m full-scale) when T = 1. There is a reasonable match between the wavelet spectra plots within the mid-range of the normalised frequencies. However, as with the full-scale passenger train, the simulation is not as accurate at the lowest frequency or at the highest frequencies. Figure 3.21 gives an example of how accurately the model simulates a slipstream in the frequency domain, and Section 3.6.3.5 investigates this accuracy further by giving the values of d at all values of T and y_s

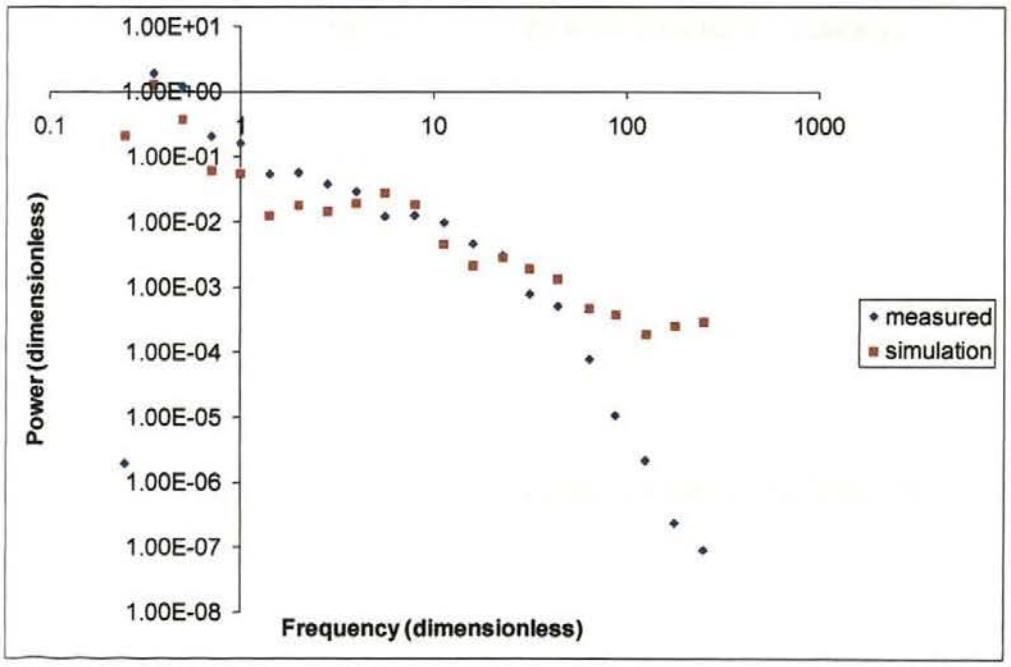

Figure 3.21. Wavelet spectra plots of the measured and simulated slipstreams at T = 1 and y_s = 10mm (0.25m full-scale) for a model-scale passenger train travelling at 32m/s along an open track.

3.6.3.5 Model validation.

Table 3.12 gives the values of d relating to the normalised velocity time history of the model-scale passenger train which lie between 0.841 and 0.888. Therefore, the model reproduces the normalised velocity profiles with reasonable accuracy. The values of d increase with decreasing y_s, as with the full-scale passenger train. Therefore, the normalised velocity profiles are more accurately reproduced where the highest velocities occur and a person is most at risk of losing their balance. The accuracy of the model to reproduce the power spectra of the slipstreams is quantified in Figure 3.22, which shows that the values of d lie between 0.87 and 0.97. Therefore, the model simulates both the normalised velocity time history and the turbulence levels within the slipstream with reasonable accuracy.

y_s	d
10mm (0.25m full-scale)	0.888
20mm (0.5m full-scale)	0.845
40mm (1m full-scale)	0.841

Table 3.12. Index of Agreement (d) relating to the normalised velocity time history of a model-scale passenger train.

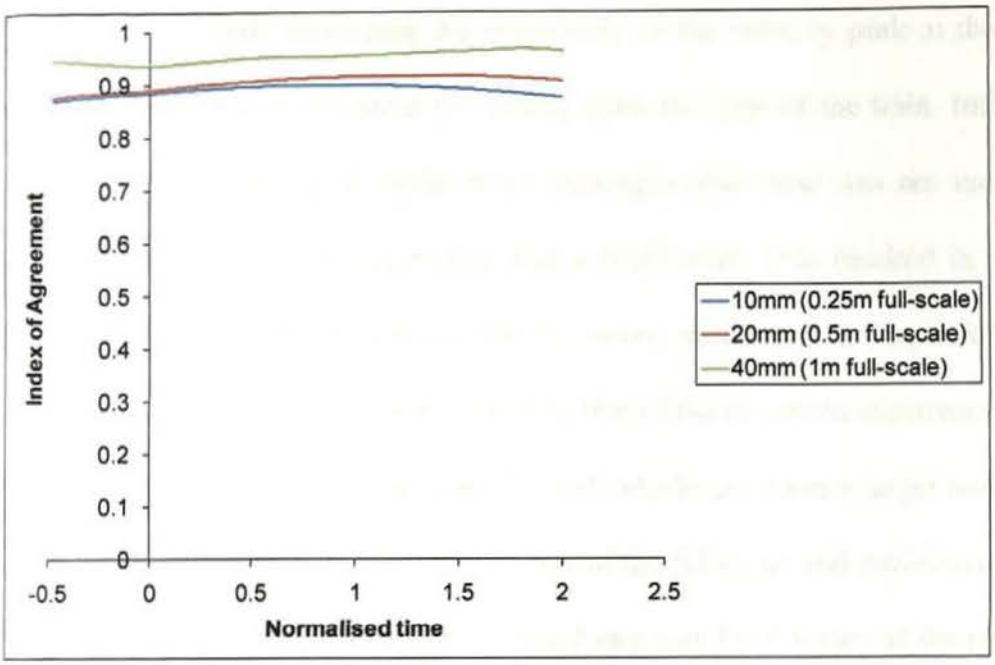

Figure 3.22. Index of Agreement (d) relating to the dimensionless power of the model-scale passenger train.

3.7 Discussion.

Previous experiments undertaken on a full-scale passenger train (Johnson *et al.*, 2004), a full-scale freightliner (Temple and Dalley, 2001), and a model-scale passenger train (Baker *et al.*, 2001) had identified a number of flow regions of a train slipstream, as described in Section 2.2.1. The theory associated with each of these regions is used as the basis of a mathematical model to simulate the mean velocity profile of a slipstream. The regions that are common to all of the train types are the upstream/nose, boundary layer and wake regions. The theories of potential flow, boundary layer growth on a flat plate, and wake decay are used for the upstream/nose region, the main body of the train, and in the wake when $T \geq 1.5$, respectively.

In order to correctly reproduce the magnitude of the velocity peak at the nose of the train certain adaptations are required depending upon the type of the train. Initially, the tapering width of the full-scale and model-scale passenger train nose was not incorporated into the model, therefore, the passenger train had a bluff nose. This resulted in simulated velocity peaks at the nose that were too large. However, modelling the tapered width reduces the magnitude of the simulated velocity peak to that of the measured slipstream. Altering the nose shape in this manner shows that a bluff-nosed vehicle generates a larger nose velocity peak, as described in Section 2.2.2. The rear carriage of the full-scale and model-scale passenger trains also tapers in width, but this is not modelled as a simulated vortex at the rear of the full-scale train generates the correct slipstream velocity magnitudes in this region, and the velocity magnitudes at the rear of the model-scale train are correct without modelling the tapering. In order to generate the correct velocity magnitude of the nose peak of the bluff-nosed freightliner, adaptations are made to the width along the locomotive. Modelling an effective Y value that is 15% greater and 18% lower than the actual Y value for the freightliner passing by a station platform and along an open track, respectively, results in the correct nose peak velocity being reproduced. That such an alteration is necessary to simulate the correct velocities suggests that the potential flow theory as adapted by Sanz-Andrés *et al.* (2004a), and used in the model, is not as appropriate for bluff-nose vehicles as it is for streamlined vehicles. This agrees with the conclusion of Sanz-Andrés *et al.* (2004a) that the adapted potential flow theory gives a quantitative representation of the velocities only for streamlined vehicles (as mentioned in Section 2.4).

In the literature reviewed for the current research, no theory has been found that reproduces the velocity peak at the rear of the train, and the first attempt to model this region involved

extending the length of the train and, therefore, the boundary layer region, into the wake and widening the width of the train along this extended length. Although this method produced a velocity peak at the rear of the train it was unsatisfactory because it did not model the phenomenon that is actually occurring at the rear of the train, namely boundary layer separation. Modelling a vortex at the rear of the train is a more appropriate method, and so a vertical cylindrical vortex with exponential decay is incorporated into the slipstream model. The vortex results in very low velocities until just before the peak then the velocity rapidly increases, reaches a maximum magnitude, rapidly decreases, then becomes very small. As the velocity is very small before the rapid increase and after the rapid decrease, the vortex's 'zone of influence' is modelled to start at $T = 1$, where the vortex velocities are added on to the final boundary layer velocity, and the 'zone of influence' acts only for the length of the vortex's diameter. In the measured slipstream, however, the velocity starts to increase before the end of the train. The maximum velocity of the simulated peak occurs shortly after $T = 1$, which accurately reproduces the measured slipstreams at the smaller values of y_s. For example, at $y_s = 0.57$m, the measured and simulated maximum velocity of the rear peak occurs at $T = 1.001$ and $T = 1.002$, respectively, for a 363.8m long train travelling at 51m/s past a station platform. As the value of y_s increases, the measured velocity peak occurs at larger values of T, hence, the accuracy of the occurrence of the simulated peak reduces. However, the magnitude of the velocity peak decreases with increasing y_s, therefore, the rear peak is modelled with reasonable accuracy for the slipstreams which impose a greater risk to a person. The vortex model reproduces the mean characteristics of the velocity at the rear of a full-scale passenger train in that the velocity peaks shortly after $T = 1$ and then dies off after the rear of the train has past. A Rankine vortex with linear velocity decay outside the circumference was also tested, but was rejected as no combination of the decay constants was

found that generated the correct maximum velocity for all distances from the train side. Vortices other than that of a vertical cylinder were considered for the model, such as a horizontal cylindrical vortex, however, these have velocities which are dependent upon height. As there is insufficient data available to determine how velocity varies with height, it is assumed that height does not affect slipstream velocity. Therefore, only a vertical cylindrical vortex can be modelled as its velocity only varies with longitudinal and lateral distance. A transitional region in the model links the wake region to the velocities at the rear of the train. Initially, a linear relationship existed between the normalised time and the normalised slipstream velocity in this region, but a quadratic relationship reproduces the shape of the normalised velocity profile more accurately, and is therefore included in the model.

A modified AR model of the order two is incorporated into the slipstream model in order to simulate the turbulence-induced fluctuations of the velocity time series. Before the AR model given in equation (3.9) was adopted, the AR model used to reproduce the turbulence originally had the equation:

$$\tilde{U}_T = U_T + \phi_1\left(\bar{\bar{U}}_{T1} - \bar{U}_{T1}\right) + \phi_2\left(\bar{\bar{U}}_{T2} - \bar{U}_{T2}\right) + \phi_3 a_t U_T \tag{3.26}$$

where:

$$\bar{\bar{U}}_{T1} = \frac{1}{10}\sum_{i=T-1}^{T-10} \tilde{U}_i \qquad \bar{U}_{T1} = \frac{1}{10}\sum_{i=T-1}^{T-10} U_i \qquad \bar{\bar{U}}_{T2} = \frac{1}{10}\sum_{i=T-11}^{T-20} \tilde{U}_i \qquad \bar{U}_{T2} = \frac{1}{10}\sum_{i=T-11}^{T-20} U_i$$

Therefore, the AR model was originally based on the average of ten previous fluctuating normalised velocities minus the average of ten previous mean normalised velocities. Also, the white noise term was multiplied by the normalised mean velocity. However, the actual AR model adopted for the slipstream model improves the accuracy of the generated turbulence in both the time and frequency domains.

In general, the shape of the velocity profile, the magnitude of the velocities and the turbulence levels of the measured slipstreams are reasonably reproduced by the simulated slipstreams. The values of d of the velocity time history of the freightliner and the model-scale passenger train are high indicating that the slipstreams of these trains are simulated with reasonable accuracy. The values of d of the velocity time history a full-scale passenger train generally increase with decreasing y_s, so that d is large close to the train side indicating that the model simulates the slipstream at small values of y_s with reasonable accuracy. Although the values of d at distances further away from the train side indicate that the model does not accurately simulate the slipstream at these greater distances, the smaller slipstream velocities at large y_s values do not impose such a risk to a person exposed to the slipstream. Therefore, it is more important to accurately simulate the velocities close to the train side than further away, and this is achieved by the model. The exception to this is at a distance of 1.07m from the side of a full-scale passenger train passing a station platform, the d value of which is low as the model does not reproduce the 'flat' shape of the velocity time history along the main body of the train. However, no combination of the values of the boundary layer constants n and C_1 result in such a 'flat' velocity profile, and the values of the constants used in the model give the best possible simulation of this region.

As turbulence affects the stability of a person it is important that the turbulence-induced velocity fluctuations are accurately simulated, and this is ascertained by investigating the frequency domain using the mathematical technique of wavelet analysis. The wavelet spectra plots produced from this analysis show that, for the full-scale and model-scale passenger trains, the worst match of the dimensionless power between the simulated and measured slipstreams occurs at the lowest frequency, i.e. the largest scale, for all values of y_s and T. However, the wavelet spectra plots of the freightliner slipstreams show that there is a good match of the dimensionless power between the simulated and measured slipstreams at the lowest frequency for all values of T. This indicates that the largest scale of a freightliner's turbulence is simpler to reproduce than that of a passenger train which is likely to be due to the simpler large scale shape of a freightliner's slipstream. The match of the dimensionless power between the simulated and measured slipstreams of all train types is good at the mid-range of frequencies for all values of y_s and T, but then decreases with increasing frequency especially with the freightliner. This shows that it is increasingly difficult to simulate the turbulence as the scale becomes smaller. In general, the values of d associated with the turbulence of the full-scale and model-scale passenger trains are high indicating that the energy distribution of the turbulence is reproduced with reasonable accuracy. The exception to this is at a distance of 0.41m from the side of a full-scale passenger train travelling along an open track. Decreasing the values of ϕ_2 and ϕ_3 reduces the values of d of this particular slipstream, therefore, increasing ϕ_1 and ϕ_2 would theoretically result in an improved simulation. However, increasing either ϕ_1 or ϕ_2 results in an extremely unrealistic velocity time history along the main body of the train that bears no resemblance to an actual velocity profile. Hence, the most accurate simulated turbulence occurs with the ϕ values used in the model. The energy distribution of the turbulence within the slipstream of a freightliner is also

not accurately simulated, and this is likely to be due to the complexity of the turbulence generated by the aerodynamically rough freightliner.

3.8 Conclusions.

The fluid dynamics theory associated with each slipstream region is used as the basis of a mathematical model to simulate a slipstream. Potential flow theory is used in the essentially inviscid flow region upstream and around the train nose where a velocity peak occurs at $T = 0$, the potential flow theory is also used throughout the length of the slipstream. The increasing velocities along the main body of the train are simulated using the theory of boundary layer development on a flat plate. The velocity peak due to boundary layer separation measured during the full-scale passenger train tests is simulated by a vertical cylindrical vortex placed immediately after the rear of this train. The velocity of the vortex decays exponentially beyond the vortex's circumference. The wake is delayed until $T = 1.5$ and its gradually decreasing velocity magnitudes are simulated using wake decay theory. A transitional region links the wake to the slipstream velocities at the rear of the train.

The above process results in a mean normalised velocity profile of a slipstream, and the turbulence-induced velocity fluctuations are simulated by incorporating a modified AR model of the order two into the model. The AR coefficient associated with the white noise term, ϕ_3, varies with train type, train location, slipstream region, and y_s. Larger values of ϕ_3 are used with a freightliner, a train travelling along an open track, along the main body of a train, and close to the train side reflecting where the greatest levels of turbulence occur. The energy distribution of the turbulence within a slipstream is investigated using the technique of

wavelet analysis in order to determine if the model simulates the turbulence-induced velocity fluctuations accurately. The main method of model validation uses the Index of Determination which shows that, in general, the velocity time histories and turbulence levels of the measured slipstreams are reproduced by the model with reasonable accuracy.

CHAPTER 4.

EXPERIMENTS INVESTIGATING THE RESPONSE OF A PERSON TO A SUDDEN GUST.

4.1 Introduction.

As the velocity of a train slipstream increases rapidly around the train's nose (described in Section 2.2) a set of full-scale experiments was undertaken to investigate the effects of a sudden change in wind velocity on a person. The aim of the experiments was to determine what wind velocities cause a person to be displaced and to what extent. The results were used when modelling a person's response to a train slipstream, as described in Section 5.3.4. The experiments described in this chapter are presented in a paper entitled Evaluating and modelling the response of an individual to a sudden change in wind speed. This has been accepted by the journal Building and Environment and is given in Appendix 2.

4.2 Equipment and volunteers.

The experiments were undertaken in the environmental working section of the dynamic circuit of the Jules Verne Climatic Wind Tunnel at CSTB in Nantes, France. This section is 25m long, ranges from 10m to 15m wide, and has an average cross-sectional area of $100m^2$. Six variable-pitch propeller fans with 3200kW propulsion generate the airflow within the tunnel, and can be controlled to vary the oncoming flow. However, the rotation of the fans immediately after being at rest is not fast enough to be able to reproduce the rapid change in wind velocity as would be experienced by an individual exposed to a train slipstream.

Therefore, in order to generate a wind velocity time history which approximates that required a novel gust generating device was created by attaching two 2m high wooden boards to the side of a forklift truck. Figure 4.1 shows the modified forklift truck in the wind tunnel. The truck was positioned in the wind tunnel perpendicular to the oncoming flow so creating a sheltered region immediately behind the screen where up to three volunteers could stand at any one time. When the required upstream wind velocity was established, the forklift truck was driven across the wind tunnel, thereby exposing the volunteers to the oncoming flow, i.e. they experienced a sudden gust.

Figure 4.1. Forklift truck with wooden boards attached.

The responses of twenty nine individuals involved in the experiments are presented in this chapter, twelve of the individuals were female and seventeen male. For purposes of classification the volunteers were divided into the age ranges of 18-24, 25-30, 31-40 and 41-50, with 69%, 14%, 7% and 10% of the volunteers being in the age ranges respectively. No

volunteers were over the age of fifty years, and therefore were all young or middle-aged. The average mass was 53.4kg and 72.2kg for the females and males, respectively. Details of the volunteers' mass, height, and age are given in Appendix 3.

4.3 Initial tests.

Initial tests were undertaken without the presence of the volunteers in order to determine the velocity time history produced immediately downwind of the modified forklift truck when the forklift truck was driven across the wind tunnel. A Gill Solent ultrasonic anemometer recorded the wind velocities at a height of 1.5m above the ground immediately behind the wooden boards attached to the forklift truck when the oncoming longitudinal wind velocity in the wind tunnel was set at 7, 10, 12, 15 and 20m/s. Figure 4.2 shows the resultant velocity time history of the longitudinal and lateral components of the wind for each of the sudden gusts. The resultant is presented because the simulated train slipstreams generated by the model in the current research are based upon the resultant of the longitudinal and lateral components of the train slipstreams measured during previous experiments (described in Section 2.2). The average velocities recorded by the anemometer prior to the forklift truck being driven away are not zero due to the circulation of air within the sheltered region. A rapid change in velocity is illustrated clearly, and occurs in less than 0.5s for each of the oncoming flows. The turbulence intensity during the initial 5s after the rapid velocity change is 0.22, 0.22, 0.22, 0.15 and 0.07 with the oncoming flow of 7, 10, 12, 15 and 20m/s respectively. The turbulence intensity was only calculated for the initial 5s as the volunteers had attained their maximum displacement by this time, therefore, a person's response

occurred during this time interval. However, the turbulence levels would have played a minor role in a volunteer's destabilisation compared to the step change in velocity.

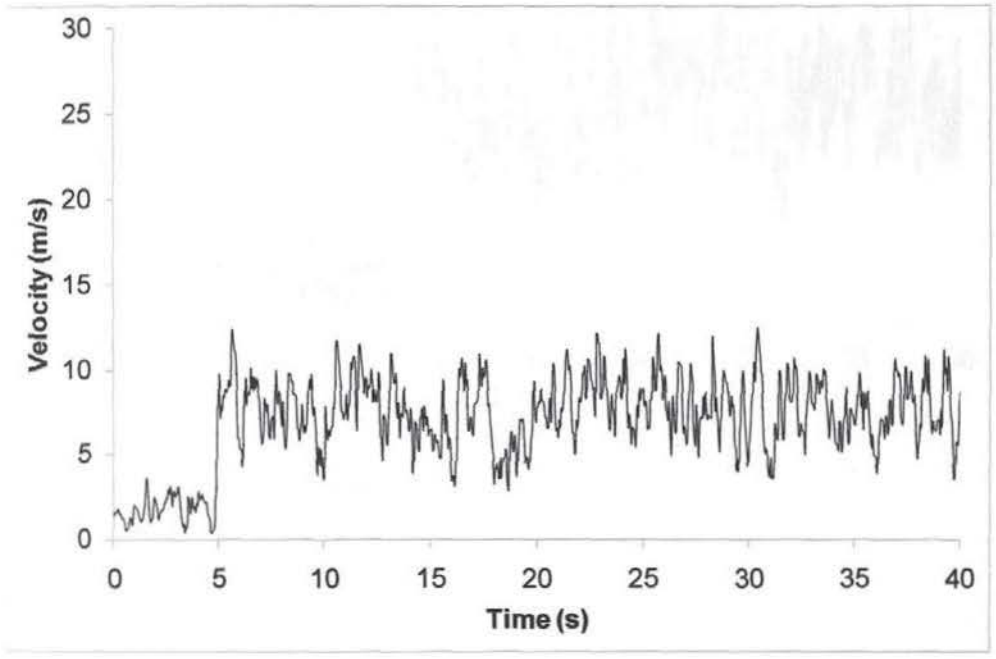

Figure 4.2a. Oncoming flow of 7m/s.

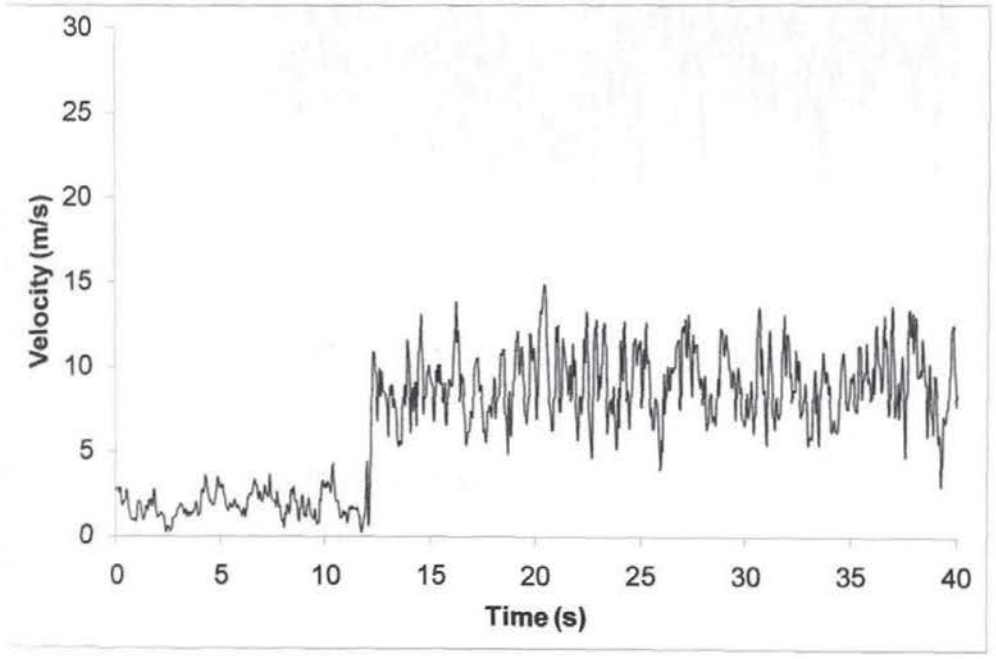

Figure 4.2b. Oncoming flow of 10m/s.

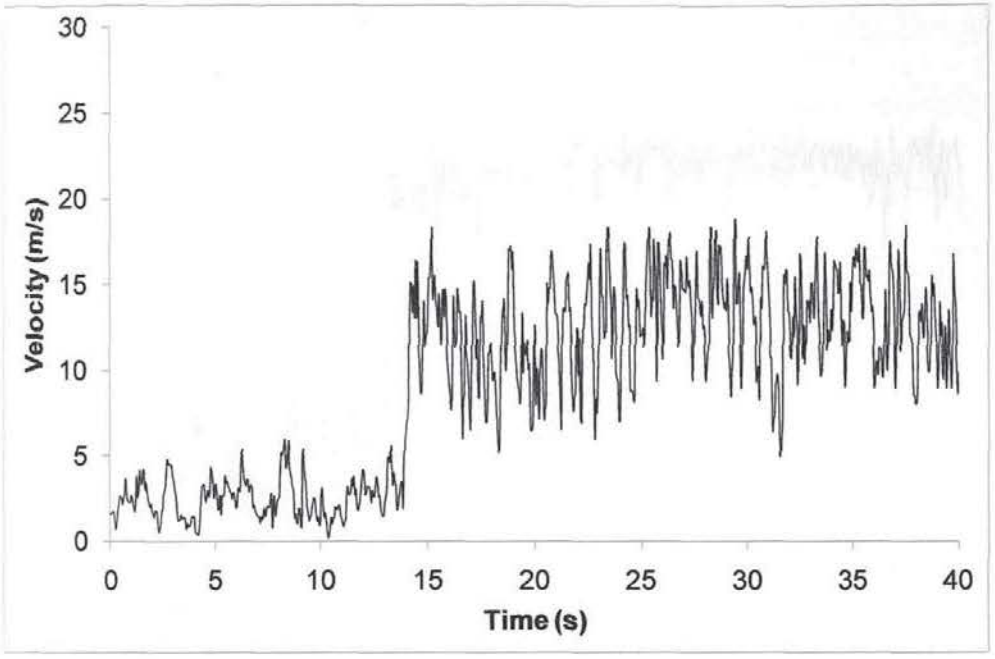

Figure 4.2c. Oncoming flow of 12m/s.

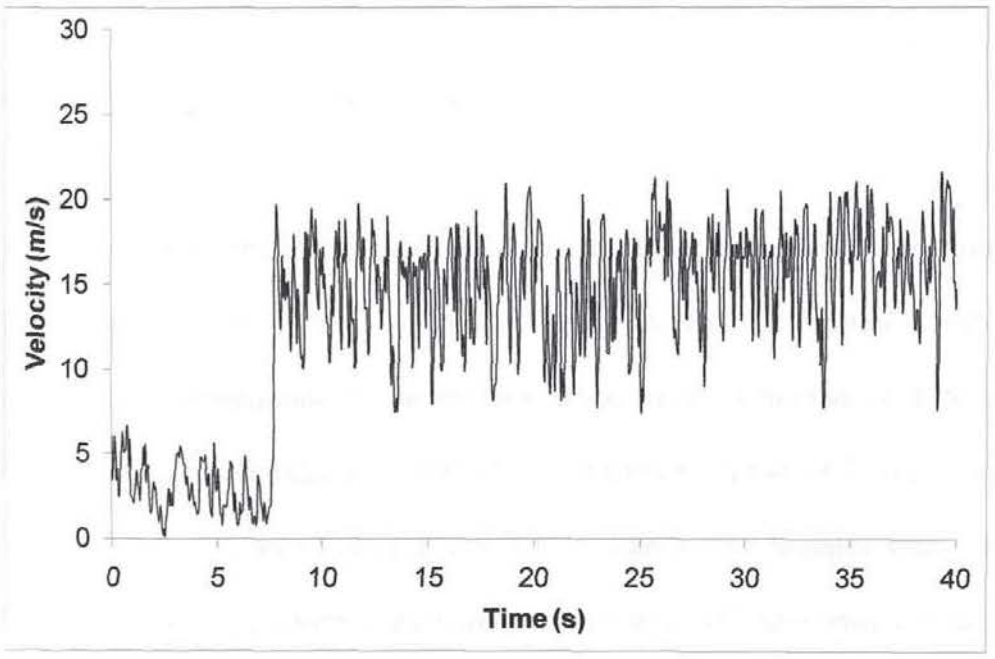

Figure 4.2d. Oncoming flow of 15m/s.

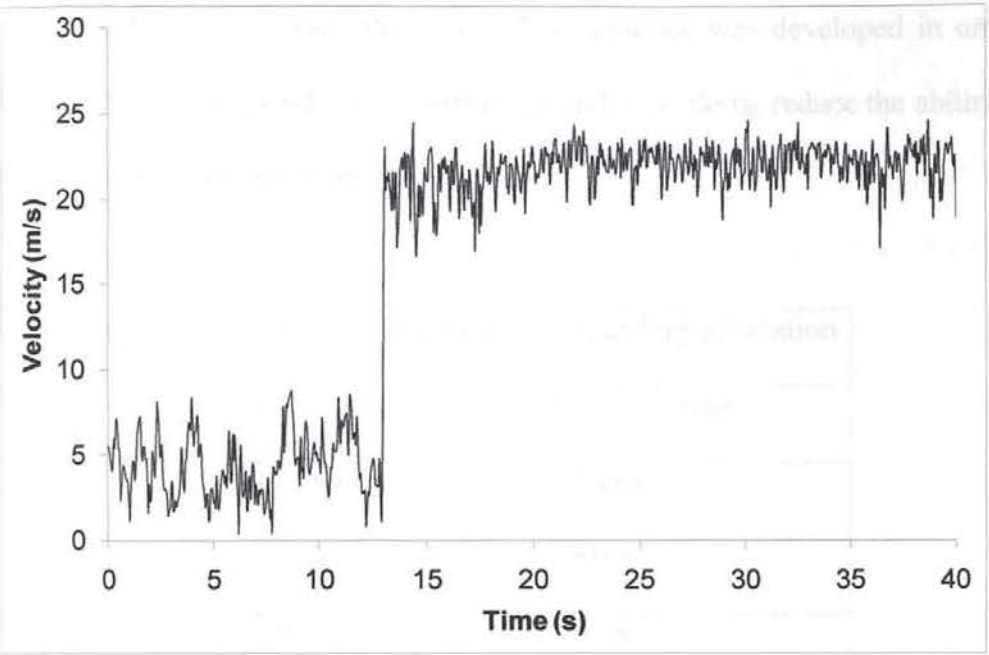

Figure 4.2e. Oncoming flow of 20m/s.

Figure 4.2. Velocity time histories of the gusts generated in the wind tunnel.

4.4 Experimental procedure.

For each experiment undertaken the volunteers stood in the sheltered region behind the screen in groups of two or three, either facing the screen (front orientation), with their backs to the screen (back orientation) or side-on (side orientation). A number of different wind velocities were used, with all individuals tested with oncoming flows of 7, 10, 12 and 15m/s, and the males tested with an additional velocity of 20m/s. The females were not tested with this higher velocity as a safety precaution because some of them were displaced significantly at 15m/s. Each standing position experienced all the different oncoming wind velocities, and Table 4.1 shows the sequence of tests carried out on the female and male volunteers, with the column headed 'Gust velocity' representing the predetermined oncoming wind velocity. The volunteers were first subjected to 10m/s with the front orientation, and were then subjected to

12m/s with the side orientation, etc. This sequence was developed in order to introduce a degree of uncertainty into the experiments and in so doing reduce the ability of the volunteers to prepare for changes in the wind velocity.

Gust velocity (m/s)	Standing orientation	Standing orientation
	Female	Male
10	Front	Front
12	Side	Side
7	Back	Back
15	Front	Front
20		Side
10	Side	Back
12	Back	Front
7	Front	Side
15	Side	Back
20		Front
10	Back	Side
12	Front	Back
7	Side	Front
15	Back	Side
20		Back

Table 4.1. Sequence of gust velocities and standing positions.

The responses of the volunteers to the rapid change in wind velocity were recorded using a digital video camera. An individual was judged to have been displaced if they stepped in any direction with either one or both feet when exposed to the oncoming wind. However, if an individual pivoted on their toes or heels then they were not judged to have been displaced.

4.5 Experimental stability analysis.

4.5.1 Qualitative analysis.

Figure 4.3 is a series of photographs from an experiment involving a group of females facing an oncoming wind velocity of 15m/s. Figure 4.3a shows the individuals sheltered behind the screen, and Figure 4.3b illustrates that after one second the screen had been completely removed and the individuals were subjected to the oncoming flow. Figure 4.3b also shows that there is a slight time delay in the response of the individuals, with the person farthest from the camera being displaced last of all. Figure 4.3c illustrates the displacement of the participants two seconds after the screen had been removed and shows the maximum displacement of each of the participants. The squares on the wind tunnel floor measure 2m by 2m; therefore, the volunteer closest to the camera has one foot displaced by nearly 2m in Figure 4.3c. This figure shows the two largest displacement distances recorded during the whole series of experiments, although during some tests certain people were not displaced at all. Details of the experimental results are given in Appendix 3.

Figure 4.3a. A group of individuals sheltered behind the screen.

Figure 4.3b. A group of individuals mid experiment.

Figure 4.3c. The maximum displacement position of the individuals.

Figure 4.3. A group of individuals subjected to a gust velocity of 15m/s.

4.5.2 Percentage of people displaced.

Figure 4.4 illustrates the percentage of people displaced for the different gust velocities and standing orientations. The percentage of displaced people with the front orientation is given in Figure 4.4a, and this shows that the percentage of people displaced increases with increasing gust velocity and that all individuals are displaced at 15m/s. A higher percentage of females than males are displaced at all other wind velocities tested, especially at 10m/s, when 67% and 18% of females and males are displaced respectively.

Figure 4.4b concerns the percentage of people displaced by the gust velocities with the back orientation. The figure shows that the percentage of people displaced increases with increasing gust velocity and that all females and males are displaced at gust velocities of

15m/s and 20m/s respectively. There is a higher percentage of females displaced than males at all gust velocities and, as with Figure 4.4a, the difference is most noticeable at 10m/s. Comparing Figures 4.4a and 4.4b shows that the percentages displaced are similar for the front and back orientations except with 10m/s, when 18% and 0% of males are displaced with the front and back orientations respectively, and when 67% and 42% of females are displaced with the front and back orientations respectively.

Figure 4.4c concerns the percentage of individuals displaced with the side orientation, and again shows that the percentage increases with increasing gust velocity. It also shows an almost linear relationship between the percentage displaced and gust velocity for both genders. No one is displaced until 12m/s, and only 50% of the females, and 71% of males are displaced by gust velocities of 15m/s and 20m/s, respectively. This leads to the conclusion that the side orientation is significantly more stable than the other orientations tested. As with Figures 4.4a and 4.4b there are lower percentages associated with the males than females.

In Figures 4.4a-4.4c there are greater percentages of females displaced than males. However, using a t-test and testing at the 5% confidence level to investigate if males are more stable than females shows that the percentages of males displaced are only significantly lower for a gust velocity of 10m/s for the front and back orientations. For all other gust velocity/orientation combinations there is no statistical difference between males and females. Details of the results of all the t-tests undertaken for Chapter 4 are given in Appendix 4.

As the males are not significantly more stable than females, except with a gust velocity of 10m/s for the front and back orientations, the data for both genders are combined in Figure

4.4d. Figure 4.4d does not include the gust velocity of 20m/s as only males were tested with this oncoming flow. This figure shows that there is almost a linear relationship between the percentage displaced and gust velocity with the front and side orientations. The percentages displaced at 7, 12 and 15m/s are very similar for the front and back orientations; however, at 10m/s the percentage displaced for the back orientation is less than half of that for the front orientation, with 17% and 38% of individuals displaced with the back and front orientations respectively. Using a t-test and testing at the 5% confidence level confirms that the front orientation is more stable than the back orientation only for a gust velocity of 10m/s. Figure 4.4d shows that the side orientation is more stable than either the front or back orientations, and using a t-test and testing at the 5% confidence level confirms that both the front and back orientations are less stable than the side orientation for the gust velocities of 10m/s and above.

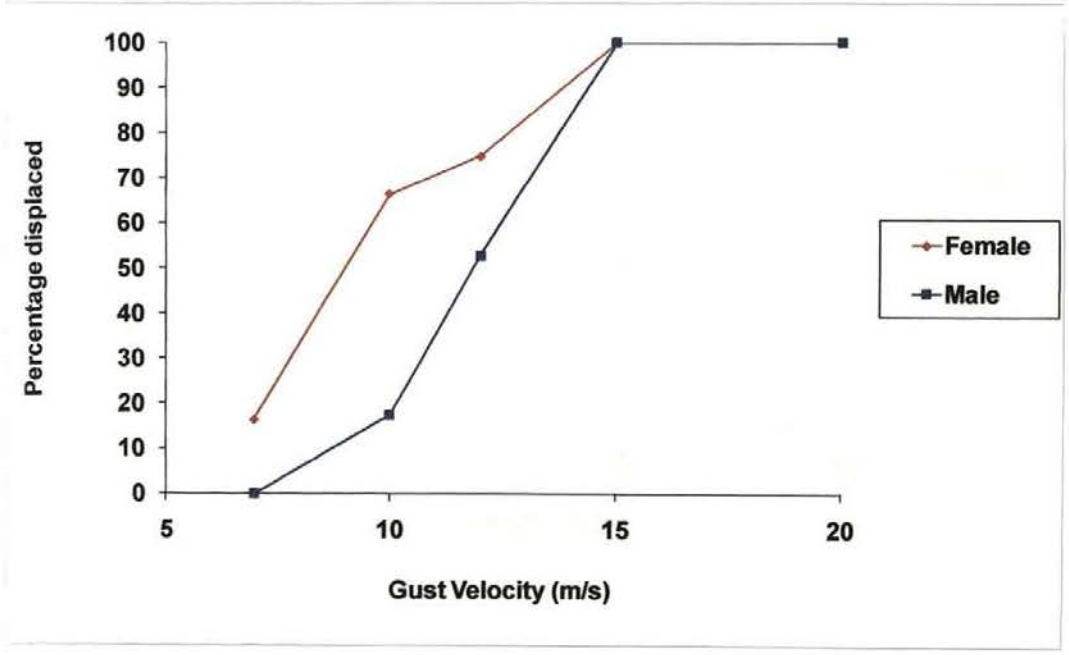

Figure 4.4a. Front orientation.

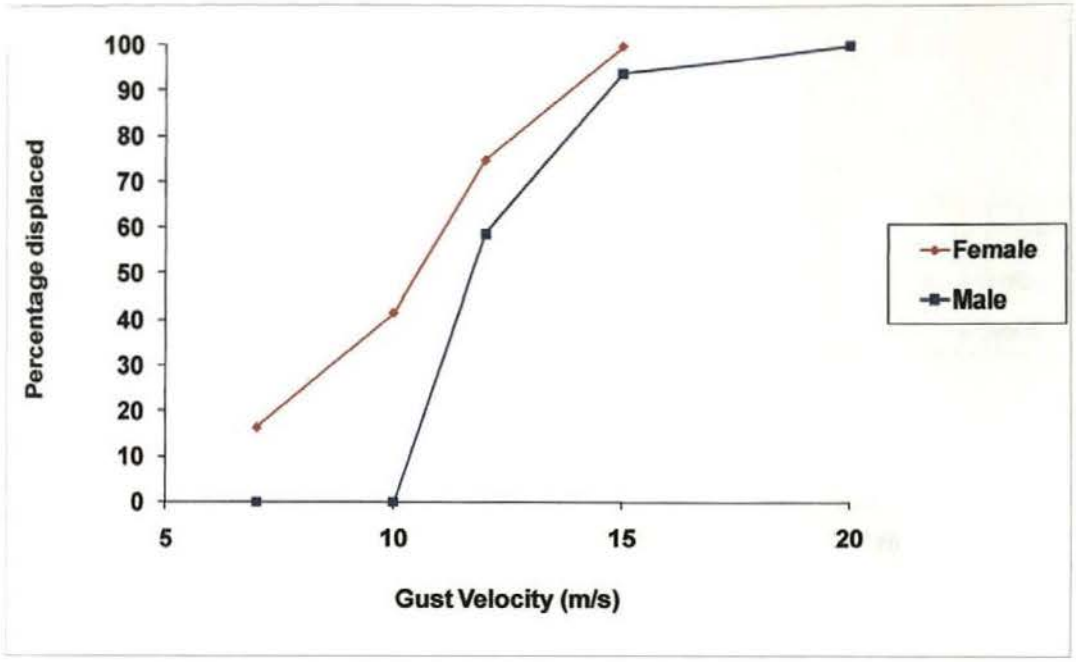

Figure 4.4b. Back orientation.

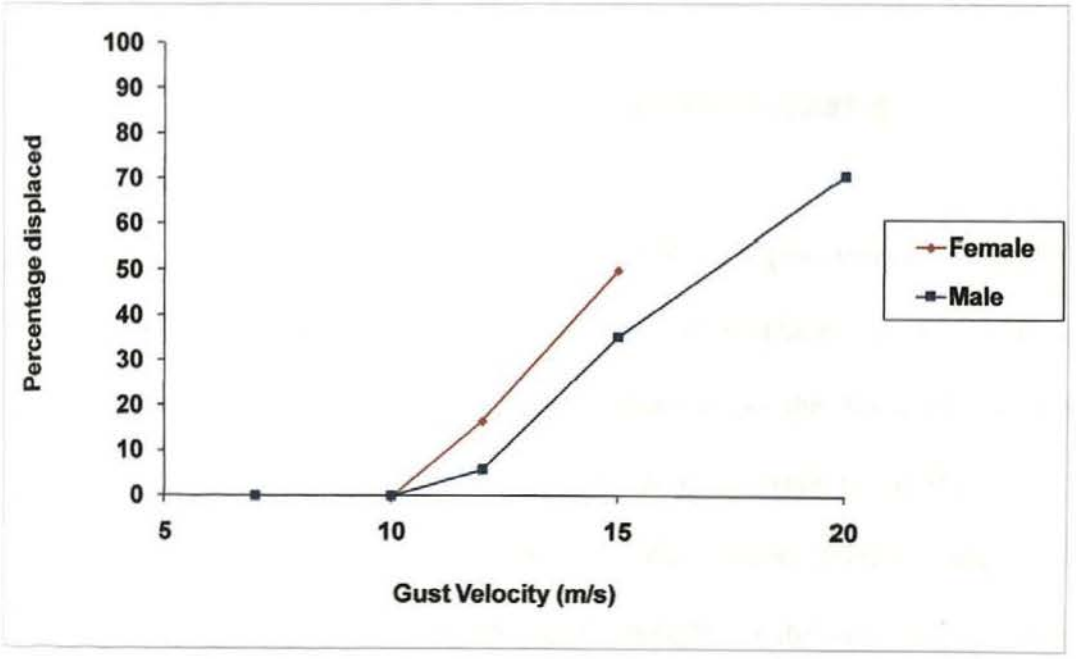

Figure 4.4c. Side orientation.

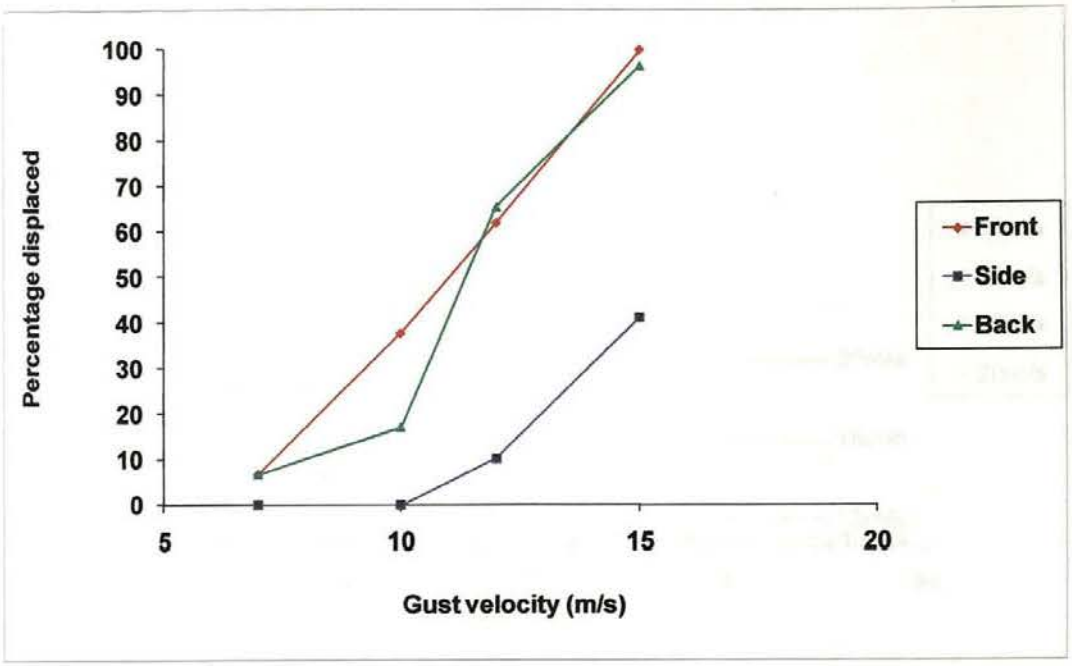

Figure 4.4d. All individuals and all orientations.

Figure 4.4. Percentage of people displaced by the gust velocities.

4.5.3 Investigating how weight affects displacement distance.

As well as determining if a person was displaced by a gust velocity, analysis of the video footage allowed the actual distance the person was displaced to be ascertained. This was possible as there were 2m by 2m squares marked on the floor of the wind tunnel, as mentioned in Section 4.5.1; however, as the distances were taken from video footage the displacements could only be determined to the nearest 50mm. Figure 4.5 shows the displacement distance of an individual against weight for the various gust velocities, and for the front and back orientations. Figure 4.5 shows a large degree of scatter, which indicates the variety in responses within the group of individuals, and the straight solid lines are the average displacement distances of the volunteers for each of the gust velocities.

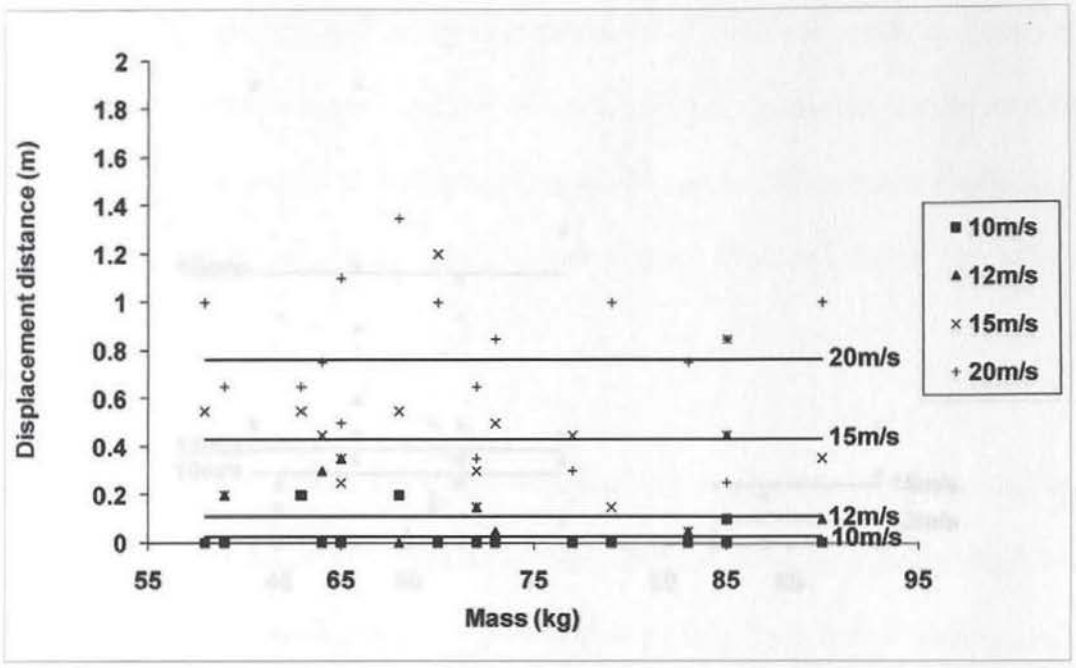

Figure 4.5a. Front orientation of males.

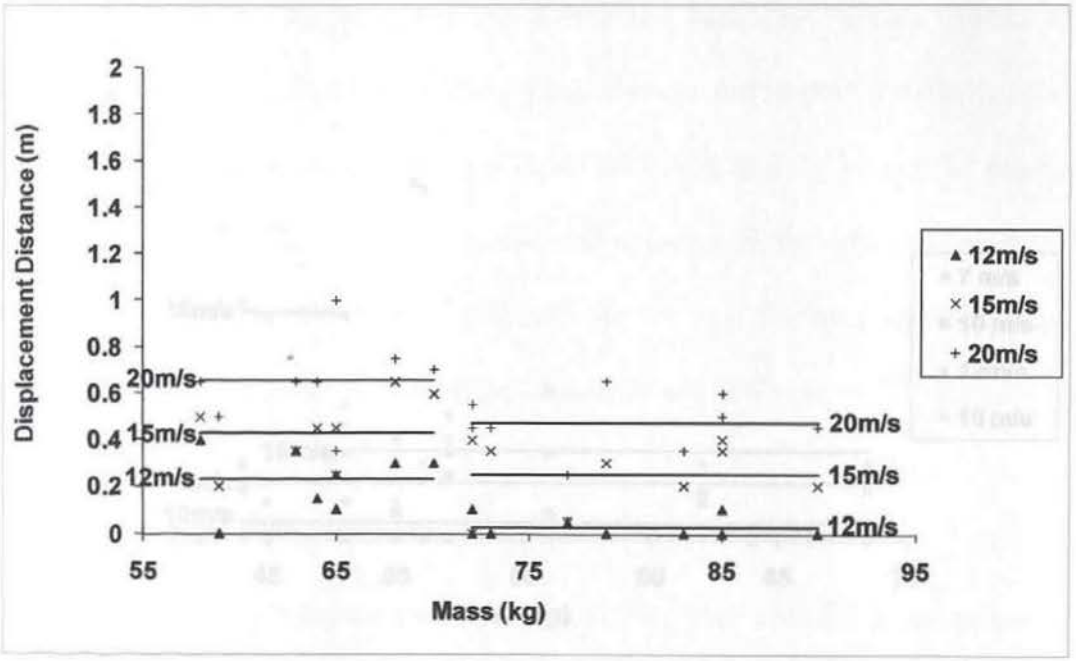

Figure 4.5b. Back orientation of males.

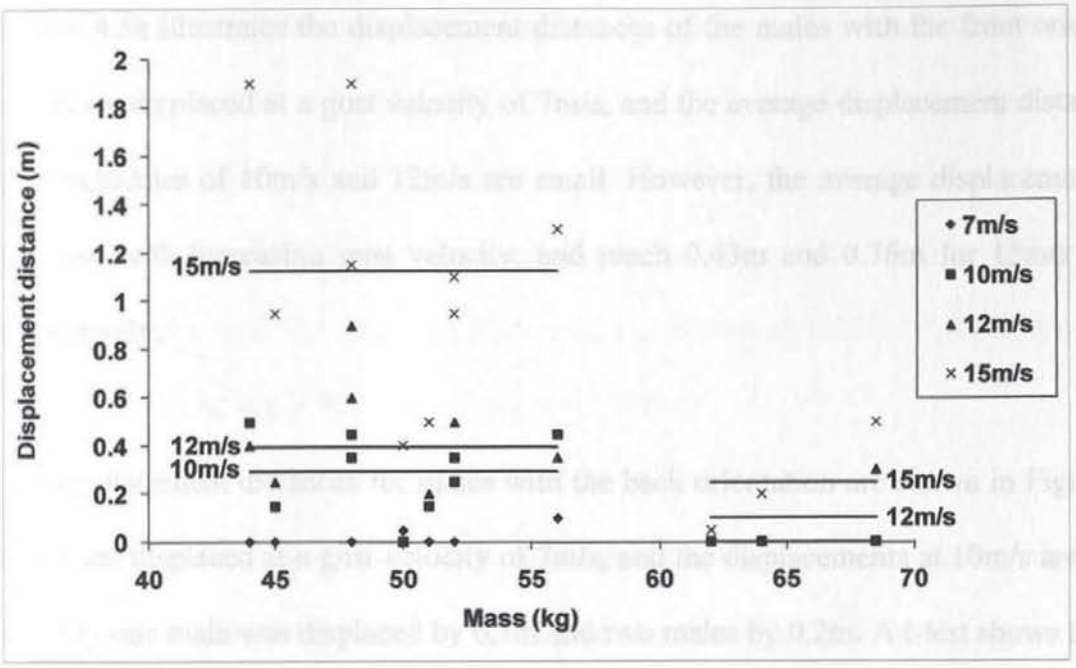

Figure 4.5c. Front orientation of females.

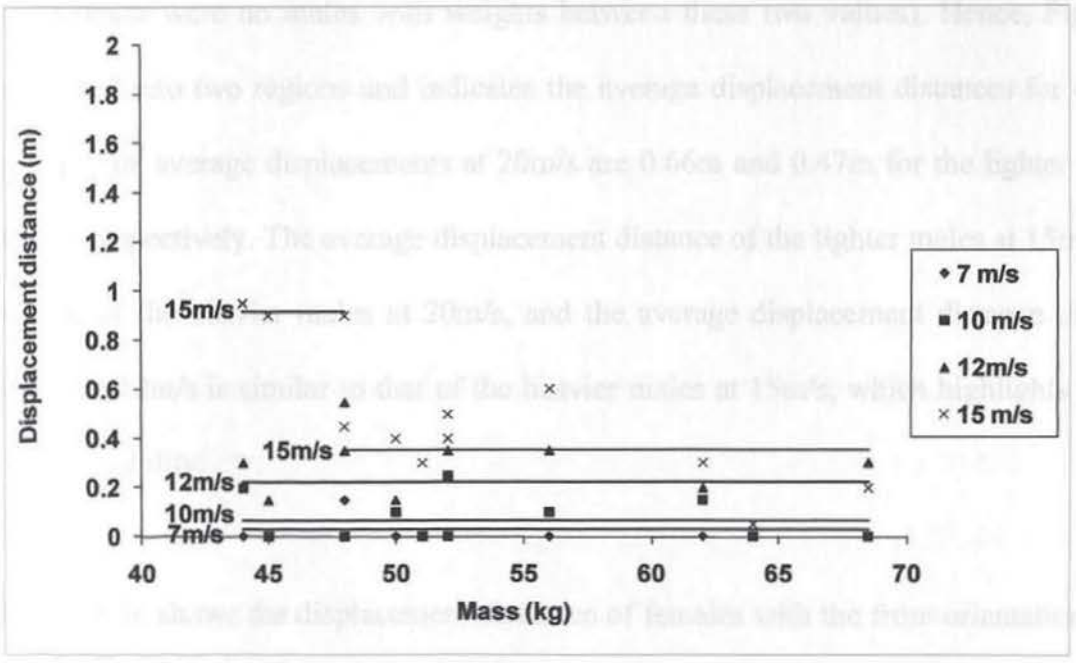

Figure 4.5d. Back orientation of females.

Figure 4.5. Displacement distances and average displacement distances of the individuals for the gust velocities.

Figure 4.5a illustrates the displacement distances of the males with the front orientation. No males are displaced at a gust velocity of 7m/s, and the average displacement distances for the gust velocities of 10m/s and 12m/s are small. However, the average displacement distances increase with increasing gust velocity, and reach 0.43m and 0.76m for 15m/s and 20m/s, respectively.

The displacement distances for males with the back orientation are shown in Figure 4.5b. No males are displaced at a gust velocity of 7m/s, and the displacements at 10m/s are very small, i.e. only one male was displaced by 0.1m and two males by 0.2m. A t-test shows that, for gust velocities of 12m/s and above, males weighing 72kg or more had significantly lower displacement distances than males weighing 70kg or less when testing at the 5% confidence level (there were no males with weights between these two values). Hence, Figure 4.5b is separated into two regions and indicates the average displacement distances for each weight group. The average displacements at 20m/s are 0.66m and 0.47m for the lighter and heavier males, respectively. The average displacement distance of the lighter males at 15m/s is similar to that of the heavier males at 20m/s, and the average displacement distance of the lighter males at 12m/s is similar to that of the heavier males at 15m/s, which highlights how weight affects stability.

Figure 4.5c shows the displacement distances of females with the front orientation, which are very low with a gust velocity of 7m/s, i.e. only two females are displaced and these by 0.05m and 0.1m. Undertaking a t-test on this data and testing at the 5% confidence level indicates that there are two separate regions in the graph, one relating to weights 56kg or less, and one corresponding to weights 62kg or more, for gust velocities of 10m/s and above (there were no

females with weights between these two values). At 15m/s, the average displacement distance of the lighter females is 1.13m which is the largest average displacement distance of all the participants, and is three and a half times greater than the average displacement distance of 0.25m of the heavier females. The average displacement distance of the heavier females at 15m/s is lower than the average displacement distance of 0.29m of the lighter females at 10m/s, indicating the effect weight has on stability.

Figure 4.5d shows the displacement distances for females with the back orientation and, as with Figures 4.5a-4.5c, illustrates that increased gust velocity is associated with increased displacement distance. Using a t-test and testing at the 5% confidence level shows that the females weighing 44kg-47.5kg, i.e. the lightest females, are less stable than the other females at the gust velocity of 15m/s. The average displacement distance of the lightest females and all other females at 15m/s is 0.92m and 0.36m respectively, therefore, the average displacement distance of the lightest females is more than two and a half times greater than that of the others.

Comparing Figure 4.5a with Figure 4.5b, and Figure 4.5c with Figure 4.5d shows that the average displacement for an individual with their back to the wind is generally less than when facing the wind. For example, males facing into a gust velocity of 20m/s have an average displacement distance of 0.76m, whereas the average displacement distance of males with the back orientation is 0.66m and 0.46m for the lighter and heavier weight group respectively for the same gust velocity. The side orientation is not included in the analysis as the displacements are very small and reasonable conclusions cannot be drawn further than that the side orientation is the most stable.

4.5.4 Wind-induced force and how it affects stability.

As the displacement distance of a person is dependent upon the gust velocity, this section investigates the relationship between the displacement distance and the wind induced force, which is a function of gust velocity. The drag force acting upon a person is given by:

$$F = {}^{1}/_{2}\,\rho C_D A u^2 \tag{4.1}$$

where F is the wind induced force, ρ is the density of air and takes the value of 1.22kg/m^3, C_D is the drag coefficient, A is the projected area, and u is the gust velocity.

Gender	Gust velocity (m/s)	$C_D A$ (m^2)	
		Front	Side
Female	7	0.546	0.373
Female	10	0.530	0.335
Female	12	0.503	0.319
Female	15	0.459	0.297
Male	7	0.649	0.438
Male	10	0.627	0.395
Male	12	0.611	0.368
Male	15	0.589	0.341
Male	20	0.557	0.308

Table 4.2. Values of drag area for stationary people in uniform flow as determined using Murakami and Deguchi (1981).

Murakami and Deguchi (1981) give values of the drag area ($C_D A$) for stationary average females and males in uniform flow for front and side orientations at various wind velocities. Interpolation of this data obtains values of the drag area for the gust velocities used in the current study, and these are given in Table 4.2. Using equation (4.1) and Table 4.2, the wind force acting on a person with the front or side orientation can be calculated, and this is given in Table 4.3.

Gender	Gust velocity (m/s)	Force (N)	
		Front orientation	Side orientation
Female	7	16.5	11.2
Female	10	32.6	20.6
Female	12	44.5	28.3
Female	15	63.5	41.1
Male	7	19.6	13.2
Male	10	38.6	24.3
Male	12	54.1	32.6
Male	15	81.5	47.2
Male	20	137.0	75.8

Table 4.3. Forces on the volunteers as calculated using Murakami and Deguchi (1981).

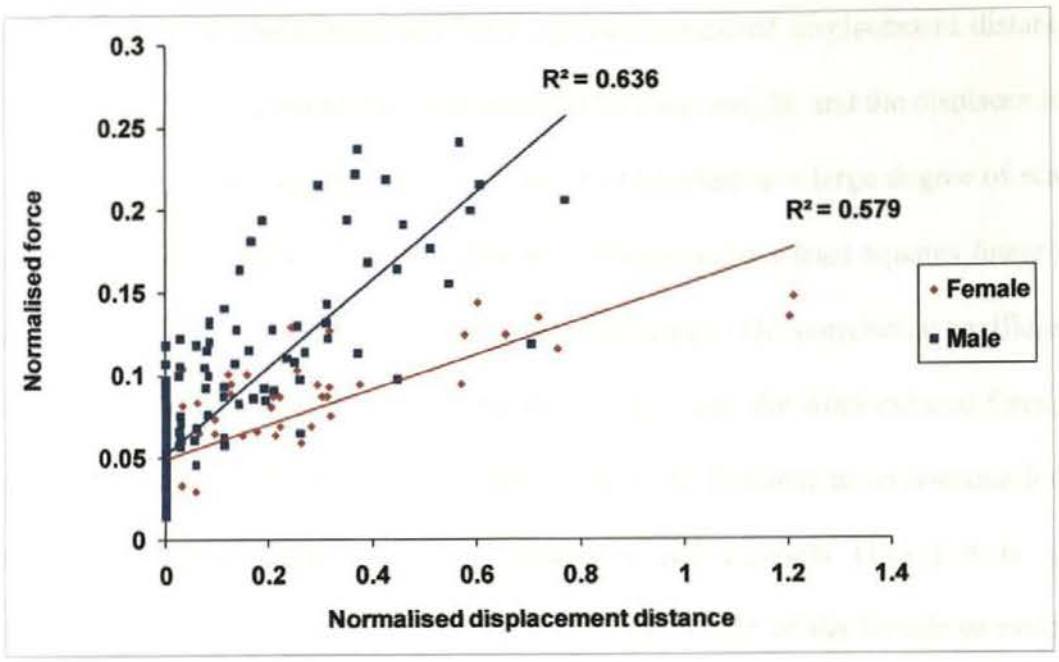

Figure 4.6. Normalised force against normalised displacement distance.

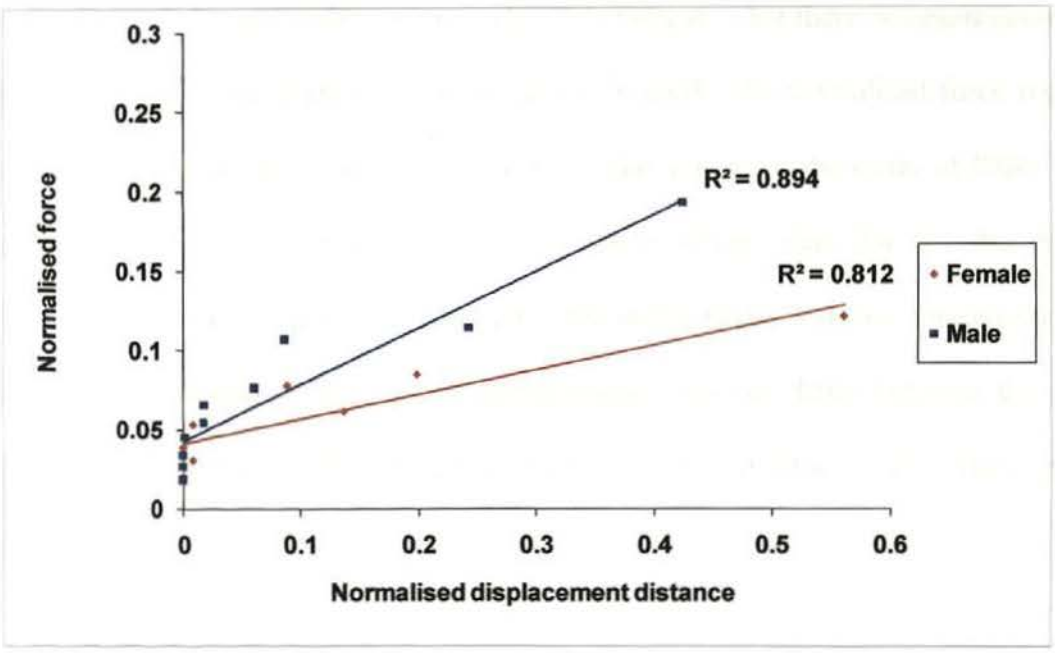

Figure 4.7 Normalised force against normalised displacement distance for an average female or male.

Figure 4.6 shows the normalised force against normalised displacement distance, where the force acting on each individual is normalised by their weight, and the displacement distance is normalised by their height. This figure shows that there is a large degree of scatter which is reflected in the values of the correlation coefficients for a least squares linear regression of normalised force on normalised displacement distance. The correlation coefficients are 0.579 and 0.636 for females and males, respectively. However, the wind induced force was obtained using data from Murakami and Deguchi (1981) which relates to an *average* female or male. Hence, to remain consistent with Murakami and Deguchi (1981) it is perhaps more appropriate to normalise the force by the average weight of the female or male participants. Figure 4.7 shows that this improves the correlation coefficients of a least squares linear regression of normalised force on normalised displacement distance, which are now 0.812 and 0.894 for females and males respectively. This indicates that there is a clear linear relationship between the two parameters when averaging is used. The normalised force required to first displace an individual is similar for both genders and is of the order of 0.04. However, the gradient of the line relating to the male data is steeper than that for the females, which indicates that for a given normalised force the males have a smaller normalised displacement distance. Although the normalised displacement distances differ between the genders for a given normalised force, both genders remain balanced until the value of the normalised force exceeds 0.04.

4.6 Discussion.

A set of full-scale experiments were undertaken to investigate the effect of a sudden change in wind velocity as would be experienced by an individual exposed to a train slipstream. A novel

gust generating device was created by attaching wooden boards to the side of a forklift truck which was positioned in a wind tunnel perpendicular to the oncoming flow, thus creating a sheltered region immediately behind the screen where volunteers could stand. When the required wind velocity was established within the wind tunnel, the forklift truck was driven across the wind tunnel so exposing the volunteers to a sudden gust. Initial tests showed that a rapid change in velocity occurred in less than 0.5s for each of the oncoming wind flows, which is a step change in velocity. This rapid change in velocity occurs within a slipstream at the nose of both a freightliner and a passenger train (see Section 2.2.1). However, a passenger train's slipstream velocity then decreases before increasing again along the train's main body, whereas a freightliner's slipstream velocity remains at a similar magnitude until after the rear of the train has past. Therefore, the experiments generated a gust velocity that reproduced the sudden velocity increase at a train's nose, and also the continued high velocity of a freightliner's slipstream.

For each experiment undertaken, the participants stood in the sheltered region behind the screen, either facing the screen (front orientation), with their backs to the screen (back orientation) or side-on (side orientation). All individuals were tested with velocities of 7, 10, 12 and 15m/s, and the males were tested with an additional velocity of 20m/s. Although it would have been useful to have had all the individuals tested with the same gust velocities, the large displacements of some females with a gust velocity of 15m/s precluded this on safety grounds. An individual was judged to have been displaced during an experiment if they stepped in any direction with either one or both feet when exposed to the oncoming wind. An individual was judged not to have been displaced if they only pivoted on their toes or heels, as it would have been impossible to tell from the video footage if a participant in heavy winter

shoes had pivoted only slightly. Also, the model is concerned with the number of people who are destabilised, and a person who only pivots without stepping has not been destabilised as their centre of gravity has not moved outside of their base. Although the responses of twenty nine individuals are presented in this chapter there were thirty one participants involved in the experiments, however, two were excluded from the results as the video footage showed that they were bracing themselves excessively whilst in the sheltered region in preparation for the oncoming wind. This deliberate bracing was reflected in their response to the gust velocity, making them much more stable than any other participant.

Analysis of the results shows that both the percentage of people displaced and their actual displacement distances increase with increasing gust velocity, as would be expected due to the increased applied force. A person's stability is also affected by their standing orientation, with the side orientation resulting in a significantly lower percentage of displaced people and lower displacement distances than either the front or back orientations. Also, the greatest displacement distances occur with the front orientation. Therefore, the participants of the experiments were the least stable when facing the oncoming flow and the most stable when side-on to the flow, and this agrees with the experimental results in De Graaf and Van Weperen (1997). De Graaf and Van Weperen (1997) conclude that although a person standing side-on can withstand the least amount of acceleration their projected area and hence the applied force is smaller which results in the side orientation being the most stable, whereas the front orientation is the least stable. The difference in stability between the front and back orientations can at least in part be explained by the position of a person's centre of gravity over their feet between their heels and toes. Winter (1995) gives the position of one particular person's centre of gravity as being in the order of 5-6cm from their ankle joint when standing

quietly. Assuming that this person is an adult, the centre of gravity would be positioned less than half the foot length from the heel for even a small footed adult. When a person's centre of gravity moves outside their base of support, i.e. their feet, they become unstable (Hof *et al.*, 2005). As there is a greater horizontal distance for the centre of gravity to move to go beyond a person's toes than it is to go beyond their heels, a person is more stable when pushed from the back than from the front, i.e. the back orientation is more stable than the front orientation.

A statistical analysis undertaken in order to investigate the effect a person's mass has upon their displacement distance shows that the results can be separated into different regions depending on weight for the front orientation of females and the back orientation of both females and males. Lighter individuals have greater displacement distances for a given gust velocity than the heavier individuals. As most females involved in the experiments had lower masses than the males the smallest and largest displacement distances were associated with the heaviest males and the lightest females respectively. Although the average displacement distances for each weight group cannot be taken to be accurate for all the population within the weight groups, the difference between the groups indicates that weight affects a person's response to a slipstream. As a person's weight provides a counter moment to the moment due to the applied force, increasing a person's mass increases the counter moment and thereby increases a person's stability. The effect of the height of a participant was also investigated. As all the participants had similar builds, with only two people being of significantly heavier build than the others, height increased proportionally with weight, hence, when the displacement distance data was arranged with increasing height the results were very similar to those when the displacement distance data was arranged in increasing weight. As the effect

of height could not be separated from the effect of weight, only the effect of weight on the displacement distance is presented.

As the gust velocity affects a person's displacement distance, the relationship between the drag force and the displacement distance is also investigated. Values of the drag area of an average female or male are determined by using the data in Murakami and Deguchi (1981), from which the drag force acting on a person is calculated. There is a clear linear relationship between the normalised force and the normalised displacement distance of females or males when the force is normalised by the *average* weight of the female or male subjects. Although the normalised displacement distances differ between the genders for a given normalised force, with the males having lower normalised displacement distances, the normalised force required to first displace an individual is similar for both genders and is of the order of 0.04. Therefore, both genders remain balanced until subjected to the same normalised force, after which the females have greater normalised displacement distances. The drag force was also calculated using drag coefficient values given by Penwarden *et al.* (1978), and projected area values calculated using the work of Dubois and Dubois (1916) (cited in Penwarden *et al.*, 1978). This method gives similar results to those when using the values of Murakami and Deguchi (1981), therefore, only the latter are presented here.

4.7 Conclusions.

The results of experiments undertaken to investigate the response of an individual to a step change in velocity time history show that:

- Increasing gust velocities result in a decreased stability.
- Increasing weight results in increased stability.
- Stability is a function of standing orientation, with the front orientation being the least stable and the side orientation being the most stable.
- Generally, gender does not affect the percentage of people displaced.
- A normalised force of 0.04 is required to destabilise both females and males.
- Males have lower normalised displacement distances for a given normalised force than females.

CHAPTER 5.

THEORETICAL MODELLING OF A PERSON'S RESPONSE TO A TRAIN SLIPSTREAM.

5.1 Introduction.

A person's response to a slipstream is modelled in two parts, initially as a simple solid object and then as a mass-spring-damper system. The model calculates the displacement of a person throughout their response and compares this with a critical displacement. If the critical displacement is reached, then the model identifies the person as having become destabilised. Sections 5.2 and 5.3 describe the simple solid object and the mass-spring-damper system respectively. The method of calculating the critical displacement is given in Section 5.4, and Section 5.5 describes how the model generates random people.

5.2 Simple solid object.

When a person is subjected to an applied force their muscles are not able to react instantaneously, therefore, a person's body is effectively a non-responsive object until the inception of the muscular response occurs after the short time delay. Johnson and Prevezer (2005) present a model to evaluate the response of a person during this initial time period which, following the work of Fukuchi (1961) (cited in Johnson and Prevezer, 2005), is assumed to occur for 0.375s after the application of the force. The model of Johnson and Prevezer (2005) consists of a rectangular cuboid representing the body of a person where the height of the cuboid is equal to the person's height, and the position of the centre of gravity

(COG) occurs at half the cuboid's height and at half the width and breath of the cuboid. This model is adapted for the current study so that the COG is at a height that is 55% of the cuboid's height (Miller, 1998). In the model developed in this thesis the width of the two opposite faces of the cuboid representing a person's front and back is taken to be equal to the person's shoulder width, and a person's side is taken to be two thirds of the shoulder width, which is a reasonable length when clothing is allowed for. The values of a person's shoulder width are given in Section 5.4. Figure 5.1 illustrates the cuboid that is used to model the initial response of a person. A further adaptation of the model allows for the 27% slower reaction time of an elderly person compared to that of a younger person as determined from the balance recovery experiments of Mackey and Robinovich (2006). Therefore, the adapted model has a young and middle-aged person responding as a simple solid object for the first 0.375s after being exposed to a slipstream, and an elderly person responding as a simple solid object for a 27% longer time than that of a younger person, i.e. for the first 0.476s.

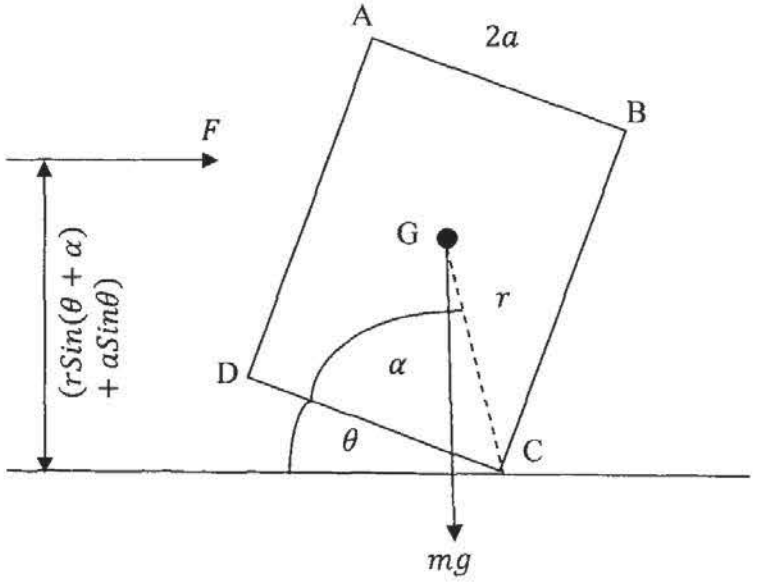

Figure 5.1a. Pivoting cuboid.

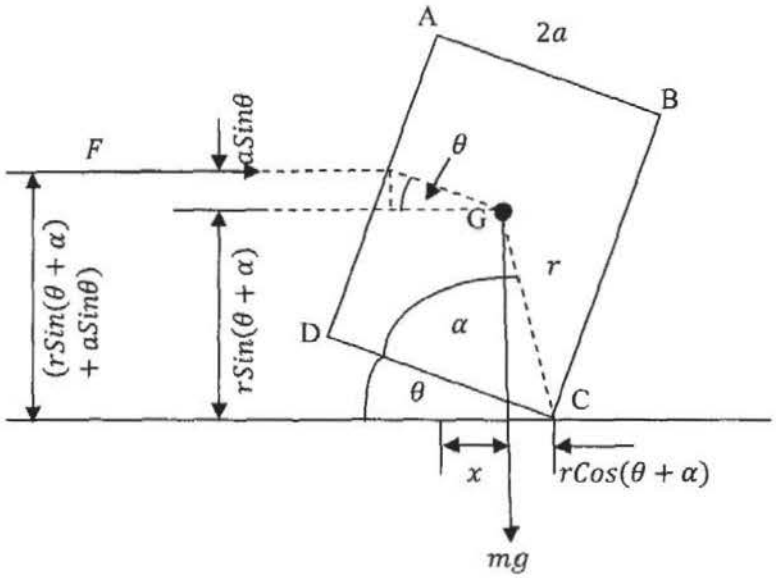

Figure 5.1b. Showing how equations of the cuboid are determined.

Figure 5.1. The cuboid representing a person before the inception of the muscular response.

5.2.1 Wind loading and displacements.

The instantaneous wind velocity of a train slipstream subjects a person to an instantaneous wind force, F, which is given by:

$$F = {}^{1}/_{2}\,\rho C_D A u^2 \qquad (5.1)$$

where ρ is the air density and takes the value of 1.22kg/m^3, C_D is the drag coefficient, A is the projected area of the person and u is the slipstream velocity. The values of C_D are taken from Penwarden *et al.* (1978) and are 1.17 and 1.01 for a person standing facing the wind and side-on to the wind respectively. Although no test on a person standing with their back to the

oncoming flow was included in Penwarden *et al.* (1978) the model assumes that for this standing position the value of C_D is the same as when a person faces the wind. A is determined using the Dubois area (A_{DU}) (Dubois and Dubois, 1916) (cited in Penwarden *et al.* 1978) which relates the total surface area of the body to the person's weight (w) in Newtons and height (h) in metres, thus:

$$A_{DU} = 0.0769w^{0.425}h^{0.725} \tag{5.2}$$

Penwarden *et al.* (1978) give a relationship between A_{DU} and A, so that $\frac{A}{A_{DU}}$ is 0.32 and 0.22 for a person facing and standing side-on to a slipstream respectively. As with C_D, the value of $\frac{A}{A_{DU}}$ for a person standing with their back to the slipstream is taken to be the same as when facing the flow. The values of C_D and $\frac{A}{A_{DU}}$ stated above are for people wearing trousers with a shirt, sweater or a buttoned jacket, as determined by Penwarden *et al.* (1978). Using A_{DU} and $\frac{A}{A_{DU}}$ in place of A, equation (5.1) becomes:

$$F = \frac{1}{2}\rho C_D \frac{A}{A_{DU}} A_{DU} u^2 \tag{5.3}$$

Figure 5.1 illustrates the cuboid being subjected to the force (F) and rotating about its pivotal edge (C), with the cuboid's weight (mg) acting vertically down from its COG (G). The force moment, M_F, acting about C is:

$$M_F = F(rSin(\theta + \alpha) + aSin\theta) \tag{5.4}$$

Equation (5.4) is applicable before and after the COG has moved beyond C. The weight moment, M_W , acting about C, before the COG has moved beyond C is:

$$M_W = mgrCos(\theta + \alpha) \tag{5.5}$$

After the COG has moved beyond C the angle $(\theta + \alpha)$ is greater than 90°, therefore, M_W is negative and acts to destabilise the cuboid. In equations (5.3), (5.4) and (5.5), r is the distance of GC in Figure 5.1, a is half the distance of AB, θ is the angle of rotation between the base of the cuboid (CD) and the ground, and α is the angle DCG. When the force moment becomes greater than the mass moment the cuboid starts to rotate about the pivotal edge. When the horizontal distance of the COG is beyond that of C, i.e. the COG has moved beyond the pivotal axis, both the mass moment and force moment act to destabilise the cuboid and at this point the cuboid will topple over. Although a person will become destabilised when the centre of gravity is beyond the pivotal axis they may be able to alter their standing position, e.g. by stepping, and thereby regain their balance. The horizontal displacement of the COG that results in the destabilisation of a person is discussed in Section 5.4. In the simple solid object model the distributed slipstream force is represented by a single equivalent force acting through the cuboid's centre of gravity before the cuboid has started to rotate. When the cuboid rotates the force acts at the same point on the face of the cuboid as when the cuboid is upright, i.e. not at the same height as the COG. The horizontal displacement of the cuboid's COG (x) is:

$$x = a - \big(rCos(\theta + \alpha)\big) \tag{5.6}$$

The term $(rCos(\theta + \alpha))$ is positive before the COG has moved beyond C, and negative when it has moved beyond C. The model calculates the displacement distance of the cuboid throughout its response and uses the final value of x as the initial displacement for the mass-spring-damper system described in Section 5.3.

5.3 Mass-spring-damper model.

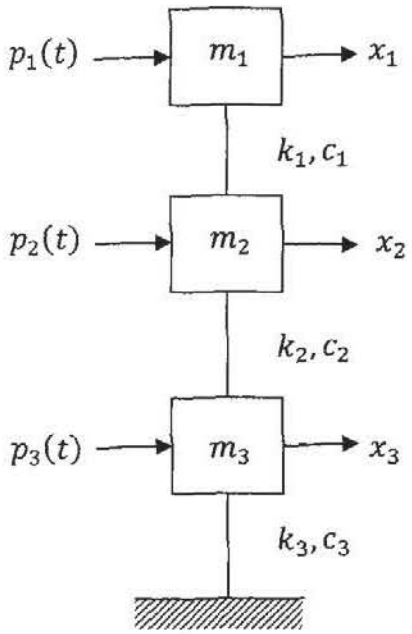

Figure 5.2. The mass-spring-damper model representing a person after the inception of the muscular response.

A mass-spring-damper model, illustrated in Figure 5.2, simulates the response of a person to a train slipstream after the inception of a person's muscular response, and comes into effect after the simple solid object model, i.e. after 0.375s from the onset of the slipstream for a young and middle-aged person, or 0.476s for an elderly person. The three masses, m_1, m_2 and m_3 represent the person's head, upper body and lower body respectively, and are connected

by springs with stiffness k, and dampers with damping c. The masses m_1 and m_2 are connected by k_1 and c_1, whereas m_2 and m_3 are connected by k_2 and c_2, and m_3 is connected to the base by k_3 and c_3. The proportions of the values of m_1, m_2 and m_3 to the total body mass are taken from National Highway Traffic Safety Administration (2002) and are 6%, 64% and 30% respectively. The springs and dampers represent the elastic components of the muscles (Wexler *et al.*, 1997) and the viscous resistance of the muscles (Martin *et al.*, 1994) respectively. During the vibration of the system the masses m_1, m_2 and m_3 have a horizontal displacement with distances of x_1, x_2 and x_3 respectively. The externally applied wind force due to the slipstream is represented by $p(t)$.

5.3.1 Equations of motion.

The equations of motion of the mass-spring-damper system can be expressed as:

$$m_1\ddot{x}_1 + c_1\dot{x}_1 - c_1\dot{x}_2 + k_1x_1 - k_1x_2 = p_1(t) \tag{5.7}$$

$$m_2\ddot{x}_2 - c_1\dot{x}_1 + (c_1 + c_2)\dot{x}_2 - c_2\dot{x}_3 - k_1x_1 + (k_1 + k_2)x_2 - k_2x_3 = p_2(t) \tag{5.8}$$

$$m_3\ddot{x}_3 - c_2\dot{x}_2 + (c_2 + c_3)\dot{x}_3 - k_2x_2 + (k_2 + k_3)x_3 = p_3(t) \tag{5.9}$$

(Warburton, 1964). Equations (5.7), (5.8) and (5.9), can also be expressed symbolically as:

$$\mathbf{m}\ddot{\mathbf{x}} + \mathbf{c}\dot{\mathbf{x}} + \mathbf{k}\mathbf{x} = \mathbf{p}(t) \tag{5.10}$$

where $\mathbf{x}$, $\dot{\mathbf{x}}$ and $\ddot{\mathbf{x}}$ are the displacement vector, the velocity vector and the acceleration vector respectively, $\mathbf{p}(t)$ is the applied load vector, and $\mathbf{m}$, $\mathbf{c}$, and $\mathbf{k}$ are the mass matrix, the damping matrix and the stiffness matrix respectively, so that:

$$\mathbf{m} = \begin{bmatrix} m_1 & 0 & 0 \\ 0 & m_2 & 0 \\ 0 & 0 & m_3 \end{bmatrix} \tag{5.11}$$

$$\mathbf{c} = \begin{bmatrix} c_1 & -c_1 & 0 \\ -c_1 & c_1 + c_2 & -c_2 \\ 0 & -c_2 & c_2 + c_3 \end{bmatrix} \tag{5.12}$$

$$\mathbf{k} = \begin{bmatrix} k_1 & -k_1 & 0 \\ -k_1 & k_1 + k_2 & -k_2 \\ 0 & -k_2 & k_2 + k_3 \end{bmatrix} \tag{5.13}$$

5.3.2 Determining the eigenvalues and the eigenvectors.

In order to model the vibration of the mass-spring-damper system and thereby determine the displacements of the system, the eigenvalues and eigenvectors are determined for the system which is taken to be freely vibrating after the termination of an initial perturbation. The eigenvalues are the square of the undamped natural angular frequencies (ω_n^2) at which the system vibrates, and the eigenvectors represent the mode shapes which give the relative position of the three masses when vibrating and thereby indicate the shape of the system. Assuming that the system is undamped and vibrating freely, i.e. after an initial disturbance the system is allowed to vibrate freely with no external force applied, equations (5.7), (5.8) and (5.9) become:

$$m_1\ddot{x}_1 + k_1x_1 - k_1x_2 = 0 \tag{5.14}$$

$$m_2\ddot{x}_2 - k_1x_1 + (k_1 + k_2)x_2 - k_2x_3 = 0 \tag{5.15}$$

$$m_3\ddot{x}_3 - k_2x_2 + (k_2 + k_3)x_3 = 0 \tag{5.16}$$

Equations (5.14), (5.15) and (5.16) can be expressed symbolically as:

$$\mathbf{m\ddot{x} + kx = 0} \tag{5.17}$$

Assuming a simple harmonic response, the displacement of the three masses is:

$$x_1 = \hat{x}_1 Sin(\omega_n t + \theta) \tag{5.18}$$

$$x_2 = \hat{x}_2 Sin(\omega_n t + \theta) \tag{5.19}$$

$$x_3 = \hat{x}_3 Sin(\omega_n t + \theta) \tag{5.20}$$

or, symbolically:

$$\mathbf{x} = \hat{\mathbf{x}} Sin(\omega_n t + \theta) \tag{5.21}$$

where $\hat{x}$ is the shape of the system which does not change with time, ω_n is the free vibration undamped angular natural frequency, the subscript n refers to the mode (n = 1, 2 or 3 in the case of the three mass model), t is the time since the termination of the initial disturbance, and θ is the phase angle.

Differentiating equations (5.18), (5.19) and (5.20) twice with respect to time gives:

$$\ddot{x}_1 = -\omega_n^2 \hat{x}_1 Sin(\omega_n t + \theta) \tag{5.22}$$

$$\ddot{x}_2 = -\omega_n^2 \hat{x}_2 Sin(\omega_n t + \theta) \tag{5.23}$$

$$\ddot{x}_3 = -\omega_n^2 \hat{x}_2 Sin(\omega_n t + \theta) \tag{5.24}$$

or, symbolically:

$$\ddot{\mathbf{x}} = -\omega^2 \hat{\mathbf{x}} Sin(\omega_n t + \theta) \tag{5.25}$$

Substituting equations (5.18), (5.19) and (5.22) into (5.14), equations (5.18), (5.19), (5.20) and (5.23) into (5.15), and equations (5.19), (5.20) and (5.24) into (5.16), and omitting the term $Sin(\omega_n t + \theta)$ gives:

$$(k_1 - \omega_n^2 m_1)\hat{x}_1 - k_1 \hat{x}_2 = 0 \tag{5.26}$$

$$-k_1 \hat{x}_1 + (k_1 + k_2 - \omega_n^2 m_2)\hat{x}_2 - k_2 \hat{x}_3 = 0 \tag{5.27}$$

$$-k_2 \hat{x}_2 + (k_2 + k_3 - \omega_n^2 m_3)\hat{x}_3 = 0 \tag{5.28}$$

Equations (5.26), (5.27) and (5.28) can be expressed symbolically as:

$$[\mathbf{k} - \omega_n^2 \mathbf{m}]\hat{\mathbf{x}} = \mathbf{0} \tag{5.29}$$

For a non-trivial solution $\hat{\mathbf{x}} \neq \mathbf{0}$, therefore:

$$|\mathbf{k} - \omega_n^2 \mathbf{m}| = \mathbf{0} \tag{5.30}$$

where the | | brackets represent the determinant of the matrix. Equation (5.30) can be solved by rearranging equation (5.26) to give $\hat{x}_2$ in terms of $\hat{x}_1$:

$$\hat{x}_2 = \frac{(k_1 - \omega_n^2 m_1)}{k_1}\hat{x}_1 \tag{5.31}$$

and substituting equation (5.31) into equation (5.28) and rearranging to give $\hat{x}_3$ in terms of $\hat{x}_1$:

$$\hat{x}_3 = \frac{k_2(k_1 - \omega_n^2 m_1)}{k_1(k_2 + k_3 - \omega_n^2 m_3)}\hat{x}_1 \tag{5.32}$$

Substituting equations (5.31) and (5.32) into equation (5.27) and simplifying, gives:

$$\begin{aligned} -m_1 m_2 m_3 \omega_n^6 + (m_1 m_2(k_2 + k_3) + m_1 m_3(k_1 + k_2) + m_2 m_3 k_1)\omega_n^4 \\ - \big(k_1 k_2(m_1 + m_2 + m_3) + k_2 k_3 m_1 + k_1 k_3(m_1 + m_2)\big)\omega_n^2 \\ + k_1 k_2 k_3 = 0 \end{aligned} \tag{5.33}$$

Solving this gives three values of ω_n^2, i.e. three eigenvalues, one for each of the three modes of the system used in the model.

For a single degree of freedom system ω is defined as:

$$\omega = 2\pi f = \sqrt{\frac{k}{m}} \tag{5.34}$$

where f is the cyclic natural frequency of the system, k is the spring stiffness and m is the single mass. As the person model involves a multi-degrees-of-freedom system, the values of ω_n of the person model relate to the mass and the stiffness of a single-degree-of-freedom system equivalent of a multi-degrees-of-freedom system (the reason for which is described in Section 5.3.4). The single-degree-of-freedom system equivalent of a multi-degrees-of-freedom system is given in Figure 5.3.

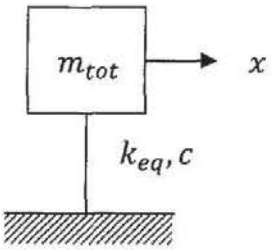

Figure 5.3. Single-degree-of-freedom equivalent of a multi-degrees-of-freedom system.

The parameters m_{tot} and k_{eq} are a person's total mass and the equivalent stiffness respectively. The value of k_{eq} is calculated using the springs in series equation and, for a system with three degrees of freedom such as that used in the person model, k_{eq} is:

$$k_{eq} = \frac{1}{\frac{1}{k_1} + \frac{1}{k_2} + \frac{1}{k_3}} \tag{5.35}$$

In the model the three eigenvalues determined from equation (5.33) are proportional to k_{eq} and inversely proportional to m_{tot} thus:

$$\omega_n^2 = \begin{Bmatrix} e_1 \\ e_2 \\ e_3 \end{Bmatrix} \frac{k_{eq}}{m_{tot}} \tag{5.36}$$

where $e_1 \frac{k_{eq}}{m_{tot}}$, $e_2 \frac{k_{eq}}{m_{tot}}$ and $e_3 \frac{k_{eq}}{m_{tot}}$ are the eigenvalues of the first, second and third modes of vibration respectively, and $e_1 \frac{k_{eq}}{m_{tot}} < e_2 \frac{k_{eq}}{m_{tot}} < e_3 \frac{k_{eq}}{m_{tot}}$.

The three eigenvalues are then substituted into each of equations (5.31) and (5.32), and the values of $\hat{x}_2$ and $\hat{x}_3$ in terms of $\hat{x}_1$ are called the eigenvectors and denoted by ϕ, so that:

$$\boldsymbol{\phi}_n = \frac{1}{\hat{x}_{1n}} \begin{Bmatrix} \hat{x}_{1n} \\ \hat{x}_{2n} \\ \hat{x}_{3n} \end{Bmatrix} \tag{5.37}$$

which in matrix form is:

$$\boldsymbol{\Phi} = \begin{bmatrix} \hat{x}_{11}/\hat{x}_{11} & \hat{x}_{12}/\hat{x}_{12} & \hat{x}_{33}/\hat{x}_{13} \\ \hat{x}_{21}/\hat{x}_{11} & \hat{x}_{22}/\hat{x}_{12} & \hat{x}_{23}/\hat{x}_{13} \\ \hat{x}_{31}/\hat{x}_{11} & \hat{x}_{32}/\hat{x}_{12} & \hat{x}_{33}/\hat{x}_{13} \end{bmatrix} = \begin{bmatrix} 1 & 1 & 1 \\ \phi_{21} & \phi_{22} & \phi_{23} \\ \phi_{31} & \phi_{32} & \phi_{33} \end{bmatrix} \tag{5.38}$$

with the notation being $\hat{x}_{rn}$, where the subscripts r and n identify the mass and mode respectively, e.g. ϕ_{23} relates to m_2 in the third mode. $\boldsymbol{\Phi}$ gives the mode shapes of the system, as illustrated in Figure 5.4, which indicates how the masses vibrate with respect to each other.

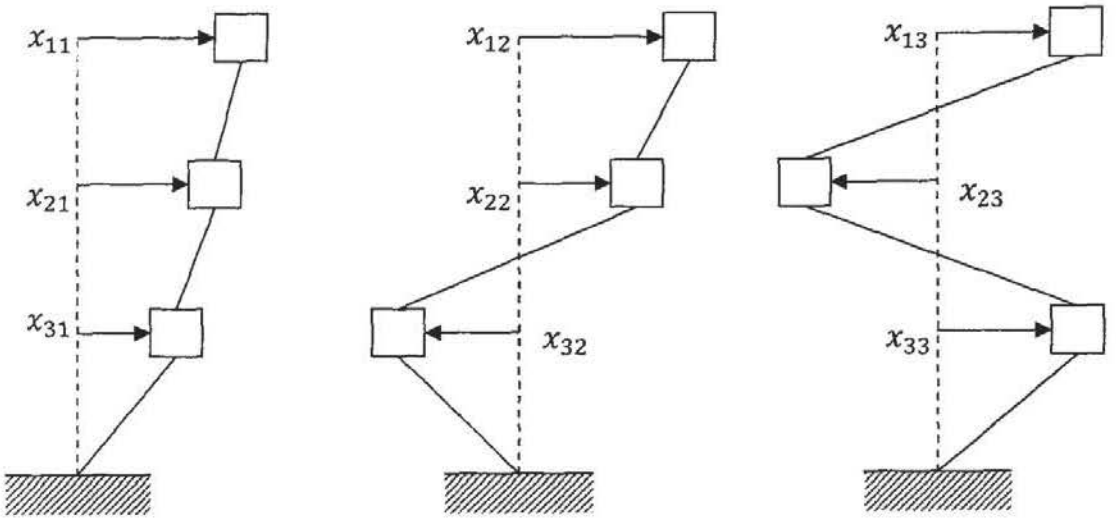

Figure 5.4. Mode shapes of a mass-spring-damper system with three degrees of freedom.

5.3.3 Determining the damped angular natural frequency and the damping ratio.

The damped angular natural frequencies, ω_{Dn}, and the damping ratio, ε, are also required to determine the displacements of the mass-spring-damper system, and this section describes how these parameters are calculated. The three values of ω_n are determined from an undamped system freely vibrating after an initial disturbance, but in order to obtain ω_{Dn} the damping of the system is considered. Clough and Penzien (1993) express equation (5.10) as:

$$M_n\ddot{Y}_n + C_n\dot{Y}_n + K_nY_n = P_n(t) \tag{5.39}$$

where M_n, C_n, K_n and $P_n(t)$ are called the normal-coordinate generalised mass, generalised damping, generalised stiffness, and generalised load for mode n respectively These are defined as:

$$M_n \equiv \boldsymbol{\phi}_n^T \mathbf{m} \boldsymbol{\phi}_n \tag{5.40}$$

$$C_n \equiv \boldsymbol{\phi}_n^T \mathbf{c} \boldsymbol{\phi}_n \tag{5.41}$$

$$K_n \equiv \boldsymbol{\phi}_n^T \mathbf{k} \boldsymbol{\phi}_n \tag{5.42}$$

$$P_n(t) \equiv \boldsymbol{\phi}_n^T \mathbf{p}(\mathrm{t}) \tag{5.43}$$

The damping ratio, ε_n, is defined as the ratio of a system's actual damping to the critical damping, thus:

$$\varepsilon_n = \frac{C_n}{2\omega_n M_n} \tag{5.44}$$

where $2\omega_n M_n$ is the critical damping. When $\varepsilon_n < 1$, $\varepsilon_n = 1$ and $\varepsilon_n > 1$, the system is undercritically damped, critically damped and overcritically damped respectively. As Clough and Penzien (1993, p.32) state that '...it is very unusual under normal conditions to have overcritically damped structural systems...', the damped system representing the response of a person is assumed to be undercritically damped, i.e. $0 < \varepsilon_n < 1$. When $\varepsilon_n < 1$, the system will oscillate about its original position with oscillations of decreasing amplitude. The damped angular natural frequency, ω_{Dn}, is related to ε_n and defined as:

$$\omega_{Dn} = \omega_n \sqrt{1 - \varepsilon_n^2} \tag{5.45}$$

5.3.4 Determining values of the natural frequency and the total damping.

The cyclic natural frequency, f, of a person is required in order to determine k_{eq}, and the total damping of the system, c_{tot}, is required to determine the damping ratio; hence, both f and c_{tot} are involved in calculating the displacements of the mass-spring-damper system. Morasso and Scieppati (1999) present a single-degree-of-freedom system to model a person's sway occurring during upright standing and use a value of f that is below 1Hz. As this value of f is associated with a single-degree-of-freedom system, a single-degree-of-freedom system equivalent of the multi-degrees-of freedom system used in the current research is used with f < 1Hz. The equivalent system is illustrated in Figure 5.3 and, using equation (5.34), f is defined as:

$$f = \frac{1}{2\pi}\sqrt{\frac{k_{eq}}{m_{tot}}} \tag{5.46}$$

The values of f and c_{tot} are determined by utilising the data from previous full-scale experiments which were undertaken in a wind tunnel to test a person's response to a sudden gust for the purposes of the current research (Chapter 4). In order to reproduce the results of the experiments the twenty nine participants were simulated by the model by using the information of their heights, weights, gender and standing orientation. All of the participants were young or middle-aged, and the relationship between k_1, k_2 and k_3 was taken to be $k_1 = k_2 = k_3$ (see Section 5.3.5). Additionally, the relationship between c_1, c_2 and c_3 was taken to be $c_1 = c_2 = c_3$ (see Section 5.3.6). The people generated by the model were exposed to the wind velocity profiles that were recorded during the full-scale tests, as shown

in Figure 4.2, with each person simulated to be either standing facing the oncoming flow, or with their back, left side or right side to the flow. Values of f between 0 and 1Hz were tested in the model with varying values of c_{tot} using a trial-and-improvement method until the percentage of people displaced in the full-scale experiments was reasonably reproduced by the model. In determining the values of f and c_{tot} the value of ε has to be considered so that $\varepsilon < 1$ as the system is undercritically damped. As ε is inversely proportional to m_{tot} (which is indicated in equation (5.44)), the smallest value of m_{tot} has to be large enough so that $\varepsilon < 1$.

Wind velocities (m/s)	Percentage of people displaced		Absolute error of percentage of people displaced (b-a)	Percentage error of percentage of people displaced (100×(b-a)/a)
	Full-scale wind tunnel tests (a)	Simulated by the model (b)		
7	8.6%	7.8%	-0.8%	-9.3%
10	13.8%	17.2%	3.4%	+24.6%
12	38.3%	42.2%	-3.9%	+10.2%
15	65.5%	50%	15.5%	+23.7%

Table 5.1. Percentages of people displaced during the full-scale wind tunnel tests and generated by the model (f = 0.9Hz, c_{tot} = 215Ns/m).

Table 5.1 gives the percentages of people displaced by the various wind velocities during the full-scale tests and simulated by the model using values of 0.9Hz and 215Ns/m for f and c_{tot} respectively. The percentages relate to a person being displaced when either standing facing the oncoming flow, with their back, their left side or their right side to the flow, i.e. the results of each of these standing positions are combined. Although it would be more accurate to reproduce the percentages displaced for each standing orientation, the results of the full

working model do not differentiate between standing orientations so it was deemed appropriate to not differentiate between standing orientations when determining f and c_{tot}. Table 5.1 also shows the absolute error and percentage error of the simulated results compared with the measured results. The largest percentage error is associated with the wind velocity of 10m/s and is 24.6%, however, the absolute error associated with this wind velocity is only 3.4%. The absolute and percentage errors associated with the wind velocities of 7m/s and 12m/s are quite small, therefore, the model generates the percentages of people displaced at these wind velocities with reasonable accuracy. The least accurately reproduced results are associated with the wind velocity of 15m/s. Altering the values of f and c_{tot} in order to more accurately reproduce the results at the wind velocity of 15m/s significantly reduces the accuracy of the results at 7, 10 and 12m/s. The best overall reproduction of the results occurs when f = 0.9Hz and c_{tot} = 215Ns/m.

5.3.5 Values of the eigenvalues and the eigenvectors for modelled individuals.

In order to determine ω_n^2 and $\mathbf{\Phi}$ the relationship between the three mass values and m_{tot} is utilised, as is the relationship between the three stiffness values and k_{eq}. As described in Section 5.3, the three masses of the system relate to a person's total mass by:

$$m_1 = 0.06m_{tot} \tag{5.47}$$

$$m_2 = 0.64m_{tot} \tag{5.48}$$

$$m_3 = 0.30m_{tot} \tag{5.49}$$

Therefore, the mass matrix is:

$$\mathbf{m} = \begin{bmatrix} 0.06 & 0 & 0 \\ 0 & 0.64 & 0 \\ 0 & 0 & 0.30 \end{bmatrix} m_{tot} \tag{5.50}$$

Taking the values of k_2 and k_3 in terms of k_1, so that $k_2 = gk_1$ and $k_3 = hk_1$, where g and h are constants, the equivalent stiffness is:

$$k_{eq} = \frac{1}{\frac{1}{k_1} + \frac{1}{gk_1} + \frac{1}{hk_1}} = \frac{ghk_1}{gh + g + h} \tag{5.51}$$

Thus:

$$k_1 = \frac{gh + g + h}{gh} k_{eq} \tag{5.52}$$

$$k_2 = \frac{gh + g + h}{h} k_{eq} \tag{5.53}$$

$$k_3 = \frac{gh + g + h}{g} k_{eq} \tag{5.54}$$

The scarcity and contradictory nature of the data relating to the appropriate values of stiffness of a model representing the response of a standing person to a horizontal force (as discussed in Section 2.8) has led to the assumption that $k_1 = k_2 = k_3$ for young and middle-aged people, so the values of both g and h are equal to one. Therefore, for a young and middle-aged person, equations (5.52), (5.53) and (5.54) give:

$$k_1 = k_2 = k_3 = 3k_{eq} \tag{5.55}$$

It is conjectured that elderly people standing on a station platform have a different response to younger people when exposed to the slipstream of a passing train. This difference is incorporated into the model by delaying the reaction time, as described in Section 5.2, and also by altering the relationship between k_1, k_2 and k_3. Liu *et al.* (2006) examines the effects of age on active leg stiffness adjustment and concludes that the leg stiffness of elderly subjects is 70% that of younger subjects when performing a counter movement jump, therefore, the model takes this reduced stiffness to be a feature of an elderly person's leg. The reduced leg stiffness is reflected in the model by assuming that the value of k_3 of an elderly person is 70% of the k_3 value of a younger person, i.e. $k_{3E} = 0.7k_{3Y}$, for a given total body mass. The subscripts E and Y refer to an elderly and a younger (young and middle-aged) person respectively, and are used for clarification when deemed necessary. It is also assumed that, as with a younger person, $k_{1E} = k_{2E}$. Therefore, $g = 1$ in equation (5.51), which leads to the relationship between k_{eqE} and k_{1E}:

$$k_{eqE} = \frac{hk_{1E}}{2h+1} \tag{5.56}$$

which, with $hk_{1E} = k_{3E} = 0.7k_{3Y}$, leads to:

$$k_{eqE} = \frac{0.7k_{3Y}}{2h+1} \tag{5.57}$$

Van der Burg *et al.* (2007) indicate that the stiffness of an elderly person's trunk is greater than that of a younger person, although it does not quantify the increase, therefore, the values of k_1 and k_2 of an elderly person are taken to be greater than those of a younger person. This

can be achieved by assuming that $k_{eqY} = k_{eqE}$, as $k_{1Y} = k_{2Y}$, $k_{1E} = k_{2E}$ and $k_{3Y} > k_{3E}$ thus resulting in k_{1E} and k_{2E} being larger than k_{1Y} and k_{2Y} respectively. Equation (5.55) leads to:

$$k_{eqY} = \frac{k_{3Y}}{3} \tag{5.58}$$

Substituting equation (5.57) into equation (5.58), with $k_{eqY} = k_{eqE}$, leads to the solution $h = \frac{11}{20}$. As $k_3 = hk_1$, the relationship between k_1, k_2 and k_3 of an elderly person is $k_1 = k_2 = \frac{20}{11}k_3$. Using this relationship and equation (5.56), the relationship between each of the stiffnesses and k_{eq} of an elderly person are determined to be:

$$k_{eq} = \frac{11}{42}k_1 = \frac{11}{42}k_2 = \frac{10}{21}k_3 \tag{5.59}$$

Equations (5.55) and (5.59) show that k_1, k_2 and k_3 are dependent upon k_{eq} which in turn is dependent upon m_{tot} as f is constant (equation (5.46)), therefore, the values of stiffness vary with m_{tot}.

Substituting equations (5.47), (5.48), (5.49) and (5.55) into equation (5.33) leads to the eigenvalues associated with a young and middle-aged person:

$$\omega_n^2 = \begin{Bmatrix} 1.910 \\ 22.205 \\ 55.260 \end{Bmatrix} \frac{k_{eq}}{m_{tot}} \tag{5.60}$$

Similarly, substituting equations (5.47), (5.48), (5.49) and (5.59), into equation (5.33) leads to the eigenvalues associated with an elderly person:

$$\omega_n^2 = \begin{Bmatrix} 1.618 \\ 23.366 \\ 70.308 \end{Bmatrix} \frac{k_{eq}}{m_{tot}} \tag{5.61}$$

With f = 0.9Hz the value of $\frac{k_{eq}}{m_{tot}}$ for a person irrespective of age can be calculated using equation (5.46), thus:

$$\frac{k_{eq}}{m_{tot}} = 31.978 \tag{5.62}$$

The units are s^{-2}. The eigenvalues, ω_n^2, can then be calculated for a young and middle-aged person from equation (5.60) giving:

$$\omega_n^2 = \begin{Bmatrix} 61.078 \\ 710.071 \\ 1767.104 \end{Bmatrix} \tag{5.63}$$

and for an elderly person from equation (5.61), thus:

$$\omega_n^2 = \begin{Bmatrix} 51.740 \\ 747.198 \\ 2248.309 \end{Bmatrix} \tag{5.64}$$

With units of $rad^2.s^{-2}$. In order to determine the eigenvector matrix (**Φ**) for a young and middle-aged person, equations (5.47), (5.55) and (5.60) are substituted into equation (5.31) to

give $\hat{x}_2$ in terms of $\hat{x}_1$. Also, equations (5.47), (5.49), (5.55) and (5.60) are substituted into equation (5.32) to give $\hat{x}_3$ in terms of $\hat{x}_1$. Therefore:

$$\boldsymbol{\Phi} = \begin{bmatrix} 1 & 1 & 1 \\ 0.962 & 0.556 & -0.105 \\ 0.532 & -2.521 & 0.030 \end{bmatrix} \tag{5.65}$$

for a young and middle-aged person. Similarly, $\boldsymbol{\Phi}$ for an elderly person is determined by substituting equations (5.47), (5.59) and (5.61) into equation (5.31), and substituting equations (5.47), (5.49), (5.59) and (5.61) into equation (5.32). Thus:

$$\boldsymbol{\Phi} = \begin{bmatrix} 1 & 1 & 1 \\ 0.975 & 0.633 & -0.105 \\ 0.685 & -2.213 & 0.026 \end{bmatrix} \tag{5.66}$$

for an elderly person.

5.3.6 Values of the damped angular natural frequency and damping ratio of individuals.

In order to determine ε_n and ω_{Dn}^2 the relationship between each damping value and c_{tot} is utilised. As the data relating to the appropriate values of damping of a mass-spring-damper system representing the response of a standing person to a horizontal force is scarce and contradictory (as discussed in Section 2.8) it is assumed that $c_1 = c_2 = c_3$ for all people irrespective of age. In the model $c_{tot} = c_1 + c_2 + c_3$, therefore, $c_1 = c_2 = c_3 = \frac{1}{3}c_{tot}$, and the damping matrix, $\mathbf{c}$, from equation (5.12), is given by:

$$\mathbf{c} = \begin{bmatrix} 0.333 & -0.333 & 0 \\ -0.333 & 0.667 & -0.333 \\ 0 & -0.333 & 0.667 \end{bmatrix} c_{tot} \tag{5.67}$$

In order to obtain the damping ratio, ε_n, of a young and middle-aged person the matrices M_n and C_n are determined from equations (5.40) and (5.41) respectively, thus:

$$M_n = \begin{bmatrix} 0.737 & -3.352 \times 10^{-5} & 1.416 \times 10^{-4} \\ -3.352 \times 10^{-5} & 2.164 & -5.220 \times 10^{-5} \\ 1.416 \times 10^{-4} & -5.220 \times 10^{-5} & 0.067 \end{bmatrix} m_{tot} \tag{5.68}$$

$$C_n = \begin{bmatrix} 0.156 & -3.967 \times 10^{-4} & -3.333 \times 10^{-5} \\ -3.967 \times 10^{-4} & 5.340 & -1.350 \times 10^{-4} \\ -3.333 \times 10^{-5} & -1.350 \times 10^{-4} & 0.413 \end{bmatrix} c_{tot} \tag{5.69}$$

Substituting equations (5.63), (5.68) and (5.69) into equation (5.44), the damping ratio for a young and middle-aged person is:

$$\varepsilon_n = \begin{Bmatrix} 0.077 \\ 0.261 \\ 0.413 \end{Bmatrix} \frac{c_{tot}}{\sqrt{m_{tot} k_{eq}}} \tag{5.70}$$

The matrices M_n and C_n for an elderly person are also determined from equations (5.40) and (5.41), thus:

$$M_n = \begin{bmatrix} 0.809 & 2.205 \times 10^{-4} & -1.770 \times 10^{-4} \\ 2.205 \times 10^{-4} & 1.786 & 2.010 \times 10^{-4} \\ -1.770 \times 10^{-4} & 2.010 \times 10^{-4} & 0.067 \end{bmatrix} m_{tot} \tag{5.71}$$

$$C_n = \begin{bmatrix} 0.185 & -0.227 & 2.482 \times 10^{-3} \\ -0.227 & 4.377 & -8.276 \times 10^{-3} \\ 2.482 \times 10^{-3} & -8.276 \times 10^{-3} & 0.413 \end{bmatrix} c_{tot} \tag{5.72}$$

Substituting equations (5.64), (5.71) and (5.72) into equation (5.44), the damping ratio for an elderly person is:

$$\varepsilon_n = \begin{Bmatrix} 0.079 \\ 0.136 \\ 0.366 \end{Bmatrix} \frac{c_{tot}}{\sqrt{m_{tot} k_{eq}}} \tag{5.73}$$

Using c_{tot} = 215Ns/m and equation (5.62), ε_n becomes:

$$\varepsilon_n = \frac{1}{m_{tot}} \begin{Bmatrix} 2.928 \\ 9.923 \\ 15.702 \end{Bmatrix} \tag{5.74}$$

for a young and middle-aged person, and,

$$\varepsilon_n = \frac{1}{m_{tot}} \begin{Bmatrix} 3.004 \\ 5.171 \\ 13.915 \end{Bmatrix} \tag{5.75}$$

for an elderly person.

The values of ω_{Dn} are determined by substituting equation (5.74) into equation (5.45) for a young and middle-aged person, thereby giving:

$$\omega_{Dn} = \begin{Bmatrix} 7.815 \\ 26.647 \\ 42.037 \end{Bmatrix} \sqrt{1 - \frac{1}{m_{tot}^2} \begin{Bmatrix} 8.573 \\ 98.466 \\ 246.553 \end{Bmatrix}} \tag{5.76}$$

Substituting equation (5.75) into equation (5.45) gives ω_{Dn} for an elderly person:

$$\omega_{Dn} = \begin{Bmatrix} 7.193 \\ 27.335 \\ 47.416 \end{Bmatrix} \sqrt{1 - \frac{1}{m_{tot}^2} \begin{Bmatrix} 9.024 \\ 26.739 \\ 193.627 \end{Bmatrix}} \tag{5.77}$$

With units of rad.s^{-1}.

5.3.7 Wind loading and displacements.

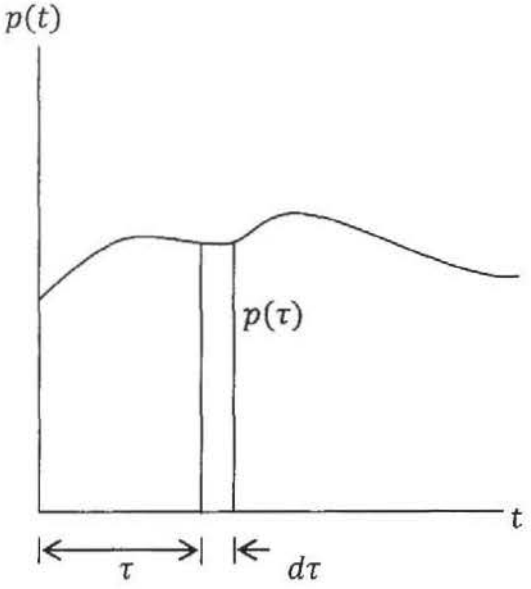

Figure 5.5. Time history of an arbitrary general loading $p(t)$.

If a system is subjected to an impulse loading which acts in isolation it freely vibrates after the termination of such an impulse, and the displacement of each of the system's masses can be determined. In the model developed in the current research, the entire wind loading of a slipstream acting on a person is considered to consist of a succession of very short-duration impulse loads, with a person's displacement being the sum of the displacements due to each of the impulses. Summing all the individual free vibration responses gives the total response

of the system to the entire wind loading. Figure 5.5 illustrates the time history of an arbitrary general loading $p(t)$, with an intensity of loading $p(\tau)$ acting at $t = \tau$. The loading acting during the time interval of $d\tau$ is an impulse loading, $p(\tau)d\tau$ (Clough and Penzien, 1993).

The displacement of an under-critically damped single-degree of freedom system after the termination of an isolated impulse load is given by:

$$x = e^{-\varepsilon\omega(t-\tau)}\frac{p(\tau)d\tau}{m\omega_D}Sin\omega_D(t-\tau) \qquad t \geq \tau \quad (5.78)$$

Equation (5.78) gives the response of a system to an isolated impulse but the loading due to a slipstream is considered to consist of a succession of impulses, therefore, the displacement given by equation (5.78) is actually $dx(t)$, thus:

$$dx(t) = e^{-\varepsilon\omega(t-\tau)}\frac{p(\tau)d\tau}{m\omega_D}Sin\omega_D(t-\tau) \qquad t \geq \tau \quad (5.79)$$

where $dx(t)$ is the displacement time history due to one impulse load for $t \geq \tau$, not the change in displacement during dt. The displacement of a single-degree-of-freedom system subjected to the slipstream loading, is determined by summing the displacements due to all of the individual impulse loads over the entire time $t \geq 0$, thus:

$$x = \frac{1}{m\omega_D}\int_0^t p(\tau)\,Sin\omega_D(t-\tau)e^{-\varepsilon\omega(t-\tau)}d\tau \qquad t \geq 0 \quad (5.80)$$

Equation (5.80) is known as the Duhamel integral equation, and this can be adapted for a multi-degrees-of-freedom system subjected to a wind loading thus:

$$Y_n = \frac{1}{M_n \omega_{Dn}} \int_0^t P_n(\tau)\, Sin\omega_{Dn}(t-\tau) e^{-\varepsilon_n \omega_n (t-\tau)} d\tau \qquad t \geq 0 \quad (5.81)$$

where Y_n is the modal amplitude, and $P_n(\tau)$ is the load function for the nth mode which takes into consideration the relative forces acting upon each mass, so that:

$$P_n(\tau) = {}^1/_2\, \rho C_D A u^2 \sum_r \phi_{rn} \eta_r \qquad (5.82)$$

where ρ, C_D, A and u are defined as for equation (5.1), ϕ_{rn} are the eigenvectors, and η_r is the relative amplitude of the force acting upon the three masses. As there is insufficient slipstream data to determine conclusively how the slipstream velocity varies with height (as described in Section 3.3) the model assumes that the force acting on each of the three masses is the same, therefore, $\eta = 1$ for each mass. To help solve equation (5.81) the following expression is used:

$$Sin(\omega_{Dn} t - \omega_{Dn} \tau) = Sin(\omega_{Dn} t) Cos(\omega_{Dn} \tau) - Cos(\omega_{Dn} t) Sin(\omega_{Dn} \tau) \qquad (5.83)$$

Therefore, equation (5.81) becomes:

$$Y_n = \frac{Sin(\omega_{Dn}t)}{M_n\omega_{Dn}} \int_0^t P(\tau)Cos(\omega_{Dn}\tau)e^{-\varepsilon_n\omega_n(t-\tau)}d\tau \tag{5.84}$$

$$-\frac{Cos(\omega_{Dn}t)}{M_n\omega_{Dn}} \int_0^t P(\tau)Sin(\omega_{Dn}\tau)e^{-\varepsilon_n\omega_n(t-\tau)}d\tau$$

The displacement vector, $\boldsymbol{x}_n$, for each mass is obtained from the product of the mode shape vector, $\boldsymbol{\phi}_n$, and the modal amplitude, Y_n, (Clough and Penzien, 1993) so that:

$$\boldsymbol{x}_n = \boldsymbol{\phi}_n Y_n \tag{5.85}$$

Summing the modal vectors gives the total displacement vector, **x**, for each mass:

$$\mathbf{x} = \boldsymbol{\phi}_1 Y_1 + \boldsymbol{\phi}_2 Y_2 + \cdots + \boldsymbol{\phi}_N Y_N \tag{5.86}$$

Therefore, the actual horizontal displacements for each mass, x_r, are determined by summing the product of ϕ_n and Y_n for each mode:

$$x_1 = \phi_1 Y_1 + \phi_2 Y_2 + \phi_3 Y_3 \tag{5.87}$$

$$x_2 = \phi_1 Y_1 + \phi_2 Y_2 + \phi_3 Y_3 \tag{5.88}$$

$$x_3 = \phi_1 Y_1 + \phi_2 Y_2 + \phi_3 Y_3 \tag{5.89}$$

5.3.7.1 Displacement of an entire person.

The displacement of the person as a whole (x_p) is taken to be the displacement occurring at the COG of the whole body. This height (h_p) occurs at 55% of the person's full height, as mentioned in Section 5.2. As equations (5.87) to (5.89) give the displacements of the three masses the value of x_p is calculated using these displacements, and this is achieved by first determining the heights at which the three masses are positioned.

The displacement distances of the three masses of the system representing a person occur at the COG of each mass. The centres of gravity of m_1, m_2 and m_3 of a person standing up straight are taken to be at the person's full height (h_1), at the navel (h_2), and a little above the knees at half the height to the navel (h_3), respectively. The person is proportioned so that $h_1 : h_2$ approximates the Golden Ratio. i.e. is 1.618:1 (Parveen, n.d.) Therefore, $h_2 = 0.618h_1$ and $h_3 = 0.309h_1$, as illustrated in Figure 5.6, and $h_p = 0.55h_1$. As the masses exhibit only horizontal displacements the height of each COG remains the same throughout the duration of the vibration.

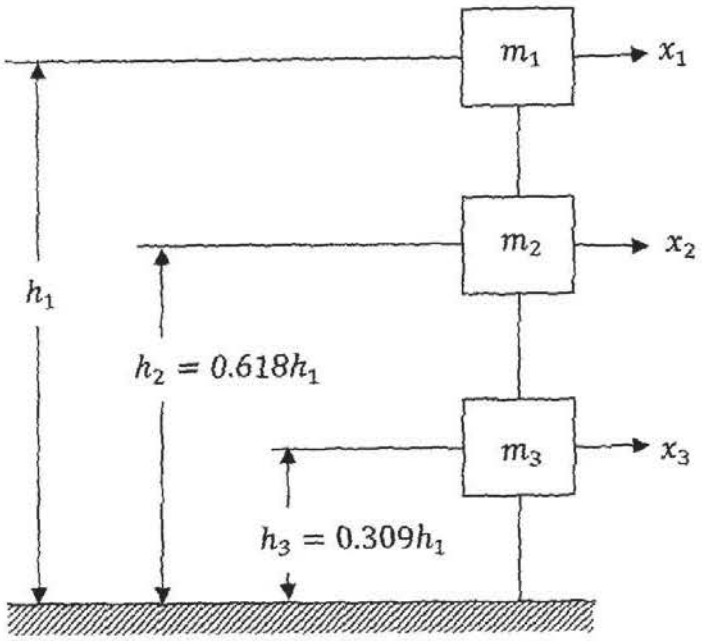

Figure 5.6. Relative heights of the centre of gravity of each mass.

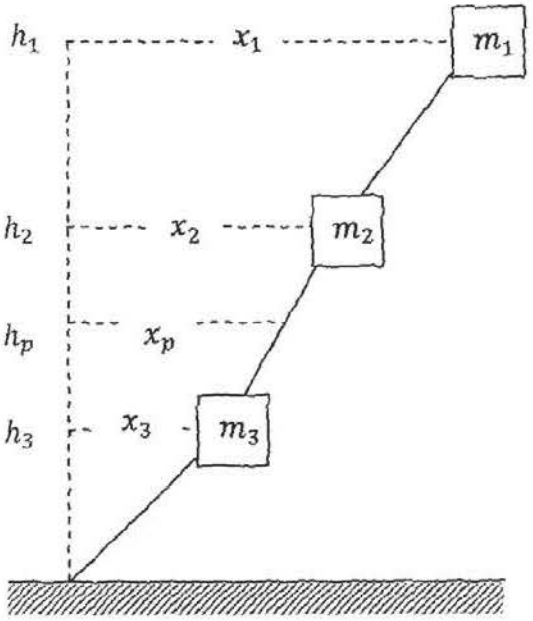

Figure 5.7a. Heights and displacements of the centre of gravity of each mass.

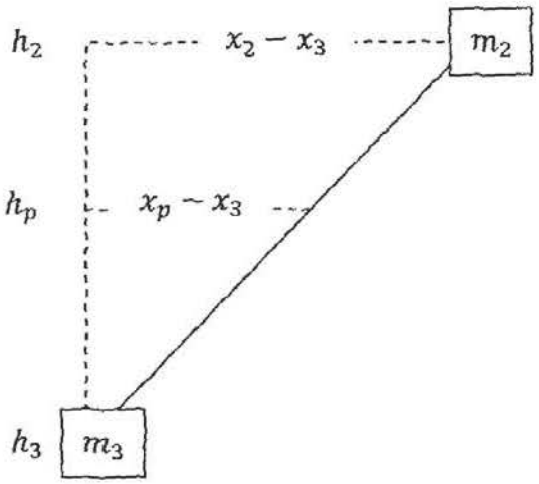

Figure 5.7b. Section of the displaced system between m_2 and m_3.

Figure 5.7. Details required in order to determine the displacement of the whole person.

Figure 5.7a shows arbitrary displacements of the three masses and illustrates that x_p is equal to x_3 plus an additional length. This additional length is shown in Figure 5.7b as $x_p - x_3$, with Figure 5.7b illustrating the section of the displaced system between m_2 and m_3. The length $x_p - x_3$ can be determined from similar triangles, thus:

$$(x_p - x_3) = \frac{(x_2 - x_3)(h_p - h_3)}{(h_2 - h_3)} \tag{5.90}$$

Adding this to x_3 gives the displacement of the person:

$$x_p = \left(\frac{(x_2 - x_3)(h_p - h_3)}{(h_2 - h_3)}\right) + x_3 \tag{5.91}$$

With $h_2 = 0.618h_1$, $h_p = 0.55h_1$ and $h_3 = 0.309h_1$, equation (5.91) becomes:

$$x_p = 0.780x_2 + 0.220x_3 \tag{5.92}$$

When the person's displacement moves beyond the critical displacement the person has become destabilised. The calculation of the critical displacement is detailed in Section 5.4.

5.4 Critical displacement.

When the COG of the person, either represented as a simple solid object or as a mass-spring-damper system, is displaced beyond a certain critical distance the person has become unstable and will have to alter their standing position, for example by moving their feet, so as not to

lose their balance. A person will be blown in different directions depending on how they are standing in relation to the oncoming flow of the slipstream, therefore, their critical displacement is dependent upon their standing orientation. A person will be blown to their side, backwards over their heels or forwards over their toes if they are standing side-on to the oncoming flow, facing the flow or with their back to the flow respectively. A person becomes unstable when their COG moves outside their base (Hof *et al.*, 2005), therefore, instability occurs when the COG is either beyond the side of the foot, the heels or the toes when a person is standing side-on to the oncoming flow, facing the flow or with their back to the flow respectively.

Assuming that a person stands with both feet facing directly forward and shoulder width apart, and taking the person's COG to be positioned on the midline of the body through the sagittal plane, i.e. half way between the right and left sides, a person will become unstable when their COG has been displaced by a distance equal to half the shoulder width when standing side-on to the oncoming flow. The shoulder width of a person is calculated using the data given in the German DIN33402-2 as quoted by Schlick (2003). This data give values of the 50^{th} percentile shoulder width and the 50^{th} percentile height for women and men, and is reproduced in Table 5.2. A person's shoulder width is assumed to be proportional to their height, therefore, dividing a person's shoulder width by their height gives the shoulder width in terms of a person's height (h_1), the values of which are given in Table 5.2. The shoulder width to height ratio of a man is greater than that of a woman, i.e. $0.23h_1 > 0.22h_1$, reflecting the broader shoulders that occur in men. The critical displacement is half the shoulder width, and is therefore $0.110h_1$ and $0.115h_1$ for a woman and a man respectively. The shoulder width of a child is assumed to be $0.22h_1$, i.e. the same as for an adult female, as a child's

shoulders will not be as broad in relation to their height as an adult male's, therefore, a child's critical displacement is $0.110h_1$.

Person	50^{th} percentile body height (h_1) (m)	50^{th} percentile shoulder width (m)	Shoulder width in terms of h_1
Adult female	1.619	0.355	$0.22h_1$
Adult male	1.733	0.398	$0.23h_1$

Table 5.2. A person's height, shoulder width, and shoulder width in terms of h_1.

Standing orientation		Critical displacement
Facing the flow		$0.050h_1$
Back to the flow		$0.100h_1$
Side on to the flow	Adult female	$0.110h_1$
	Adult male	$0.115h_1$
	Child	$0.110h_1$

Table 5.3. Critical displacement related to height.

For a person either facing or with their back to the flow the critical displacement is determined from the length of a person's foot, which is 15% of a person's height (Van Bogaert, 1999). As the torso is positioned towards the rear of the foot, the model assumes that a person's COG is above a position one third of their foot length from the back of the heel when standing upright. Therefore, the critical displacement is taken to be a third and two thirds of the foot length when being pushed over the heels and over the toes respectively. The critical displacement, in terms of a person's height, is therefore $0.05h_1$ ($0.333\times0.15h_1$) and

$0.10h_1$ ($0.666 \times 0.15h_1$) when a person is facing the oncoming flow and has their back to the flow respectively. The critical displacement values relating to the various standing orientations are given in Table 5.3.

The model calculates the critical displacement of each generated person and identifies if their displacement reaches the critical value when they are represented as either a simple solid object or a mass-spring-damper system. If the critical displacement is reached at any time during the person's response that person is identified as having become destabilised. However, a person identified by the model as being destabilised will not necessarily fall over in reality, but will have to alter their stance in order to regain their stability.

5.5 Generating random people.

A wide section of the British population travel by train, therefore, within certain limits, the model generates people standing on a station platform that have random weights, heights, ages, gender and standing positions. It is assumed that young children are likely to either be in a pushchair or otherwise securely positioned when waiting for a train, therefore, the model generates people that are aged seven years or older on a station platform. A statistical bulletin of travel by Scottish residents (The Scottish Government, 2005) gives the number of trips per person per year by the main mode of transport and shows details relating to age and gender. Under the transport category that includes rail, the number of trips per person is 17, 87 and 20 for children aged under 16, adults between 16 and 59 inclusive, and adults aged 60 and over. If it is assumed that there is a uniform distribution of children's ages, then the number of children aged between 7 and 15 inclusive is 17 × 9/16, i.e. 9.6. Therefore, the ratio of children

to adults (excluding the elderly) to elderly adults is 9.6 : 87 : 20, which is approximately 1 : 9 : 2. The model generates children between the ages of 7 and 16 inclusive, adults (excluding the elderly) between 17 and 59 inclusive, and elderly adults between 60 and 84 inclusive, and generates the people within these age categories using the above ratio. The model assumes that people's ages are uniformly distributed within each age category. Although the statistical data define children as being aged under 16, the model defines 16 year olds as children because height and weight only stop increasing rapidly at the age of 17 according to the graphs presented by Halls (2004). The same statistical bulletin also gives the number of trips for a woman and a man as 34 and 33 respectively, so the number of females and males standing on a station platform is taken to be equal. The model reproduces the age and gender ratios when generating people standing on a station platform. A report by Network Rail (2006) states that 96% of its maintenance workers are male, and as allowing for the small proportion of female trackside workers will not effect the results the model only generates men standing alongside an open track. The ages of the trackside workers are generated to be uniformly distributed between 17 and 59 inclusive to reflect the probable age range of these workers.

The model generates the heights and weights of all the people by using a normal distribution, the means and standard deviations of which are calculated using the data given in Halls (2004) on the 5^{th}, 50^{th} and 95^{th} percentile values of height and weight. The data in Halls (2004) is taken from the National Health and Nutrition Examination Survey (NHANES III) that was undertaken in the US during the years 1988 – 1994. The data show that both height and weight change with age, with the changes occurring more rapidly in children, as would be expected, therefore, the heights and weights of children are calculated for each particular age

(7, 8, 9 years, etc.). As an adult's weight and height do not change as much as those of a child, these parameters are calculated using the nearest decade to the adult's age (20, 30, 40 years, etc.); for example, a forty-seven year old will have the weight and height associated with a fifty year old. The data show that the distribution of height is only slightly skewed, therefore, the mean height of the normal distribution is taken to be the 50^{th} percentile value corresponding to the age of the person. The probability of a person being below the 5^{th} percentile height is 0.05, and this is used to determine the standard deviation of the height using a normal distribution table. The distribution of the weight, however, is positively skewed, i.e. there's a greater range of weights between the 95^{th} and 50^{th} percentiles than between the 5^{th} and 50^{th} percentile; for example, the 5^{th}, 50^{th} and 95^{th} percentile weights of a girl aged 16 are 46kg, 57kg and 90kg respectively. The 50^{th} percentile weight value is taken to be the mean, as with the height data, but an effective 5^{th} percentile value is used to determine the standard deviation of the normal distributions. The effective 5^{th} percentile is the value of the 50^{th} percentile minus half the difference between the 5^{th} and 95^{th} percentiles of weight, thereby approximating a non-skewed distribution. Table 5.4 gives the mean and standard deviations used to generate the random heights and weights of children and adults.

Person	Age (years)	Female				Male			
		Height (m)		Weight (kg)		Height (m)		Weight (kg)	
		Mean	Standard deviation	Mean	Standard deviation	Mean	Standard deviation	Mean	Standard deviation
Child	7	1.210	0.055	23.0	5.167	1.220	0.061	23.5	4.559
	8	1.270	0.063	25.5	6.383	1.280	0.064	26.5	5.623
	9	1.340	0.066	29.0	7.751	1.340	0.067	30.0	6.991
	10	1.410	0.070	33.5	9.119	1.405	0.070	35.0	8.359
	11	1.470	0.070	38.5	10.182	1.475	0.075	40.0	9.726
	12	1.520	0.073	45.5	11.246	1.540	0.078	45.0	10.942
	13	1.575	0.070	51.0	12.310	1.600	0.078	50.5	12.614
	14	1.615	0.066	55.0	12.918	1.650	0.078	56.0	13.830
	15	1.630	0.061	56.0	13.374	1.705	0.073	61.0	14.894
	16	1.635	0.060	57.0	13.374	1.750	0.075	66.0	15.198
Adult	20	1.640	0.061	59.0	15.198	1.770	0.067	72.0	14.590
	30	1.640	0.061	63.0	16.413	1.770	0.067	79.0	15.198
	40	1.640	0.061	67.0	17.021	1.775	0.067	82.0	16.109
	50	1.630	0.061	69.0	16.413	1.770	0.067	83.0	16.109
	60	1.615	0.061	70.0	15.805	1.760	0.061	83.0	14.894
	70	1.590	0.061	68.0	15.198	1.735	0.061	81.0	13.374
	80	1.565	0.061	63.0	14.286	1.710	0.061	76.5	12.462

Table 5.4. Mean and standard deviation values of height and weight.

The train side is assumed to be alongside the platform edge when the train passes through a station so that a person standing 1m from the platform edge is also 1m from the train side. The model allows the generated people to be standing between two distances from the side of

a passenger train. However, the maximum distance that a person can stand is 3.5m and 2.5m from the side of a passenger train passing a station platform and travelling along an open track respectively, as slipstreams can only be simulated to these distances due to the limitations of the data from the train slipstream tests (described in Section 2.2). A person can only be positioned at 1.5m and 0.705m from the side of a freightliner passing a station platform and travelling along an open track respectively, as the slipstream measurements were only taken at these distances during the tests. The standing orientation of a person on a station platform is randomly generated using a uniform distribution so that there is an equal chance of a person standing with their right side, left side, front or back towards the oncoming flow of the slipstream. A man standing alongside an open track is modelled with his side towards the flow, as it is probable that when he moves back from an approaching train he stands with his back to the tracks (Bates, 2004).

5.5.1 Checking the suitability of the generated people.

Certain limits are set and adjustments made to the weights and heights of the simulated people to ensure that realistic values are generated for the person's age and gender, e.g. there are no 2.4m (8') tall people or 1.8m (6') tall people weighing 32 kg (5 stone). A limit of 2cm below the 5th percentile and above the 95th percentile is allowed for the heights of both children and adults. A limit of 1.5kg below the 5th and above the 95th percentile is allowed for an adult's weight, and a 1.5kg limit above the 95th percentile is also set for a child's weight. However, due to a child's weight being more positively skewed than an adult's, a limit of only 0.5kg is allowed below the 5th percentile weight, and if a child's weight is generated to be more than 1kg below the 5th percentile their weight is increased to be the mean value. The values of

these limits are used as it is reasonable to assume that only a small percentage of people, if any, will have heights or weights beyond them. Therefore, excluding anyone who does have a height or weight beyond the limits will not affect the model's results. Table 5.5 gives the ranges of height and weight values of children and adults.

Person	Age (years)	Female		Male	
		Height range (m)	Weight range (kg)	Height range (m)	Weight range (kg)
Child	7	1.110 – 1.330	17.5 – 36.5	1.090 – 1.330	17.5 – 34.5
	8	1.160 – 1.400	19.5 – 42.5	1.150 – 1.400	19.5 – 39.5
	9	1.220 – 1.480	21.5 – 49.5	1.210 – 1.470	22.5 – 47.5
	10	1.280 – 1.550	24.5 – 56.5	1.270 – 1.540	25.5 – 55.5
	11	1.340 – 1.620	27.5 – 63.5	1.330 – 1.620	29.5 – 62.5
	12	1.390 – 1.670	31.5 – 70.5	1.390 – 1.680	33.5 – 71.5
	13	1.440 – 1.710	36.5 – 79.5	1.460 – 1.750	37.5 – 80.5
	14	1.480 – 1.740	40.5 – 85.5	1.520 – 1.800	42.5 – 89.5
	15	1.510 – 1.750	43.5 – 89.5	1.570 – 1.850	46.5 – 97.5
	16	1.520 – 1.760	45.5 – 91.5	1.600 – 1.890	50.0 – 102.5
Adult	20	1.530 – 1.770	45.0 – 97.5	1.655 – 1.910	55.0 – 106.5
	30	1.520 - 1.770	46.5 – 104.0	1.660 – 1.920	60.5 – 103.5
	40	1.520 – 1.760	48.5 – 107.0	1.650 – 1.910	61.5 – 117.5
	50	1.515 – 1.755	49.5 – 106.5	1.650 – 1.900	62.0 – 117.5
	60	1.500 – 1.740	49.5 – 104.5	1.640 – 1.880	61.5 – 113.5
	70	1.480 – 1.720	48.5 – 101.5	1.620 – 1.860	60.5 – 107.5
	80	1.445 – 1.685	46.5 – 96.0	1.590 – 1.830	58.0 – 101.5

Table 5.5. Ranges of height and weight.

Another consideration regarding weight is that ε_n is inversely proportional to m_{tot} and $\varepsilon_n < 1$, as described in Section 5.3.3. From equations (5.74) and (5.76), the minimum mass of a young and middle-aged person must be greater than 15.702kg and greater than 13.915kg for an elderly person to ensure that $\varepsilon_n < 1$. Table 5.5 shows that no elderly person is simulated with such an unnaturally low weight of 13.915kg. Although a child does have a low weight its minimum weight is 17.5kg, which is associated with a 7 year old child, and this is larger than the required 15.702kg. Therefore, the value of ε_n is less than unity for all generated people.

BMI value	Weight status
≤ 18.5	Underweight
18.5 - 24.9	Normal weight
25.0 - 29.9	Overweight
≥ 30	Obese

Table 5.6. BMI values and weight status of adults.

Body mass index (BMI) is also utilised to ensure that reasonable weights and heights are generated, and to check that the model produces the correct proportion of underweight, normal weight, overweight and obese people that are within the current general population. The BMI of a person is their weight (kg) divided by the square of their height (m^2), and Table 5.6, which is taken from Halls (2004), gives the weight status of adults as determined by their BMI. A health survey of England in 2003 (Sproston and Primatesta, 2004) shows that over half of the adult population is either overweight or obese, with one in five being obese, and the model generates similar percentages of overweight and obese adults. A similar approach is taken for children. However, the BMI relating to each weight status of a child increases with

increasing age, e.g. a girl aged 7 and 10 is categorised as obese when her BMI reaches 19.7 and 23 respectively. The BMI weight status also differs between girls and boys. Therefore, the BMI values associated with underweight, normal weight and obese children are determined for each age and each gender. A report of the Royal College of Physicians of London, the Royal College of Paediatrics and Child Health, and the Faculty of Public Health (2004) shows that 16% of UK children were obese in 2001, and the model generates children with a similar incidence of obesity. For example, one set of randomly generated people produces 35%, 22% and 18% of overweight adults, obese adults and obese children respectively.

5.6 Discussion.

The response of a person subjected to a train slipstream is modelled in two parts, they are initially considered to respond as a simple solid object until the inception of the muscular response after which they are modelled as a mass-spring-damper system with both stiffness and damping. The initial response of a young and middle-aged person lasts for 0.375s, whereas an elderly person has a slower reaction time and is modelled as a simple solid object for 0.476s. This results in a person responding as a simple solid object during most, if not all, of the slipstream velocity peak at the train nose, except at low train speeds.

Various mass-spring-damper models of a standing person available in the literature (e.g. Nigg and Liu, 1999) give values for stiffness and damping. However, these values are appropriate for a response to a vertical force only, and could not even be used as a basis for determining appropriate stiffness and damping values in the current research as the values in the literature vary greatly between models. Therefore, the model assumes that $c_1 = c_2 = c_3$ for everyone,

and $k_1 = k_2 = k_3$ for young and middle-aged people, and uses the results from the wind tunnel tests investigating the effect of a sudden gust on a person to determine the values of f and c_{tot}. The values of f and c_{tot} that result in the closest match between the simulated and measured proportion of displaced people are 0.9Hz and 215Ns/m, respectively, although it can be conjectured that the values of f and c_{tot} change from person to person. The experimental data presented by Wei and Griffin (1998), and used in their model of a seated person subjected to vertical vibration, show that damping varies between people, e.g. the total damping of an average child is lower than that of an average adult. As all the factors that affect the values of f and c_{tot} are not known, and the amount by which these parameters vary is also unknown, the variation is not modelled. However, the values of f and c_{tot} used by the model will be the average of the range of values associated with the people involved in the sudden gust experiments. The sudden gust experiments exposed the participants to a very rapid change in wind velocity from an initial velocity close to zero, i.e. there was a step change in velocity, and the increased velocity continued for a few seconds. Although there is a rapid increase in slipstream velocity at a train's nose, only the slipstream velocity profile of a freightliner has continuing high velocities as the slipstream velocity of a passenger train decreases after the nose until the high boundary layer velocities are generated. Therefore, the values of f and c_{tot} that were calculated from the sudden gust tests may have been different if the velocity profile of a passenger train's slipstream had been used in the tests.

An elderly person is likely to have a different response to a train slipstream than a younger person, and although no elderly people participated in the wind tunnel tests, the model assumes that the values of f and c_{tot} are applicable for people of all ages. However, the model uses the results of Liu *et al.* (2006) from experiments examining the effects of age

upon leg stiffness, and so takes the value of k_3 of an elderly person to be 70% that of a younger person. The experiments described in Liu *et al.* (2006) involved participants performing a counter movement jump in which they rapidly squatted down from an upright position then jumped into the air with maximum effort. Although this is not the response of a person of any age to a slipstream, the reduced stiffness determined from the experiments is taken to be a feature of an elderly person's leg.

The value of f of a person corresponds to a slipstream frequency that is simulated with reasonable accuracy by the model. For example, a person exposed to the slipstream of a full-scale 363.8m passenger train passing a station platform at 51m/s has a dimensionless f value of 6.4, where f is normalised by $\frac{L}{U}$. A wavelet spectra plot for this train, given in Figure 3.11, shows that the dimensionless power of the measured and simulated slipstreams is similar at the dimensionless frequency of 6.4. The dimensionless f value does not correspond to either the lowest or higher slipstream frequencies that are not as accurately reproduced. This is true for the entire length of the slipstream of this train and also for a full-scale passenger train passing an open track (see Figure 3.12), a full-scale freight train (Figures 3.17 and 3.18) and a model-scale passenger train (Figure 3.21). As an applied force with a frequency that coincides with the natural frequency of a person will result in large oscillations, the slipstream frequency that would create the largest displacements of a person is modelled with reasonable accuracy. Although the higher frequencies of a passenger and freight train's slipstream and the lower frequencies of a passenger train are not as accurately simulated they will not affect a person's response to the same extent as the middle range frequencies that include the f value of a person.

The force acting on a person is calculated using parameters C_D and $\frac{A}{A_{DU}}$ which are appropriate for people wearing trousers with a shirt, sweater or a buttoned jacket. People wearing skirts are not considered by the model as it is not possible to determine the proportion of skirt wearers in the commuting population, however, it is likely that the majority of people standing on a station platform wear trousers. As all trackside workers also wear trousers, the model assumes that all people wear trousers. It is also not possible to determine the proportion of people wearing coats that are flapping in the slipstream, especially as it depends upon the season. However, it can be assumed that only a few people on a station platform are wearing coats as opposed to jackets, and only a small proportion of these will allow their coats to flap in the slipstream on a station platform. Furthermore, it is assumed that no trackside workers wear flapping coats. The value of $C_D.\frac{A}{A_{DU}}$, hence the drag force, relating to people wearing skirts is lower than for those wearing trousers, and is highest for people with a flapping coat. Therefore, for a given height and weight, a person wearing a skirt is more stable than when they wear trousers, and a person with a flapping coat is less stable. Although the greater instability of a person wearing a flapping coat is not modelled, neither is the greater stability of a person wearing a skirt; therefore, by only modelling people wearing trousers without a flapping coat, an approximate average response is generated for all clothing types. The values of C_D and $\frac{A}{A_{DU}}$ are smaller for a person standing side-on to a slipstream than when either facing the oncoming flow or have their back to the flow, and this will result in a lower force acting upon a person who is standing side-on.

The model calculates the horizontal displacements of a person, and when the displacement of a person's COG moves outside the person's base, i.e. beyond a critical displacement, the

person is said to have become destabilised. The base of a person encompasses their feet and the space in-between, and the person's COG is modelled to be at an equal distance from the outer edge of the side of their feet. It is also modelled to be one third of the foot length from the outer edge of their heels; although this is not based on any literature, it is a reasonable assumption as it results in a person being more unstable when facing the slipstream than when they have their back to the flow, as shown by the results of the wind tunnel tests. The critical displacement of a person standing side on to the flow is greater than with either of the other orientations, and this will contribute to the greater stability of a side-on person exhibited by the participants of the wind tunnel tests. The model assumes that a person stands with their feet shoulder width apart, however, this will not be true of all people as some will stand with their feet together and some with their feet very wide apart, e.g. at either side of a suitcase. With the possibility of such extremes of foot placement the assumption that a person's feet are shoulder width apart is an approximate average of the standing position and is, therefore, not an unreasonable assumption to make. Another assumption of the model is that the feet are facing directly ahead whereas in reality the feet will be at an angle, but this will have a negligible effect on the size of a person's base and, therefore, on their stability. The ratio of a person's shoulder width to their height is developed from the data in the German DIN33402-2, where Deutsches Institute für Normung (DIN) is Germany's ISO member body. The model assumes that the ratio is the same for UK citizens, and as the shoulder width measurement is the biacromial width, i.e. the distance between the highest point of the scapula bone of each shoulder, it is unaffected by body fat and therefore applicable to most of the population regardless of body mass. As both the foot length and shoulder width are proportional to a person's height, the critical displacement can be determined for all standing orientations for a given height.

On a station platform there are people from the age of seven up to eighty-five years. The youngest person generated on a station platform is aged seven, as children below the age of seven are assumed to be either in a pushchair or otherwise securely positioned, and so not at risk of losing their balance from a slipstream whilst standing. Although in reality some young children will be allowed to wander about the platform unattended, their number is likely to be very small and will, therefore, have a negligible effect on the results of the model. The maximum age of a person generated on a station platform is eighty-five as the data pertaining to weight and height are only available up to the age of eighty and seventy, respectively, from the source used. The data allow reasonable extrapolation up to the age of eighty-five, but any extrapolation beyond this would be increasingly inaccurate. It is likely, however, that there will be very few people above the age of eighty-five on a station platform and those present are likely to be seated. Therefore, their exclusion from the model will have a negligible effect on the results. The proportion of children, young and middle-aged adults, and elderly adults simulated on a station platform reflects that found in the actual commuting population, with the population consisting mainly of young and middle-aged adults. Trespassers on the tracks are not included in the model as the numbers of these are assumed to be very small in comparison to the numbers of trackside workers and consequently will not affect the results.

Although the data used to determine the weight and height of a person is based on the US population it can be assumed to apply to the current UK population. The weight and height data is from the NHANES III survey which was undertaken during 1988 – 1994. This survey, as described by the National Center for Health Statistics (2007), reports that 56.0% of US citizens aged twenty and over were overweight or obese, while 22.9% were obese. A health survey undertaken in England in 2003 (Sproston and Primatesta, 2004), shows that over half the adult population are overweight or obese, with one in five being obese. The surveys show

that the proportions of overweight and obese US citizens in 1988 – 1994 are similar to those of UK citizens in 2003; therefore, the US data is applicable for the current UK population. The BMI values of the simulated people also show that the correct proportions of overweight and obese people in the UK population are generated by the use of the NHANTES III survey data.

5.7 Conclusions.

A person's response to a slipstream is modelled as a simple solid object for a fraction of a second after first being exposed to a train slipstream and before the inception of their muscular response. If the force due to the slipstream is large enough the simple solid object will rotate about its pivotal axis. An elderly person is modelled as a simple solid object for a 27% greater time period than a younger person in order to allow for their slower response. The final horizontal displacement distance of the simple solid object's COG is taken to be the initial displacement of a mass-spring-damper system. This system models a person's response after the muscular response is initiated, and consists of three masses, springs representing the elastic components of the muscles, and dampers representing the viscous resistance of the muscles. The stiffness of an elderly person's lower body is taken to be less than that of a younger person in order to further simulate the age-dependent response of a person. The force acting upon the system is taken to be a succession of individual short-duration impulses, and a person's response is the sum of the responses to each impulse. The displacements of each of the three masses are determined, and from these the displacement of the COG of the body as a whole is calculated. When the person's displacement reaches a critical distance the person is recorded as having become destabilised. The critical displacement is dependent upon a

person's standing position, their height and, when standing side on to the oncoming flow, their gender. Random people are generated using realistic values of height and weight, and appropriate gender, age and standing orientation proportions are generated depending upon whether the person is standing on a station platform or by the side of an open track.

CHAPTER 6.

A PERSON'S RESPONSE TO A SLIPSTREAM.

6.1 Introduction.

The model generates a thousand individual slipstream velocity time histories based on chosen train parameters and distances from the train side/platform edge. It also generates an equal number of randomised people, each of which is exposed to one velocity time history. The maximum displacement of each person is calculated and if this is greater than the critical displacement the person is recorded as having been destabilised. The model goes on to calculate the percentage of the thousand people that are destabilised by the train slipstream. A thousand slipstreams and people are generated as this number results in statistically stable results for all of the train types.

6.2 A person's displacement during the passing of a train.

In order to visualise the response of a person generated by the model the normalised displacements of a woman weighing 65kg and 1.64m tall (the 50^{th} percentile values for a thirty-year-old female), standing 0.25m from a station platform edge and facing into a slipstream generated by a passenger train travelling at 85m/s are illustrated in Figure 6.1. The displacement is normalised by the height to the woman's centre of gravity, where a positive and a negative normalised displacement corresponds to this person being pushed backwards and tipping forwards respectively. Figure 6.1 shows that this person first starts to move after the nose of the train has past. She then oscillates backwards and forwards, and reaches the

normalised critical displacement of 0.09 at the normalised time (T) of 0.18, therefore, this person becomes destabilised when the main body of the train passes. Although the figure shows the person continuing to oscillate after the critical displacement is reached the continuing oscillations are superfluous, as at $T = 0.18$ the person has either altered their standing position in order to remain upright or has fallen over.

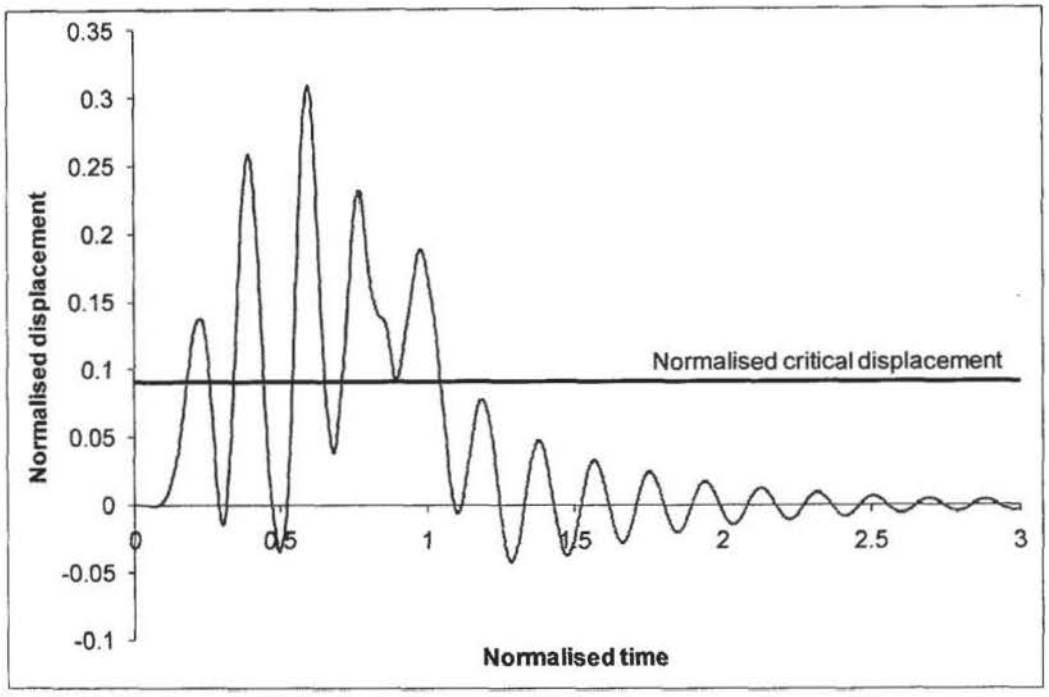

Figure 6.1. Normalised displacement distance of a woman standing 0.25m from a station platform edge and facing into a slipstream generated by a passenger train travelling at 85m/s.

Table 6.1 gives the normalised displacement distances of each mass in each mode of vibration when the critical displacement distance is reached during the response illustrated in Figure 6.1. The largest normalised displacements are associated with the first mode for all of the three masses showing that the displacements in the second and third modes contribute relatively little to the displacement of each mass.

Mass	Mode		
	1st	2nd	3rd
m_1	0.112m	0.002m	0.013m
m_2	0.108m	0.001m	-0.001m
m_3	0.060m	-0.004m	0m

Table 6.1. Normalised maximum displacement distances of the three masses in the three modes.

6.3 Investigating when a person is destabilised.

Figure 6.1 shows that a thirty year old woman weighting 65kg and 1.64m tall is destabilised when the main body of the train is passing and she is subjected to the velocities generated in the boundary layer region of the slipstream. In order to determine if a particular region is associated with the destabilisation of people more than any other region, the value of T was recorded when a person's displacement became greater than their critical displacement. This was undertaken for people standing at 0.25m from a station platform edge with a passenger train travelling at 85m/s. Of the thousand people modelled, 697 are destabilised; with 657, 4 and 36 destabilised when the boundary layer region, the vortex and the transition region passes respectively. No one is destabilised when the velocity peak at the nose of the train passes. The small number of people destabilised when the transition region passes lose their stability before T = 1.09, i.e. immediately after the velocity peak at the rear of the train, suggesting that it is the velocity peak that causes their destabilisation. There are 39.1% of people destabilised when modelled to be standing at 1.5m from the side of a freightliner travelling past a station platform at 40m/s, and all of the people who lose their balance in this

instance do so when the main body of the train passes. Therefore, the critical region with regards to a person's stability is the boundary layer region along the main body of the train.

6.4 The effect of train speed, train type and distance from the train side on a person's stability.

In order to determine how train speed, train type and distance from the train side effect a person's stability the model randomly generated people standing on a station platform and subjected them to increasing speeds of both a full-scale passenger train and a freightliner, and positioned them at increasing distances from the side of the full-scale passenger train. Both train types were 363.8m in length in order to facilitate comparison between the results. Table 6.2 gives the percentages of people destabilised by the slipstream of a passenger train travelling by a station platform at various speeds, with the commuters standing between the platform edge (0m) and 1.5m, between 0.25m and 1.5m, and between 0.5m and 1.5m. Figure 6.2 gives a graphical representation of this data. The results show that the percentage of people destabilised increases with increasing train speed, as would be expected. For example, when people are standing between the platform edge and 1.5m the percentage destabilised goes up from 3.5% to 24.6% when the train speed is increased from 45m/s to 85m/s. As people are positioned further from the platform edge the percentages reduce. For example, 18.3% of people are destabilised when standing between 0m and 1.5m from the side of the train travelling at 75m/s, whereas approximately half this proportion are destabilised when standing between 0.25m and 1.5m, i.e. 9.2%. Also, people are first destabilised by a train speed of less than 45m/s when standing between 0m and 1.5m, however, when they are standing between 0.25m and 1.5m they are not destabilised until the train reaches a speed of

between 55m/s and 65m/s. This reflects that the slipstream velocities decrease with increasing distance from the train side, as described in Section 2.2.1.

Train speed (m/s)	Distance from platform edge		
	0m – 1.5m	0.25m – 1.5m	0.5m – 1.5m
45	3.5%	0%	0%
55	6.7%	0%	0%
65	13.7%	4.6%	1.4%
75	18.3%	9.2%	6.3%
85	24.6%	17.6%	8.5%

Table 6.2. Effect of train speed and distance from the station platform edge on the percentage of people destabilised by a passenger train.

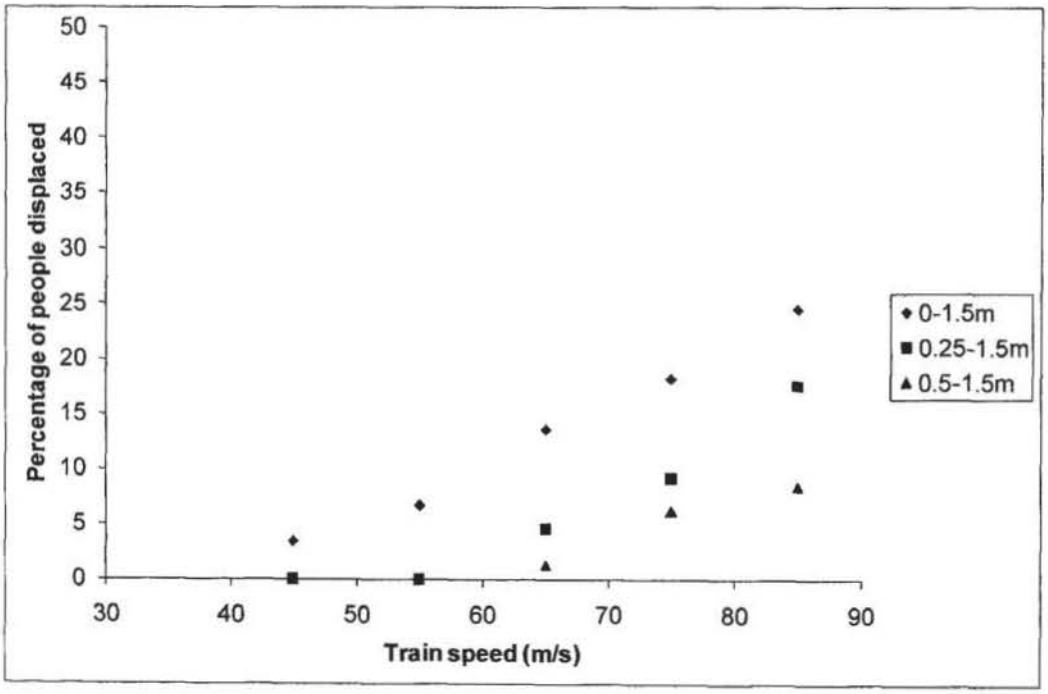

Figure 6.2. Percentage of people destabilised when standing at various distances from the station platform edge by the slipstream of a passenger train travelling at various speeds.

Table 6.3 gives the percentage of people destabilised who are standing 1.5m from the edge of a station platform when a freightliner passes by, and Figure 6.3 gives these results in graphical form. The percentage of destabilised people increases with increasing freightliner speed as with the passenger train results. For example, 0.7% and 39.1% of people are destabilised by a freightliner travelling at 20m/s and 40m/s, respectively. However, a greater proportion of people are destabilised at lower freightliner speeds than passenger train speeds even though the distance from the side of the freightliner is greater than the distances from the side of the passenger train. For example, 30.1% of people are destabilised when standing at 1.5m from the side of a freightliner travelling at 35m/s, but only 24.6%, 17.6% and 8.5% are destabilised at 0m – 1.5m, 0.25m – 1.5m, and 0.5m – 1.5m from the side of a passenger train travelling at 85m/s, respectively. Section 2.2.1 shows that higher slipstream velocities are associated with a freightliner than with a passenger train at comparable train speeds and distances from the train side, and this is reflected in the results presented in Tables 6.2 and 6.3, where a freightliner affects a person's stability more than a passenger train.

Train speed (m/s)	Percentage of people destabilised
20	0.7%
25	15.7%
30	21.9%
35	30.1%
40	39.1%

Table 6.3. Effect of train speed on the percentage of people destabilised by a freightliner when standing at 1.5m from the station platform edge.

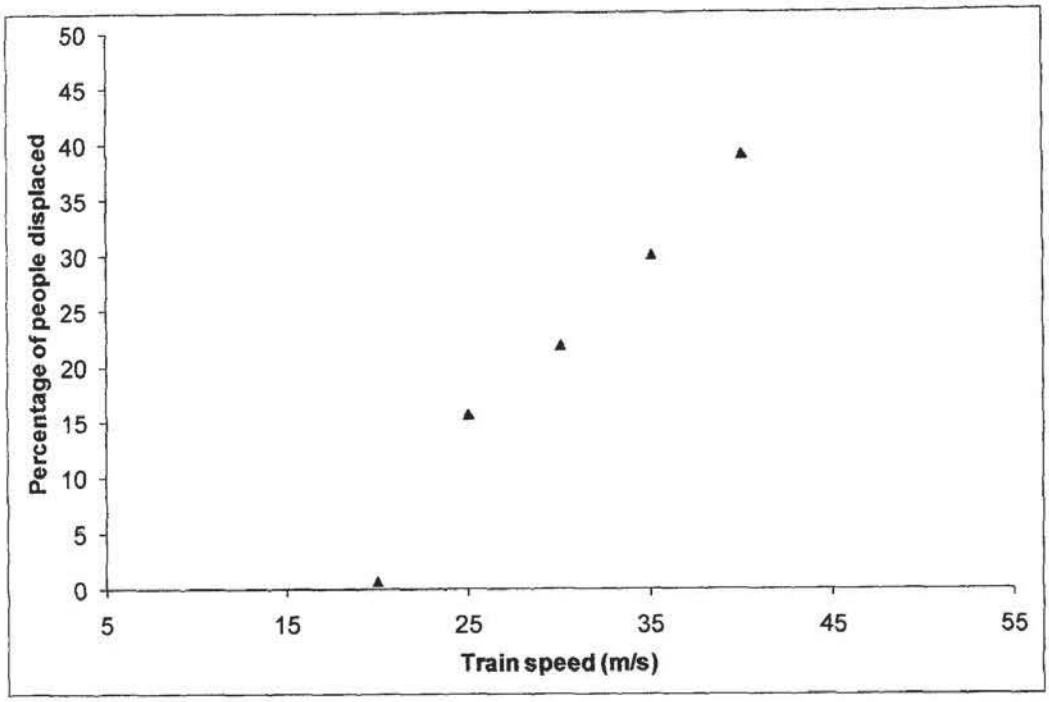

Figure 6.3. Percentage of people destabilised at 1.5m from the platform edge by the slipstream of a freightliner travelling at various speeds.

6.5 Parametric analysis.

The various parameters of the equations involved in generating a slipstream and a person are analysed to identify which have the most influence on a person's stability, and the results of this parametric analysis are given in Tables 6.4 to 6.11. A passenger train passing by a station platform at 85m/s when everyone is standing 0.25m from the platform edge results in 69.7% of the people being destabilised by the slipstream, and this result is used as the reference run for the parametric analysis. (This reference run is also used to investigate when a person is destabilised in Section 6.3.) The original value of each parameter is given in brackets in Tables 6.4, 6.5 and 6.6.

Table 6.4 shows how varying the slipstream parameters that are associated with generating the mean velocity time history affects the percentage of destabilised people. When the train

length is increased to be the same length as the eighteen carriage Eurostar trains, i.e. 400m (Jowit, 2007), there is only a 1.7% increase in the percentage of people destabilised; however, when the train length is decreased to 200m there is a decrease of 24.7% in the people destabilised. Therefore, a person's stability is affected by train length. Modelling the train's height as 4.5m to be the same as that of the E4 Series Shinkansen (Fossett, 2007) results in a 1.1% decrease in destabilised people; whereas a 2.73m tall train, such as a British Class 390 'Pendolino' train (Wikipedia, 2007b), results in 1.3% more people destabilised. Varying the width of the main body of the train to be 2.90m (British Class 390 'Pendolino') or 3.4m (E4 Series Shinkansen) results in a +3.4% and a -2.0% change in the number of destabilised people respectively. Altering the dimensions of the train's nose to those of a British Class 390 'Pendolino' so that the nose length and width are 2.9m and 2.1m respectively (as calculated from Virgin Trains (2007) in the same manner as described in Section 3.6.1.1) results in a change of only -1.9% and +0.4% of people destabilised respectively. As these percentage changes are very low they may be due to the normal variability in the results of the model. With a nose width of 3.07m the nose is modelled to be the same width as the train's main body, therefore, the train is effectively modelled to have a nose that does not taper in width. A nose length of 0m also models a nose that does not taper. The results from both these altered train dimensions are also very low, with changes of +1.4% and +1.6% for a nose length of 0m and a nose width of 3.07m respectively. Therefore, altering the nose dimensions does not affect the stability of people.

In the model the parameters of n and C_1 are dependent upon the distance from the side of the train, however, in the parametric analysis they take the values of 10 and 11.5 respectively, which are applicable to flow in pipes with a Reynolds Number (Re) of 1.6×10^6. The values

correspond to the maximum Re tested in the experiments of Nikuradse (1932) (cited in Duncan *et al.*, 1970). The values of n and C_1 corresponding to the maximum Re are used as $Re = 21.2 \times 10^8$ in the reference run, i.e. it is greater than the maximum value of the experiments. Altering n and C_1 results in a +5.6% and a -9.5% change in the number of people destabilised respectively. There are increases in the percentage of people destabilised when U_{max} is increased to the value used with a passenger train travelling along an open track, i.e. 50% of the train speed ($0.5V$), and the radius (R) of the vortex is increased to equal half the train width, i.e. 1.535m. The resulting changes to stability due to these alterations in the two parameters are +14.6% and +5.6% respectively. When the constant B is varied by +25% and by -25% the resulting changes are +9.0% and -12.1% respectively. Baker (2001) gives values of α and β for train wakes that fit the theory of Eskridge and Hunt (1979), and both these values are of the order of 20 for the distance of 0.25m from the train side. When the values of α and β are taken to be 20 there is a -3.2% and a -3.0% change in the numbers of people destabilised.

Figure 3.13 gives the values of the Index of Agreement (d) validating the slipstream model in the frequency domain for a passenger train passing a station platform at various distances from the train side (y_s). The values of d are over 0.8 along the full length of the slipstream for all y_s values. Assuming that d is also greater than 0.8 at y_s = 0.25m, although the smallest value of y_s in Figure 3.13 is 0.57m, there is less than a 20% error in modelling the slipstream of this train in the frequency domain. Therefore, the values of the AR coefficients (ϕ_1, ϕ_2 and ϕ_3) are altered by ±20% in the parametric analysis, and the results of this analysis are given in Table 6.5. The most sensitive AR coefficient is ϕ_1 in the wake. Reducing this parameter by

20% from 0.65 to 0.52 results in a decrease in stability by 8.0%, whereas increasing the parameter by 20% to 0.78 results in an increase in stability by 10.9%.

Slipstream region	Parameter		Percentage of people destabilised	Percentage change
General	Train length (364m)	400m	70.9%	+1.7%
		200m	52.5%	-24.7%
	Height (3.84m)	2.73m	70.5%	+1.3%
		4.50m	68.9%	-1.1%
	Width (3.07m)	2.90m	72.1%	+3.4%
		3.40m	68.3%	-2.0%
Upstream and around nose	Nose length (1.59m)	0m	70.7%	+1.4%
		2.90m	68.4%	-1.9%
	Nose width (2.30m)	2.10m	70.0%	0.4%
		3.07m	70.8%	+1.6%
Main body	n (16.28)	10	73.6%	+5.6%
	C_1 (8.16)	11.5	63.1%	-9.5%
Vortex	U_{max} (0.35V)	0.5V	79.9%	+14.6%
	R (0.768m)	1.535m	73.6%	+5.6%
	B (284)	213	76.0%	+9.0%
		355	61.3%	-12.1%
Wake	α (2.5)	20	67.5%	-3.2%
	β (1)	20	67.6%	-3.0%

Table 6.4. Effect of varying the slipstream parameters associated with generating the mean velocity.

Slipstream region	Parameter		Percentage of people destabilised	Percentage change
Upstream and around nose	ϕ_1 (0.5)	0.4	67.9%	-2.6%
		0.6	72.2%	+3.6%
	ϕ_2 (0.2)	0.16	70.7%	+1.4%
		0.24	70.0%	+0.4%
	ϕ_3 (0.003)	0.0024	68.6%	-1.6%
		0.0036	68.7%	-1.4%
Main body	ϕ_1 (0.35)	0.28	66.4%	-4.7%
		0.42	72.4%	+3.9%
	ϕ_2 (0.55)	0.44	70.1%	+0.6%
		0.66	68.8%	-1.3%
	ϕ_3 (0.03)	0.024	67.6%	-3.0%
		0.036	74.5%	+6.9%
Vortex and transition	ϕ_1 (0.5)	0.4	69.8%	+0.1%
		0.6	71.6%	+2.7%
	ϕ_2 (0.2)	0.16	76.2%	+9.3%
		0.24	65.1%	-6.6%
	ϕ_3 (0.0141)	0.0113	69.7%	0%
		0.0169	69.8%	+0.1%
Wake	ϕ_1 (0.65)	0.52	75.3%	+8.0%
		0.78	62.1%	-10.9%
	ϕ_2 (0.1)	0.08	68.8%	-1.3%
		0.12	69.3%	-1.0%
	ϕ_3 (0.0039)	0.0031	68.7%	-1.4%
		0.0047	69.2%	-0.7%

Table 6.5. Effect of varying the slipstream parameters associated with generating the turbulence.

Tables 6.6 to 6.11 are concerned with an analysis undertaken on the parameters associated with modelling a person. Table 6.6 shows that when a person is not modelled to have any damping, i.e. $c_{tot} = 0$, the number of people destabilised increases by 11.4%. The model of a person developed by Morasso *et al.* (1999) has a natural frequency (f) of 0.5Hz, therefore, f in the parametric analysis is reduced to 0.5Hz which results in 39.3% more people destabilised than when $f = 0.9$Hz. The analysis of the parameters of a person is continued by investigating how clothing affects a person's stability. The model assumes that everyone wears trousers with a shirt, sweater or buttoned jacket in the choice of C_D and $\frac{A}{A_{DU}}$ values. In order to investigate how clothing affects stability the model generated the commuting population to all be wearing skirts, or to all be wearing trousers with a flapping coat. Table 6.7 gives the values of C_D and $\frac{A}{A_{DU}}$ associated with the various clothing types, which are taken from Penwarden *et al.* (1978), and Table 6.8 shows the effect that clothing has on stability. With all the commuting population wearing skirts there is a 12.3% reduction in destabilised people compared to when they all wear trousers, which indicates that wearing a skirt increases a person's stability. Conversely, wearing a flapping coat decreases a person's stability, with 26.0% more people being destabilised than when a shirt, sweater or buttoned jacket is worn.

Parameter	Value	Percentage of people destabilised	Percentage change
C_{tot} (215Ns/m)	0Ns/m	78.0%	+11.4%
f (0.9Hz)	0.5Hz	97.5%	+39.3%

Table 6.6. Effect of varying the mass-spring-damper parameters.

Clothing	Facing or with back to slipstream		Side-on to slipstream	
	C_D	$\frac{A}{A_{DU}}$	C_D	$\frac{A}{A_{DU}}$
Trousers with shirt, sweater or buttoned jacket	1.17	0.32	1.01	0.22
Skirt with shirt, sweater or buttoned jacket	1.08	0.30	0.95	0.21
Trousers with flapping coat	1.33	0.35	1.12	0.26

Table 6.7. C_D and $\frac{A}{A_{DU}}$ values for various clothing.

Clothing	Percentage of people destabilised	Percentage change
Skirt with shirt, sweater or buttoned jacket	61.1%	-12.3%
Trousers with flapping coat	87.8%	+26.0%

Table 6.8. Effect of clothing on stability.

The effect that weight and height have upon a person's stability is investigated by changing these parameters of a thirty year old woman standing at 0.25m from a station platform edge and subjected to the slipstream of a passenger train travelling at 85m/s. The reference weight and height are 63kg and 1.64m respectively, which are the 50th percentile values for a thirty year old woman. When the model subjects one particular generated person to a thousand slipstreams the percentage presented by the model can be taken to be equivalent to the probability that the particular individual will be destabilised. Therefore, the probability of the generated thirty year old woman becoming destabilised is 0.721, and this is used as the reference result. Table 6.9 shows how this probability varies with varying weight and height. When the weight is increased to the 75th percentile value, but the height remains at the 50th

percentile value, the probability of destabilisation decreases by 8.7%, and with the 95th percentile weight the probability decreases further so that it is 20.8% lower than with the reference run. The probability of destabilisation increases by only 1.1% and 2.6% when the height is increased to the 75th and the 95th percentile values, with the weight at the 50th percentile value. However, increasing the weight and height from the 50th percentile to the 75th and 90th percentiles does not alter the parameter values by the same proportion. For example, weight increases by 20.6% from the 50th percentile value of 63kg to the 75th percentile value of 76kg, whereas the height only increases by 2.7% from the 50th percentile value of 1.64m to the 75th percentile value of 1.685m. Table 6.9 also shows the effect that increasing the weight and height by the same proportion has on stability. An increase of 5% of the weight or height results in a change of only -2.2% or +2.1% respectively. The effect on stability of a larger change to these parameters cannot be investigated as height can only change by a small proportion to remain realistic.

Initially, the model assumed that the lower body stiffness (k_3) of all people irrespective of age was the same for a given total body mass. However, in the final model the value of k_3 for an elderly person is 70% that of a younger person for a given total body mass. The effect that age has upon a person's stability is investigated by showing how the percentage of people destabilised varies when k_3 is independent of and dependent upon age, and the results of this investigation are given in Table 6.10. People are subjected to the simulated slipstream of a passenger train passing a station platform at 85m/s while they are stood at 0.25m from the platform edge. Table 6.10 shows that 68.1% of people aged between seven and sixty years are destabilised by the slipstream. Similarly, 68.1% of elderly people are destabilised when k_3 is independent of age, i.e. k_3 is the same for everyone for a given total body mass. However,

when k_3 is dependent upon age, i.e. the k_3 value of an elderly person is 70% that of a younger person for a given total body mass, the percentage of destabilised elderly people is 79.5%, which is 16.7% greater than that of the younger people. Therefore, a decrease in the lower body stiffness of an elderly person results in a reduced stability compared to a younger person. As no one was displaced whilst their response was modelled as a simple solid object, the delayed reaction of an elderly person did not interfere with the above results. The model incorporated the age-dependence of k_3 in order to simulate an elderly person's reduced stability, and this result has shown that the desired effect has been achieved.

Weight	Height	Probability of the person being destabilised	Percentage change from results for 50th percentile values
63kg (50th percentile)	1.64m (50th percentile)	0.721	-
76kg (75th percentile)	1.64m (50th percentile)	0.658	-8.7%
102.5kg (95th percentile)	1.64m (50th percentile)	0.571	-20.8%
63kg (50th percentile)	1.685m (75th percentile)	0.729	+1.1%
63kg (50th percentile)	1.75m (95th percentile)	0.740	+2.6%
66.15kg (an increase of 5% on the 50th percentile)	1.64m (50th percentile)	0.705	-2.2%
63kg (50th percentile)	1.722m (an increase of 5% on the 50th percentile)	0.736	+2.1%

Table 6.9. Effect of weight and height on the stability of a thirty-year-old woman.

Age		Percentage of people destabilised
7 – 60 years		68.1%
60+	k_3 is same as that of a younger person for a given total body mass	68.1%
	k_3 is 70% that of a younger person for a given total body mass	79.5%

Table 6.10. Effect of lower body stiffness (k_3) on stability.

Standing orientation	Percentage of people destabilised
Front	95.8%
Back	30.0%
Side	1.7%

Table 6.11. Effect of standing orientation on stability.

The results of the full-scale wind tunnel tests undertaken in the current research to investigate the effect of a sudden gust on a person indicate that standing orientation affects stability. Of the three standing orientations, facing the oncoming flow is the least stable, followed by standing with the back to the flow, and being side-on to the flow is the most stable orientation. The effect that standing orientation has on a person generated by the model is shown in Table 6.11 which gives the percentages of people destabilised whilst standing at 0.25m from the station platform edge when a passenger train passes by at 60m/s. In Table 6.11 the orientations front and back refer to a person facing the flow and with their back to the flow respectively. The model reproduces the results of the wind tunnel tests in that the simulated people are least stable when facing the flow and most stable when standing side-on to the flow. For this particular simulation nearly everyone is destabilised by the slipstream

when facing the flow whereas only a very small percentage are destabilised when standing side-on to flow.

6.6 Discussion.

A person's response is initially modelled by a simple solid object, and after a short time period modelled by a mass-spring-damper system. If the wind load is large enough the simple solid object will rotate and the mass-spring-damper system will oscillate. When a person faces or has their back to the flow they will oscillate backwards and forwards, and will oscillate side-to-side when standing side-on to the flow. The oscillations eventually decrease to zero after the train has past, and this is indicative of an undercritically damped system as described in Section 5.3.3. All of the people destabilised by a freightliner passing a station platform and most of the people destabilised by a passenger train passing a station platform became unstable when the main body of the train past, therefore, the boundary layer region is the critical region for most people. However, a small proportion of people on a station platform were destabilised when the velocity peak at the rear of a passenger train past or had just past. Both the boundary layer region and the region immediately after the rear of the train are associated with high velocities and turbulence levels which increase a person's risk of losing their balance. The percentage of destabilised people increases with increasing train speed and decreasing distance from the train side due to the larger slipstream velocities and turbulence levels involved in these circumstances, as described in Section 2.2.1. Also, more people are destabilised by the slipstream of a freightliner than by that of a passenger train with comparable train lengths, speeds and distances from the train side. That a freightliner's slipstream has a greater effect on a person's stability is due to the aerodynamically rough

shape of a freightliner compared to the streamlined shape of a passenger train, therefore a freightliner produces higher slipstream velocities and turbulence levels (Section 2.2.1).

A parametric analysis indicates how varying the values of the parameters involved in simulating a slipstream and a person affects the stability of a person. Of the parameters associated with generating a slipstream, the greatest change in the proportion of people destabilised occurs when the length of the train is reduced to 200m. Therefore, train length is a sensitive parameter, with a longer train associated with decreased stability. A longer train will have a more developed boundary layer region resulting in higher velocities along the length of its main body, thereby exposing a person to greater slipstream forces. The velocity peak at the nose of the train is not a critical region for the stability of a person, and altering the parameters of the train's nose does not alter the velocity peak enough to affect the number of people destabilised. The boundary layer parameters of n and C_1 are considered as 'curve fit' parameters in the current work, and are modelled to be a function of y_s with a passenger train travelling past a station platform or along an open track in order to reproduce the magnitude and shape of the velocity profile. In the parametric analysis, however, they take the values that are appropriate for the boundary layer theory of flow in pipes, i.e. $n = 10$ and $C_1 = 11.5$, which were originally used in the model. Altering these boundary layer parameters, however, has only a small affect on a person's stability. The parameter to have the greatest affect after the train length is U_{max}, which is associated with the generation of the vortex at the rear of the train. Increasing U_{max} results in the generation of a larger velocity peak at the rear of the train, hence, a larger number of people are destabilised. When the vortex parameters R and B are increased and decreased respectively, the maximum rear peak velocity increases (see equation 3.4), hence, the percentage of destabilised people increases. The wake is not a

critical region and increasing the parameters α and β by 700% and 1900% respectively, does not alter the wake's velocity profile enough to affect the proportion of destabilised people. Varying the AR coefficients by ±20% generally has only a small affect on the number of people destabilised, therefore, the values of the AR coefficients used in the model are reasonable.

Some of the parameters associated with the person simulation affect stability more than the slipstream parameters. A large change in the number of people destabilised, i.e. +39.3%, occurs when f is decreased to 0.5Hz from 0.9Hz. Decreasing f results in a decrease in k_{eq} for a given m_{tot} value, as shown in equation (5.46), which leads to the greater instability of a person. The damping of a person serves to reduce the oscillations of the mass-spring-damper system, therefore, larger numbers of people are destabilised when they are modelled to have no damping. The values of f and c_{tot} used in the model were determined by reproducing the results of the full-scale sudden gust experiments and, although the results were not reproduced with complete accuracy, the values of f and c_{tot} used give the best reproduction. The values of f and c_{tot} may change from person to person, however, the values used in the model represent the average values of these parameters of the people involved in the experiments. As f and c_{tot} are sensitive parameters the model would be improved if accurate values of these parameters were ascertained, for example, by undertaking experiments of people exposed to train slipstreams. A person's clothing also affects their stability, and using the values of C_D and $\frac{A}{A_{DU}}$ appropriate for various clothing shows that people wearing skirts are more stable than those wearing trousers, and people wearing flapping coats are less stable. The wearing of skirts and flapping coats results in 12.3% fewer and 26.0% more destabilised people, respectively, than the reference run of people wearing trousers with a shirt, jumper or fastened

jacket. The model does not generate anyone wearing a skirt or a flapping coat and, as mentioned in Section 5.5, a person wearing trousers with a shirt, jumper or fastened jacket is assumed to represent the average person on a station platform. The percentage reduction resulting from the wearing of a skirt is not equal to the percentage increase resulting from the wearing of a flapping coat, therefore, if there were equal numbers of people wearing these clothes on a station platform the average response could not be represented by people wearing trousers with a shirt, jumper or fastened jacket. It is, however, likely that there are more people on a station platform wearing skirts than wearing coats that are allowed to flap in the wind, especially during summer, consequently the average response can be represented by people wearing trousers with a shirt, jumper or fastened jacket. The increased stability associated with wearing a skirt is due to both C_D and $\frac{A}{A_{DU}}$ being smaller for this clothing type for all standing orientations, thereby reducing the force acting upon the person. The parameters are, however, greater with a flapping coat resulting in a larger force and hence a decrease in stability.

Increasing a person's weight and height from the 50th percentile value to the 75th and 95th percentile values shows that weight affects a person's stability whereas height does not, with an increase in weight resulting in an increase in stability. However, increasing the weight and height of the woman used in the analysis to the 75th and 95th percentiles is an increase in the actual weight of 20.6% and 62.7% respectively, whereas the height only increases by 2.7% and 6.7% respectively. Therefore, the distribution of weight has a larger spread than that of the height, and this will affect the results of the model. When the weight is increased by a proportion similar to that suitable for height, i.e. 5%, the change in the percentage of people destabilised is very small, therefore, small percentage changes in weight or height do not alter

stability. Larger increases in weight affect a person's stability, and this could be conjectured to also be true of a large increase in height. However, large changes in height do not occur in reality; for example, if the height increased by 20.6% (as weight does between the 50^{th} and 75^{th} percentiles), the height of the woman used in the analysis would be 1.978m, which is unusually tall for anyone. Therefore, as the distribution of weight has a large spread it can affect the percentage of destabilised people. A greater mass of a person increases their stability as it produces a larger mass moment which counteracts the moment due to the force of the slipstream acting on the simple solid object. Also, a larger mass results in a larger value of k_{eq} due to f being constant, as shown by equation (5.46), and this leads to greater stability. The results of the wind tunnel tests undertaken to investigate the response of a person to a sudden gust show that a person's standing orientation also affects their stability and the parametric analysis shows that a person is correctly modelled as being the least stable when facing the oncoming flow and the most stable when they are side-on to the flow. The side-on orientation is modelled to be the most stable as the values of C_D and $\frac{A}{A_{DU}}$ associated with this orientation are smaller than with the other orientations, therefore, there is a smaller force acting on a side-on person. Also, the critical displacement distance of a side-on person is larger than with the other orientations thus further contributing to the stability of a person standing side-on to the flow. A person facing the flow is modelled to have the smallest critical displacement distance, hence, they are the least stable.

6.7 Conclusions.

The main conclusions that can be drawn regarding a person's response to a train slipstream can be summarised as:

- When the slipstream force is large enough a modelled person will oscillate in the direction of the flow and against the flow. The oscillations decrease to zero after the train has past.
- The boundary layer region is the critical region for a person's stability with both a passenger train and a freightliner. However, a small percentage of people are also destabilised immediately after the rear of a passenger train due to the velocity peak present in that region.
- The percentage of destabilised people increases with increasing train speed, decreasing distance from the train side, and is greatest when a freightliner slipstream is involved.
- The parameters that are the most sensitive are the train length, a person's natural frequency (f), their clothing, weight, standing orientation, and age.

CHAPTER 7.

EXPERIMENTS INVESTIGATING THE RESPONSE OF A PUSHCHAIR TO A TRAIN SLIPSTREAM.

7.1 Introduction.

A train slipstream will impinge upon objects positioned along the side of a track as well as people. Temple and Johnson (2003) state that most reported slipstream incidents occurring on UK station platforms involve pushchairs, therefore, it is important that the model develops and incorporates the response of a pushchair to a train slipstream. A pushchair responds by either toppling over or by moving along the ground on its wheels. The former response is modelled using an adapted version of the simple solid object as used for the initial response of a person and described in Section 5.2. The force required to move a pushchair along the ground on its wheels is calculated using the coefficient of static friction, which has been determined from the results of a series of experiments. The experiments were also used to verify the adapted simple solid object model.

7.2 Coefficient of static friction.

In order for an applied force to cause sliding between two horizontal objects it needs to be greater than the maximum attainable value of an opposing static friction force. Until the applied force is greater than this maximum, the static friction force will be of equal magnitude to the applied force; therefore, sliding will not occur between the two objects. Sliding will

occur when the maximum frictional force is reached. The coefficient of static friction defines the threshold of movement and is given by:

$$F_{max} = \mu N \tag{7.1}$$

where F_{max} is the maximum frictional force that occurs before the onset of movement between the two objects, μ is the coefficient of static friction, and N is the normal force between the objects. In the case of the pushchair experiments, N is the total weight of the pushchair and its contents.

7.3 Pushchair experiments.

7.3.1 Experimental equipment.

Experiments were undertaken on two single pushchairs and one double pushchair. The single pushchairs were a Maclaren Quest Stroller and a Mamas and Papas (M&P) Freestyler Advance Travel System weighing 5.321kg and 9.200kg respectively, and the double pushchair was a 13.571kg Maclaren Twin Techno Stroller. These were used in order to test the response of different styles and weights of pushchairs, and thereby draw conclusions applicable to the full range of available pushchairs. Figures 7.1, 7.2 and 7.3 show the Maclaren Quest Stroller, the M&P Freestyler Advance Travel System and the Maclaren Twin Techno Stroller, respectively. The Maclaren Quest Stroller had its hood removed and the other pushchairs had their hoods down during the experiments. The wheels of the pushchairs consisted of pairs of castors, with the single and double pushchairs having four and six pairs

of castors respectively. The front wheels of all the pushchairs could rotate by 360°, whereas the back wheels were fixed so that they were always in line with the longitudinal axis of the pushchair. Brakes could be applied to the back wheels of each pushchair. Figures 7.4 and 7.5 show a photograph taken during the experiments and a schematic diagram of the experimental equipment, respectively. As Figures 7.4 and 7.5 show, an overturned table was utilised to set up a pulley system with one end of a length of cord attached horizontally to a pushchair and the other end tied to a container into which weights and lead shot could be added in order to apply a horizontal force to the pushchair.

Figure 7.1. Maclaren Quest Stroller.

Figure 7.2. M&P Freestyler Advance Travel System.

Figure 7.3. Maclaren Twin Techno Stroller.

Figure 7.4. Experimental equipment.

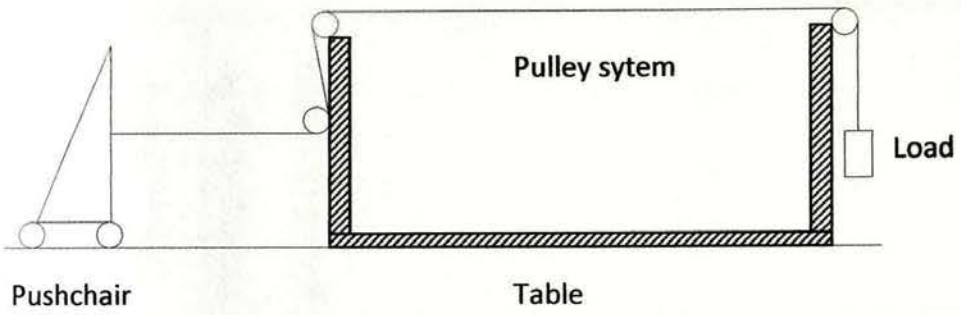

Figure 7.5. Schematic diagram of the experimental equipment.

7.3.2 Experimental method.

The experiments were undertaken with the length of cord either attached to the back or to the side of the pushchair so that the applied force acted along the pushchair's longitudinal or lateral axis respectively. The back wheels were either unbraked or braked, and the front wheels were either facing forwards and in line with the pushchair or perpendicular to the pushchair. Additional tests were undertaken on the three pushchairs to investigate the effects on the coefficient of static friction (μ) of rotating the front wheels so that they were facing backwards but still in line with the pushchair. One test was undertaken on the empty Maclaren Quest Stroller with the length of cord attached to the back of the braked pushchair in order to verify the adapted simple solid object model. In this instance the pushchair toppled over backwards, and this toppling was independent of the position of the front wheels. All other tests were undertaken to determine the value of μ and resulted in the pushchair moving along the ground on its wheels when the applied force was large enough. Table 7.1 lists the tests undertaken on the pushchairs.

Pushchair tested	Pushchair axis the force acts along	Brakes	Front wheels	Masses added to pushchair (kg)	Manner of destabilisation
Maclaren Quest Stroller, M&P Freestyler Advance Travel System, Maclaren Twin Techno Stroller	Longitudinal	Unbraked	In line with pushchair (facing forwards)	0, 1, 2, 3 and 4	Moving along the ground on wheels
			In line with pushchair (facing backwards)		
			Perpendicular to pushchair		
	Lateral	Unbraked	In line with pushchair (facing forwards)		
			Perpendicular to pushchair		
		Braked	In line with pushchair (facing forwards)		
			Perpendicular to pushchair		
Maclaren Quest Stroller	Longitudinal	Braked			Toppling

Table 7.1. Tests undertaken on the pushchairs.

In the toppling experiment, the length of cord was attached to the upright pushchair at the height of the pushchair's centre of gravity in order to replicate the loading on the simple solid object. The height to the centre of gravity was determined by placing the pushchair on a wooden beam between two tables with the beam underneath the back of the pushchair so that it was across the pushchair's width. The beam was across the pushchair's centre of gravity when the pushchair was balanced on the beam. The length of cord was attached at an equal distance between the pushchair's back wheels to allow an equal moment to act on each of the wheels due to the applied force, and thereby prevent the pushchair rotating to the side. The applied load which caused the pushchair to topple over was recorded. During the tests to determine μ, the pushchair was either empty, or had weights of 1kg, 2kg, 3kg or 4kg added to the seat. The length of cord was attached to the pushchair at an equal distance between the two back wheels when the pushchair was pulled from the back, and at an equal distance between the front and back wheels when the pushchair was pulled from the side. As with the toppling experiment, this was to allow an equal moment to act on each of the wheels. The pushchair always moved along the ground on its wheels during these tests and did not topple over even when the length of cord was attached to the highest point of the pushchair, therefore, the length of cord could be attached at any convenient height. The load was recorded which first caused the wheels to move along the ground with each incremental weight, and the increasing total pushchair weight required an increasing applied force in order to start the pushchair moving.

7.3.3 Results.

7.3.3.1 Toppling experiment.

In the toppling experiment, the force that caused toppling of the Maclaren Quest Stroller was 61.8N. Figure 7.6 is a simplified diagram of the Maclaren Quest Stroller showing that its height, height to the centre of gravity, and distance between the front and back wheels are 1.04m, 0.38m and 0.52m respectively. The pushchair rotates about its back wheels, and the horizontal distance between this rotational axis and the centre of gravity is termed the critical distance. The critical distance was determined in a similar manner as the height to the centre of gravity, as described in Section 7.3.2, but with the pushchair balanced on its side with its handles and back wheels to one side of the beam and its front wheels to the other. The critical distance of the Maclaren Quest Stroller is also shown on Figure 7.6 and is 0.25m.

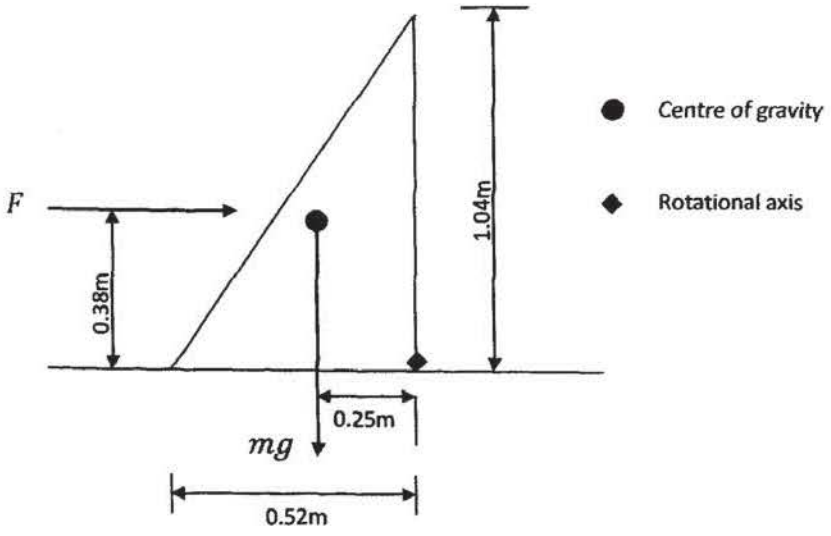

Figure 7.6. Dimensions of the Maclaren Quest Stroller.

The force (F) expected to be required to topple the pushchair is calculated by considering the moment due to F and the mass moment, thus:

$$0.38F = 0.25mg \tag{7.2}$$

where m is the pushchair's mass, i.e. 9.2kg, and g is the acceleration due to gravity. Equation (7.2) leads to the expected toppling force of 59.4N, which is similar to the actual force that caused toppling of 61.8N. The actual force required to cause toppling is 4.0% greater than the expected force. The small discrepancy between the expected and actual force will largely be due to the experimental error inherent in the method of ascertaining the position of the pushchair's centre of gravity. This involved placing the pushchair on a wooden beam between two tables and determining the position of the centre of gravity by eye when the pushchair was balanced in a particular plane. Taking into consideration this probable cause of error, the results of the experiment appear to confirm the applicability of the adapted simple solid object for modelling a pushchair susceptible to toppling.

7.3.3.2 Experiments to determine the coefficient of static friction.

Initial tests were undertaken to investigate the effects on the force required to move a pushchair along the ground on its wheels, and hence the value of μ, of rotating the front wheels by 180°. The front wheels remained in line with the longitudinal axis of the pushchair, i.e. were facing forwards or backwards. The tests were undertaken on all three pushchairs when unbraked and with the applied force acting along the longitudinal axis of the pushchair. The results of these initial tests with the Maclaren Quest Stroller, M&P Freestyler Advance

Travel System, and Maclaren Twin Techno Stroller are given in Tables 7.2, 7.3 and 7.4 respectively. A statistical analysis of these results using a t-test and testing at the 5% confidence level shows that there is no significant difference in the force required to move the pushchairs when the front wheels are facing forwards or backwards. This is true of all three pushchairs, and from this it is assumed that a pushchair has the same value of μ when its front wheels are rotated by 180°. All other results relate to the experiments undertaken to determine μ of a pushchair with the front wheels either in line with or perpendicular to the longitudinal axis of the pushchair.

Total weight of pushchair (N)	Force required to move pushchair (N)		Result of t-test (5%)
	Front wheels facing forwards	Front wheels facing backwards	
5.321	2.357	3.416	Not significant
6.321	2.628	3.710	
7.321	3.537	3.952	
8.321	3.913	4.207	
9.321	4.769	5.067	

Table 7.2. Results of the tests investigating the rotation of the front wheels by 180° (in line with the pushchair) of the Maclaren Quest Stroller.

Total weight of pushchair (N)	Force required to move pushchair (N)		Result of t-test (5%)
	Front wheels facing forwards	Front wheels facing backwards	
9.200	1.961	2.462	Not significant
10.200	3.030	2.834	
11.200	4.462	3.599	
12.200	5.472	4.266	
13.200	5.992	4.658	

Table 7.3. Results of the tests investigating the rotation of the front wheels by 180° (in line with the pushchair) of the M&P Freestyler Advance Travel System.

Total weight of pushchair (N)	Force required to move pushchair (N)		Result of t-test (5%)
	Front wheels facing forwards	Front wheels facing backwards	
13.571	5.031	5.595	Not significant
14.571	7.483	6.355	
15.571	8.797	6.620	
16.571	7.855	7.924	
17.571	11.661	8.493	

Table 7.4. Results of the tests investigating the rotation of the front wheels by 180° (in line with the pushchair) of the Maclaren Twin Techno Stroller.

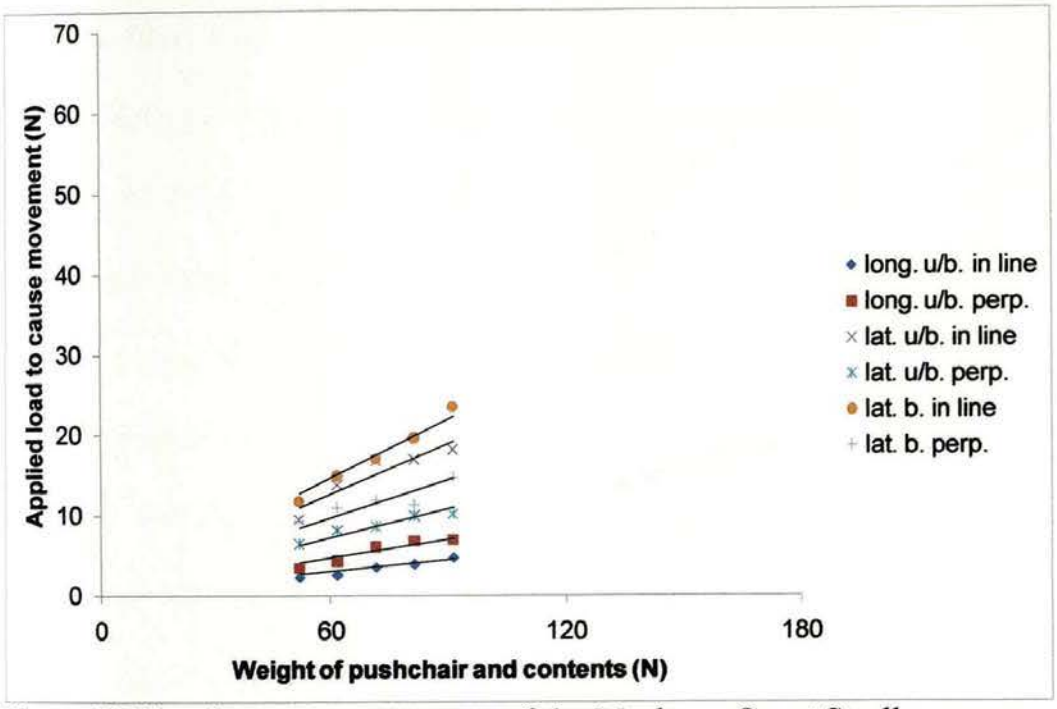

Figure 7.7. Load to cause movement of the Maclaren Quest Stroller.

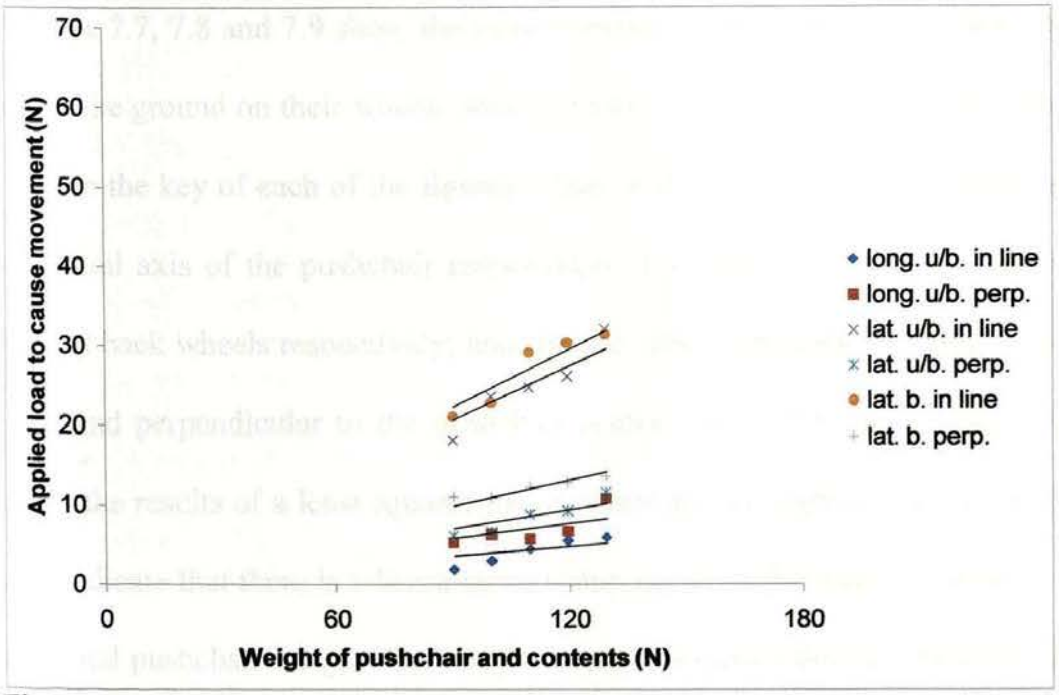

Figure 7.8. Load to cause movement of the M&P Freestyler Advance Travel System.

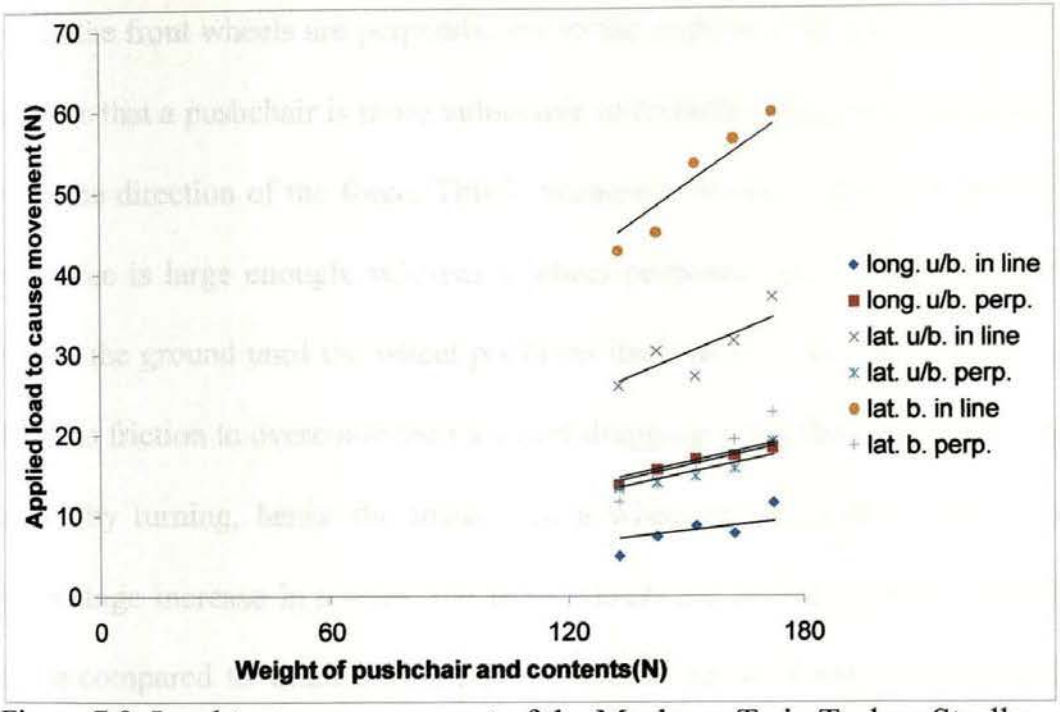

Figure 7.9. Load to cause movement of the Maclaren Twin Techno Stroller.

Figures 7.7, 7.8 and 7.9 show the force required to start each of the three pushchairs moving along the ground on their wheels with increasing total pushchair weight. The terms 'long' and 'lat' on the key of each of the figures refers to the applied force acting along the longitudinal or lateral axis of the pushchair respectively. The terms 'u/b' and 'b' refer to unbraked and braked back wheels respectively; and 'in line' and 'perp' refer to front wheels that are in line with and perpendicular to the pushchair respectively. The straight trendlines on the figures show the results of a least squares linear regression of applied load on total pushchair weight and indicate that there is a linear relationship between the force required to move a pushchair and total pushchair weight. Each of the trendlines passes through the origin and has a gradient equal to μ. Table 7.5 gives the values of μ and the correlation coefficient for the least squares linear regression (R^2) of the data shown in Figures 7.7, 7.8 and 7.9. It can be seen from Table 7.5 that for a pushchair with a force applied along its longitudinal axis, the values of μ are lower when the front wheels are in line with the pushchair than perpendicular to the pushchair. Conversely, for a pushchair with a force applied along its lateral axis, μ is lower

when the front wheels are perpendicular to the pushchair than in line with the pushchair. This implies that a pushchair is more vulnerable to destabilisation when the front wheels are in line with the direction of the force. This is because a wheel in line with the force will turn when the force is large enough, whereas a wheel perpendicular to the force will first be dragged across the ground until the wheel positions itself so as to be able to turn. As a turning wheel has less friction to overcome than a wheel dragging along the ground it is easier for a wheel to move by turning, hence the lower μ of a wheel in line with a force. Table 7.6 gives the percentage increase in μ when the front wheels are in line with the direction of the applied force compared to when they are perpendicular to the force. For example, when a force is applied along the longitudinal axis of an unbraked Maclaren Quest Stroller, μ is 0.048 and 0.076 when the front wheels are in line with and perpendicular to the direction of the force, respectively. Thus, the increase in μ is 58.3%. The lowest and highest values of R^2 are 0.504 and 0.996 respectively. The lowest value of R^2 is associated with the Maclaren Twin Techno Stroller which was the heaviest pushchair tested and moved along the ground slowly so that it was difficult to determine when it had actually started to move. This difficulty in determining pushchair motion was a source of error in the experiments leading to measurements that did not completely conform to a linear relationship between the force required to cause movement and the pushchair weight.

Pushchair axis the force acts along	Brakes	Front wheels in relation to pushchair	Maclaren Quest Stroller		M&P Freestyle Travel System		Maclaren Twin Techno Stroller	
			μ	R^2	μ	R^2	μ	R^2
Longitudinal	Unbraked	In line	0.048	0.924	0.039	0.578	0.054	0.504
Longitudinal	Unbraked	Perpendicular	0.076	0.881	0.064	0.521	0.107	0.947
Lateral	Unbraked	In line	0.209	0.860	0.228	0.855	0.199	0.708
Lateral	Unbraked	Perpendicular	0.119	0.883	0.078	0.771	0.101	0.814
Lateral	Braked	In line	0.243	0.996	0.246	0.885	0.338	0.888
Lateral	Braked	Perpendicular	0.159	0.678	0.109	0.655	0.110	0.607

Table 7.5. Values of μ and R^2 for the various experimental setups.

Pushchair axis the force acts along	Brakes	Maclaren Quest Stroller	M&P Freestyle Travel System	Maclaren Twin Techno Stroller
Longitudinal	Unbraked	58.3%	64.1%	98.1%
Lateral	Unbraked	75.6%	192.3%	97.0%
Lateral	Braked	52.8%	125.7%	207.3%

Table 7.6. Percentage increase in μ when the front wheels are in line with the direction of the applied force compared to when they are perpendicular to the force.

The three pushchair types mostly have similar values of μ for a given experimental setup. For example, a braked pushchair with the force applied along its longitudinal axis and with its front wheels in line with the pushchair has a μ value of 0.048, 0.039 and 0.054 for the Maclaren Quest Stroller, the M&P Freestyle Travel System, and the Maclaren Twin Techno

Stroller, respectively. Statistical analysis using a t-test and testing at the 5% confidence level shows that there is no significant difference between the pushchair types for a given experimental setup. The exception is between the unbraked M&P Freestyle Travel System and Maclaren Twin Techno Stroller pushchairs when the force is applied along the longitudinal axis with the front wheels perpendicular to the pushchair. However, this may be due to the R^2 value of the M&P Freestyle Travel System for this experimental setup being 0.521, which is the second lowest value. Therefore, μ of this experimental setup and pushchair is not as accurate as others. As with the Maclaren Twin Techno Stroller, the low R^2 value will be due to the difficulty in determining when the pushchair had actually started to move. Table 7.7 summarises the results of the above statistical analysis.

Pushchair axis the force acts along	Brakes	Front wheels in relation to pushchair	Maclaren Quest Stroller versus M&P Freestyle Travel System	Maclaren Quest Stroller versus Maclaren Twin Techno Stroller	M&P Freestyle Travel System versus Maclaren Twin Techno Stroller
Longitudinal	Unbraked	In line	Not significant	Not significant	Not significant
Longitudinal	Unbraked	Perpendicular	Not significant	Not significant	Significant
Lateral	Unbraked	In line	Not significant	Not significant	Not significant
Lateral	Unbraked	Perpendicular	Not significant	Not significant	Not significant
Lateral	Braked	In line	Not significant	Not significant	Not significant
Lateral	Braked	Perpendicular	Not significant	Not significant	Not significant

Table 7.7. Summary of the statistical analysis undertaken to investigate the difference between μ of the various pushchair types.

Parameters compared	Fixed parameters	Maclaren Quest Stroller	M&P Freestyle Travel System	Maclaren Twin Techno Stroller
Pushchair axis the force acts along: longitudinal versus lateral	Unbraked, front wheels in line with pushchair	Significant	Significant	Significant
	Unbraked, front wheels perpendicular to pushchair	Significant	Not significant	Not significant
Brakes: braked versus unbraked	Force along lateral axis, front wheels in line with pushchair	Not significant	Not significant	Significant
	Force along lateral axis, front wheels perpendicular to pushchair	Significant	Significant	Significant
Front wheels: in line with pushchair versus perpendicular to pushchair	Force along longitudinal axis, unbraked	Significant	Significant	Significant
	Force along lateral axis, unbraked	Significant	Significant	Significant
	Force along lateral axis, braked	Significant	Significant	Significant

Table 7.8. Summary of the statistical analysis undertaken to investigate the difference between μ of the various parameters.

A statistical analysis was also undertaken to investigate if experimental setup affects μ, i.e. if there is a difference in the value of μ between a pushchair with a force acting along the longitudinal axis and one with the force applied along the lateral axis, between a braked and an unbraked pushchair, or between a pushchair with its front wheels in line with or perpendicular to the pushchair. Table 7.8 summarises the results of t-tests undertaken at the 5% confidence level, and shows that generally there is a significant difference between μ for each of the experimental setups of a particular pushchair. However, there is no significant difference in μ between a braked and an unbraked Maclaren Quest Stroller with a force applied along the lateral axis with the front wheels in line with the pushchair. Neither is there a significant difference between an unbraked Maclaren Twin Stroller with the front wheels perpendicular to the pushchair when the force is applied along the longitudinal axis or along the lateral axis. There is also no significant difference between an unbraked M&P Freestyle Travel System with the force applied along the longitudinal axis or along the lateral axis when its front wheels are perpendicular to the pushchair, and between this pushchair braked or unbraked when the force acts along the lateral axis with its front wheels in line with the pushchair. Apart from these four exceptions, the remaining seventeen comparisons give significant differences between the experimental setups, from which it can be concluded that experimental setup affects the value of μ.

In summary, statistical analysis shows that there is generally no significant difference in μ between the pushchair types for a given experimental setup, however, there is generally a significant difference between the experimental setups for a given pushchair. Given the level of complexity of the model and the other assumptions that have been made, it is not unreasonable to take an average value for μ for all the pushchairs with a given experimental

setup. However, each experimental setup has a different value of μ, and Table 7.9 gives the average values of μ for the various experimental setups. The model of a pushchair's response to a train slipstream, which will be described in Chapter 8, uses the values of μ given in Table 7.9. As larger values of μ result in greater stability of a pushchair, Table 7.9 shows that a pushchair is less stable when a force acts along its longitudinal axis rather than along its lateral axis. For example, the value of μ of an unbraked pushchair with its front wheels in line with the force is 0.047 and 0.099 when the force is applied along the longitudinal axis and the lateral axis, respectively. An unbraked pushchair is less stable than a braked pushchair. For example, when a force acts along the lateral axis of a pushchair which has its front wheels perpendicular to the force, the value of μ is 0.212 and 0.276 when the pushchair is unbraked and braked respectively. Also, a pushchair is less stable when its front wheels are in line with the force. For example, when a force acts along the longitudinal axis of an unbraked pushchair the value of μ is 0.047 and 0.082 when the front wheels are in line with and perpendicular to the force respectively.

Pushchair axis the force acts along	Brakes	Front wheels in relation to pushchair	Average μ
Longitudinal	Unbraked	In line	0.047
Longitudinal	Unbraked	Perpendicular	0.082
Lateral	Unbraked	In line	0.212
Lateral	Unbraked	Perpendicular	0.099
Lateral	Braked	In line	0.276
Lateral	Braked	Perpendicular	0.129

Table 7.9. Average μ values for the various experimental setups.

7.4 Discussion.

A pushchair is destabilised by a slipstream by either toppling over or by moving along the ground on its wheels. The value of μ is required in order to determine the force that would move a pushchair along the ground on its wheels, therefore, a series of experiments was undertaken in order to determine μ, as well as to verify the suitability of an adapted simple solid object model to predict the force required to cause toppling. During the experiments the results were checked for repeatability, with several experimental setups being tested three times. The applied load required to cause movement was very similar for each of the three tests in all of the experimental setups, therefore, the results were repeatable.

Only a braked pushchair with a force applied along its longitudinal axis was destabilised by toppling, with the angle of the front wheels having no effect. The expected and actual force to cause toppling of the Maclaren Quest Stroller was 59.4N and 61.8N respectively, and the small discrepancy between the expected and actual force will largely be due to the method of ascertaining the position of the centre of gravity. This involved placing the pushchair on a 0.025m wide wooden beam between two tables, and determining by eye the position of the beam when the pushchair was balanced in a particular plane. The errors inherent in this procedure are due to the pushchair balancing on a beam with a width of 0.025m and not on an extremely thin edge, the complex unsymmetrical design of a pushchair, and taking the measurements by eye. If the height to the centre of gravity was measured correctly as 0.38m a critical distance of 0.26m would give the expected toppling force, which differs from the measured distance of 0.25m by 0.01m. If, however, the critical distance was measured correctly then a height to the centre of gravity of 0.365m would give the expected toppling

force, which differs by 0.015m from the measured height. The friction between the length of cord and the three pulleys would also affect the results. Taking into consideration the possible causes of error, the similarity of the two values shows that it is not unreasonable to use the adapted simple solid object for modelling a pushchair susceptible to toppling.

The experiments undertaken to determine μ involved three different pushchairs with a force applied either along the longitudinal axis or the lateral axis of the pushchair, with or without the brakes applied, and with the front wheels either in line with or perpendicular to the pushchair. A horizontal force was applied to the pushchair until it started to move along the ground on its wheels. The pushchair was tested in this manner when it was empty and when additional masses of 1kg, 2kg, 3kg and 4kg were placed on its seat. Greater masses were initially used but they caused the pushchair to move along the ground extremely slowly so that it was difficult to determine when the pushchair had actually started to move, especially the Maclaren Twin Techno Stroller which was the heaviest pushchair tested. Therefore, the additional masses were kept at 4kg and less. A strain gauge was temporarily attached to a wheel in order to facilitate the observation of movement when masses greater than 4kg were used. However, because of the very slow movement of the pushchair, it was just as difficult to recognise when the pushchair had started to move when using the strain gauge as by looking at the actual wheels. Increasing forces were required in order to move a pushchair with increasing total weight, and the results show that there is a linear relationship between these two parameters. The gradient of the trendline showing the linear relationship between the applied load and the pushchair's total weight gives the value of μ. Even with small additional weights it was not easy to determine pushchair motion and this was a source of error in the experiments leading to measurements that did not completely conform to a linear relationship.

A statistical analysis of the experimental results shows that the μ values of the three pushchair types are generally not significantly different from each other for a given experimental setup. Although the pushchairs were of differing styles, all the wheels were made of a hard rubber material. As the μ value is dependent upon the surfaces that sliding occurs between, the similar μ values reflect that the wheels were made of a similar material. This fact makes the modelling of a pushchair's response to a slipstream simpler.

The stability of a pushchair decreases when a force acts along the pushchair's longitudinal axis rather than the lateral axis. This is due to the pushchair's back wheels being fixed so as to always be in line with longitudinal axis of the pushchair, therefore, when a force acts along the pushchair's longitudinal axis the back wheels are in line with the force. The back wheels are able to turn when they are in line with the force, whereas they would initially be dragged across the ground if perpendicular to the force as would be the case when the force acts along the lateral axis of the pushchair. As a turning wheel has less friction to overcome than a wheel dragging along the ground, a lower force is required to move a wheel by turning. Similarly, a pushchair with its front wheels perpendicular to the force is more stable than when the front wheels are in line with the force, and a braked pushchair is more stable than an unbraked pushchair.

The lowest and highest average values of μ are 0.047 and 0.276 respectively. The extent of how this difference affects a pushchair's stability can be determined from the following example using the Maclaren Twin Techno Stroller with its hood down. The empty pushchair weighs 133.09N and, using equation (7.1), would require a force of 6.26N to move it along the ground on its wheels when it is most vulnerable to destabilisation, i.e. when $\mu = 0.047$.

The magnitude of the slipstream velocity that will cause destabilisation of this pushchair can be calculated from the drag force equation given by equation (5.1). The value of a pushchair's drag coefficient (C_D) is not described in literature nor was it possible to conduct experiments in the current research to ascertain its value. The value of C_D of an average modern car, a bicycle with cyclist, and a standing person is in the order of 0.3, 0.9 and 1.0, respectively. The C_D value of a person is taken from Penwarden *et al.* (1978) whereas the other values are taken from Wikipedia (2006b). A pushchair is an aerodynamically rough and unstreamlined object, therefore, using the above information, a pushchair's C_D is assumed to take a value of one. The projected area of the pushchair was measured during the experiments to be 0.44m^2 when the force acts along the pushchair's longitudinal axis. Therefore, taking 6.26N to be the drag force acting upon the pushchair, the destabilising slipstream velocity for this particular setup of the pushchair is 4.8m/s. With the pushchair in its most stable placement, i.e. $\mu = 0.276$, the force required to cause destabilisation is 36.73N. The projected area of the pushchair was measured to be 0.14m^2 when the force acts along the pushchair's lateral axis. Assuming $C_D = 1$, the slipstream velocity would need to be 20.7m/s to destabilise the pushchair. As 20.7m/s is more than four times greater than 4.8m/s, the most stable setup of a pushchair requires a much larger slipstream velocity to cause destabilisation than the most vulnerable setup. A full analysis of the parameters involved in modelling a moving pushchair is given in Section 8.4.

The floor of the location that the experiments were undertaken in was made of concrete which had been laid to provide a smooth indoor surface. The floor had been mopped before the experiments commenced in order to remove dust and any other particles present. The value of μ is dependent upon the two surfaces that the sliding occurs between, therefore, the values of μ determined by the experiments reflect the fact that the pushchairs were on a concrete

surface. A surface of tarmac, for example, would have resulted in different results. As the surface of a station platform is usually made of concrete the experiments were undertaken on a surface similar to that found at stations, thereby reducing the potential for error in determining μ. A concrete station platform floor may have a different finish to the floor on which the experiments were conducted on, however, it was beyond the scope of the experiments to determine the effects such differences have on μ.

7.5 Conclusions.

Experiments were undertaken to determine the force required to cause a pushchair to topple, and so verify the adapted simple solid object model. The expected and actual applied forces to cause toppling were similar, therefore, it is not unreasonable to assume that a pushchair can be modelled as a simple solid object when it is vulnerable to toppling. Most of the experiments were, however, undertaken to determine the value of μ which is used to calculate the force required to cause a pushchair to begin moving along the ground on its wheels. The results of the experiments show that there is no significant difference between μ for the various pushchair types for a given experimental setup, however, experimental setup makes a significant difference to μ. Therefore, an average value of μ for the three pushchairs is calculated for each of the experimental setups. A pushchair is more vulnerable to destabilisation by moving along the ground on its wheels when it is unbraked rather than braked, when the applied force acts along the longitudinal axis rather than the lateral axis, and with the front wheels in line with the direction of the applied force rather than perpendicular to the direction of the force. Therefore, the most stable placement for a pushchair vulnerable to moving along the ground on its wheels is when the force is applied along the lateral axis of

a braked pushchair with the front wheels in line with the pushchair. With this setup $\mu = 0.047$. Conversely, the least stable placement is when a force is applied along the longitudinal axis of an unbraked pushchair with its front wheels in line with the pushchair, where $\mu = 0.276$.

CHAPTER 8.

THEORETICAL MODELLING OF A RESPONSE OF A PUSHCHAIR TO A TRAIN SLIPSTREAM.

8.1 Introduction.

A pushchair vulnerable to toppling, i.e. one that is braked and facing into a slipstream, is modelled using the adapted version of the simple solid object as used for the initial response of a person and described in Section 5.2. Therefore, this pushchair is modelled to rotate about its back wheels and topple over when its centre of gravity (COG) has moved beyond the horizontal position of the back wheels, i.e. has reach its critical distance. The model of a pushchair positioned so as to be at risk of moving along the ground on its wheels utilises the coefficient of static friction (μ). The force required to move this pushchair along the ground is determined by multiplying μ by the pushchair's total weight, as shown in equation (7.1). When this force is exceeded by the slipstream force, given in equation (5.1), the model recognises that the pushchair has been made to move along the ground on its wheels and records the pushchair as having been destabilised by the slipstream. Figure 8.1 gives a schematic diagram of the forces involved when a pushchair moves along the ground on its wheels.

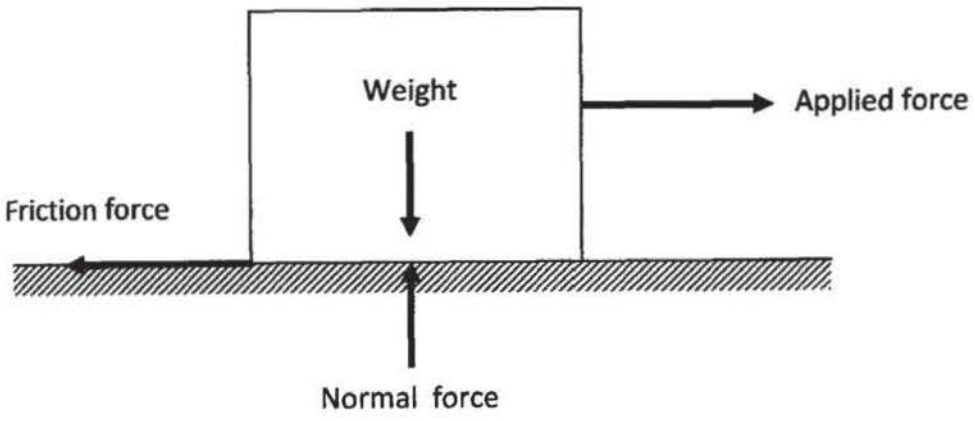

Figure 8.1. Forces involved when a pushchair moves along the ground on its wheels.

8.2 Determining the parameters of a pushchair.

The parameters of a range of pushchairs are required in order to be able to model the response of a random pushchair to a train slipstream. The parameters of mass, projected area (A), drag coefficient (C_D), height to the COG, and critical distance (which is the horizontal distance to the COG from the back wheels) are required to simulate a toppling pushchair as a simple solid object. The parameters of mass, A, C_D and μ are required to model a pushchair destabilised by moving along the ground on its wheels.

In the model the height to the COG is dependent upon the actual height of the pushchair, so that the height to the COG is equal to the pushchair's height multiplied by the ratio between these two parameters. The height of a pushchair is taken from the pushchairs used in the experiments and also from the websites of Mothercare UK Ltd. and Mamas and Papas Ltd.[1] which give details of various pushchair makes and designs. Thus the model uses a uniform distribution of pushchair height between 0.75m and 1.1m. The value of the ratio between the

[1] www.mothercare.co.uk and www.mamasandpapas.co.uk.

height to the pushchair's COG and its full height was of the order 0.38 for the Maclaren Quest Stroller when it was empty and without a hood. Further ratios are estimated from the pushchairs portrayed on the websites of Mothercare UK Ltd. and Mamas and Papas Ltd. which appear to have a variety of weight distributions, e.g. a pushchair may have a frame which has a lot of metal near its base. The estimated range of the ratio values also considers the possible positions of the pushchair's contents, e.g. shopping may be contained in a compartment within the pushchair's hood. Therefore, in the pushchair model the ratio has a uniform distribution lying between 0.25 and 0.75, with a low ratio corresponding to a pushchair with baggage stored under the child's seat and a high ratio to a pushchair with its hood up and baggage stored close to the handles, respectively.

The critical distance is dependent upon the distance between the front and back wheels which in turn is dependent upon the pushchair's height. The critical distance is equal to the distance between the front and back wheels multiplied by the ratio between these two distances. The ratio between the critical distance and the distance between the front and back wheels of the Maclaren Quest Stroller is of the order of 0.48 with the pushchair empty and without a hood. However, if a child were seated in the pushchair the ratio would increase as the seat is positioned towards the front of the pushchair, whereas the ratio would decrease if a hood was attached as the hood is positioned at the rear of pushchair. In the model the ratio between the critical distance and the distance between the wheels is assumed to take a uniform distribution between the values of one third and two thirds. This range, although estimated, considers the placement of a child in the seat, the various positions of baggage, and the style of the pushchair and its attachments such as hoods and leg coverings. The distance between the front and back wheels is equal to the pushchair's height multiplied by the ratio between these two

distances, with the ratio taking a uniform distribution between the values of 0.5 and 0.6 in the model. These values were determined from the pushchairs involved in the experiments and also from a variety of pushchairs shown on the relevant websites. The dimensions of the MacLaren Quest Stroller, from which its various ratios were determined, are given in Figure 7.6.

The smallest and greatest mass of a pushchair in either the experiments or detailed on the relevant websites is approximately 5kg and 15kg respectively. Also, the websites give a maximum child's age of three years that the pushchair is suitable for, alternatively the maximum additional mass that can be added is stated to be up to 15kg. The 50^{th} percentile mass of a three year old child is given by Halls (2004) to be approximately 15kg, which corresponds to the maximum allowable mass of the pushchair contents when this is stated. Therefore, the maximum total mass of a pushchair is taken to be the mass of the empty pushchair plus 15kg. Thus the model takes the minimum and maximum total pushchair masses to be 5kg and 30kg respectively, and these are generated using a uniform distribution.

Parameter	Calculation method
Height to COG	Pushchair height × (height to COG / pushchair height)
Distance between front and back wheels	Pushchair height × (distance between front and back wheels / pushchair height)
Critical distance	Distance between front and back wheels × (critical distance / distance between front and back wheels)

Table 8.1. Calculation method of parameters.

Parameter		Range of values
Pushchair height (m)		0.75 – 1.1
Height to COG / pushchair height		0.25 – 0.75
Distance between front and back wheels / pushchair height		0.5 – 0.6
Critical distance / distance between front and back wheels		0.333 – 0.667
A (m^2)	Pushchair in line with the force	0.2 – 0.5
	Pushchair side on to the force	0.1 – 0.35
Mass of pushchair plus contents (kg)		5 - 30
μ		0.047 – 0.276

Table 8.2. Values for various pushchair parameters.

An approximate value of A was measured from the pushchairs used in the experiments and estimated from pushchairs on the relevant websites. As the Maclaren Quest Stroller was small compared to other pushchairs, had its hood removed and was without a baggage compartment under the seat, its value of A was used as the minimum value for a pushchair either in line with or side-on to a force. The Maclaren Twin Techno Stroller was a double pushchair with a baggage compartment and a hood, and was large compared to other pushchairs. Therefore, its value of A was used as the maximum value for a pushchair either in line with or side-on to a force when it had its hood up. Thus the minimum and maximum A of a pushchair side-on to the force is $0.10m^2$ and $0.35m^2$ respectively, and a pushchair in line with the direction of the force has a minimum and maximum A of $0.20m^2$ and $0.50m^2$ respectively. The model generates A values of a pushchair between the minimum and maximum values using a uniform distribution. The range of values used allows for various styles of pushchairs and

attachments. The calculation method and the relationship between the various parameters is summarised in Table 8.1, and the range of values of the parameters is given in Table 8.2.

The pushchair experiments (Chapter 7) were undertaken with the pushchairs in line with the applied force and side-on to the force. A pushchair would, however, actually be placed on a station platform at any angle to the slipstream and each of the pushchair's front wheels could be at any angle in their 360° rotation. As the experimental results show that μ is the same when the front wheels are rotated by 180°, the values given in Table 7.9 are the lower and upper limits of a range of μ values for each particular pushchair setup. Therefore, the coefficients lie within the range of 0.047-0.082, 0.099-0.212 and 0.129-0.276 for an unbraked pushchair in line with the direction of the applied force, an unbraked pushchair side-on to the force, and a braked pushchair side-on to the force, respectively. Of all the possible setups, an unbraked pushchair in line with the force with its front wheels also in line with the force will define the lowest value of μ. A braked pushchair side-on to the force with its front wheels perpendicular to the direction of the force will define the greatest value of μ. All other pushchair setups, including pushchairs or front wheels positioned diagonally to the slipstream, will have a value of μ between these limits. Therefore, the lower and upper values of μ are 0.047 and 0.276, respectively. Due to time constraints, a test to determine the value of μ for a braked pushchair that would have its back to the oncoming slipstream was not undertaken. Therefore, in order to determine the full distribution of μ values between 0.047 and 0.276 the range of μ is approximated for such a pushchair. Both the lower and upper values of the range of μ associated with the pushchair side-on to the force are 30% greater when the brakes are applied than when the pushchair is unbraked. If this increase is also assumed to exist for a pushchair in line with the direction of the force the values of μ would be 0.061–0.107 when

the brakes were applied, i.e. an increase of 30% on the coefficients of 0.047–0.082 for an unbraked pushchair. Figure 8.2 gives the ranges of μ with each of the four pushchair setups, and this schematic diagram shows that there is a large amount of overlay between the μ values. Although there is not a full overlay of μ, there are only small regions where the overlaying does not occur, therefore, the distribution of μ can be approximated as uniform. The model generates a uniform distribution of μ between 0.047 and 0.276, thereby allowing for all placements of a pushchair at risk of being destabilised by moving along the ground on its wheels.

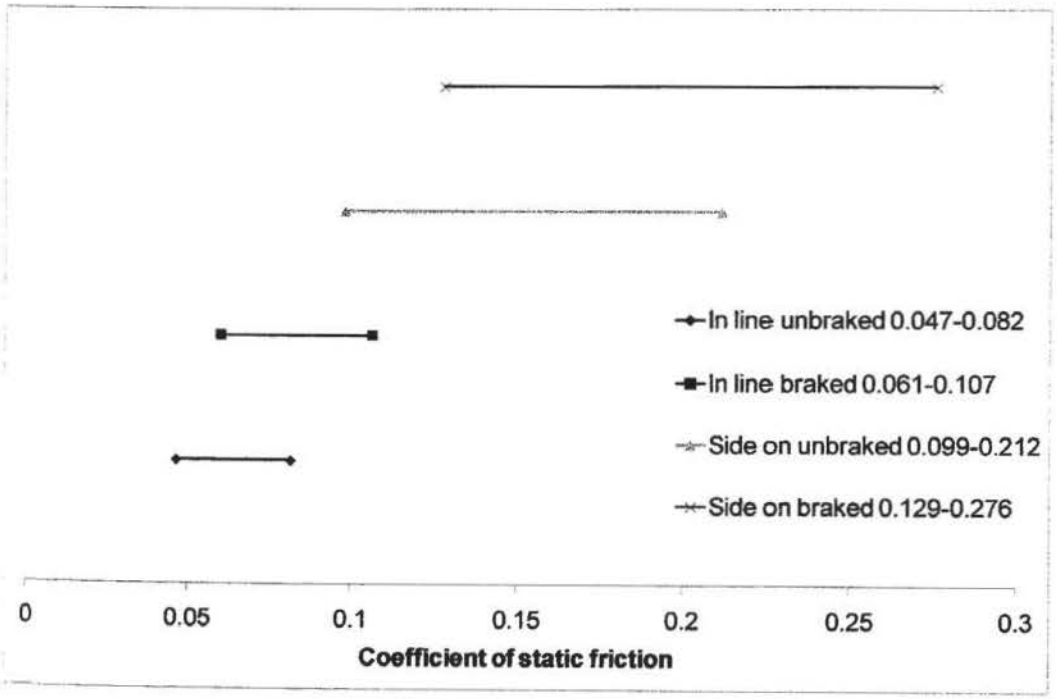

Figure 8.2. Distribution of μ.

Both A and μ are dependent upon the pushchair's position. A pushchair in line with the force has A values in the range of $0.20m^2$ to $0.50m^2$ and μ between 0.047 and 0.107, whereas a pushchair side on to the force has A values between $0.10m^2$ and $0.35m^2$ and μ in the range of 0.099 and 0.276. In order to relate these two parameters to one another the model generates

values of μ between 0.047 and 0.276 as described above, and then generates A values that are dependent upon the value of μ. As the maximum μ value of a pushchair in line with the force is 0.107, and the minimum μ value of a pushchair side-on to the force is 0.099, the model assumes that when $\mu < 0.1$ the pushchair is in line with the force and generates a value of A appropriate to such an alignment, i.e. will generate A values between $0.20m^2$ and $0.50m^2$. Conversely, if $\mu \geq 0.1$ the model assumes that the pushchair is side-on to the force and generates a value of A which lies between $0.10m^2$ and $0.35m^2$, i.e. values for a side-on pushchair.

The value of C_D of a pushchair is not described in literature nor was it possible to conduct experiments in the current study to ascertain the value, therefore, the model assumes that $C_D = 1$, as described in Section 7.4.

8.3 Results from the theoretical model.

The model calculates the percentage of pushchairs destabilised by moving along the ground on their wheels by assuming that all the pushchairs on a station platform are positioned so as to be susceptible to this manner of destabilisation. It calculates the percentage of pushchairs destabilised by toppling separately, and for this calculation assumes that all the pushchairs are positioned so as to be susceptible to toppling. The model does not consider the proportion of pushchairs on a station platform that are susceptible to the different methods of destabilisation. However, this does not affect the overall results, as will be described later. Therefore, two percentages are presented by the model, one giving the percentage of pushchairs that moved along the ground on their wheels and one giving the percentage of

toppled pushchairs. The pushchair experiments recorded the force required to initialise movement of a pushchair along the ground on its wheels, therefore, a pushchair recorded by the model as being destabilised in this manner has moved, but the displacement distance is not calculated.

Tables 8.3 and 8.4 give the percentages of pushchairs destabilised by a train slipstream when positioned on a station platform for various train speeds and for both types of pushchair response, namely, toppling and moving along the ground on the wheels. Table 8.3 relates to pushchairs destabilised by the slipstream of a passenger train when positioned between 0m and 1.5m from the platform edge, and between 0.25m and 1.5m. Table 8.4 relates to pushchairs destabilised by a freightliner when positioned at 1.5m from the platform edge. Figure 8.3 gives the percentages of pushchairs destabilised by moving along the ground on their wheels in graphical form; the results relating to toppling pushchairs are not included in the figure as they are very low. The train speeds and distances from the train side/platform edge presented in Tables 8.3 and 8.4, and in Figure 8.3, are the same as those used when investigating a person's response to a slipstream, and thereby facilitate comparison with a person's response as given in Tables 6.2 and 6.3 and Figures 6.2 and 6.3. The results of destabilised pushchairs due to a freightliner's slipstream are given for a distance of 1.5m from the platform edge as this is the only lateral distance that can be modelled for such a train type, as discussed in Section 3.6.2. Figure 8.3 shows that the percentage of pushchairs destabilised by moving along the ground on their wheels increases with increasing train speed, as would be expected. For example, 37.8% and 81.2% of pushchairs move along the ground on their wheels when positioned at 0m - 1.5m from the side of a passenger train travelling at 45m/s and 85m/s respectively. An increase in the distance from the platform edge results in a lower

percentage of destabilised pushchairs for a given train speed. For example, 37.8% and 18.8% of pushchairs move along the ground on their wheels when positioned at 0m - 1.5m and at 0.25m - 1.5m from the side of a passenger train travelling at 45m/s, respectively. Therefore, there is a 50.3% decrease in destabilised pushchairs when the pushchairs are positioned beyond 0.25m. As with the response to a passenger train's slipstream, the percentage of pushchairs destabilised by moving along the ground on their wheels increases with increasing freightliner speed. For example, 53.7% and 98.0% of pushchairs are destabilised at speeds of 20m/s and 40m/s respectively. Although the response to the freightliner and passenger train slipstreams are not directly comparable due to the pushchairs being placed at different distances from the train side, it can be seen that the slipstream of a freightliner has a greater effect on the response of a pushchair than that of a passenger train. This can be inferred as the percentage of pushchairs destabilised by a freightliner slipstream and a passenger train slipstream are similar although the freightliner speed is lower and the distance from the freightliner side is greater. For example, 52.5% of pushchairs move along the ground on their wheels when positioned between 0m and 1.5m from the side of a passenger train travelling at 55m/s, whereas 53.7% of pushchairs are destabilised when positioned at 1.5m from the side of a freightliner travelling at 20m/s. Of the pushchairs that would be susceptible to toppling only 0.1% and 1.2% actually topple when positioned at 0m – 1.5m and at 0.25m – 1.5m, respectively, when exposed to the slipstream of a passenger train travelling at 85m/s. No pushchairs at y_s = 1.5m topple due to the slipstream of a freightliner travelling at 40m/s, whereas 98.0% move along the ground on their wheels. Only at a speed of 45m/s do 1.8% of pushchairs topple when exposed to a freightliner. Therefore, the destabilisation of a pushchair is more likely to involve the wheels moving along the ground than the pushchair toppling over.

Train speed (m/s)	Distance from platform edge			
	0m – 1.5m		0.25m – 1.5m	
	Moving along the ground on the wheels	Toppling	Moving along the ground on the wheels	Toppling
45	37.8%	0%	18.8%	0%
55	52.5%	0%	33.8%	0%
65	65.8%	0%	46.5%	0%
75	74.6%	0%	58.9%	0%
85	81.2%	0.1%	68.9%	1.2%

Table 8.3. Effect of train speed and distance from the platform edge on the percentage of pushchairs destabilised by a passenger train passing a station platform.

Train speed (m/s)	Percentage of pushchairs destabilised	
	Moving along the ground on the wheels	Toppling
20	53.7%	0%
25	76.1%	0%
30	89.0%	0%
35	95.2%	0%
40	98.0%	0%

Table 8.4. Effect of train speed on the percentage of pushchairs destabilised by a freightliner passing a station platform when positioned at 1.5m from the platform edge.

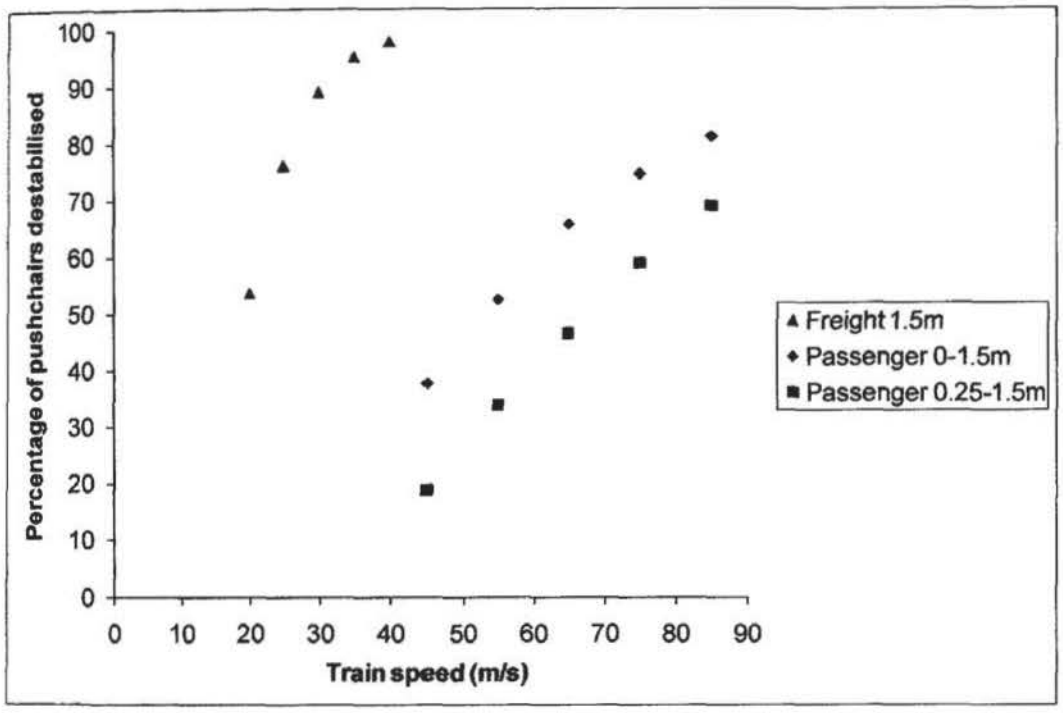

Figure 8.3. Percentage of pushchairs destabilised with increasing train speed.

8.4 Parametric analysis.

Section 8.3 shows how train type, train speed and distance from the platform edge affect the stability of a pushchair subjected to a slipstream. Section 8.4 analyses the various parameters used to generate a random pushchair in order to identify which have the most influence on a pushchair's stability. The slipstream of a passenger train passing by a station platform at 55m/s when the pushchairs are positioned between 0m and 1.5m from the platform edge results in 52.5% of the pushchairs being destabilised by moving along the ground on the wheels, and this result is used as the reference run for the analysis of the parameters involved when a pushchair is destabilised in this manner. The slipstream of a passenger train passing by a station platform at 85m/s when all pushchairs are positioned at 0.2m from the platform edge results in 21.1% of the pushchairs toppling over, and this result is used as the reference run for the analysis of the parameters involved when a pushchair topples. The large train

speed and small distance from the platform edge of the reference run for the toppling pushchairs are used in order to produce a reasonably large percentage of toppled pushchairs that can be used in the parametric analysis. Tables 8.5 and 8.6 show how altering the pushchair parameters affects the percentage of pushchairs destabilised by moving along the ground on the wheels, and Table 8.7 shows the effects of altering the parameters on the percentage of toppling pushchairs. The percentage change in the number of destabilised pushchairs compared to the reference run due to altering the parameters is also given in Tables 8.5, 8.6 and 8.7.

Table 8.5, which relates to pushchairs moving along the ground on their wheels, shows that when all the pushchairs have the minimum modelled mass of 5kg there is an increase of 70.9% in the number of pushchairs destabilised compared to the reference run. When all the pushchairs have the maximum modelled mass of 30kg there is decrease of 47.2% in the number of destabilised pushchairs, therefore, increasing a pushchair's mass results in greater stability. The stability of a pushchair also increases with decreasing values of C_D, for example, a 20% reduction in C_D, i.e. $C_D = 0.8$, results in a 13.9% reduction in the amount of pushchairs destabilised. Table 8.6 shows that a pushchair's setup, which involves the parameters of μ and A, also affects the percentage of pushchairs moving along the ground on their wheels. The least stable setup occurs when all the pushchairs are positioned so that the force acts along the pushchair's longitudinal axis, the back wheels are unbraked, and the front wheels are in line with the pushchair. With this setup 78.9% of pushchairs move along the ground on their wheels, which is an increase of 50.3% from the reference run. The most stable setup occurs when all the pushchairs are modelled with the force acting along the pushchair's lateral axis, the back wheels are braked, and the front wheels are in line with the pushchair. This results in

a 35.0% reduction in the amount of pushchairs destabilised. An unbraked pushchair is less stable than a braked pushchair, for example, when the force is applied along the pushchair's lateral axis and the front wheels are in line with the pushchair, 45.0% and 34.1% of pushchairs are destabilised when the pushchair is unbraked and braked respectively. When a force is applied along the longitudinal axis, a pushchair is more stable when its front wheels are perpendicular to the pushchair. Conversely, when a force is applied along the lateral axis, a pushchair is more stable when its front wheels are in line with the pushchair. For example, when the force is applied along the lateral axis, 34.1% and 64.8% of braked pushchairs are destabilised when the front wheels are in line with and perpendicular to the pushchair, respectively. Therefore, a pushchair with its front wheels in line with the direction of the applied force is more vulnerable to destabilisation than when its front wheels are perpendicular to the force. That stability decreases when a force acts along a pushchair's longitudinal axis rather than its lateral axis, when the pushchair is unbraked rather than braked, and when the front wheels are in line with the direction of the force rather than perpendicular to the force, agrees with the experimental results described in Section 7.3.3.2.

Table 8.7, which relates to toppling pushchairs, shows that when all the pushchairs have the minimum modelled mass of 5kg nearly all, i.e. 96.8%, of the pushchairs susceptible to toppling will actually topple, whereas at the maximum mass of 30kg no pushchairs topple. At a mass of 20kg 0.1% of pushchairs topple, therefore, all pushchairs are stable with masses greater than approximately 20kg when positioned at 0.2m from the side of a passenger train travelling at 85m/s. The height of the pushchair has only a small affect on its stability, with the minimum (0.75m) and the maximum (1.1m) heights resulting in a decrease of 6.2% and an increase of 9.0% in the amount of pushchairs toppling respectively. Therefore, a greater

height slightly decreases a pushchair's stability. The ratio between the height to the pushchair's COG and the full height affects the percentage of toppling pushchairs even less than the height. The minimum (0.25) and maximum (0.75) values result in 20.8% and 21.5% of pushchairs toppling which, considering the reference run resulted in 21.1% of pushchairs toppling, is a negligible change. A negligible change also occurs when altering the ratio between the critical distance and the distance between the front and back wheels. At both the minimum (0.333) and maximum (0.667) values 20.7% of pushchairs topple. A larger change in the number of topping pushchairs occurs due to the ratio of the distance between the front and back wheels and the pushchair height. At the minimum value of 0.5 and the maximum value of 0.6 the percentage of destabilised pushchairs increases by 20.9% and decreases by 16.1% respectively Therefore, a larger distance between the front and back wheels for a given height increases a pushchair's stability. As with the pushchairs susceptible to being destabilised by moving along the ground on their wheels, an increase in C_D results in a decrease in stability. Increasing C_D by 20% to 1.2 increases the number of pushchairs destabilised by 36.5%. Varying A also affects the numbers of toppling pushchairs, with the minimum value of 0.1m^2 and the maximum value of $0.35\ \text{m}^2$ resulting in 0.5% and 44.5% of pushchairs destabilised respectively. Therefore, a lower A exposed to a slipstream increases the stability of a pushchair.

Parameter		Percentage of pushchairs destabilised	Percentage change
Mass	5kg	89.7%	+70.9%
	30kg	27.7%	-47.2%
C_D	1.2	60.4%	+15.0%
	1.1	56.3%	+7.2%
	0.9	49.9%	-5.0%
	0.8	45.2%	-13.9%

Table 8.5. Effect of altering the pushchair parameters on the percentage of pushchairs destabilised by moving along the ground on their wheels.

Pushchair setup			Percentage of pushchairs destabilised	Percentage change
Pushchair axis the force acts along	Brakes	Front wheels in relation to pushchair		
Longitudinal	Unbraked	In line	78.9%	+50.3%
Longitudinal	Unbraked	Perpendicular	62.1%	+18.3%
Lateral	Unbraked	In line	45.0%	-14.3%
Lateral	Unbraked	Perpendicular	56.4%	+7.4%
Lateral	Braked	In line	34.1%	-35.0%
Lateral	Braked	Perpendicular	64.8%	+23.4%

Table 8.6. Effect of altering the pushchair setup on the percentage of pushchairs destabilised by moving along the ground on their wheels.

Parameter		Percentage of pushchairs destabilised	Percentage change
Mass	5kg	96.8%	+358.8%
	20kg	0.1%	-99.5%
	30kg	0%	-100%
Height of pushchair	0.75m	19.8%	-6.2%
	1.1m	23.0%	+9.0%
Height to COG / pushchair height	0.25	20.8%	-1.4%
	0.75	21.6%	+2.4%
Distance between front and back wheels / pushchair height	0.5	25.5%	+20.9%
	0.6	17.7%	-16.1%
Critical distance / distance between front and back wheels	0.333	20.7%	-1.9%
	0.666	20.7%	-1.9%
C_D	1.2	28.8%	+36.5%
	1.0	25.1%	+19.0%
	0.9	17.1%	-19.0%
	0.8	12.8%	-39.3%
A	0.1	0.5%	-97.6%
	0.35	44.4%	+110.4%

Table 8.7. Effect of altering the pushchair parameters on the percentage of pushchairs destabilised by toppling.

8.5 Discussion.

A pushchair exposed to a train slipstream on a station platform will be destabilised either by toppling over, in which case it is modelled as a simple solid object, or by moving along the ground on its wheels. A series of experiments was undertaken to determine the range of μ values applicable to a pushchair and required in order to model a pushchair moving along the ground on its wheels. The values of pushchair mass, height, distance between the front and back wheels, and A were measured during the experiments, and taken or estimated from the relevant sources. This allows a range of values for these parameters to be ascertained. The position of a pushchair's COG was also measured during the experiments, however, this position would be affected by the mass and placement of a child and baggage. It was not possible to determine the position of the COG when the pushchair either contained a child or baggage as such additions would be likely to either fall out of the pushchair or move from their intended position during the measuring procedure, therefore, the COG's position is estimated. In the model, the distance between the front and back wheels is dependent upon the pushchair's height, the vertical position of the pushchair's COG is also dependent upon the pushchair's height, and the critical distance is dependent upon the distance between the front and back wheels. Relating one parameter to another generates the parameters more accurately for a particular pushchair, and so prevents unrealistic pushchairs being generated. As it was not possible to ascertain what style of pushchair is the most popular, or how and with what they are loaded whilst on a station platform, the parameters described above are taken to have a uniform distribution. Although this is unlikely to be totally accurate, an assumption of a normal distribution may also be incorrect. For example, people may choose to take only lightweight pushchairs onto a train, which would result in a positively skewed distribution of

mass. A uniform distribution generates more lightweight pushchairs than a normal distribution, and so would be more suitable in this instance.

The experiments described in Chapter 7 give values of μ when an unbraked and braked pushchair is side-on to an applied force, and when an unbraked pushchair is in line with a force. In order to determine the full range of μ values of a pushchair, the values of μ for a braked pushchair with its back to the oncoming slipstream is required. However, due to time constraints, an experiment to determine these values could not be undertaken, hence a range of μ values is approximated for such a pushchair setup. As the range of μ values associated with a braked pushchair side on to the force is 30% greater than that of an unbraked pushchair in the same position, it is assumed that a braked pushchair with its back to the flow has μ values that are 30% greater than those associated with an unbraked pushchair in line with a force. This results in a large amount of overlay of μ values for the four pushchair setups, therefore, μ is modelled to have a uniform distribution between the lowest and highest values. The assumption that the range of μ for a braked pushchair with its back to the flow is 30% greater than the μ value of an unbraked pushchair in line with the flow may not be accurate. However, with any increase in such a range there would still be a large amount of overlay of all μ values due to the large amount of overlay between the values associated with a braked and an unbraked pushchair side on to the force. Therefore, assuming a uniform distribution is not unreasonable.

Both A and μ are dependent upon the position of the pushchair, and this fact is reflected in the model by having the value of A dependent upon whether the μ is associated with a pushchair in line with or side-on to a force. The maximum μ value of a pushchair in line with the force

and the minimum μ value of a pushchair side-on to the force is 0.107 and 0.99, respectively. As these values are similar, the model assumes that the pushchair is in line with the force when $\mu < 0.1$, and that the pushchair is side-on to the force when $\mu \geq 0.1$. The value of 0.107 is the upper limit of the approximated range of μ for a braked pushchair in line with the force, therefore, it may not be a totally accurate value. However, the value of 0.99 was ascertained from the experiments. If the actual value of the upper limit of the approximated range of μ is greater than 0.107, then 0.1 may be too low a value at which to define whether a pushchair is in line with or side-on to a force. However, if the actual value of the upper limit of the approximated range is less than 0.107, then 0.1 may indeed be an accurate defining value, unless the value of 0.107 is very much too high. Without undertaking further experiments to determine the actual value of the maximum μ value for a braked pushchair in line with the force the above assumptions are the best method that the model can employ.

The model's results show that a pushchair's setup affects its stability when moving along the ground on its wheels. A pushchair is less stable when in line with the applied force rather than side-on to the force, when it is unbraked rather than braked, and when the front wheels are in line with the force rather than perpendicular to the force. This agrees with the results of the experiments undertaken on pushchairs as described in Section 7.3.3.2, and is the result of a lower force being required to overcome friction when turning a wheel than when dragging a wheel across the ground (see Section 7.4).

The destabilisation of a pushchair is much more likely to involve the wheels moving along the ground than the pushchair toppling over, for example, 0.1% and 81.2% of pushchairs topple and move along the ground on their wheels, respectively, when positioned at 0m – 1.5m from

the side of a passenger train travelling at 85m/s. Also, most pushchairs will be positioned on a station platform so that they are susceptible to being destabilised by moving along the ground on their wheels as there is only one particular setup which puts a pushchair at risk from toppling, namely a braked pushchair facing into the oncoming slipstream. Due to the small proportion of pushchairs positioned so as to be vulnerable to toppling and the fact that only a small number of these will actually topple over, the chance of a pushchair toppling over is very small. This means that the probability of a pushchair toppling on a station platform has a negligible effect on the total percentage of pushchairs destabilised, and the percentage of pushchairs destabilised by moving along the ground on their wheels can be taken to be the overall result. The results of the two types of pushchair response are presented separately by the model and not combined, and this needs to be taken into consideration when interpreting the model's results.

The results of the model show that increasing train speed and decreasing distance from the side of a train results in larger percentages of pushchairs being destabilised by a slipstream. This is due to increasing slipstream velocity magnitudes and turbulence levels, as described in Section 2.2.1. A freightliner's slipstream has a greater effect on the stability of a pushchair than a passenger train's slipstream, and this is due to the freightliner being aerodynamically rough, hence, it generates larger slipstream velocities and turbulence levels. These results are also true for the stability of people, as described in Section 6.4.

Comparing the response of a pushchair to that of a person (as described in Chapter 6) shows that there is a greater percentage of pushchairs than people destabilised for a given train speed and distance from the train side. For example, 37.8% of pushchairs are destabilised by

moving along the ground on their wheels when positioned between 0m and 1.5m from the side of a passenger train travelling at 45m/s, hence, it can be concluded that 37.8% of all pushchairs are destabilised. However, only 3.5% of people are destabilised when similarly positioned. At 1.5m from the side of a freightliner travelling at 40m/s, 98.0% and 39.1% of pushchairs and people are destabilised respectively. Therefore, a pushchair is more likely to be destabilised than a person, and as the slipstream of a freightliner has a greater effect on stability than a passenger train, a pushchair exposed to a freightliner's slipstream is most at risk of being destabilised. Although the distances associated with the destabilisation of a pushchair and a person are not calculated by the model, the greater vulnerability of a pushchair exposed to the slipstream of a freightliner agrees with the reported incidents involving slipstreams on UK station platforms, as described by Temple and Johnson (2003).

A parametric analysis shows that an increase in a pushchair's mass increases its stability. For a pushchair moving along the ground on its wheels, this greater stability is due to the larger force required to destabilise a pushchair with a greater mass, as show by equation (7.1). A larger mass of a toppling pushchair results in a larger mass moment which acts against the moment due to the force (equation (5.1)), hence the greater stability. An increase in mass also increases the stability of a person, as described in Section 6.5. Increasing C_D or A of a pushchair results in an increased force acting on the pushchair resulting in a decreased stability. The value of C_D of a pushchair is assumed to be one as data on this value is not given in literature nor was it possible to undertake experiments in the current research to ascertain the value. However, in order to more accurately reproduce the response of a pushchair to a slipstream it would be beneficial to undertake experiments to determine C_D of a range of pushchairs. Increasing the values of C_D and A of a person also results in a decrease of

stability, as shown when investigating the effect of clothing or standing orientation (Section 6.5). Altering the height of a pushchair results in only a small change in the percentage of toppling pushchairs, with an increase in height decreasing stability. Decreasing the height results in the height to the pushchair's COG also decreasing, therefore, the moment due to the applied force is reduced and stability increases. This would also be expected to be true when the ratio between the height to the COG and the pushchair's height is increased, however, altering this ratio has a negligible effect on the results. Therefore, the moment due to the applied force varies more when the height varies than when the ratio between the COG's height to pushchair height varies. Increasing the ratio of the distance between the front and back wheels to the pushchair height results in fewer pushchairs toppling over. A larger value of this ratio results in a larger critical distance, therefore, there is a larger mass moment acting against the moment due to the force, and a pushchair's stability increases. However, varying the ratio of the critical distance to the distance between the front and back wheels has a negligible affect on stability. Therefore, the mass moment increases more when the distance between the front and back wheels increases than when the ratio between the critical distance and the distance between the front and back wheels increases.

8.6 Conclusions.

A pushchair situated on a station platform either moves along the ground on its wheels or topples over when the force due to a train slipstream is large enough. The model uses values of μ, which were determined from experiments, to calculate the force required to move a pushchair along the ground on its wheels. The toppling response of a pushchair is modelled using the adapted version of the simple solid object as used for the initial response of a

person. In order to model the response of a pushchair moving along the ground on its wheels the parameters of pushchair mass, A, C_D and μ are required, where A and μ are dependent upon whether the pushchair is in line with or side-on to the applied force. The response of a toppling pushchair is modelled using the parameters of pushchair mass, pushchair height, height to the COG, critical distance, A, and C_D. All of these parameters are based on uniform distributions, except for C_D which is assumed to take the value of one. For a pushchair vulnerable to toppling the height to the COG is dependent upon the pushchair's height, and the critical distance is dependent upon the distance between the front and back wheels which in turn is dependent upon the pushchair's height.

The results show that the percentage of pushchairs destabilised increases with increasing train speed and decreasing distance from the platform edge, and that the effect of a freightliner's slipstream is greater than that of a passenger train. Only a very small proportion of pushchairs that are vulnerable to toppling actually topple over. A parametric analysis shows that mass, C_D and pushchair setup affect the response of a pushchair moving along the ground on its wheels. A pushchair in line with the direction of the force is less stable than a pushchair side-on to the force, an unbraked pushchair is less stable than a braked pushchair, and stability also decreases when the front wheels are in line with the force rather than perpendicular to the force. Mass, C_D, A, and the ratio of the distance between the front and back wheels to the pushchair's height affect the response of a toppling pushchair. However, as the contribution to the overall results by toppling pushchairs is negligible, the sensitivity of the parameters of a toppling pushchair will not influence the overall results.

CHAPTER 9.

CONCLUSIONS.

9.1 Introduction.

A mathematical model has been developed to simulate the slipstream of a train, and the response of a person and a pushchair to the slipstream. The model determines if a slipstream causes a person or a pushchair to become destabilised, and presents the results as a percentage of the total number of people or pushchairs exposed to the slipstream.

9.2 Model's methodology.

The model allows the user to choose various model parameters in order to investigate the response of a person or a pushchair. A User Guide is given in Appendix 5 informing the user how to operate the model. The parameters that are selected by the user are:

- Train type.
- Speed of train.
- Full length of train.
- Width of the main body of the train.
- Height of the main body of the train.
- Length of the freight locomotive (if applicable).
- Width of the freight locomotive (if applicable).
- Height of the freight locomotive (if applicable).

- Person's location.
    - Station platform or an open track.
    - Distance from the train side/platform edge.
- Pushchair's location.
    - Distance from the train side/platform edge.

The above parameters are chosen by the user to enable the model to correctly simulate the slipstream of the train under investigation. The parametric analysis shows that train type, train speed, the full length of the train, and the location of a person and pushchair are sensitive parameters (see Sections 6.4 and 6.5). The model allows the user to alter these sensitive parameters and thereby investigate their effect on destabilisation.

Figure 9.1 is a flow chart outlining the model's methodology, i.e. how the model arrives at its results. In the flow chart, the sequence of events follows a downward direction except where shown otherwise by an arrow or by wording. The model generates an individual slipstream velocity time history based on the chosen train parameters and the distance from the train side/platform edge. It also generates a randomised person who is exposed to the velocity time history. The maximum displacement of the person is calculated and if this is greater than the critical displacement the person is recorded as having been destabilised. If the train is chosen to pass by a station platform then a randomised pushchair is also generated which is positioned so as to be capable of toppling and also positioned so as to be capable of moving along the ground on its wheels. The pushchair is then exposed to the velocity time history. As with a person, the maximum displacement of the toppling pushchair is calculated and if this is greater than the critical displacement the pushchair is recorded as having toppled. If the

slipstream force is greater than the frictional force between the wheels and the ground surface the pushchair is recorded as being destabilised by moving along the ground on its wheels. The model then generates another slipstream, person and pushchair, and determines if destabilisation has occurred. This is undertaken a thousand times, and from the results the model calculates the percentage of people and pushchairs that are destabilised by the train slipstream. A thousand runs are generated in order to obtain stable results.

The conclusions regarding the model of a slipstream, and a person and a pushchair's response to a slipstream are given in Section 9.3. There are a number of assumptions embodied within the slipstream, person and pushchair models, therefore, the conclusions below should not be interpreted or extrapolated beyond the limits of the model.

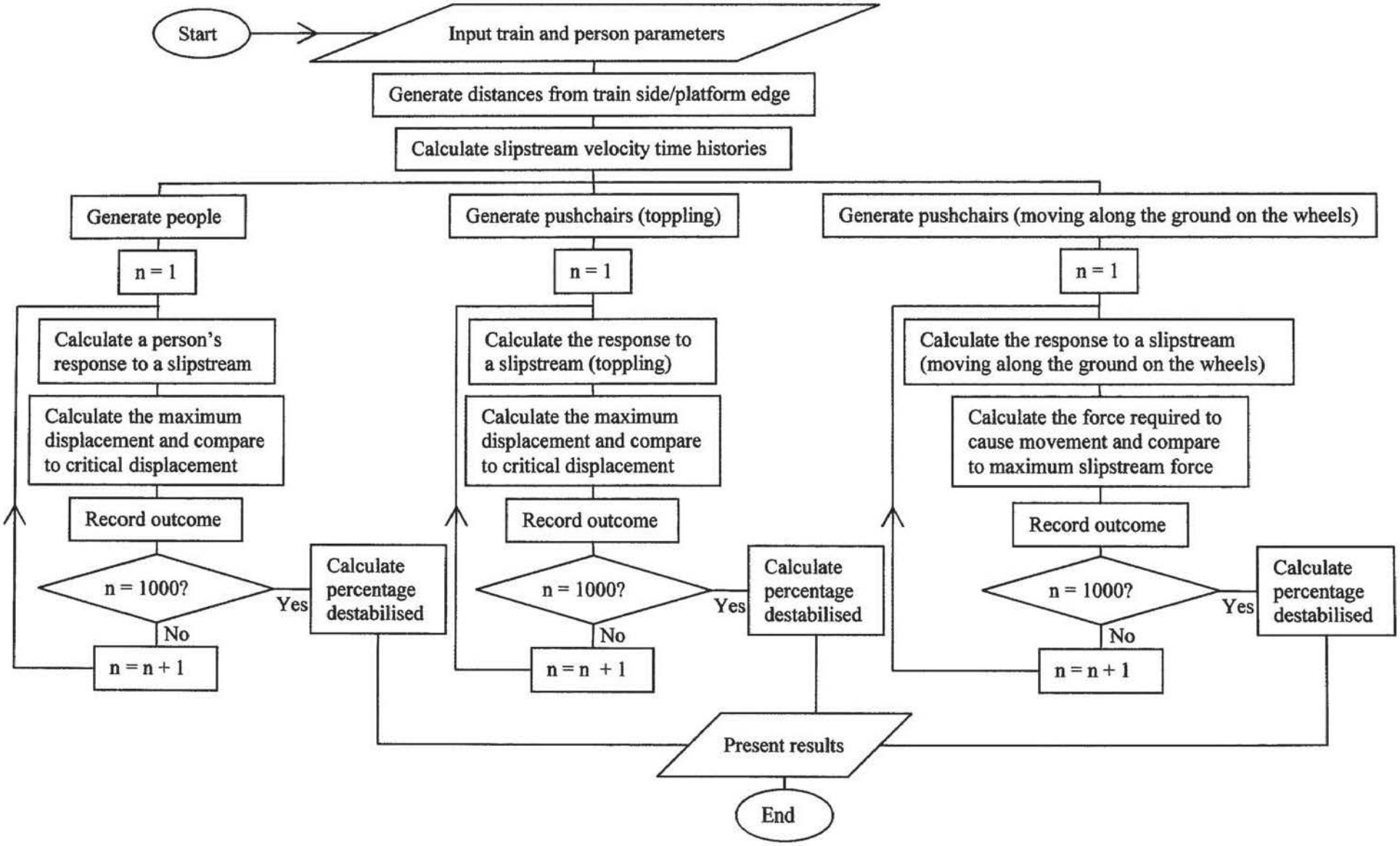

Figure 9.1. Flowchart outlining the model's methodology.

9.3 Modelling the response of a person and a pushchair to a train's slipstream.

The main conclusions relating to the mathematical model of a person and a pushchair's response to a train's slipstream can be summarised as follows:

1. The simulated mean velocity time history of a train has the shape and magnitudes resembling those of measured slipstreams.
2. Including turbulence, the velocity time histories of the freightliner, the model-scale passenger train, and close to the side of the full-scale passenger train are reproduced with reasonable accuracy.
3. The turbulence levels of the passenger train slipstream are reproduced with reasonable accuracy, however, those of the freightliner slipstream are not as accurately simulated.
4. The natural frequency and total damping of a person when modelled as a mass-spring-damper system are determined from experiments to be 0.9Hz and 215Ns/m respectively.
5. The natural frequency of a person corresponds to a slipstream frequency that is simulated with reasonable accuracy for each of the train types.
6. The drag force due to the slipstream acts upon the simple solid object that models a person's initial response and a pushchair's response.
7. A series of short-duration impulse loads acts upon the mass-spring-damper system that models a person's response after the initial response.
8. A large enough wind force causes the simple solid object to rotate or the three masses of the mass-spring-damper system to be displaced.

9. The least stable standing orientation of a person occurs when they are standing facing into the slipstream, and the most stable orientation is standing side-on to the slipstream.
10. The destabilisation of a pushchair is more likely to involve the wheels moving along the ground than by the pushchair toppling over.
11. For pushchairs moving along the ground on their wheels, the least stable set-up occurs when an unbraked pushchair and its front wheels are in line with the slipstream force. The most stable set-up occurs when the force is applied along the lateral axis of a braked pushchair with the front wheels in line with the pushchair.
12. The percentage of people and pushchairs destabilised by a slipstream increases with increasing train speed, decreasing distance from the train side and is greatest when a freightliner slipstream is involved.
13. The model predicts that 3.5% of people standing at 0m – 1.5m from the platform edge are destabilised by the slipstream a passenger train travelling at 45m/s. Therefore, people standing at this distance will start to be destabilised with a train speed of less than 45m/s.
14. Approximately one quarter (24.6%) of the people standing at 0m – 1.5m from the platform edge are destabilised by the slipstream of a passenger train travelling at 85m/s.
15. People standing at 0.25m – 1.5m from the platform edge will start to be destabilised with a passenger train speed of between 55m/s and 65m/s.
16. People standing at 0.5m – 1.5m from the platform edge will also start to be destabilised with a passenger train speed of between 55m/s and 65m/s.

17. People standing at 1.5m from the platform edge will start to be destabilised with a freightliner speed of approximately 20m/s.
18. 39.1% of people are destabilised when standing at 1.5m from the platform edge by the slipstream of a freightliner travelling at 40m/s.
19. 37.8% of the pushchairs positioned at 0m - 1.5m from the platform edge are destabilised by moving along the ground on their wheels by the slipstream of a passenger train travelling at 45m/s. This increases to 81.2% with a train speed of 85m/s.
20. 18.8% of the pushchairs positioned at 0.25m - 1.5m from the platform edge are destabilised by moving along the ground on their wheels by the slipstream of a passenger train travelling at 45m/s.
21. Over half (53.7%) of the pushchairs positioned at 1.5m from the platform edge are destabilised by moving along the ground on their wheels by the slipstream of a freightliner travelling at 20m/s.
22. Nearly all (98.0%) of the pushchairs positioned at 1.5m from the platform edge are destabilised by moving along the ground on their wheels by the slipstream of a freightliner travelling at 40m/s.
23. The most sensitive parameters of a person's response are the train length, the person's weight, clothing, standing orientation, natural frequency and age.
24. The most sensitive parameters of a pushchair moving along the ground on its wheels are mass, drag coefficient and setup. The most sensitive parameters of a toppling pushchair are mass, drag coefficient, projected area, and the ratio between the front and back wheels to the pushchair's height.

9.3.1 The effect of increasing a passenger train's speed from 55m/s to 65m/s.

The top speed of the British Class 390 'Pendolino' train before the completion of the upgraded West Coast Main Line was 177km/h (49m/s). However, it will be able to travel at 220km/h (61m/s) if further improvements to the rail network are undertaken, as mentioned in Section 1.1. Using the results from the model for a passenger train travelling at 45m/s, 55m/s and 65m/s past a station platform, as given in Table 6.2, the effect of this increase in train speed on a person's stability can be investigated. Table 9.1 summarises the results from Table 6.2 relating to these three train speeds.

Distance from platform edge	Train speed		
	45m/s	55m/s	65m/s
0m – 1.5m	3.5%	6.7%	13.7%
0.25m – 1.5m	0%	0%	4.6%
0.5m – 1.5m	0%	0%	1.4%

Table 9.1. Percentages of people destabilised by a passenger train travelling past a station platform at 45m/s, 55m/s and 65m/s.

Using interpolation between the train speeds, Table 9.1 shows that the proportion of destabilised people at 0m – 1.5m from the platform edge is between 3.5% and 6.7% with a train speed of 49m/s. However, the model predicts that no one will be destabilised if they stand between 0.25m and 1.5m from the platform edge when a passenger train passes through the station at 49m/s. With the increased train speed of 61m/s, between 0% and 4.6% of people are destabilised when standing at 0.25m – 1.5m. Therefore, it can be conjectured that a small proportion of people standing between these distances will be destabilised with a train speed

of 61m/s. However, as 0% and 1.4% of people at 0.5m – 1.5m are destabilised with a train speed of 55m/s and 65m/s, respectively, it is likely that standing at or beyond 0.5m will result in no one being destabilised with a train speed of 61m/s. This leads to the conclusion that no one will be destabilised when standing at or beyond 0.25m from the platform edge when a train passes at 49m/s, but the minimum safe distance from the platform edge increases to 0.5m when a train passes at the increased speed of 61m/s. This shows the effect of increasing the train speed from 49m/s to 61m/s on the safe distance from the platform edge at which a person can stand. An increase in the safe distance would need to be considered when planning such a change in the speed at which a non-stopping train passes through a station.

9.4 Future work.

In order to improve the model's ability to simulate freightliner slipstreams there needs to be further full-scale experiments undertaken to measure the slipstreams at a variety of distances from the freightliner side. This would allow freightliner slipstreams to be simulated for lateral distances other than 1.5m and 0.705m on a station platform and along an open track respectively. Also, how freightliner slipstreams vary depending on the consist of the train would be better understood, and therefore modelled, if a variety of consists were involved in the experiments, i.e. the number, size, spacing and type of wagons were varied. It would be beneficial if further experiments were undertaken on all train types with measurements taken at various heights in order to correctly model the manner in which the slipstream velocities vary with height. The model assumes that the slipstream velocities do not alter with height as there is insufficient data to determine the variation conclusively. Also, the model does not allow for the interaction between crosswinds and the slipstream. The model-scale experiments

of Baker *et al.* (2001) included runs with a crosswind generated perpendicular to the vehicle motion, and the slipstream velocities increased by the same amount as the crosswind velocity magnitude. However, until experiments are undertaken which involve a variety of yaw angles of the crosswind the model cannot incorporate this effect.

The modelling of a person's response would be improved if accurate values of a person's natural frequency and total damping were determined, including how these parameters vary between individuals. A person's level of preparedness for the train slipstream is also likely to affect their response, with people who have 'braced' themselves to the oncoming slipstream being less vulnerable to destabilisation. Therefore, incorporating a person's preparedness into the model would allow for this variation in the response. Further experiments with people may identify the above parameters and determine how a person's level of preparedness affects their response. Ideally, for the modelling, these experiments would be conducted using actual train slipstreams, however, in the interests of safety they are unlikely to be undertaken.

REFERENCES.

Allum, H.J., Carpenter, M.G., Honegger, F., Adkin, A.L. and Bloem, B.R. (2002) Age-dependent variations in the directional sensitivity of balance corrections and compensatory arm movements in man. **Journal of Physiology**, 542: 643-663.

Baker, C.J. (2001) Flow and Dispersion in ground vehicle wakes. **Journal of Fluids and Structures**, 15 (7): 1031-1060.

Baker, C.J., Dalley, S., Yang, X., Kettlewell, P.J. and Hoxey, R.P. (1996) An investigation of the aerodynamics and ventilation of poultry transport vehicles; part 2. Wind tunnel experiments. **Journal of Agricultural Engineering Research**, 65: 97-113.

Baker, C.J., Dalley, S.D., Johnson, T., Brown, M., Gaylard, A., Quinn, A.D. and Wright, N.G. (2000) Measurements of the slipstream and wake of a model lorry. **Proceedings of MIRA conference on vehicle aerodynamics**, Rugby, UK.

Baker, C.J., Dalley, S.D., Johnson, T., Quinn, A.D. and Wright, N.G. (2001) The slipstream and wake of a high speed train. **Proceedings of the Institution of Mechanical Engineers F Journal of Rail and Rapid Transit**, 215: 83-99.

Baker, C.J. and Sterling, M. (2004) The effects of the slipstreams of passing high speed trains on waiting passengers. **Proceedings of the 6th Conference on Wind Engineering (Wind Engineering Society)**, Cranfield, UK.

Bates, M. (2004) **Personal communication**.

Bottema, M. (1992) Wind Climate and Urban Geometry, Report No. 92.63k, Technical University of Eindhoven.

Box, E.P.G. and Jenkins, G.M. (1970) **Time series analysis: forecasting and control**. 1st ed. San Francisco: Holden-Day.

Cali, P.M. and Covert, E.E. (2000) Experimental measurements of loads induced on an overhead highway sign structure by vehicle-induced gusts. **Journal of Wind Engineering and Industrial Aerodynamics**, 84: 87-100.

Clough, R.W. and Penzien, J. (1993) **Dynamics of Structures**. 2nd ed. New York; London: McGraw-Hill.

De Graaf, B. and Van Weperen, W. (1997) The retention of balance: An exploratory study into the limits of acceleration the human body can withstand without losing equilibrium. **Human Factors: The Journal of the Human Factors and Ergonomics Society**, 39 (1): 111-118.

Dubois, D. and Dubois, E.F. (1916) Clinical calorimetry 10th paper: A formula to estimate the approximate surface area if height and weight be known. **Archives of Internal Medicine**, 17: 863-871.

Duncan, W., Thom, A. and Young, A. (1970) **Mechanics of Fluids**. 2nd ed. London: Edward Arnold.

Durov, V. (1967) Questions Relating to the Aerodynamics of High-Speed Trains. **Zheleznodorozhni Transport**, 49: 34-36.

Eskridge, R.E. and Hunt, J.C.R. (1979) Highway modeling. Part I: Prediction of velocity and turbulence fields in the wake of vehicles. **Journal of Applied Meteorology**, 18 (4): 387-400.

Farge, M. (1992) Wavelet transform and their application to turbulence. **Annual review of fluid mechanics**, 24: 395-458.

Fossett, D. A. J. (2007) **Technical data – E4 series** [online]. http://www.h2.dion.ne.jp/~dajf/byunbyun/tech/e4.htm [Accessed November 2007].

Fukuchi, G. (1961) Field measurements of train drafts. **Permanent Way No. 11**, 4 (2), Translated from 'Tetsudo Senro', bulletin of Permanent Way Society of Japan, 9 (4).

Gawthorpe, R. (1978) Aerodynamics of trains in the open air. **Railway Engineering International (Institution of Mechanical Engineers)**, 3 (3): 7–20.

Gerhardt, H. J. and Kruger, O. (1998) Wind and train driven movements in train stations. **Journal of Wind Engineering and Industrial Aerodynamics**, 74-76: 589-597.

Halls, S.B. (2004) **Health calculators and charts** [online]. www.halls.md [Accessed July 2005].

Hof, A.L., Gazendam, M. G. J. and Sinke, W.E. (2005) The condition of dynamic stability. **Journal of Biodynamics**, 38: 1-8.

Hoxey, R.P., Kettlewell, P.J., Meehan, A.M., Baker, C.J. and Yang, X. (1996) An investigation of the aerodynamics and ventilation of Poultry transport vehicles; part 1. Full-scale experiments. **Journal of Agricultural Engineering Research**, 65: 77-85.

Hsiao, E.T. and Robinovich, S.N. (1999) Biomechanical influences on balance recovery by stepping **Journal of Biomechanics**, 32: 1099-1106.

Huggins, T.C.B., Baker, C.J. and Kinnersley, R.P. (2002) Wind and vehicle induced turbulence very close to a road surface. **Proceedings of the 5th Conference on Wind Engineering (UK Wind Engineering Society)**, Nottingham, UK.

Hunt, J.C.R., Poulton, E.C. and Mumford, J.C. (1976) The effects of wind on people: New criteria based on wind tunnel experiments. **Building and environment**, 11: 15-28.

Johnson, T., Dalley, S. and Temple, J. (2004) "Recent studies in train slipstreams." In McCallen, R., Browand, F. and Ross, J. (eds.) **The aerodynamics of heavy vehicles: trucks, buses and trains. Series: Lecture notes in applied and computational mechanics**, 19, Berlin: Springer.

Johnson, T. and Prevezer, T. (2005) Mechanical model of human loss of balance due to wind gusts. **EACWE4 – The Fourth European and African Conference on Wind Engineering**, Prague, Czech Republic.

Jowit, J. (2007) **The amazing secrets of Eurostar** [online]. http://observer.guardian.co.uk/print/0,,330847378-102285,00.html [Accessed November 2007].

Kim, T-H., Kim, Y-T. and Yoon Y-S. (2005) Development of a biomechanical model of the human body in a sitting posture with vibration transmissibility in the vertical direction. **International Journal of Industrial Ergonomics**, 35: 817-829

Köhler, T. B. J. (2001) **InterCityExpress (ICE) / InterCity-NeiTech (ITC)** [online]. www.railfaneurope.net/ice/ice2.html [Accessed June 2005].

Laughton, C.A., Slavin, M., Katdare, K., Nolan, L., Bean, J.F., Kerringan, D.C., Phillips, E., Lipsitz, L.A. and Collins, J.J. (2003) Aging, muscle activity, and balance control: physiological changes associated with balance impairment. **Gait and Posture**, 18: 101-108.

Legates, D. R. and McCabe, G.J. (1999) Evaluating the use of 'goodness-of-fit' measures in hydrologic and hydroclimatic model validation. **Water Resources Research**, 35 (1): 233-241.

Liao, S., Mosier, P., Kennedy, W. and Andrus, D. (1999) The aerodynamic effect of high-speed trains on people and property at stations in the northeast corridor. U.S. Department of Transportation, Federal Railroad Administration, Report Number DOT/FRA/ORD-99/12, November 1999.

Liu, Y., Peng, C-H., Wei, S-H., Chi, J-C., Tsai, F-R. and Chen, J-Y. (2006) Active leg stiffness and energy stored in the muscles during maximal counter movement jump in the aged. **Journal of Electromyography and Kinesiology**, 16: 342-351.

Luchies, C.W., Alexander, N.B., Schultz, A.B. and Ashton-Miller, J. (1994) Stepping responses of young and old adults to postural disturbances: kinematics. **Journal of the American Geriatrics Society**, 42: 506-512.

Mackey, D. and Robinovich, S. (2006) Mechanisms underlying age-related differences in ability to recover balance with the ankle strategy. **Gait and Posture**, 23: 59-68.

Maki, B.E., McIlroy, W.E. and Fernie, G.R. (2003) Change-in-support reactions for balance recovery. **IEEE Engineering in Medicine and Biology Magazine**, March/April: 20-26.

Mamas and Papas [online]. www.mamasandpapas.co.uk [Accessed April 2007].

Martin, A., Martin, L. and Morlon, B. (1994) Theoretical and experimental behaviour of the muscle viscosity coefficient during maximal concentric actions. **European Journal of Applied Physiology**, 69 (6): 539-544.

Matsumoto, Y. and Griffin, M.J. (2001) Modelling the dynamic mechanisms associated with the principle resonance of the seated human body. **Clinical Biomechanics**, 16, Supplement No.1: S31-S44.

Matsumoto, Y. and Griffin, M.J. (2003) Mathematical models for the apparent masses of standing subjects exposed to vertical whole-body vibration. **Journal of Sound and Vibration**, 260: 431-451.

Melbourne, W.H. (1978) Criteria for environmental wind conditions. **Journal of Industrial Aerodynamics**, 3: 241-249.

Melbourne, W.H. and Joubert, P.N. (1971) Problems of wind flow at the base of tall buildings. **Proceedings of the 3rd International Conference on Wind effects on Buildings and Structures**, Tokyo, Japan.

Miller, B.C. (1998) **Investigating slips and falls: The complex dynamics behind simple accidents** [online]. http://www.safety-engineer.com/complex.htm [Accessed June 2005].

Morasso, P.G., Baratto, L., Capra, R. and Spada, G. (1999) Internal models in the control of posture. **Neural Networks**, 12: 1173-1180.

Morasso, P.G. and Schieppati, M. (1999) Can muscle stiffness alone stabilise upright standing? **Journal of Neurophysiology**, 82 (3): 1622-1626.

Mothercare [online]. www.mothercare.co.uk [Accessed April 2007].

Murakami, S. and Deguchi, K. (1981) Measurement of drag force on people walking in a wind tunnel. **CSTB Colloque – Designing with the wind**, Nantes, France.

National Center for Health Statistics (2007) **Prevalence of Overweight and Obesity Among Adults: United States, 2003-2004** [online]. http://www.cdc.gov/nchs/products/pubs/pubd/hestats/overweight/overwght_adult_03.htm [Accessed August 2007].

National Highway Traffic Safety Administration (2002) **NHTSA VRTC Pedestrian and Applied Biomechanics Division, Adult crash test dummies, hybrid III 50th percentile male** [online]. www-nrd.nhtsa.dot.gov/vrtc/bio/adult/hybIII50dat.htm [Accessed July 2005].

Network Rail (2006) **Playing our part, a corporate responsibility report** [online]. www.networkrail.co.uk/browse%20documents/corporate%20responsibility%20report/networkrailcrreport2006.pdf [Accessed January 2006].

Nigg, B.M. and Liu, W. (1999) The effect of muscle stiffness and damping on simulated impact force peaks during running. **Journal of Biomechanics**, 32: 849-856.

Nikuradse, J. (1932) Gesetzmäßigkeiten der turbulenten Strömung in glatten Rohren. In: Forschungsarb. Ing.-Wesen.

Parveen, N. (n.d.) **Golden ratio in art and architecture** [online]. http://jwilson.coe.uga.edu/EMAT6680/Parveen/GR_in_art.htm [Accessed July 2005].

Penwarden, A.D., Grigg, P.F. and Rayment, R. (1978) Measurements of wind drag on people standing in a wind tunnel. **Building and Environment**, 13: 75-84.

Quinn, A.D., Baker, C.J. and Wright N.G. (2001) Wind and vehicle induced forces on flat plates- Part 2: Vehicle induced force. **Journal of Wind Engineering and Industrial Aerodynamics**, 89: 831-847.

Robertson, A.P., Quinn, A.D. and Rees, E.J. (2004) Pressure-wave loading from a large road-vehicle and response of a cantilever mast for traffic signals. **Proceedings of the 6th Conference on Wind Engineering (UK Wind Engineering Society)**, Cranfield, UK.

The Royal College of Physicians of London, the Royal College of Paediatrics and Child Health, and the Faculty of Public Health (2004) Storing up problems: The medical case for a slimmer nation.

Sanz-Andrés, A., Santiago-Prowald, J., Baker, C.J. and Quinn, A. (2003) Vehicle-induced loads on traffic sign panels. **Journal of Wind Engineering and Industrial Aerodynamics**, 91: 925-942.

Sanz-Andrés, A., Laverson, A., Cuerva, A. and Baker, C.J. (2004a) Vehicle induced force on pedestrians. **Journal of Wind Engineering and Industrial Aerodynamics**, 92: 185-198.

Sanz-Andrés, A., Laverson, A., Baker, C. and Quinn, A. (2004b) Vehicle induced loads on pedestrian barriers. **Journal of Wind Engineering and Industrial Aerodynamics**, 92: 413-426.

Schlick, C.M. (2003) **Ergonomic design and usability engineering** [online]. http://www.iaw.rwth-aachen.de/download/lehre/vorlesungen/2003-ws-ie1/aw1bo_07_ws2003-englisch.pdf [Accessed August 2005].

Schulte-Werning, B., Matschke, G., Gregoire, R. and Johnson, T. (1999) RAPIDE: A project of joint aerodynamics research of the European high-speed rail operators. **Proceedings, 4th World Congress on Railway Research**, Tokyo, Japan.

The Scottish Government (2005) **Statistical Bulletin Transport Series: Trn / 2005 / 3: Travel by Scottish residents: some National Travel Survey results for 2002/2003 and earlier years, Table M** [online]. http://www.scotland.gov.uk/Publications/2005/04/1894658/47101 [Accessed August 2005].

Sproston and Primatesta (eds.) (2004) **Health survey for England 2003**. 1st ed. London: The stationary office.

Temple, J. and Dalley, S. (2001) RAPIDE Project; Analysis of the slipstream data. AEA Technology Rail AEATR-T&S-2001-197.

Temple, J. and Johnson, T. (2003) Review of slipstream effects on platforms, A report produced for Rail Safety and Standards Board, June 2003.

Torrence, C. and Compo, G.P. (1998) A practical guide to wavelet analysis. **Bulletin of the American Meteorological Society,** 79 (1): 61-78.

Torrence, C. and Compo, G.P. (n.d.) **A practical guide to wavelet analysis, software to generate scalograms** [online]. http://atoc.colorado.edu/research/wavelets/ [Accessed March 2005].

Van Bogaert, L.J. (1999) The relation between height, foot length, pelvic adequacy and mode of delivery. **European Journal of Obstetrics and Gynecology and Reproductive Biology**, 82: 195-199.

Van der Burg, J.C.E., Pijnappels, M. and Van Dieën, J.H. (2007) The influence of artificially increased trunk stiffness on the balance recovery after a trip. **Gait and Posture**, 26: 272-278.

Virgin Trains (2007) **Pendolino Tour** [online]. http://www.virgintrains.co.uk/travelling_with_us/our_trains/pendolino_tour/default.aspx [Accessed August 2007].

Vuchic, V. (1981) **Urban public transportation systems and technology**. 1st ed. Englewood Cliffs, NJ: Prentice-Hall.

Warburton, G. B. (1964) **The dynamical behaviour of structures**. 1st ed. Oxford ; New York : Pergamon Press : Macmillan.

Wei, L. and Griffin, M. J. (1998) Mathematical models for the apparent mass of the seated human body exposed to vertical vibration. **Journal of Sound and Vibration**, 212 (5): 855-874.

Wexler, A.S., Ding, J. and Binder-Macleod, S.A. (1997) A mathematical model that predicts skeletal muscle force. **IEEE Transaction on Biomedical Engineering**, 44 (5): 337-448.

Wikipedia (2006a) **British Rail Class 92** [online]. http://en.wikipedia.org/wiki/British_Rail_Class_92 [Accessed October 2006].

Wikipedia (2006b) **Drag coefficient** [online]. http://en.wikipedia.org/wiki/Drag_coefficient [Accessed February 2007].

Wikipedia (2007a) **Morlet wavelet** [online]. http://en.wikipedia.org/wiki/Morlet_wavelet [Accessed April 2007].

Wikipedia (2007b) **British rail class 390** [online]. http://en.wikipedia.org/wiki/British_Rail_Class_390 [Accessed November 2007].

Willmott, C.J. (1981) On the validation of models. **Physical Geography**, 2: 184-194.

Winter, D.A. (1995) **A.B.C. (anatomy, biomechanics and control) of balance during standing and walking**. 1st ed. Waterloo, Canada: Waterloo Biomechanics.

Yu, K. and Luo, C.J. (2004) The periodic responses and stability of a human body in a vehicle travelling on rough terrain. **Journal of Sound and Vibration**, 272: 267-286.

Zong, Z. and Lam, K.Y. (2002) Biodynamic response of shipboard sitting subject to ship shock motion. **Journal of Biomechanics**, 35: 35-43.